AFRPL-TR-81-097

LINER TECHNOLOGY PROGRAM

Fracture Energy Method Development

Authors: K. W. Bills, Jr.
          R. A. Schapery

AEROJET STRATEGIC PROPULSION COMPANY
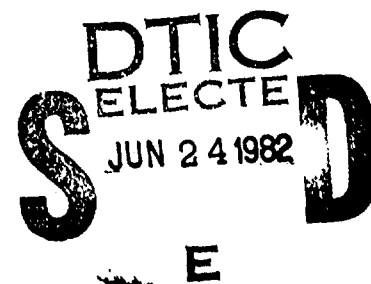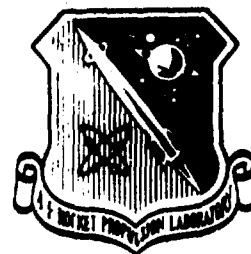P.O. Box 15699C
Sacramento, California 95813

May 1982

Final Report for the Period August 1978 through November 1981

AD A115977

APPROVED FOR PUBLIC RELEASE; DISTRIBUTION UNLIMITED

Prepared for

AIR FORCE ROCKET PROPULSION LABORATORY
DIRECTOR OF SCIENCE AND TECHNOLOGY
AIR FORCE SYSTEMS COMMAND
EDWARDS AFB, CALIFORNIA 93523

DTIC
ELECTE
JUN 24 1982
S
D
E

82   06   24   041

DTIC FILE COPY

NOTICES

When U.S. Government drawings, specifications, or other data are used for any purpose other than a definitely related Government procurement operation, the fact that the Government may have formulated, furnished, or in any way supplied the said drawings, specifications, or other data, is not to be regarded by implication or otherwise, or in any manner licensing the holder or any other person or corporation, or conveying any rights or permission to manufacture, use, or sell any patented invention that may be related thereto.

FOREWORD

This report was submitted by Aerojet Strategic Propulsion Company, P.O. Box 15699, Sacramento, CA 95813 under Contract F04611-78-C-0076, Job Order No. 573013JJ with the Air Force Rocket Propulsion Laboratory, Edwards AFB CA 93523. The report is contained in three volumes each with its own report number:

Volume I - Fracture Energy Method Development, AFRPL-TR-81-97.

Volume II - Liner Development, Characterization, and Aging, AFRPL-TR-81-98.

Volume III - Liner Development Methodology Manual. AFRPL-TR-81-99

This Final Report is approved for release and publication in accordance with the distribution statement on the cover and on the DD Form 1473.

RUSS G. STACER
Project Manager

R. JOHN MOSS, Capt, USAF
Ch, Mechanical Behavior and
Aging Section

FOR THE DIRECTOR

CHARLES R. COOKE
Director, Solid Rocket Division

REPORT DOCUMENTATION PAGE		READ INSTRUCTIONS BEFORE COMPLETING FORM
1. REPORT NUMBER AFRPL-TR-81-097	2. GOVT ACCESSION NO. AD-A115 9947	3. RECIPIENT'S CATALOG NUMBER
4. TITLE (and Subtitle) LINER TECHNOLOGY PROGRAM FRACTURE ENERGY METHOD DEVELOPMENT		5. TYPE OF REPORT & PERIOD COVERED Final Report August 1978 – November 1981
		6. PERFORMING ORG. REPORT NUMBER
7. AUTHOR(s) Mr. Kenneth W. Bills, Jr. Dr. Richard A. Schapery		8. CONTRACT OR GRANT NUMBER(s) F04611-78-C-0076
9. PERFORMING ORGANIZATION NAME AND ADDRESS Aerojet Strategic Propulsion Company Chemical Research and Development P.O. Box 15699C, Sacramento, California 95813		10. PROGRAM ELEMENT, PROJECT, TASK AREA & WORK UNIT NUMBERS 573013JJ
11. CONTROLLING OFFICE NAME AND ADDRESS Air Force Rocket Propulsion Laboratory/MKPA Edwards AFB, California 93523		12. REPORT DATE May 1982
		13. NUMBER OF PAGES 286
14. MONITORING AGENCY NAME & ADDRESS(if different from Controlling Office)		15. SECURITY CLASS. (of this report) Unclassified
		15a. DECLASSIFICATION/DOWNGRADING SCHEDULE

16. DISTRIBUTION STATEMENT (of this Report)

Approved for Public Release; Distribution Unlimited

17. DISTRIBUTION STATEMENT (of the abstract entered in Block 20, if different from Report)

18. SUPPLEMENTARY NOTES

19. KEY WORDS (Continue on reverse side if necessary and identify by block number)

Solid propellant
liner
adhesive bond
fracture criterion
fracture mechanics

J integral
measure of fracture energy
test methods

20. ABSTRACT (Continue on reverse side if necessary and identify by block number)

The objective was to develop a test method for the measurement of adhesive and cohesive fracture energy in a form that would permit the evaluation in engineering terms of the propellant liner bondline. After screening existing test specimens, the scarf-joint specimen was selected as the one that most closely met the AFRPL criteria. The J integral fracture criterion was extended to account for the nonlinear viscoelastic effects of solid propellant; and theoretically applied to the data analysis of this test. The test specimen was optimized using 1-, 2- and 3-dimensional stress analyses plus simple experimental

DD FORM 1 JAN 73 1473 EDITION OF 1 NOV 65 IS OBSOLETE

evaluations. Experiments included tests under superimposed pressures, combined tension and shear, and simultaneous cooling and deformation. Comparisons were made with other test methods and on specimens cut from motors.

Accession For

NTIS GRA&I

DTIC TAB

Unannounced

Justification

Distribution/

Availability Codes

Dist | Special

A

DTIC
COPY
INSPECTED
2

TABLE OF CONTENTS

TABLE OF CONTENTS (Continued)

FIGURE LIST

TABLE LIST (Continued)

1.0   INTRODUCTION

The Phase I efforts reported here were performed as part of a two-phase
study program. The Phase II final report and the Liner Development Methodology
Manual are presented in Volumes II and III, respectively.

An overview of Phase I is provided below. This includes the objectives
of the work, the approach followed, and a brief description of the J integral
fracture criterion.

1.1 OBJECTIVES

The objective of Phase I is to develop a test method for measuring
adhesive and cohesive fracture energy which will permit the evaluation of
bondline strength in engineering terms. The specific goals of the test method,
as set forth in the contract, are as follows:

- The test method must be scientifically sound and analyzable.

- The test specimen shall have the following characteristics:
    - Failure initiation from a controlled and analyzable
      singularity.
    - Allow failure at the location of weakest strength in the
      vicinity of the bond.
    - Provide engineering data that are independent of specimen
      geometry.
    - Be amenable to analysis to evaluate stresses and strains
      directly related to motor analyses.
    - Duplicate the various stress conditions that can exist
      in motors.
    - Be amenable to preparation from dissected motors.

-12-

- The test method shall be evaluated with a well-characterized, operational propellant/liner/insulation system, and verified with other well-characterized systems.

- The test method shall be evaluated for repeatability.

1.2 APPROACH

The approach taken was to employ a fracture energy relationship that would:

1. Permit direct measurements of the fracture energy (e.g., no separate measurements of material moduli, which are highly inaccurate in the stratified propellant/liner/case bond structure).

2. Permit measurements even when the material is nonlinear viscoelastic.

The J Integral criterion meets these requirements and provides for straightforward analytical and testing approaches. The theoretical basis for this criterion has been extensively improved by Dr. R. A. Schapery and is now considered to be applicable to nonlinear viscoelastic propellants tested under finite deformations.

The optimum test specimen was selected from an extensive screening of a number of possible bond test methods that have been, or could have been, used in the propellant industry. A morphological approach was developed at the end of this screening that greatly simplified the selection method. The scarf-joint design was finally selected as the optimum specimen. The dimensions were selected after extensive laboratory tests and after many 1-, 2- and 3-D structural analyses.

-13-

A sophisticated method for monitoring movement of the crack front employed the transmission of ultrasound between the end plates. Even though not utilized on any of these tests, the method could be used to monitor rates of crack propagation.

Standardized laboratory methods for preparing and testing the specimens were developed over a series of tests. The size and placement of the initial cracks were quite important, as were specimen alignment and edge effects. Data analysis methods also had to be evaluated and put into forms that were realistic for solid propellant test results.

Applications of the standardized test involved specimens cut from the Minuteman Stage II and Polaris A3 Stage II motors. These specimens required special end plates and crack cutting procedures because of the curvature in the cases.

A number of tests were conducted to determine the repeatability of the standardized test. The testing followed a Graeco-Latin square test grid and evaluated batch-to-batch and operator-to-operator variances as well as the test experimental error. The experimental error was found to be very small.

1.3 THE J INTEGRAL AND ITS RELATION TO OTHER FRACTURE CRITERIA

At this point it is sufficient to provide only a simple description of the J integral*. See Section 2 for a more complete presentation which extends the concept to nonlinear viscoelastic materials, including finite deformations.

Conceptually, J is a line integral taken around the crack tip. One of its primary strengths is that its value is independent of the path taken around the crack, even if some of the paths involve plastic deformations and

---

* In common with the stress-intensity factor K, there are separate values of J for the opening mode (J_I), shear mode (J_{II}), and tearing mode (J_{III}).

other paths do not. The illustration given below for an arbitrary path R around the crack tip begins at the lower crack surface on the left and proceeds counter-clockwise around to the upper surface of the crack.
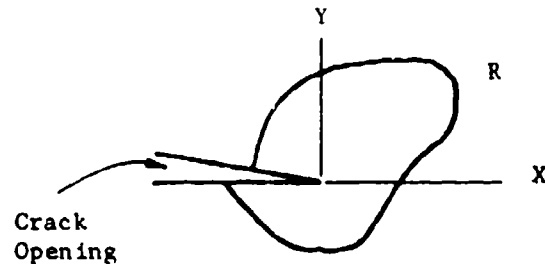
Arbitrary line integral contour
around the crack tip.

For linear-elastic behavior, the J integral is identical to G, the energy release rate per unit crack extension, and simply related to the fracture toughness, K, and the fracture energy, γ. Thus, for the opening mode case, and linear-elastic plane-strain conditions, we have the following relation.

$$J_{Ic} = G_{Ic} = \frac{(1 - \nu^2)K_{Ic}^2}{E} = 2\gamma. \tag{i}$$

This relationship illustrates the value of the J integral approach. In the laboratory it affords a straightforward characterization method. In engineering applications it can be transformed to give values of the failure criterion appropriate to other methods of analysis.

1.4 REPORT

The following report begins with a theoretical treatment of the J integral in which the concept is extended to finite deformations and non-linear viscoelastic materials. Section 3.0 describes the procedures used in screening candidate test specimens and in the selection of the scarf-joint specimen as the optimum candidate. The fourth section provides the stress and fracture analyses which led to an optimization of the specimen design.

The Scarf-joint specimen preparation and test procedures were defined in a series of tests described in Section 5.0. Sections 6.0 and 7.0 cover evaluations of the J integral under various loading conditions that exist in the motor, and evaluations using two other specimen geometries. Section 8.0 describes the tests performed on specimens dissected from motors and the statistical aspects of scarf-joint test repeatability.

2.0 CHARACTERIZATION AND ANALYSIS OF FRACTURE INITIATION IN SOLID PROPELLANT BY A GENERALIZED J INTEGRAL

The theory and application of linear viscoelastic fracture mechanics is reasonably well established [1-6]. However, because of the nonlinearity of solid propellants, application of linear theory has met with mixed success, and phenomena related to the effect of strain level and strain history have not been explained [7]. As a means of developing a criterion of fracture in nonlinear viscoelastic materials, Schapery [8] indicated that at least for initiation the J integral criterion (widely used for rate-independent elasto-plastic behavior of metals) could be extended to certain nonlinear viscoelastic materials if the stresses at each point in the body are proportional to a scalar function which obeys a power law in time with a coefficient and exponent that may vary in space. This restriction on the stress behavior has now been removed and a relatively general theory exists for both crack initiation and growth [9].

In this section of the report, we first review the basic features of standard J integral theory for nonlinear elastic media, and then deal with its extension and application to solid propellant.

2.1 J INTEGRAL THEORY FOR NONLINEAR ELASTIC MEDIA

The J integral is defined for two-dimensional problems (plane stress, plane strain, and anti-plane strain) as

$$J = \int_{\hat{\Gamma}} (W dx_2 - T_i \frac{\partial u_i}{\partial x_1} ds) \tag{2}$$

Where $\hat{\Gamma}$ (Figure 1) is a curve surrounding the crack tip that begins and ends on assumed stress-free crack faces [10]. Following standard practice, repeated indices imply summation over their range $(i,j = 1,2,3)$, and T and u are the traction and displacement vectors, respectively. Although Equation (2) is limited to small strains, it is readily generalized to large strains (Reference 11).
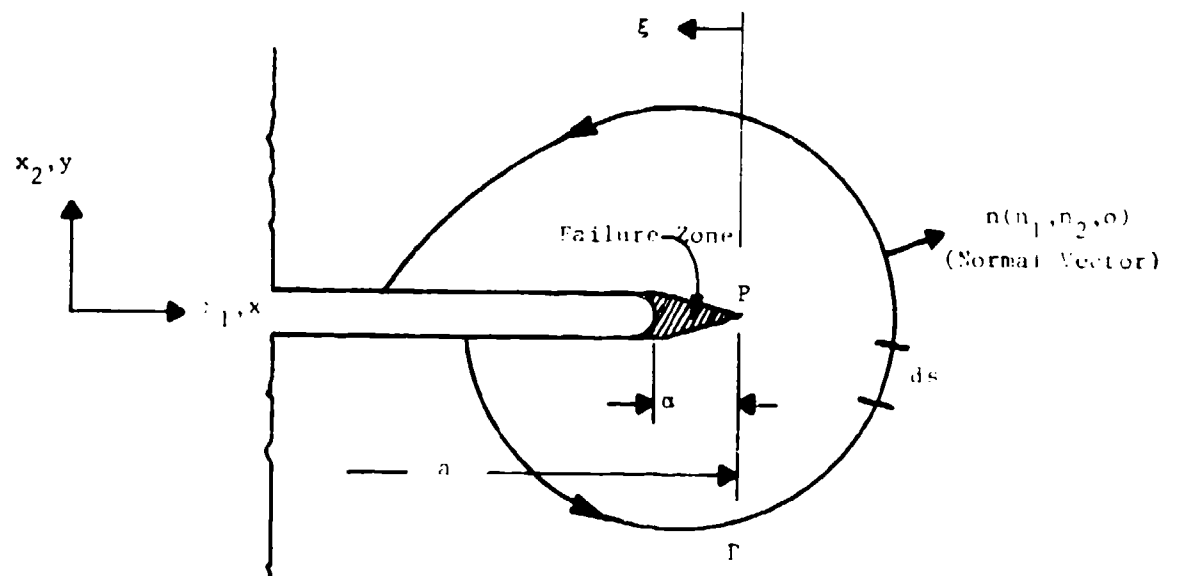
Figure 1. Contour Used to Evaluate the
J Integral in Equation (2)

The traction vector and stresses are related through the familiar expression

$$T_1 = \sigma_{ij} \; n_j \equiv \sigma_{11} \; n_1 + \sigma_{12} \; n_2 \tag{3}$$

The component T_3, corresponding to a traction in the x_3 - direction (normal to the plane of the page), is not necessarily zero; thus, the so-called anti-plane mode of loading is included in this formulation.

The quantity $W = W(\epsilon_{ij})$ is defined such that

$$\sigma_{ij} = \partial W / \partial \epsilon_{ij} \tag{4}$$

where σ_{ij} and ϵ_{ij} are the stress and strain tensors, respectively. Thus, W is the strain energy density of an elastic body. We should emphasize, however, that the body need not be elastic for Equation (4) to be valid. For elasto-plastic materials which obey the so-called deformation theory of plasticity the stresses can be written as in Equation (4), where W is a potential function consisting of both stored and dissipated energy; although the deformation theory of plasticity is usually not a good constitutive theory for metals except for proportional stressing, fracture initiation analysis of metals based on "elastic-like" Equation (4) and the J integral has been very successful [12].

As an important consequence of Equation (4), the J integral in Equation (2) is the same for all paths $\hat{\Gamma}$ [10]. Let us select a path adjacent to the crack faces (for which $dx_2 = 0$), which reduces Equation (2) to

$$J = \int_0^\alpha \sigma_{22}^f \; \frac{\partial \Delta u_2}{\partial \hat{\xi}} \; d\hat{\xi} + \int_0^\alpha \sigma_{21}^f \; \frac{\partial \Delta u_1}{\partial \hat{\xi}} \; d\hat{\xi} + \int_0^\alpha \sigma_{23}^f \; \frac{\partial \Delta u_3}{\partial \hat{\xi}} \; d\hat{\xi} \tag{5}$$

where

Δu_1 = relative displacement vector between points on the crack faces which were together prior to arrival of the crack tip. For example, Δu_2 is the crack opening displacement.

σ_{ij}^f = stress acting on the edge of the intact continuum, representing the action of the failing material near the crack tip on the adjacent continuum. For example, σ_{22}^f is the normal tensile stress tending to draw the crack faces together.

It is supposed that there is a thin layer of material between crack faces in the zone $0<\hat{\xi}<\alpha$ (Figure 1) which may be highly damaged; its constitutive properties enter the fracture theory implicitly through the values of σ_{22}^f, σ_{21}^f, and σ_{23}^f. The material in the failure zone does not have to satisfy Equation (4).

Let us now multiply Equation (5) by a small virtual crack extension, δa. One can show by direct physical considerations that the resulting expression is the work done by the continuum on the failure zone (per unit length in the x_3 direction) if the advancement takes place without change in the tractions σ_{ij}^f in the failure zone. In view of Equation (4), the body behaves as an elastic material, and thus the work $JB\partial a$ must be equal to the reduction in potential energy P_E of the body and externally applied forces, $-\partial P_E$; hence,

$$J = -\frac{1}{B}\frac{\partial P_E}{\partial a} \tag{6}$$

where B is the length of the crack edge which is advanced; $B\partial a$ is the area of the new surface projected onto the $x_1 - x_3$ plane. For advancement without external work ("fixed grips"), Equation (6) reduces to

$$J = -\frac{1}{B}\frac{\partial W_T}{\partial a} \tag{7}$$

where W_T is the total strain energy,

$$W_T \equiv \int_{V_o} W \, dV_o \qquad (8)$$

and V_o is the volume of the body.

It is important to recognize that Equations (6) and (7) provide a means for experimental determination of J in a nonlinear body without the necessity of a nonlinear stress analysis; this is discussed in the next subsection along with the use of J as a fracture parameter.

2.1.1 Experimental Determination of J Integral

Consider a sample which is quasi-statically loaded by a force F acting through the displacement U, (e.g., the biaxial strip in Figure 2). The load-displacement curve is illustrated in Figure 3 for several samples, each with a different constant crack length, $2a'$. The area under each curve from $U = 0$ to $U = U_1$ is $W_T (U_1, a)$. Plotting this integral versus the crack length*, $a = 2a'$, gives a curve like that in Figure 4.

The negative derivative of curve W_T at any value a, divided by sample thickness, B, is the J integral at $U = U_1$, Equation (7); it is supposed that both crack tips extend the same amount, $\partial a'$. If this process is repeated for additional values U_2, U_3, etc., we obtain the curves in Figure 5. For the special case of a linear elastic material, $W_T \sim U^2$, $J \sim U^2$ for a fixed value of a.

---

* Use a' as one-half the crack length and a as the full crack length.
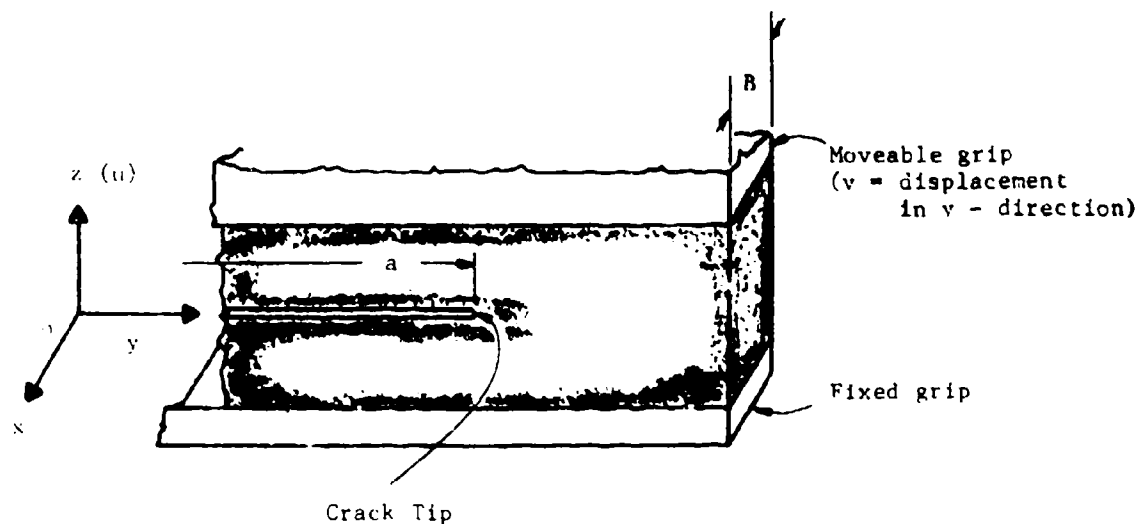
Figure 2.   Biaxial Strip Specimen

- Note that the coordinate axes
  used with this specimen are
  different from those conventionally
  used in two-dimensional problems
  (See Figure 1)
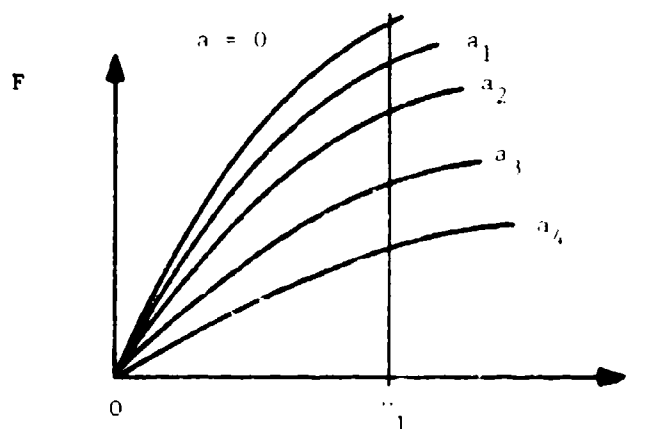
Figure 3.   Force-Displacement Curve
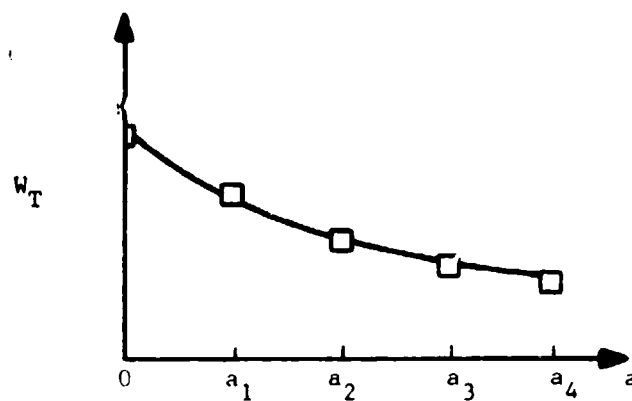
Figure 4.   Area Under F – U Curve versus Crack Length
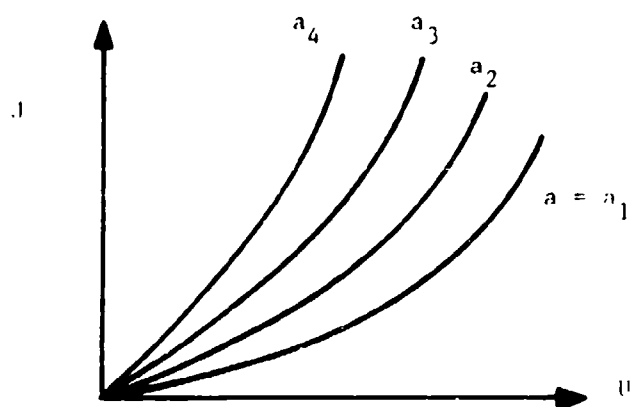
Figure 5.   J versus Axial Extension

2.1.2 Relation of J To Fracture Initiation

Suppose in a given test the crack starts to propagate at a value of $J = J_c$ (critical value of J). Since J is equal to the strain energy released per unit projected area (actually two units of area of new surface counting both top and bottom surfaces), we can say that $J_c B \partial a$ is equal to the mechanical energy needed by the material to form an amount of projected area $B \partial a$ or total surface $2B \partial a$. Thus

$$J_c = 2\Gamma_i \tag{9}$$

where Γ_i is the so-called fracture initiation energy, the energy required to form a unit of new surface.

As long as the state of the material at the crack tip (on the scale of α) is the same in different geometries (including motors), the value of J_c from the specimen test can be considered a material property; it may be compared with a predicted J-value (e.g., in a motor). If $J \geq J_c$, the crack starts to propagate; otherwise, it does not grow.

2.2 GENERALIZED J INTEGRAL FOR NONLINEAR VISCOELASTIC MATERIALS

For many linear and nonlinear viscoelastic materials under monotonic loading which obeys a power law in time [8], Equation (4) is a good approximation with W replaced by $W_v = W_v(\epsilon_{ij}, a, t)$; hence, by analogy with the elastic case,

$$J = -\frac{1}{B} \frac{\partial W_T}{\partial a} \tag{10}$$

where $W_T = W_T(U, a, t)$ is the area under the isochronal F-U curve,

$$W_T = \int_0^U F(U, a, t) dU \tag{11}$$

Note that the differentiation and integration is performed for t = constant.

The J integral for this case is, as before, the work input
to the crack tip per unit area at time t [8]. Thus J_c is equal to the
energy $2\Gamma_i$ required by the material to create the new surface at the time
of initiation t; depending on the material, Γ_i may depend on time and
temperature and other parameters such as confining pressure.

The conditions given in Reference (8) for the validity of
Equations (4) and (10) are more severe than needed. The particular
nonlinear viscoelastic constitutive equations which describe deformation
response with adequate accuracy and class of loading histories of interest,
determine whether or not a J integral method applies, and Reference (9)
discusses both this aspect and consequences for predicting crack initiation
time and crack speed.

To remove the power-law restriction on loading history given
in Reference (8), the definition of J in Reference (9) is somewhat different
than used here so far; but we shall summarize the principal results and
relate the two forms of the generalized J integral.

2.2.1 Primary Results of Reference (9) Applicable to Solid Propellant

In terms of a newly defined J integral, J_v, the governing
equation for predicting fracture initiation time t_i is

$$2\Gamma_i = E_R \int_o^{t_i} D\ (\xi - \xi') \ \frac{dJ_v}{d\tau} \ d\tau \tag{12}$$

After initiation, the crack speed $\dot{a}$ for coplanar crack growth is predicted
by using the differential equation,

$$2\Gamma = E_R \ D\left(\frac{a}{3\dot{a}a_T}\right) J_v \tag{13}$$

In these two equations:

Γ_1, Γ = fracture initiation energy and fracture
energy for continuous growth, respectively;
whether or not these energies are equal is
not known at this time.

E_R = reference modulus, a constant which is
arbitrarily selected to simplify notation.

$D(\cdot)$ = master creep compliance curve in linear
viscoelastic response range (with or without
a constant level of damage); as a good
approximation, the master relaxation modulus
is related to $D(\xi)$ by

$$E(\xi)D(\xi) = \frac{\sin m\pi}{m\pi} \tag{14}$$

where

$$m \equiv -\frac{d \log E}{d \log \xi} = \frac{d \log D}{d \log \xi} \tag{15}$$

Also, the propellant is assumed to be thermorheologically simple,

$$\xi \equiv \int_0^t dt'/a_T, \quad \xi' \equiv \int_0^t dt'/a_T \tag{16}$$

where $a_T = a_T$ (T) is the time-temperature shift factor; more general behavior
is included in Reference (9).

The quantity J_v is the generalized J integral; it obeys an
equation which is analogous to that for J in Equation (6) in that

$$J_v = -\frac{1}{B} \frac{\partial P_E^R}{\partial a} \tag{17}$$

where P_E^R is the potential energy of an elastic body that is defined below.
The quantity α is the length of the failure zone (Figure 1), which is
proportional to J_v if the strength of the material at the crack tip is constant:
when the strength varies with crack speed, one has α = function ($\dot{a}$, J_v).

-26-

The three-dimensional constitutive equation used in Reference (9) relating stresses σ_{ij} and strains ϵ_{ij} for materials exhibiting thermorheologically simple behavior is,

$$\epsilon_{ij} = E_R \int_0^t D(\xi-\xi') \frac{\partial}{\partial \tau} \left(\frac{\partial \Phi_c}{\partial \sigma_{ij}} \right) d\tau \qquad (18)$$

where $\Phi_c = \Phi_c(\sigma_{ij})$ is the complementary pseudo energy density; justification of this equation for solid propellant and other materials is given in Reference (9). The pseudo energy density Φ is defined by

$$\Phi = -\Phi_c + \sigma_{ij} \frac{\partial \Phi_c}{\partial \sigma_{ij}} \qquad (19)$$

If $D(\xi) =$ constant $\equiv E_R^{-1}$, we recover Equation (4) for an elastic material, where $\Phi \equiv W$ is the strain energy density.

For a viscoelastic material ($D(\xi)$ not constant) the quantity J_v is simply the J integral for this "reference" elastic material, and P_E^R in Equation (17) is the potential energy; for example, for the problem in Figure 2, with virtual crack growth under a fixed grip condition,

$$J_v = -\frac{1}{B} \frac{\partial \Phi_T}{\partial a} \qquad (20)$$

where $\Phi_T \equiv \int_{V_0} \Phi \, dV_0$ is the total strain energy of an elastic body.

In order to show how one can derive J_v from laboratory tests, and to illustrate its physical significance, let us first rewrite Equation (18) in an inverse form; this is easily accomplished because of its similarity to linear theory,

$$\frac{\partial \Phi_c}{\partial \sigma_{ij}} = E_R^{-1} \int_0^t E(\xi-\xi') \frac{\partial \epsilon_{ij}}{\partial \tau} d\tau \qquad (21)$$

Note that the integral is the stress in a linear viscoelastic material,

$$\sigma_{ij}^{\ell} \equiv \int_0^t E(\xi-\xi') \frac{\partial \epsilon_{ij}}{\partial \tau} d\tau \qquad (22)$$

and therefore,

$$\frac{\partial \Phi_c}{\partial \sigma_{ij}} = \frac{\sigma^{\ell}_{ij}}{E_R} \tag{23}$$

The "reference" _elastic_ material is, by definition, a material whose stress-strain equation is that in Equation (23) with _stresses_ equal to those in the actual nonlinear viscoelastic material and with the strains ϵ^R_{ij}

$$\epsilon^R_{ij} \equiv \frac{\sigma^{\ell}_{ij}}{E_R} \tag{24}$$

Similarly, the displacements in the reference material are

$$u_i^R \equiv \frac{1}{E_R} \int_o^t E(\xi - \xi') \frac{\partial u_i}{\partial \tau} d\tau \tag{25}$$

The grip displacement U for the biaxial strip and the reference elastic grip displacement U^R are related similarly through Equation (25). Inasmuch as the material's behavior is elastic in terms of U^R, we may apply the data reduction procedure covered in Figures 3 through 5 _using U^R in place of U as the abscissa._

For simultaneous cooling and straining one would have to account for thermal contraction. In this case the strains and displacements in Equations (24) and (25) should be interpreted as "strains and displacements due to stress". For a biaxial strip one should therefore subtract $\frac{3}{2}\alpha\Delta t$ from each quantity; the relation for grip displacement becomes

$$U^R - \frac{3}{2}\alpha\Delta T = \frac{1}{E_R} \int_o^t E(\xi - \xi') \frac{\partial}{\partial \tau}(U - \frac{3}{2}\alpha\Delta T) d\tau \tag{26}$$

where $\Delta T = T - T_o$, with T_o = temperature at start of cooling and T = current temperature.

-28-

2.2.2 Comparison of J Integral Methods

Consider the isothermal testing for initiation of cracking. The J in Equation (10) and J_v in Equation (20) are quite different, but lead to essentially the same criterion of fracture if the grip displacement rate is constant, or is at least monotone increasing. To show this, let us specialize Equation (26) to isothermal behavior and introduce crosshead rate $\dot{U} = R = $ constant; thus

$$U^R = \frac{R}{E_R} \int_0^t E(t-\tau) \, d\tau = \frac{R}{E_R} \frac{1}{t} \int_0^t E(\lambda) \, d\lambda \tag{27}$$

where the variable of integration has been changed from τ to $\lambda \equiv t-\tau$. Hence,

$$U^R = \frac{U \bar{E}(t)}{E_R} \tag{28}$$

where $\bar{E}$ is the time-average of the relaxation modulus.

The total pseudo strain energy in the reference elastic body is

$$\phi_T \equiv \int_0^{U^R} F(U^R, a) \, dU^R \tag{29}$$

where the elastic force F^R is equal to the viscoelastic force F at each time and crack length.

Since the stresses in the reference elastic body are equal to those in the nonlinear viscoelastic body (Reference 9) use Equations (28) and (29) (in which the variable of integration is changed from U^R to U and integration is performed at constant time) to find

$$\phi_T = \frac{\bar{E}(t)}{E_R} \int_0^U F\left(U \frac{\bar{E}(t)}{E_R}, a\right) dU \tag{30}$$

Comparing Equations (10) and (30) we see that

$$\phi_T = \frac{\bar{E}(t)}{E_R} W_T \tag{31}$$

and from Equations (9) and (19)

$$J_v = \frac{\bar{E}(t)}{E_R} J \tag{32}$$

Thus, the previously used initiation criterion $J = J_c = $ constant at $t = t_i$ is equivalent to

$$J_v = \frac{\bar{E}(t_i)}{E_R} J_c \qquad (33)$$

Or

$$J_c = \frac{E_R}{\bar{E}(t_i)} J_v \simeq C E_R \bar{D}(t_i) J_v$$

$$= C E_R J_v \frac{1}{t_i} \int_o^t D(\lambda) d\lambda \qquad (34)$$

where C is a constant that is close to unity if $m \lesssim 0.2$ (Equation (15)). One can show that Equation (34) is a good approximation to Equation (33) if $d^2 \log E / (d \log \xi)^2 \ll 1$; this inequality is obeyed by solid propellants.

Compare this result with the more basic Equation (12) for isothermal behavior,

$$2\Gamma_i = E_R \int_o^{t_i} D(t-\tau) \frac{dJ_v}{d\tau} d\tau \qquad (12)$$

Note that if J_v is constant, and if the fracture energy $\Gamma_i = J_c/2C$, then Equation (11) reduces to Equation (34). Often with monotonic loading, $J \sim t^p$ (where p is constant*) which, when used in Equation (12), leads to the same form as Equation (34); only a nearly constant factor (typically close to unity) multiplying $\bar{D}$ is different. Thus, for practical purposes in at least constant crosshead rate tests, the original method (Figures 3 through 5) is as good as the better-founded new method based on Equation (12).

The experimental determination of the time for fracture initiation t_i may not be possible with propellant; rather, one might obtain instead of t_i the time for a small amount of growth (depending on the quality of the experimenter's eyesight). In this case Equation (12) would be more

---

* When J_v is expressed in terms of stresses, it is equal to J for a linear or nonlinear elastic body which is under the same instantaneous applied loads as the viscoelastic body; cf. Equations (10) and (20).

appropriate than Equation (11). As an example let us assume the experimentally determined "initiation" time t_i^{ex}, say, is the time it takes for the crack to propagate a distance equal to a constant fraction or multiple of the failure zone length α at the speed at this time, $t_i^{ex} = k\alpha/\dot{a}$; Equation (13) becomes

$$2\Gamma = E_R \, D\left(\frac{t_i^{ex}}{3k}\right) J_v \tag{35}$$

which has the same form as Equation (34); it follows that for propellant in which $D(t)$ is practically a power law, $\bar{D}(t_i) = $ constant x $D(t_i) = $ constant x $D \, t_i^{ex}$, if Γ and Γ_i are constant. Thus, except for differences in the inferred value of fracture energy, all three methods (two for initiation, one for a small amount of growth) yield essentially the same result for isothermal, constant crosshead rate tests. However, it should be emphasized that the last result for growth is based on a somewhat arbitrary criterion of "observable growth".

Such a similarity in results is not expected for simultaneous cooling and straining; this type of test should therefore help to determine the best criterion with the hope (but not as a fundamental requirement) that Γ or Γ_i is constant, and has the same value for isothermal and nonisothermal initiation.

2.2.3 Motor Application

Consider the problem depicted in Figure 6. The stress analysis was made assuming linear elastic behavior, and some relevant predictions for pressure loading are:

Opening Mode Stress Intensity Factor, $K_I = 557$ Ksi $\sqrt{in.}$
Forward Shearing Mode Stress Intensity Factor, $K_{II} = 211$ psi $\sqrt{in.}$

Case

Pressure = 800 psi

Insulation

Liner

0.1 in. Deep Crack
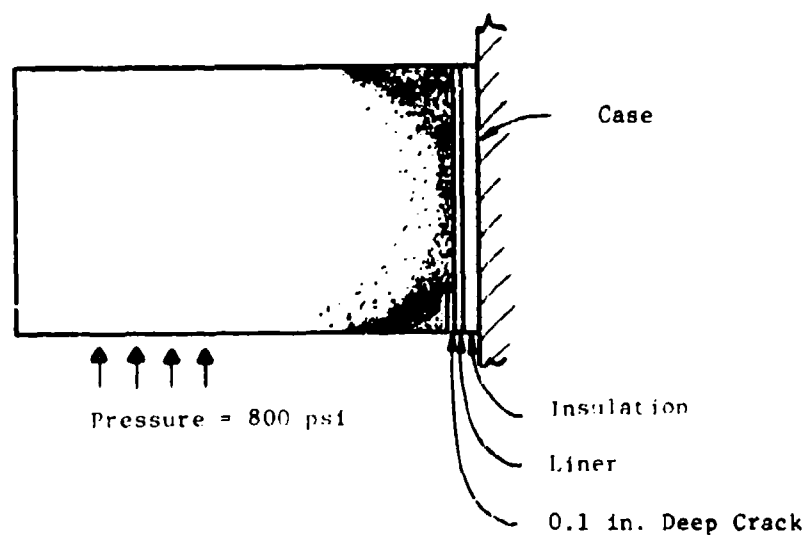
Figure 6. Sample Motor Problem (from Reference 13)

From linear elasticity theory for plane strain (the local condition in the motor around the crack):

$$J = \frac{K_I^2}{[E/(1-\nu^2)]} + \frac{K_{II}^2}{[E/(1-\nu^2)]} \tag{36}$$

where $E = 1000$ psi and $\nu = 0.5$ in the analysis [13]. We will first use elastic fracture mechanics and assume the total energy release rate, J, determines whether or not a fracture starts; but one should verify this experimentally or, more generally, establish 2Γ as a function of the K_{II}/K_I ratio. Thus, we calculate $J = 233 + 33 = 266$ lb/in. For our propellant $2\Gamma_i = J_c \sim 3$ lb/in. $<<266$ (Section 2.2.5) and thus fracture easily initiates.

If pressure $= 0$, and a thermal load only exists ($\Delta T = -100°F$), it is predicted that [13] $K_I = 10.5$, $K_{II} = 4.9$ psi $\sqrt{in.}$ Then, $J = 0.083 + 0.018 = 0.101$ lb/in. Since $J_c = 3 >> 0.101$, there is no fracture initiation in an elastic propellant.

Extension of this analysis to viscoelastic behavior may be accomplished by using Equation (33) and the fact that Equation (36) is valid for a linear reference elastic material with modulus E_R and Poisson's ratio ν_R [9]. Thus

$$J_v = \frac{K_I^2}{E_R/(1-\nu_R^2)} + \frac{K_{II}^2}{E_R/(1-\nu_R^2)} \tag{37}$$

where K_I and K_{II} are the stress intensity factors calculated for a linear viscoelastic material with a constant Poisson's ratio ν [9]. The fracture initiation time is given by the solution to

$$(1-\nu^2) K_I^2 + (1-\nu^2) K_{II}^2 = \bar{E}(t_i) J_c \tag{38}$$

where we have used Equations (33) and (37) with $\nu_R = \nu$. Thus, one uses linear viscoelastic theory to predict K_I and K_{II} as functions of time, and then checks to determine when Equation (38) is satisfied, if ever.

Referring to the pressurization problem above, the values of K_I and K_{II} are essentially independent of elastic modulus and <u>therefore they have the same values as in the viscoelastic material</u>. Assuming $2\Gamma = J_c = 3$ and $\nu = 0.5$, and using the fact that K_I and K_{II} are proportional to pressure, P, Equation (38) may be written as

$$266 \left(\frac{P}{800}\right)^2 = \frac{\bar{E}(t_1)}{1000} \times 3 \tag{39}$$

Thus, fracture initiates at the time t_1 for which

$$P(t_1) = 2.69 \sqrt{\bar{E}(t_1)} \tag{40}$$

If the actual pressure does not reach the value in Equation (40) then of course it does not have a solution and there is no initiation.

Prediction of initiation for the nonisothermal problem is more involved. Equation (12) must be used, in which the time-dependence of temperature must be accounted for in calculating reduced time, Equation (16). If the temperature is more or less uniform spacewise (which was assumed in the above problem), we may predict K_I and K_{II} from elastic analysis using an effective modulus E_{eff} (14). Then substitute Equation (37) into (11), assume $\nu_R = \nu =$ constant for the viscoelastic material and obtain,

$$\int_0^{t_1} D(\xi-\xi')\frac{d}{d\tau} (K_I^2 + K_{II}^2) \, d\tau = \frac{\Gamma_1}{1-\nu^2} \tag{41}$$

Again, the value of t_1 for which this equation is satisfied (if ever) is the initiation time. If we employ results from the above thermal problem and

introduce the effective modulus (recognizing that $K_{I,II} \Delta T E_{eff}$ for constrained cooling) and use an assumed value of $2\Gamma_i = 3$, there results

$$\int_{?}^{\xi 1} D(\xi-\xi') \frac{d(\Delta TE_{eff})^2}{d\xi'} d\xi' = 2.97 \times 10^8 \qquad (42)$$

where

$$\xi_1 = \int_0^{t_1} dt/a_T \qquad (43)$$

and

$$\Delta TE_{eff} \equiv \int_0^{\xi} E(\xi-\xi') \frac{d\Delta T}{\partial\xi'} d\xi' \qquad (44)$$

Considering the previous results for an elastic material, Equation (42) will not have a solution unless E_{eff} is much larger than 1000 psi. Note that for an elastic material $E_{eff} = E = D^{-1}$, and we obtain $E = 29,700$ psi from this equation as the modulus needed to initiate fracture for the temperature change of $T = -100°F$.

2.2.4 Summary of Specific Advantages of the J Integral

2.2.4.1 Analysis

- Theoretical anaylses of specimens are not required; but, if available, they may reduce the testing and data analysis needed.

- In motor applications, the J integral can be used with both linear and nonlinear behavior at small or large strains.

- Path-independence of the J integral reduces the requirements of numerical accuracy in predicting a fracture-controlling parameter, as compared to methods needing local crack-tip analysis.

2.2.4.2 Experiment

- J and fracture energy easily derived from force data.

- Results have simple physical meaning.

- Samples with large 3-D effects can be used without any more data analysis than for 2-D effects if crack growth is essentially uniform over most of the sample thickness.

2.2.5 Experimental Determination of Critical J Integral for Fracture Initiation

Application of Equations (10) and (11) to the characterization of fracture behavior will be illustra d by using data from cracked biaxial samples. The resulting criterion for :ractur ion will then b compared to that found by the second, more general t: ion (12).

Figure 7 shows data for three crosshead rates and two crack lengths. The initial nominal sample dimensions are:

$$H = \text{height} = 2.1 \text{ inches}$$
$$L = \text{length} = 4.0 \text{ inches}$$
$$B = \text{thickness} = 1.0 \text{ inches}$$

Prior to crack growth, the force data are fit quite well by the power law,

$$F = k_1 \, R^{0.172} \, U^{0.770} \tag{45}$$

where axial extension, U, is in inches and crosshead rate, $R \equiv \dot{U}$, is in inches per minute; also, for the two initial crack lengths employed,
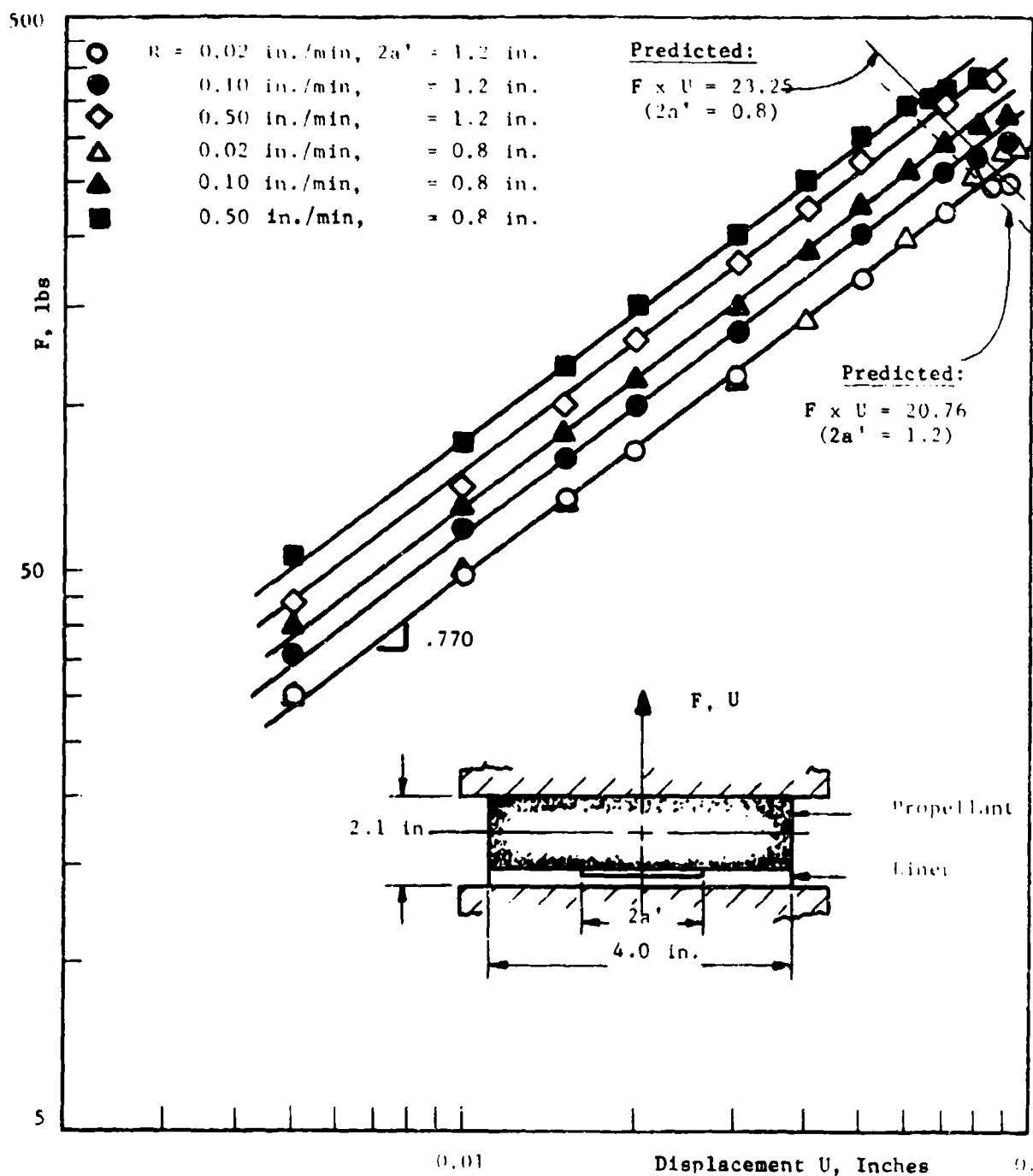
Figure 7. Force-Displacement Data from Biaxial Samples Under Tensile Loading at 0°F

$$k_1 = 3331 \text{ for } 2a' = 0.8 \text{ inches} \qquad (46)$$

$$k_1 = 2974 \text{ for } 2a' = 1.2 \text{ inches}$$

According to Equation (11), W_T is derived by integrating F, but only after R is eliminated in favor of U and t; thus, with R = U/t,

$$F = k_1 \, t^{-0.172} \, U^{0.942} \qquad (47)$$

from which

$$W_T = 0.515 k_1 \, t^{-0.172} \, U^{1.942} \qquad (48)$$

The J integral may be found from Equation (10). First, however, it is of interest to observe that the linear elastic analysis in Section 4.0 (Figures 51, 52, 55, 57 and 58) indicates that J is essentially independent of crack length for the range tested, 2a' = 0.8 and 1.2 inches. This independence will be assumed for the actual propellant samples, and thus W_T may be linearized with respect to crack length in calculating J. Hence, for $0.8 \lesssim 2a' \lesssim 1.2$,

$$J = \frac{0.515}{1.0} \, t^{-0.172} \, U^{1.942} \times \frac{2974-3331}{1.2-0.8}$$

$$\qquad (49)$$

$$= 460 \, t^{-0.172} \, U^{1.942} \, \text{lbs/in.}$$

(It is of interest to note that the value of the derivative $(2974-3331)/0.4 = 893$ is essentially equal to that predicted from linear elastic plane stress analysis.)

Referring now to Figure 7, we assumed crack growth initiates when the force-deformation data depart from a straight line. Considering the limited amount of data, the determination was crude; obviously, more data and an expanded scale are needed for a better identification of the crack initiation point.

At initiation, set $J = J_c$ in Equation (49). Because the test time does not appear explicitly in Figure 7, it is desirable to eliminate time from this equation by using Equation (47); hence,

$$J_c = \frac{460}{k_1} FU \tag{50}$$

For constant crack length and constant J_c, this equation defines a straight line having slope (-1) in Figure 7 as logarithmic coordinates are used,

$$\log \left(\frac{J_c k_1}{460} \right) = \log F + \log U \tag{51}$$

For $2a' = 0.80$, a straight line with slope (-1) has been drawn through the data where crack initiation is estimated to occur; this line is defined by $FU = 23.25$, and therefore Equations (46) and (50) yield

$$J_c = \frac{460}{3331} \times 23.25 = 3.21 \text{ lbs/in.} \tag{52}$$

Assuming that J_c is a constant, we may use Equations (46) and (50) to predict the product FU for initiation with $2a' = 1.2$ inches,

$$FU = \frac{2974}{460} \times 3.21 = 20.76 \tag{53}$$

This line is drawn in Figure 7; agreement between theory and experiment is about as good as one might expect considering the limited amount of data employed.

As a final matter, let us compare the use of Equation (49) (with $J = J_c$) as a fracture initiation criterion with that predicted from the second theory, Equation (12). Equation (32) relates J_v to the expression for J in Equation (49). We want J_v in terms of F, and therefore Equation (47) is also used to find

$$J_v = \frac{\bar{\bar{E}}(t)}{E_R} \, 460 \, k_1^{-2.062} \, t^{0.183} \, F^{2.062} \tag{54}$$

According to the second theory, this result should be identical to that for an elastic material; as time-dependence cannot exist, we must have $\bar{\bar{E}}(t) \sim t^{-.183}$, and thus for the linear viscoelastic relaxation modulus,

$$E(t) \sim t^{-.183} \tag{55}$$

Inasmuch as the relaxation modulus is predicted to obey a power law in time, Equations (14) and (34) are exact. Since $D(t) \sim t^{0.183}$, Equations (45) and (12) (with $U = Rt$) yield

$$2\Gamma_1 \sim t^{-0.172} \, U^{1.942} \tag{56}$$

Comparing this result with Equation (49), we see that if Γ_1 is constant, it provides the same fracture initiation criterion as Equation (49) with $J = J_c =$ constant, apart from an undefined constant coefficient. This coefficient is related to the (unknown) linear viscoelastic relaxation modulus; but it has no effect on the criterion. Namely, one could use any constant coefficient desired in Equation (56) if the same constant is used in deriving Γ_1 from experimental data as in applying the theory when predicting fracture initiation in motors.

3.0 SELECTION OF CANDIDATE TEST SPECIMEN

Existing test specimens and test procedures were screened to determine the best one for evaluating both adhesive and cohesive fracture energy. This evaluation effort was conducted in three steps. First, the test specimens were screened against a list of specific criteria. Second, they were evaluated morphologically in terms of the design constraints imposed by the three admissible modes of crack extension. Third, the experimental performances of the remaining candidates were compared.

The specimen survey and the results of the three-step evaluations are discussed below.

3.1 SPECIMEN SURVEY

The survey was designed to provide representatives of the various types of test specimens used in the industry, plus a few that were found in the literature for the evaluation of low modulus materials. There were fifteen candidate specimen designs gleaned from the survey. They are illustrated in Figures 8 through 22.

3.2 SCREENING AGAINST AFRPL CRITERIA

The preliminary screening of the candidate test specimen and procedures was based upon the AFRPL criteria specified in Section 1 and repeated in Table 1.

The screening criteria numbers 1 through 3 are satisfied by the principles of the J integral for all of the candidate specimens. By a rather liberal interpretation, criterion number 4 was also considered to be satisfied by the J integral concept for all specimens.

-41-
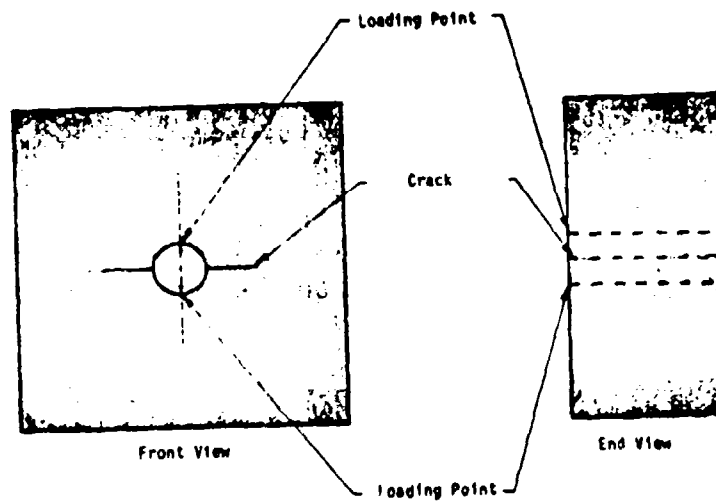
Figure 8. NOL Fracture Block
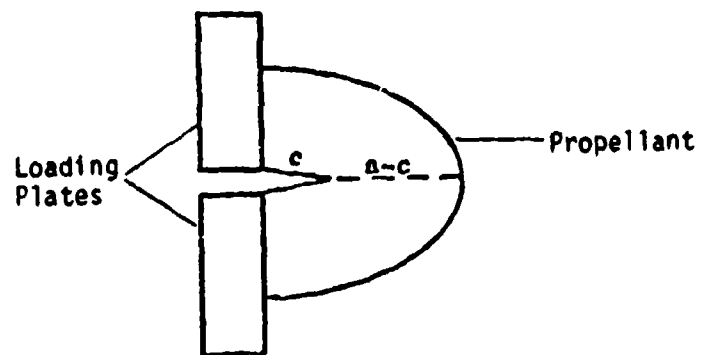
Figure 9. Anti-Plane Shear Specimen
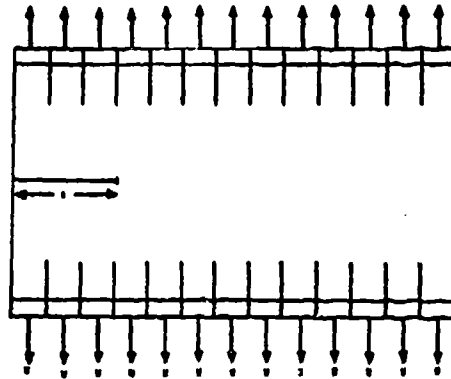
Figure 10. Plane Stress Test Specimen
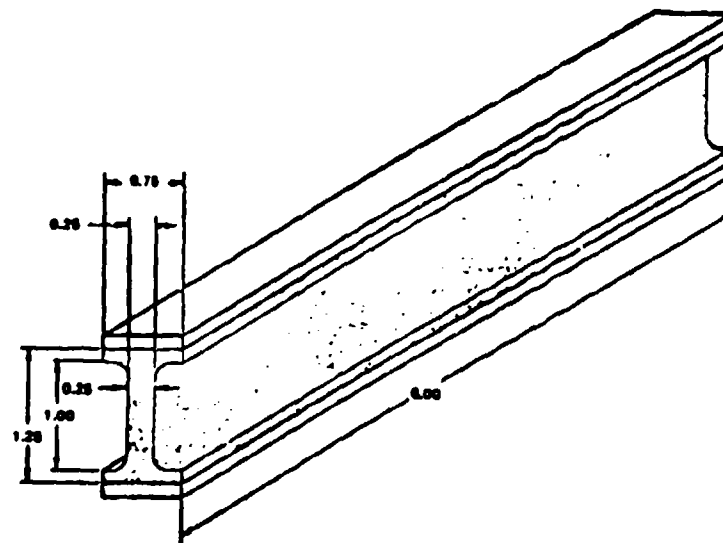
Figure 11. Strip-Biaxial Sheet Specimen
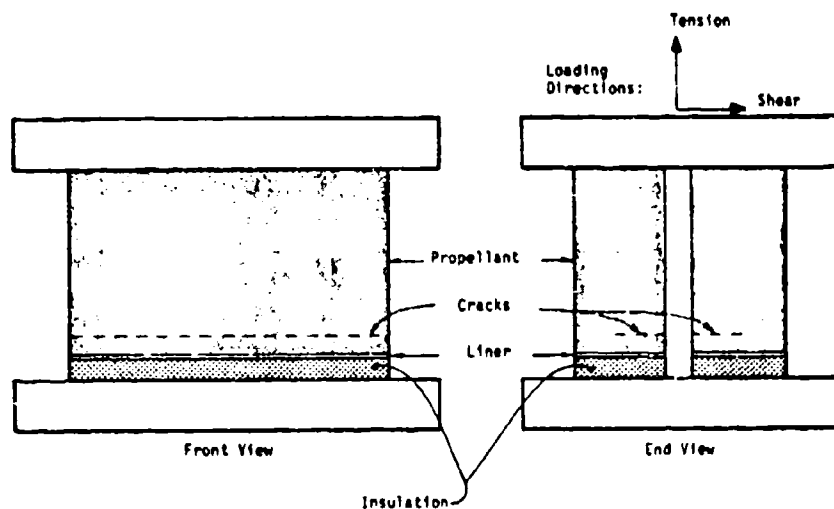
Figure 12. Twin Rail Specimen
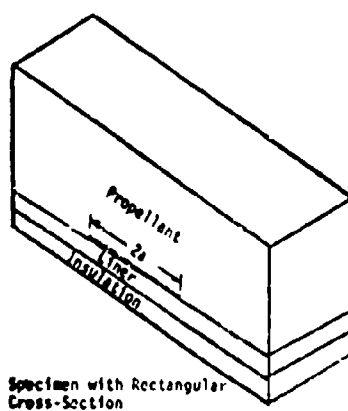
Figure 13. Scarf-Joint Specimen

ANB-3066 PROPELLANT

INITIAL FLAW

SD-851-2 LINER

V-45 INSULATION

STEEL DISK

118 Deg

PRESSURIZATION INLET
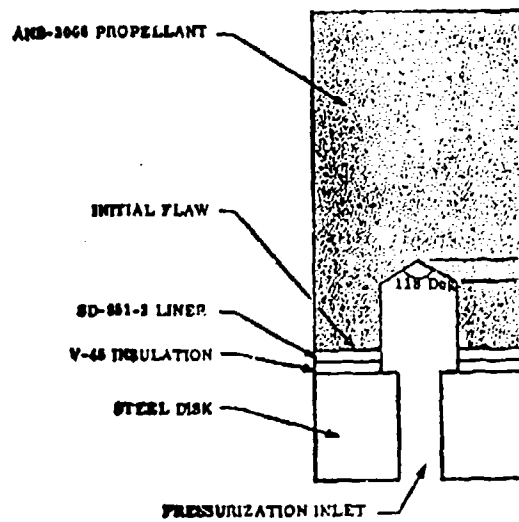
Figure 14. Cylindrical Peel Specimen

Crack

Propellant

Liner

Insulation
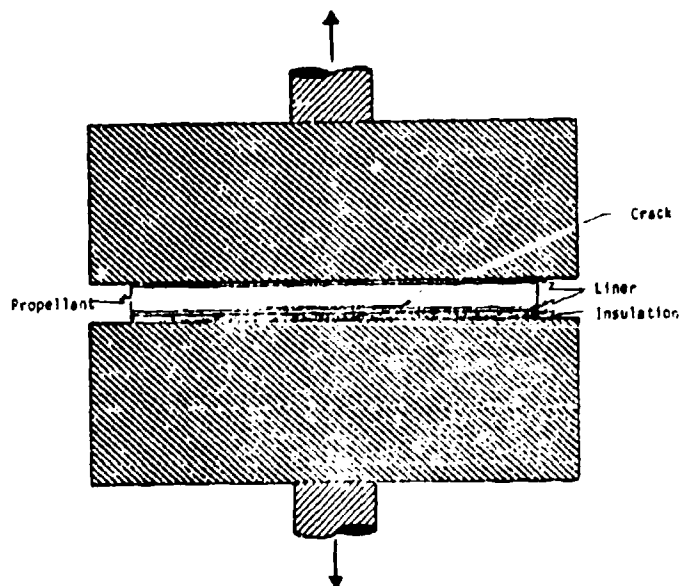
Figure 15. Poker Chip Specimen
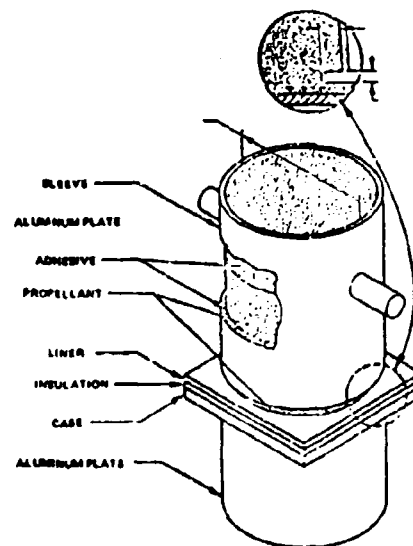
Figure 16. Tensile Sleeve Specimen
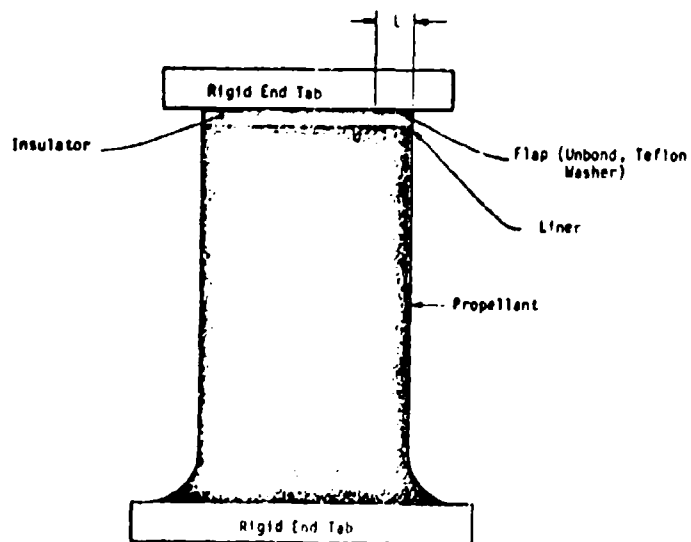
Figure 17.   Round-Flapped Case Bond Tensile Sample
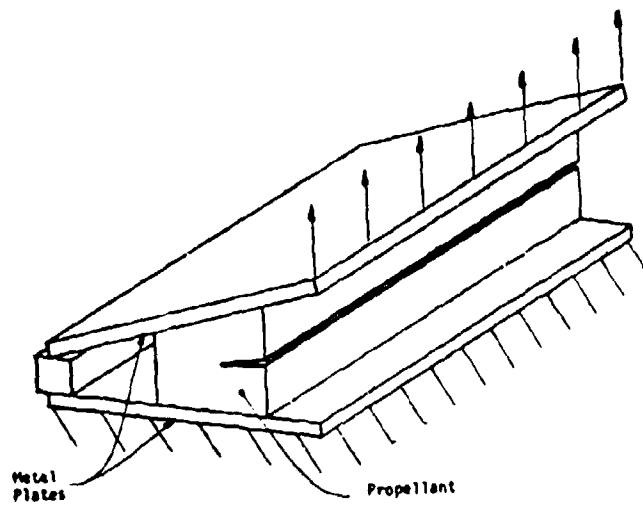
Figure 18. Plane Stress Fracture Specimen
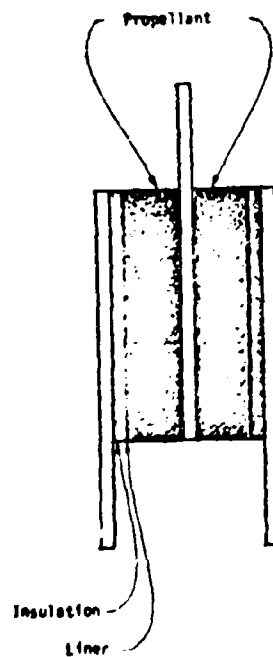
Figure 19. Double-Lap Shear Specimen
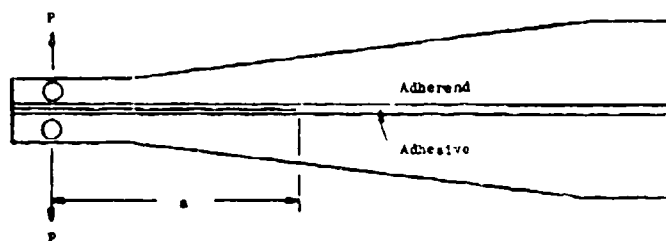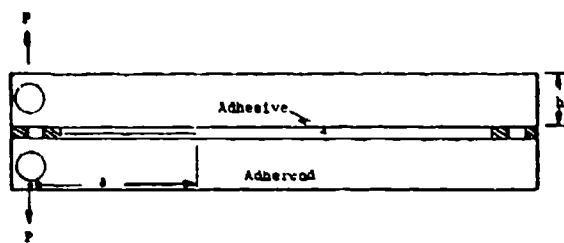
Figure 20. Adhesive Fracture Toughness Specimens
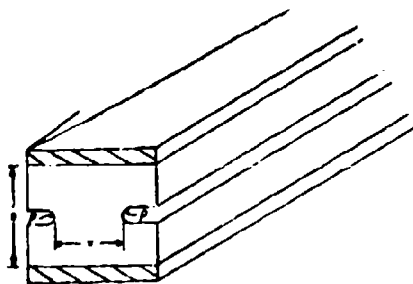
Figure 21. Double-Notch Test Specimen
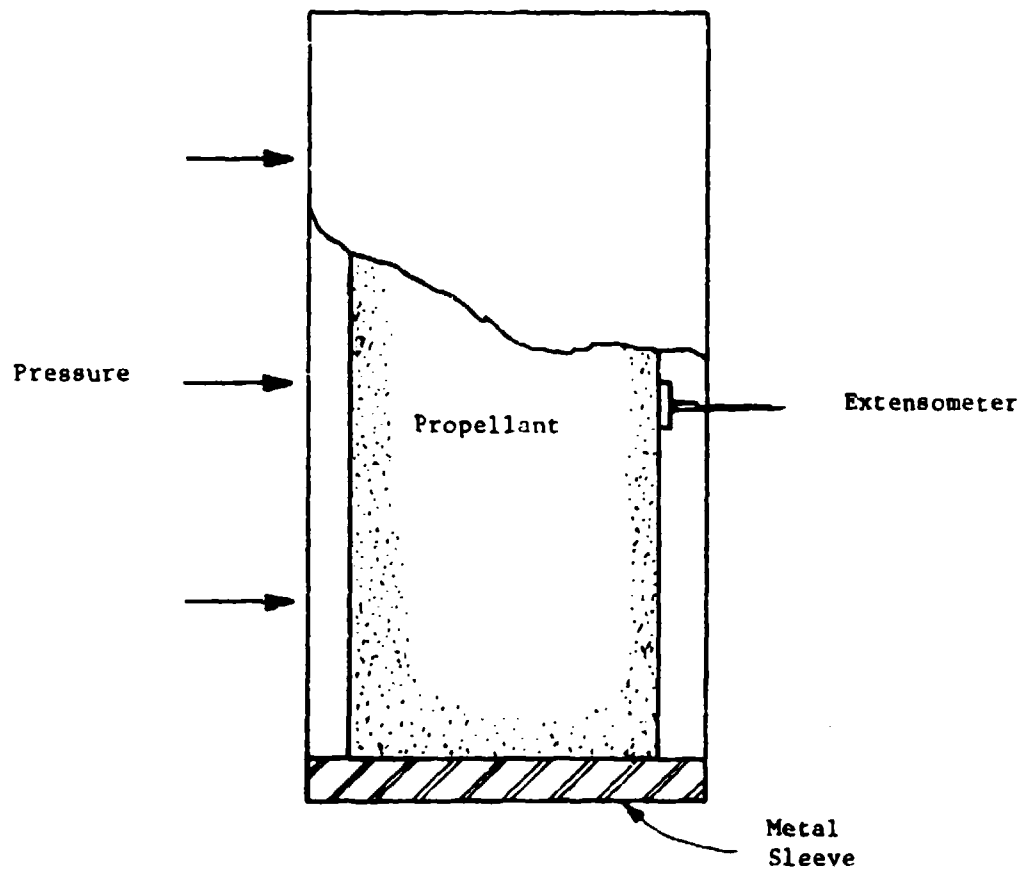
Figure 22.   End-Pressurized Cylinder

TABLE I

AFRPL SCREENING CRITERIA FOR
SELECTING CANDIDATE PROPELLANT
AND BOND TEST SPECIMENS

1.   Failure initiation from a controlled and analyzable singularity.

2.   Allow failure at the location of weakest strength in the vicinity
      of the bond.

3.   Provide engineering data that are independent of specimen geometry.

4.   Be amenable to analysis to evaluate stresses and strains directly
      related to motor analyses.

5.   Duplicate the various stress conditions that can exist in motors.

6.   Be amenable to preparation from dissected motors.

Criterion number 5 (duplicate stress conditions in motor) involves two types of thermal loading conditions (tensile alone and combined tension and shear) and one type of pressurization loading (combined shear and super-imposed pressure). A number of tests were considered to be unacceptable, for either of two reasons: (1) the motor loading condition could not be duplicated or (2) the testing could not be performed to separately identify the normal and shear components.

The following tests were considered to be unacceptable in meeting criterion number 5:

- Fracture block specimen (Figure 8)
- Anti-plane shear specimen (Figure 9)
- Cylindrical peel specimen (Figure 14)
- Tensile sleeve specimen (Figure 16)
- Round-flapped specimen (Figure 17) (After inclusion of a central crack this specimen is similar to a cylindrical peel specimen)
- Plane stress specimen (Figure 18)
- Double-lap shear specimen (Figure 19)
- Adhesive fracture toughness specimen (Figure 20)
- End-pressurized cylinder specimen (Figure 22)

Criterion number 6 (amenable to preparation from dissected motors) could be met by all except the following three specimens:

- Fracture block specimen (Figure 8)
- Anti-plane shear specimen (Figure 9)
- End-pressurized cylinder specimen (Figure 22)

The remaining specimens were subjected to further scrutiny.

3.3 DESIGN MORPHOLOGY

A simple screening tool was developed in terms of the specimen designs and the three admissible modes of crack extension (Figure 23). Combining these into a morphological assessment quickly reduces the candidate specimens to a very few.

As illustrated in Figure 24, there are only two types of specimen cross section, two crack placement methods, and three loading modes.

For the fracture tests, the torsional loading of circular cross section specimens produces a parallel shear mode of failure (see Figure 23). This mode of crack extension does not meet the requirement of duplicating bondline stress conditions that can exist in motors. That is, bondline fractures in motors consist of the opening mode or forward shear mode alone, or the opening mode plus the forward shear failure mode (see Figure 25). Thus, after eliminating torsional loading of circular cross section specimens, the optimum specimen was selected from those with rectangular cross sections.

The dimensional morphology of the rectangular specimens is illustrated in Figure 26. This category covers a broad range of specimen designs, including:

- Uniaxial specimen
- Strip-biaxial specimen
- Mid-size group
  - Scarf-joint specimen
  - Twin-rail specimen
  - Double-notch specimen
- Rectangular poker chip specimen

The laboratory testing and structural analyses of these specimens further reduced the number of candidates.
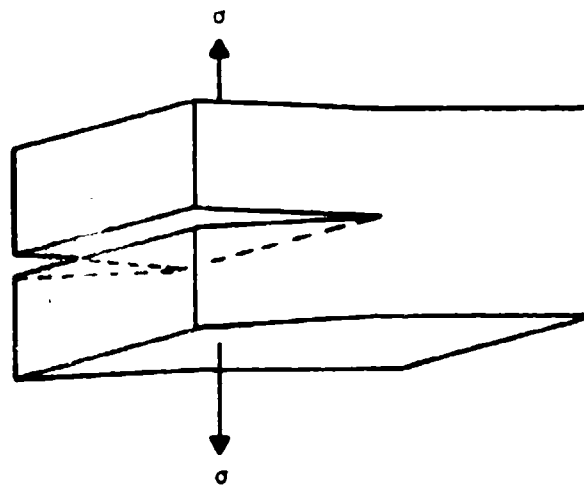
I. Opening Mode
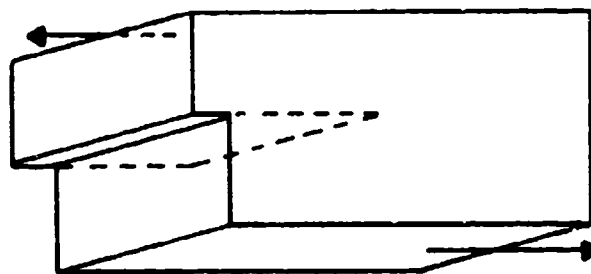
II. Forward Shear Mode
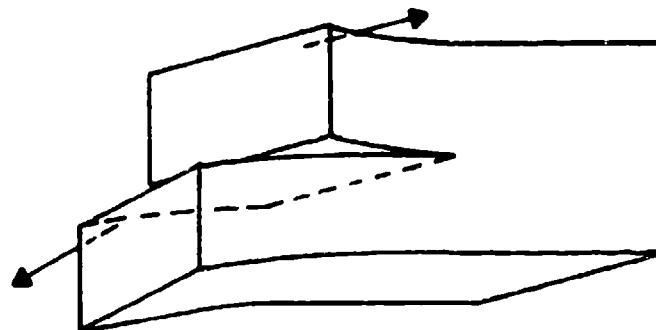
III. Parallel Shear Mode

Figure 23. Admissible Modes of Extension

-53-

SPECIMEN MORPHOLOGY

-General-

• Specimen cross-sections

•• Rectangular

•• Circular

• Crack placements

•• Central

•• Edge

• Specimens load applications

•• Normal

•• Shear

– Rectangular specimen
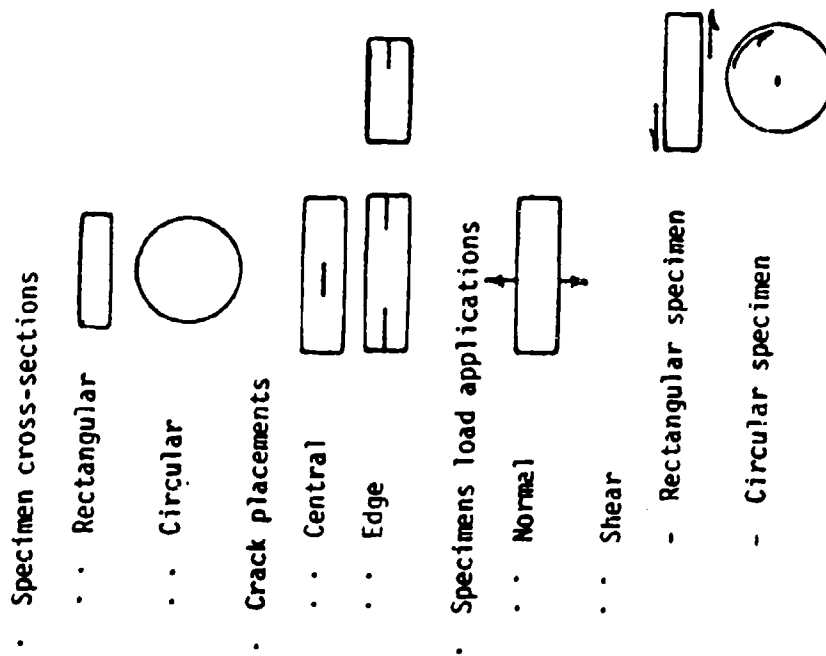
– Circular specimen

Figure 24. Specimen Morphology (General)

-54-

I. Opening Mode II. Forward III. Tear Mode
Shear Mode

Motor failures consist of:

. Opening mode alone

. Opening mode and forward shear mode

. Forward shear mode under compressive normal stress

Circular specimens can provide:

. Opening mode alone

. Opening mode and tear mode

Rectangular specimens can provide:

. Opening mode alone

. Opening mode and forward shear mode

. Opening mode under hydrostatic compressive stress

Figure 25. Modes of Crack Extension in Motors

-55-

Strip-Biaxial   Scarf-Joint   Rectangular Pokerchip
                 Twin Rail
                 Double Notch
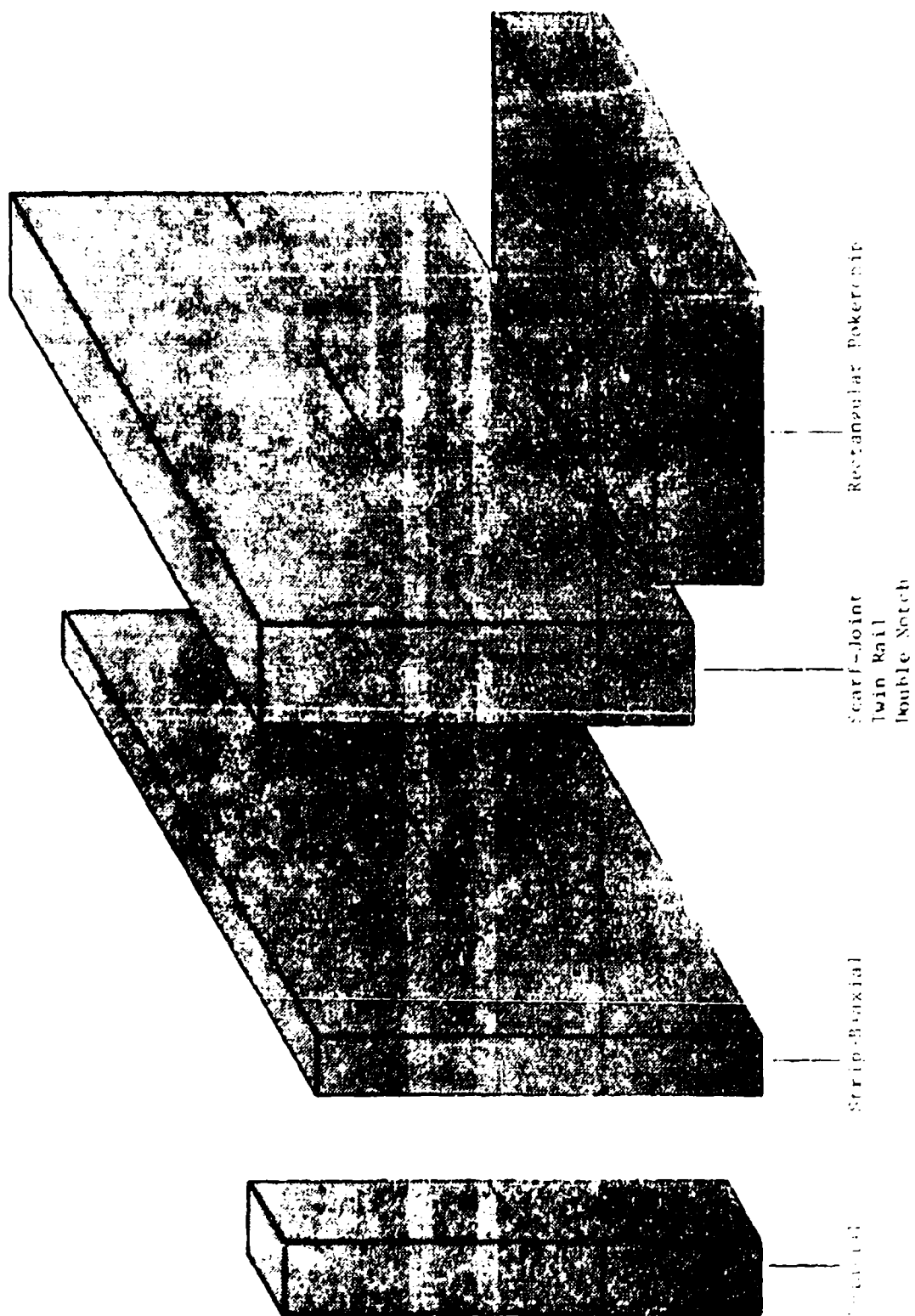
Figure 25. Dimensional Morphology of Rectangular Specimens

3.4 PRELIMINARY LABORATORY SCREENING TESTS

These preliminary tests were designed to find the best design among the rectangular specimens, then to determine its approximate dimensions. All of the tests described below were performed on samples of ANB-3066 propellant; no liner was used.

3.4.1 Specimen Behavior

The scarf-joint specimen with edge cracks and the double notch test specimen gave premature failures at the secondary bonds (adhesive bonds to the specimen end plates). This failure mechanism prevented further considerations of these designs.

The scarf-joint specimen with a central crack and the twin rail specimen both performed well with no secondary bond failures. However, to get a uniform fracture energy along the crack (e.g., a uniform propagation of the crack front) it was necessary to carefully machine the end surfaces of the propellant and, equally carefully, to align the end plates with respect to each other. This was more difficult to do in the twin rail specimens, which may rule out the design.

The strip biaxial specimen produced a behavior that seemingly contradicts elastic analyses of the design. That is, it had a tendency to premature failure due to local stress concentrations at the bonded surface. In a previous study at Aerojet [15] R. C. Sampson had made a Moire' Fringe strain analysis of this specimen (using DP-21 inert propellant). He found the biaxial strain to be greatest at 1.2 in. from the end of a seven-inch long specimen.

Figure 27 shows the variation of longitudinal strain at two different points in the specimen for extensions up to 0.12 in. The Moire' pattern for $\Delta = 0.16$ in., where the first visible failure occurred,
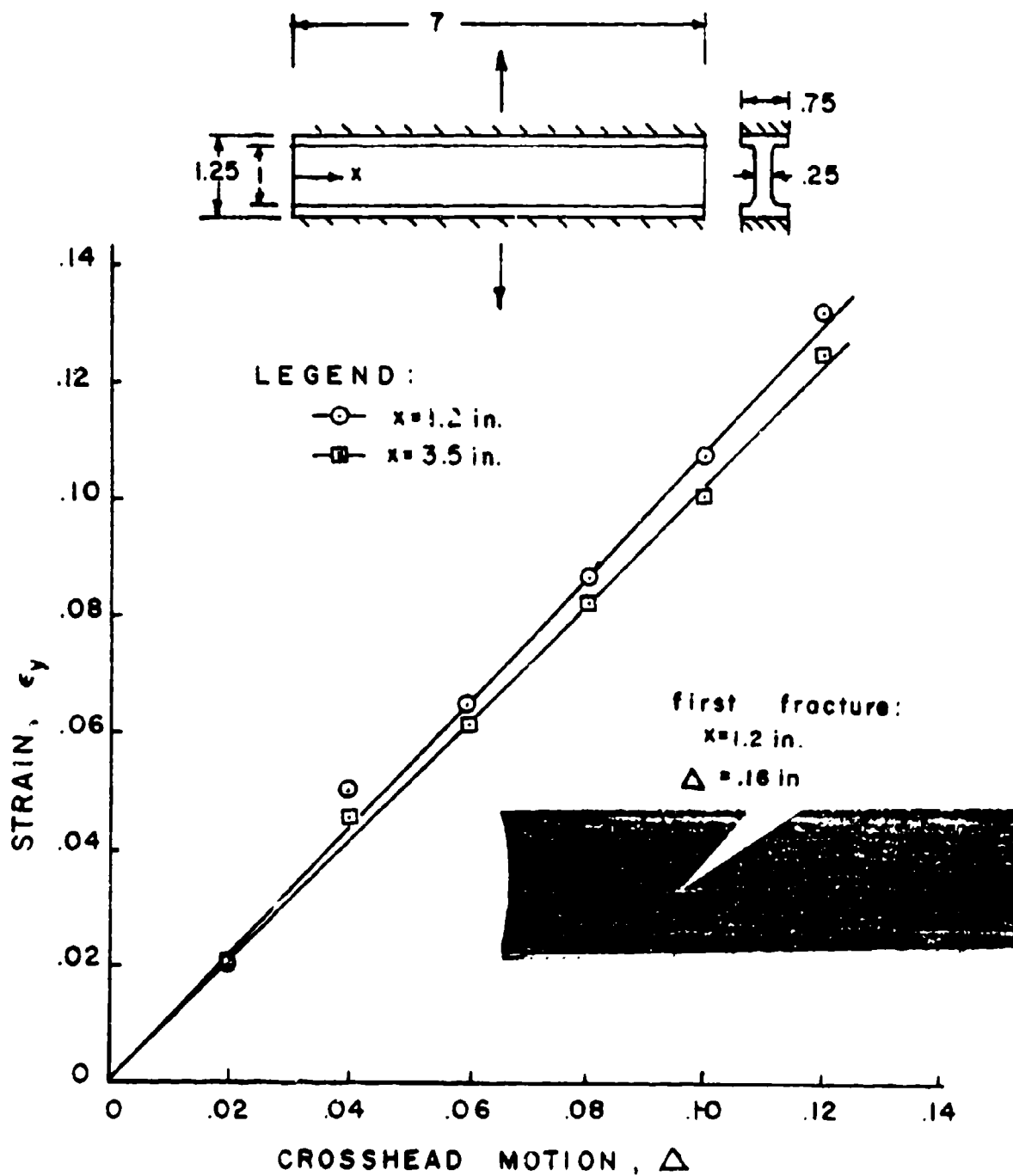
Figure 27. Strain in DP-21 Biaxial Strip

is superimposed on Figure 27. The crack is located about one-third the
distance from the end of the specimen to its midpoint. The reason for
the initial failure at this location is indicated by the measured strain
distribution for $\Delta = 0.12$ in. (Figure 28). Although some scatter of the
data appears, the strain maximum in the region around $x = 1.2$ in. is
clearly evident.

The elimination of these specimens leaves a scarf-joint
specimen with a central crack. Its dimensions could vary over a wide
range from the uniaxial to the poker chip designs.

3.4.2 Preliminary Assessment of Scarf-Joint Dimensions

A simple experimental plan was devised to determine
the performance of scarf-joint specimens of various dimensions. Evaluations
of these specimens and crack initiation tests were made in terms of the
following criteria:

- Specimen preparation
- Secondary bond failures
- The existence of a "toe" in the force-time trace
- The relative deformation at which crack initiation
  occurs
- The relative sharpness of the crack tip at initiation

It is sufficient at present to discuss only the elongation
at crack initiation. In this case the goal was to find a specimen design
whose critical elongation was sufficiently large to minimize the effect
of the "toe" in the force-time curve, but not so great that response non-
linearities should be produced prior to crack initiation. Elongation values
in the range of 5 to 7% were considered to be ideal.

The basic design for the specimen is sketched in Figure 29.
It has a height H, a length L, a depth B, and a central crack length 2a'.

-59-
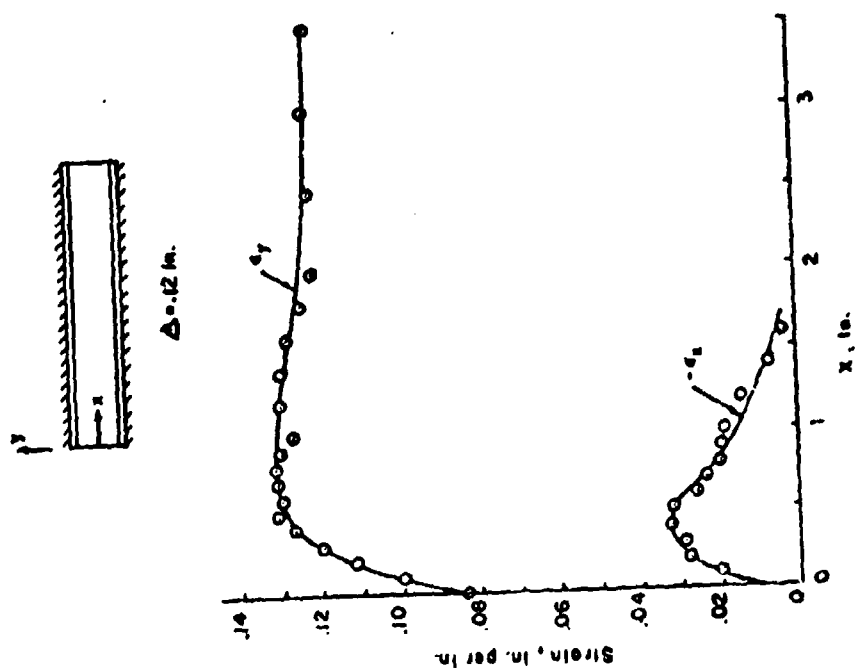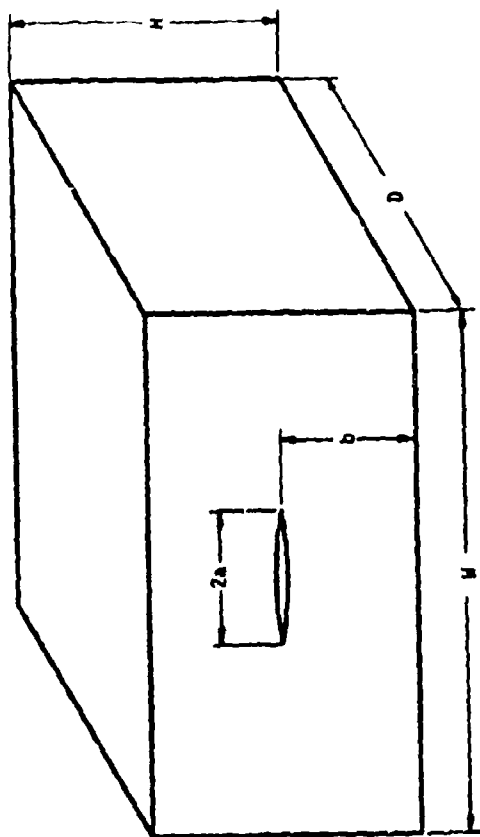
Figure 29. Dimensional Parameters in Scarf-Joint Test

FIGURE 28. STRAIN DISTRIBUTION IN QP-21 BIAXIAL STRIP

The placement of the crack was at a distance b from the lower end plate. The test plan considered the following range of specimen dimensions and crosshead rates, R:

$$2a': \quad 1.0 \text{ to } 2.0 \text{ inches}$$
$$b: \quad 0.1 \text{ to } 1.0 \text{ inches}$$
$$B: \quad 0.25 \text{ to } 1 \text{ inch}$$
$$H: \quad 1 \text{ to } 3 \text{ inches}$$
$$L: \quad 2 \text{ to } 4.5 \text{ inches}$$
$$R: \quad 0.02 \text{ to } 0.50 \text{ in./min}$$

All the testing was conducted at 77°F using ANB-3066 propellant without a liner.

Table 2 contains a tabulation of the specimen design and test parameters together with the critical elongation, $\Delta l/l$, test results. The most notable features of these test data are (a) the narrow range for the elongation data, 0.039 to 0.082 in./in. and (b) the acceptable elongation range was satisfied by most of the tests. Both the highest and the lowest values were obtained from the thin, B = 0.25 in., specimens. This probably reflects the sensitivity of the thin specimens to handling damage.

Specimens J-12 through J-32 form part of a Graeco-latin square test plan. A partial analysis of the data indicated that the elongation:

- increases as the crack size, $2a'$, and specimen height, H, decrease
- increases as specimen thickness, B, increases
- is independent of specimen length, L

The higher elongation levels within this test range were considered to be the most stable, hence the optimum specimen should lean to the smaller dimensions

TABLE 2. EXPERIMENTAL ASSESSMENTS OF DIMENSIONAL VARIATIONS IN THE SCARF-JOINT TEST USING PROPELLANT ALONE

- Tests Conducted at 77°F -

Test	H, in.	W, in.	D, in.	b, in.	2a/W	R, in./min	$\Delta l/l$, in./in.
J-1	2.0	3.004	0.479	1.0	0.7	0.02	0.054
J-2	2.0	3.020	0.495	1.0	0.5	0.02	0.053
J-3	2.0	3.033	0.491	1.0	0.3	0.02	0.053
J-4	2.0	3.028	0.497	1.0	0.7	0.10	0.048
J-5	2.0	2.947	0.500	1.0	0.5	0.10	0.059
J-6	2.0	2.968	0.520	1.0	0.3	0.10	0.060
J-7	2.0	3.048	0.435	1.0	0.7	0.50	0.050
J-8	2.0	2.922	0.528	1.0	0.5	0.50	0.055
J-9	2.0	2.945	0.460	1.0	0.3	0.50	0.055
J-10	2.0	3.0	1.0	0.5	0.4	0.10	0.060
J-11	2.0	3.0	1.0	0.5	0.6	0.10	0.071
J-12	3.0	4.5	0.5	0.1	0.4	0.10	0.065
J-13	3.022	4.5	0.48	0.1	0.4	0.10	0.058
J-14	3.033	4.483	0.438	0.1	0.6	0.10	0.044
J-15	3.0	4.5	0.5	0.1	0.6	0.10	0.044
J-16	2.0	2.0	0.25	0.1	0.4	0.10	0.055
J-17	2.0	2.0	0.25	0.1	0.6	0.10	0.039
J-18	3.0	3.0	0.25	0.2	0.4	0.10	0.044
J-19	2.982	2.8	0.241	0.2	0.6	0.10	0.060
J-20	2.0	4.5	1.0	0.2	0.4	0.10	0.068
J-21	2.0	4.5	1.0	0.2	0.6	0.10	0.064
J-22	1.0	1.968	0.514	0.2	0.4	0.10	0.070
J-23	1.011	2.038	0.414	0.2	0.6	0.10	0.068
J-24	2.019	3.008	0.422	0.5	0.4	0.10	0.069
J-25	2.0	3.018	0.496	0.5	0.6	0.10	0.048
J-26	2.0	3.047	0.472	0.5	0.6	0.10	0.047
J-27	1.0	4.466	0.267	0.5	0.4	0.10	0.082
J-28	1.0	4.466	0.260	0.5	0.4	0.10	0.073
J-29	0.963	0.484	0.264	0.5	0.6	0.10	0.074
J-30	0.964	4.488	0.263	0.5	0.6	0.10	0.071
J-31	1.0	4.5	0.30	0.5	0.6	0.10	0.060
J-32	2.988	1.953	1.01	0.5	0.6	0.10	0.056
J-33	1.0	3.0	1.0	0.5	0.8	0.10	0.058
J-34	2.992	1.991	0.971	0.5	0.4	0.02	0.058

for H and 2a', and to the larger ones for B. The value for L appears to
be at the user's discretion.

Following these rules, B was tentatively selected to be
1 in. This was done for the pragmatic reason that specimens of that thickness
have a better resistance to rough handling. The specimen height, H, according
to the available analyses, must be equal to, or greater than, 2B to give
optimum thermal behavior and independence from Poisson's ratio (Section 4).
It was expected that L could take on any dimension from 2 to 6 in. Considering
potential applications in tests on tactical-sized motors, a short specimen
is indicated. But, practical crack sizes suggest a long specimen. We have
arbitrarily (as allowed) chosen the intermediate value of 4 in. for L. Thus,
the tentatively selected standard test specimen had the dimensions:

$$L = 4 \text{ in.}, \quad H = 2 \text{ in.}, \quad B = 1 \text{ in.}$$

These dimensions were submitted for structural analyses and final selection
of the standard specimen dimensions (Section 4).

3.4.3 Experimental Determinations of Interaction Distances Between the Crack Tip and Specimen Boundaries

To help guide later studies of crack length, preliminary
measurements were made to determine the minimum acceptable dimension, d,
between the crack tip and nearest boundary of the test specimen.
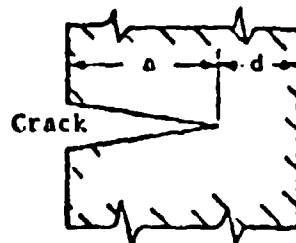
These observations were made using a rail specimen in an optical comparator. The end of the specimen, at the crack, looked like the sketch given here. The crack tip was observed at 10 and 20 diameters magnification as the crack progressed slowly towards the boundary on the right.

The distance d was taken to be that where the crack tip and the rear boundary noticeably interacted with each other (sharp indentations of the boundary and shear flows around the plane of the crack). The measured distances in three successful tests were:

0.11 in.
0.16 in.
0.11 in.

Considering the variations between propellants, and the effects of test temperature and path dependence, a value for d of at least 0.20 in. will be used.

4.0   STRESS AND FRACTURE ANALYSIS OF SCARF-JOINT SPECIMENS

4.1.   INTRODUCTION

Selection of test specimen geomet_y was guided by finite element analysis of cracked and uncracked specimens. In addition, even though they are for linear elastic behavior, these analyses provide insight into the stress distribution, estimates of the J integral, and show whether or not the stresses near crack tips have the desirable feature of being only weak functions of the thickness coordinate. Also, they enable one to determine how well plane stress analysis predicts energy release rates in three dimensional (moderately thick) samples.

In all cases, the analyses are for rectangular samples of length L, height H, and thickness B, as shown in Figure 30. They were made by Professor W. E. Haisler, Jr., of Texas A&M University using TEXGAP (Referer   16) for most two-dimensional problems and AGGIE I (Reference 17) for three-dimensional problems.

4.2   TWO-DIMENSIONAL ANALYSIS OF UNCRACKED SPECIMENS FOR THICKNESS EFFECTS

The first analytical task in the program consisted of using TEXGAP to stress analyze uncracked samples in order to guide the selection of the height-to-thickness ratio. Inasmuch as stresses due to a given overall strain or uniform temperature change are independent of absolute specimen size, the thickness B was arbitrarily taken as 1 inch, and the height H was varied, as noted in Figure 31.

In analyzing this geometry, it is necessary to keep in mind that the specimen is to be used to study experimentally fracture initiating from a crack which is in or close to a linear that is bonded between the propellant and grip. The thickness of the liner will be small compared to sample thickness B, and therefore it is not considered in the present section which is concerned with global sample characteristics.

-65-
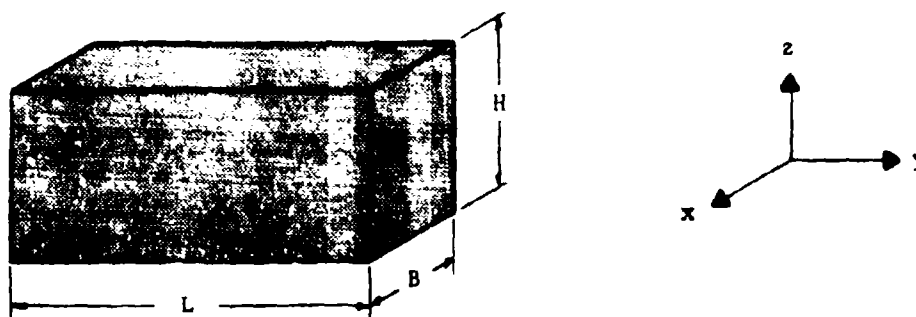
Figure 30. Scarf-Joint Specimen
Geometry and Coordinate Notation
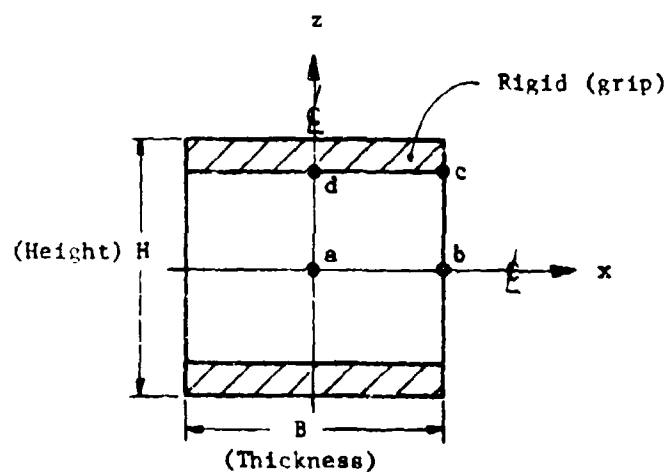
Conditions:

Plane Strain
E = Young's modulus
ν = 0.5
B = 1.0 inch
H = 0.5, 1.0, 2.0, 3.0 inches

Loading: $\bar{\epsilon}_z$ = Axial displacement (direction) divided
            by H applied to rigid grip or

            αΔT Thermal strain

Figure 31. Parameters Used in Two-Dimensional
Analysis of Uncracked Samples

From the standpoint of fracture behavior, it is desirable to use a
relatively thick sample to minimize global strains and crack tip blunting.
(A thin sample may undergo a large amount of strain prior to significant
crack growth, and therefore will not correctly produce mechanical behavior
associated with a case-bonded grain which is under three-dimensional geometric
constraint conditions.) On the other hand, it is desirable to use specimens
which are thin enough that residual thermal stresses are negligible and for
which the near-grip stresses are essentially independent of H. Also,
considering the variability of Poisson's ratio, ν, of propellant, it is
desirable to minimize the sensitivity of stresses to ν by using relatively
thin samples.

Figures 32-38 exhibit stress distributions for four different
height-to-thickness ratios. As plane strain is assumed (corresponding to
the assumption L>>H and L>>B)the limiting value of σ_{zz} for very high samples
under average axial strain $\bar{\epsilon}_z$ is

$$\sigma_{zz} = \frac{E}{1-\nu^2} \bar{\epsilon}_z \tag{57}$$

and thus with $\nu = 0.5$,

$$\sigma_{zz} / E\bar{\epsilon}_z = 4/3 \tag{58}$$

This value of 4/3 is essentially reached near the central region
of the sample when H = 3, as may be seen by referring to Figures 32, 35 and 36;
indeed, there is little difference between the H = 2 and H = 3 cases.

The specimen with a height of H = 2 has a relatively uniform
normal stress along the horizontal center plane (Figure 32) and the grip
(Figure 33) except near the edges. For a shorter specimen (H $\leq$ 1 in.) the
stress is nonuniform, according to Figure 32. Also, there is no need to
use samples taller than H = 2 as the uniformity for H = 3 in. is about the
same as H = 2 in.
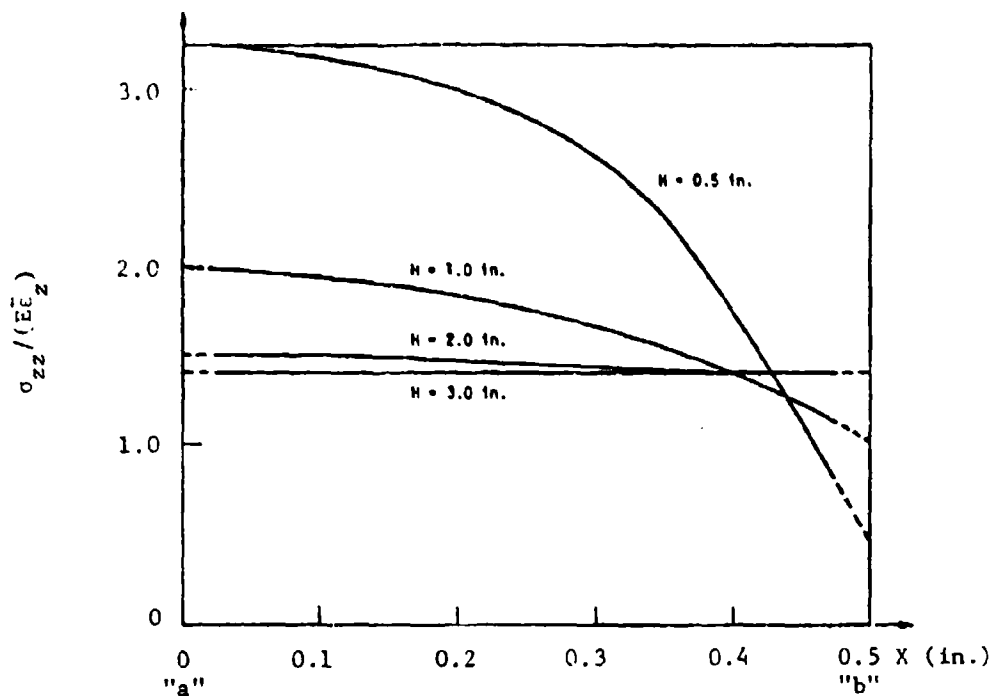
Figure 32. Axial Stress σ_{zz} Along Line a-b
(g) for $\overline{\epsilon}_z$ Axial Extension
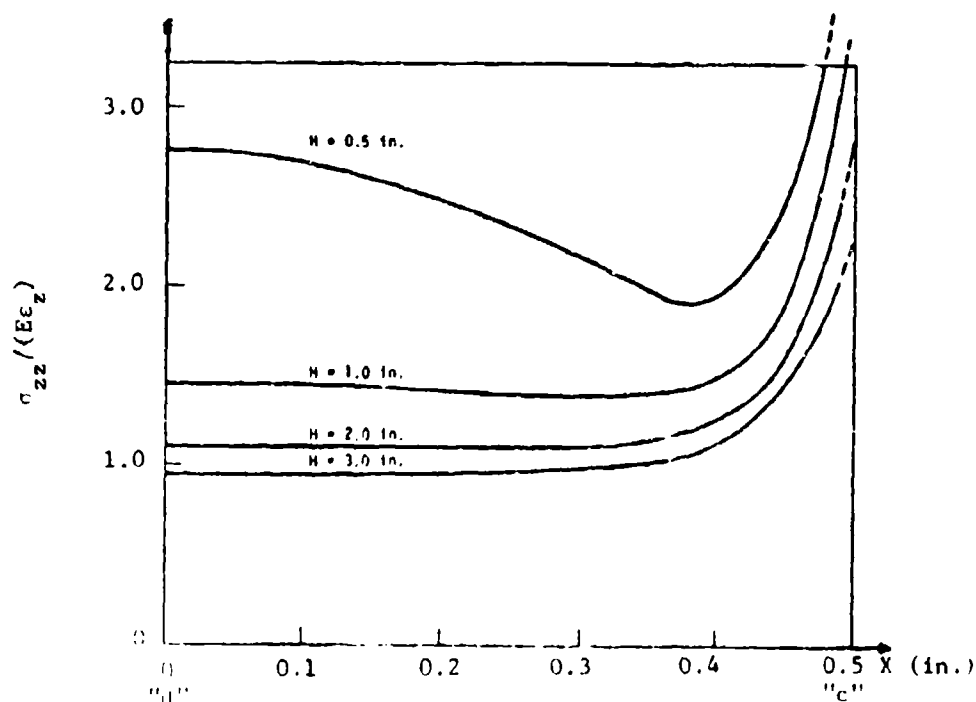
Figure 33. Axial Stress σ_{zz} Along Line d-c
(Grip Edge) for $\overline{\epsilon}_z$ Axial Extension
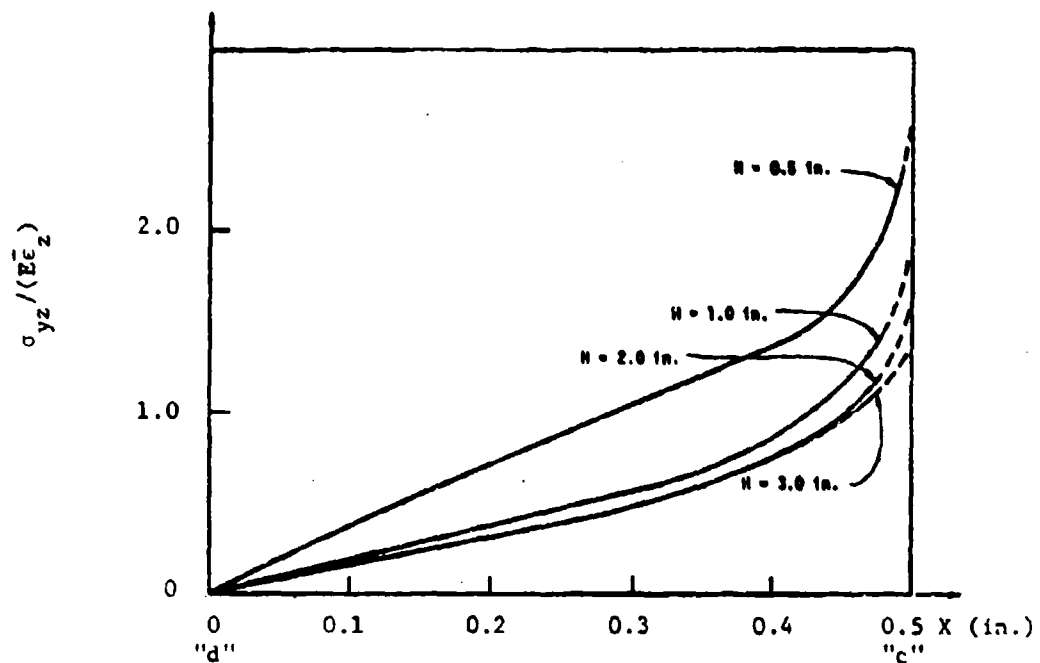
Figure 34. Shear Stress σ_{xz} Along Line d-c (Grip Edge) for $\bar{\epsilon}_z$ Axial Extension
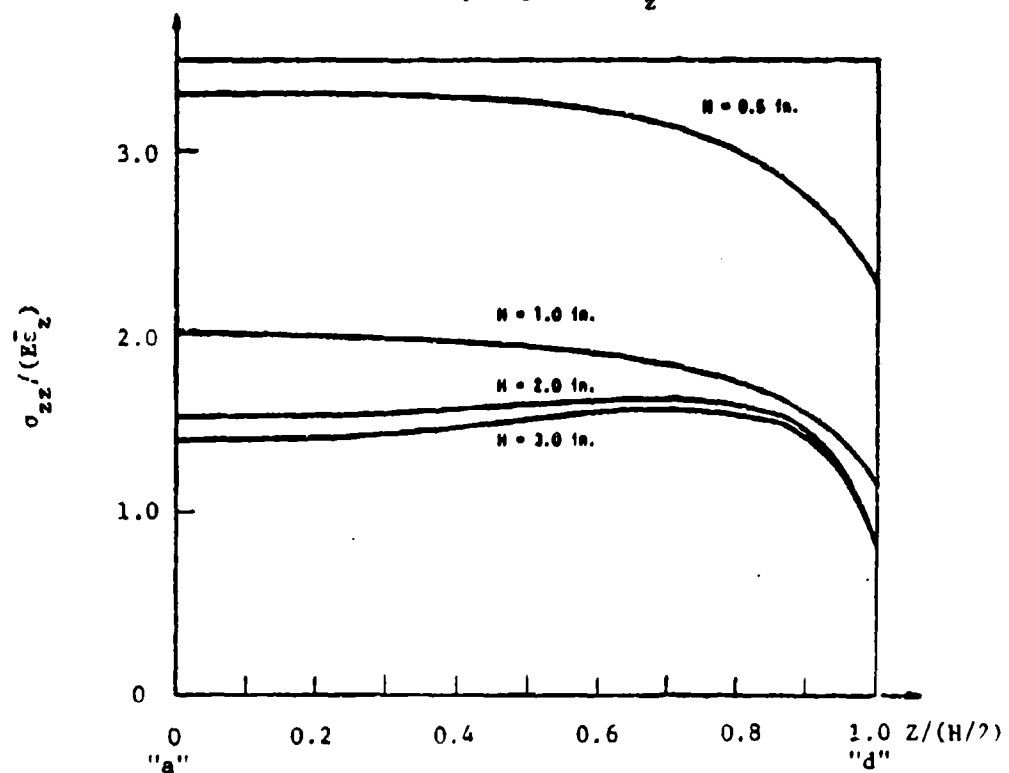
Figure 35. Axial Stress σ_{zz} Along (g) (X=0) a-d for $\bar{\epsilon}_z$ Axial Extension

-69-
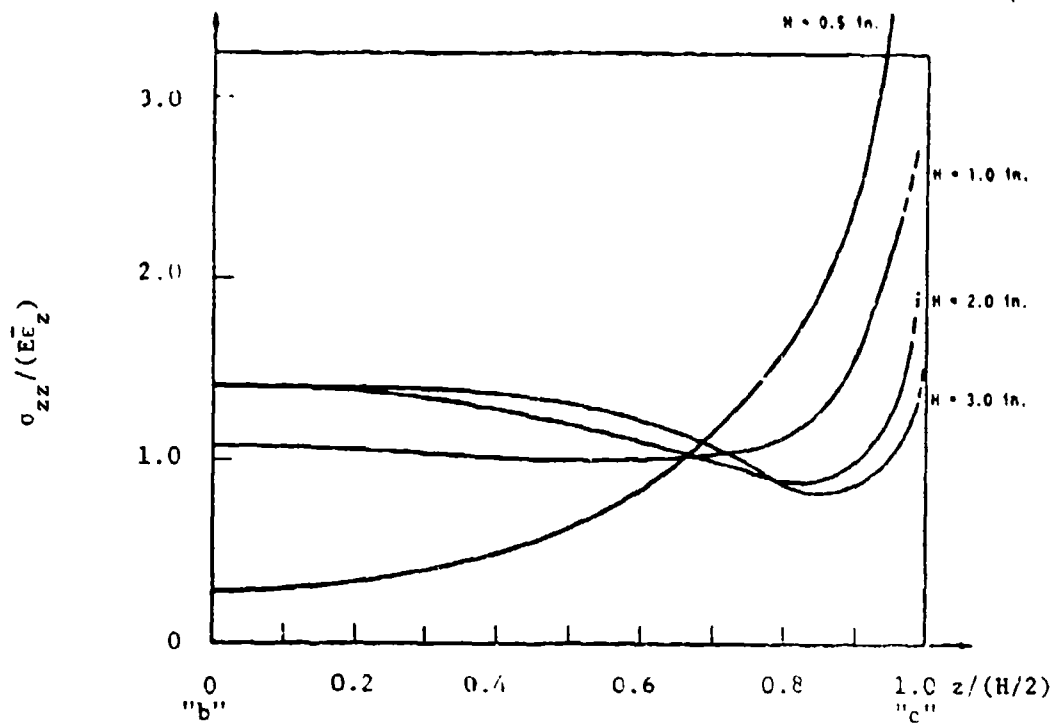
Figure 36. Axial Stress σ_{zz} Along Edge ($x=z/2$)
b-c for $\bar{\epsilon}_z$ Axial Extension
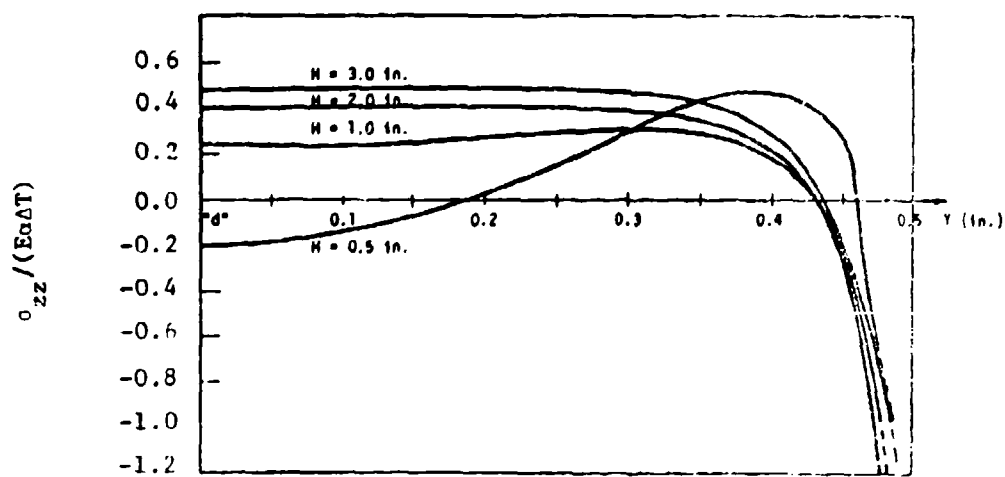
Figure 37. Axial Stress σ_{zz} Along Line d-c
(Grip Edge) for ΔT Thermal Strain

Figure 38.   Shear Stress σ_{xz} Along Line d-c

(Grip Edge) for $\alpha\Delta T$ Thermal Strain
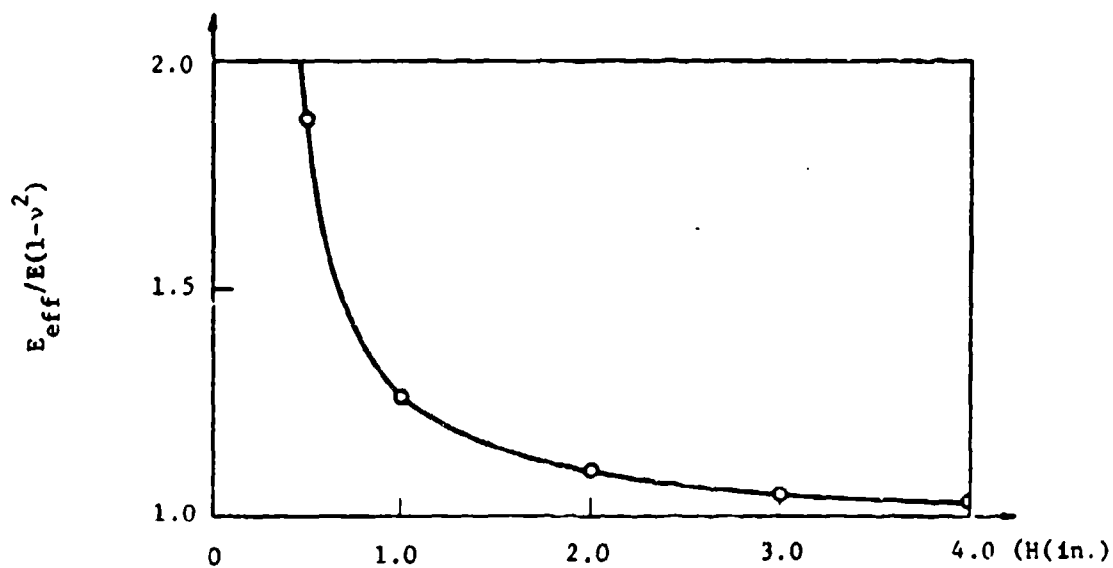
Figure 39.   Effective Modulus Ratio for Specimen Subjected to
Axial Extension Along Line a-b for $\nu = 1/2$

The shear stresses in Figure 34 for H = 2 in. and H = 3 in. are essentially the same; indeed, the distribution shown is essentially that for H = ∞; thus, the sample with H = 2 does not suffer from excessive shear stresses because of its small height (compared, say, to a standard biaxial strip sample).

Residual thermal stresses are very small for all cases even for relatively large temperature changes. Consider for example, $\Delta T = 200°F$ and $\alpha = 5 \times 10^{-5}/°F$, so that $\alpha \Delta T = 10^{-2}$. According to Figures 37 and 38, the stresses σ_{zz} and σ_{yz} are on the order of $E\alpha\Delta T$ or smaller, except very close to the corners; thus, only if specimen failure strains were on the order of 10^{-2} would the residual stress or strain have a significant influence on failure behavior. Furthermore, Figure 37 shows that triaxial constraint effects are not significant for $H \geq 1$; when H = 0.5 the strong minimum in the stress distribution at x = 0 is indicative of a thickness constraint.

Another indication of thickness constraint is the rise in effective modulus, E_{eff}, with decreasing values of height, as shown in Figure 39. By definition,

$$E_{eff} \equiv \bar{\sigma}_{zz} / \bar{\epsilon}_z \qquad (59)$$

where

$$\bar{\sigma}_{zz} = \frac{1}{A} \sum_i \sigma_i A_i \qquad (60)$$

is the average axial stress, which is calculated by summing the forces $\sigma_i A_i$ acting on each element, and $A = \sum A_i$; stresses on the plane z = 0 were used in order to minimize numerical error inherent in the calculation of stress, which would be greatest on z = H/2. It is observed from Figure 39 that E_{eff} approaches the correct limit $E/(1 - \nu^2)$ with increasing values of H.

-72-

The above study indicates the value H/B = 2 represents a good compromise for sample height. That this choice is acceptable with respect to dependence on Poisson's ratio is implied by the results in Table 3. Namely, the stresses are relatively insensitive to Poisson's ratio; very significant dependence on Poisson's ratio results for somewhat shorter samples. It should be noted that if the stresses had been divided by the plane-strain modulus $E/(1 - v^2)$ instead of E, even less dependence than shown in Table 3 would have resulted.

On the basis of the foregoing analysis, we may conclude a height-to-thickness ratio of two is large enough that:

- Thermal stresses due to heating and
  cooling are insignificant.

- Stresses due to mechanical loading are
  relatively insensitive to Poisson's ratio
  for values close to one-half.

- The variation of shear and normal stresses
  through the thickness is essentially inde-
  pendent of the height-to-thickness ratio.

4.3 TWO-AND THREE-DIMENSIONAL STRESS ANALYSIS OF CRACKED SPECIMENS

Stress analysis of the specimen geometry in Figure 30 with edge and center cracks is discussed in this section. Figures 40-42 show the finite element models employed. In all cases the total sample height is taken as H = 2 inches and the thickness as B = 1 inch, in view of the results in the preceding section.

For horizontally centered cracks, the left edge (y = 0) in Figures 40 and 41 is a plane of symmetry; i.e., the surface shear stress and

TABLE 3

EFFECT OF POISSON'S RATIO. UNIFORM AXIAL EXTENSION $\bar{\epsilon}_z$
APPLIED. H = 2.0 INCH

At x = 0.25, Z = 0

ν	$\sigma_{xx}/(E\bar{\epsilon}_z)$	$\sigma_{zz}/(E\bar{\epsilon}_z)$	$\sigma_{xx}/(E\bar{\epsilon}_z)$
0.5	-0.0285	1.49	-0.00025
0.495	-0.0276	1.47	-0.00024
0.49	-0.0267	1.46	-0.00024
0.48	-0.0250	1.43	-0.00022
0.45	-0.0207	1.35	-0.00019

At x = 0.04 and 0.25, Z = 1.0

ν	x=0.04	x=0.25	
	$\sigma_{zz}/(E\bar{\epsilon}_z)$	$\sigma_{zz}/(E\bar{\epsilon}_z)$	$\sigma_{xz}/(E\bar{\epsilon}_z)$
0.5	1.30	1.29	0.375
0.495	1.29	1.27	0.365
0.49	1.28	1.26	0.355
0.48	1.25	1.24	0.336
0.45	1.19	1.19	0.288
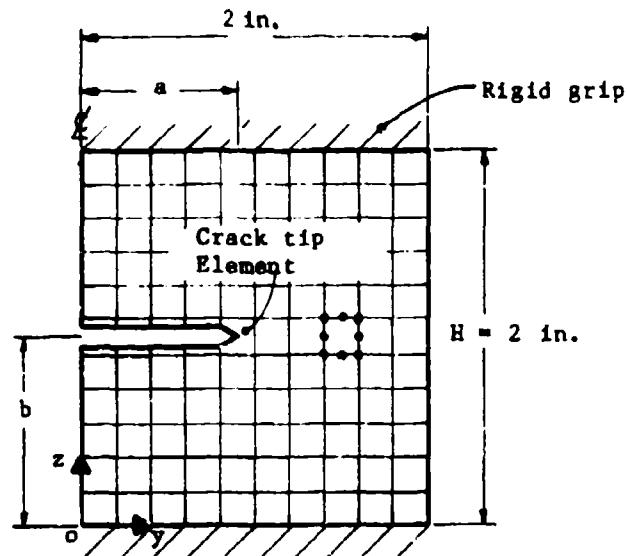
Figure 40. Typical Finite Element Representation
Used For Plane Stress/Strain Analysis With TEXGAP
(157 8-node quad elements plus crack-tip element)
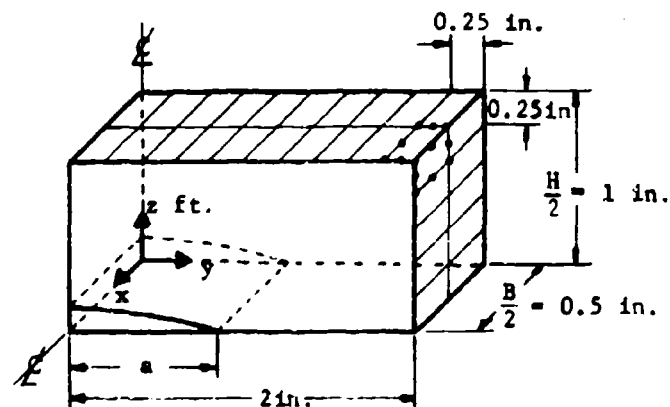
Figure 41. Typical Finite Element Representation
Used For Three-Dimensional Analysis With AGGIE I
(64 20-node elements above crack plane; quadratic
displacement function used along element edges
and cubic function used within element)
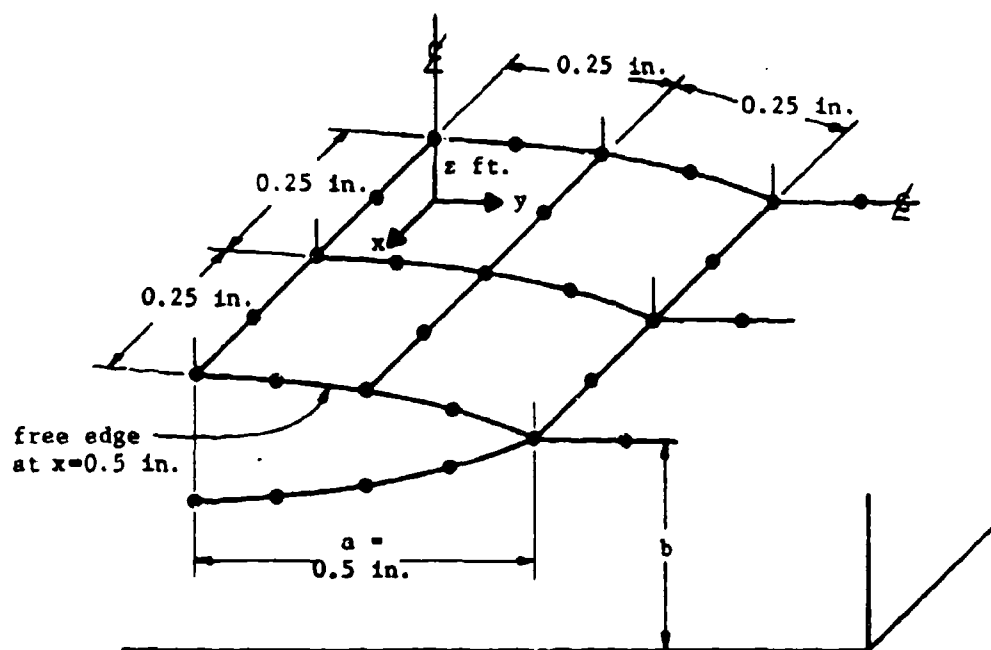
Figure 42. Nodal Points Used in Three-Dimensional
Representation of a Crack in AGGIE I

-76-

horizontal displacement vanish on y = 0 and the full sample length is L = 4 inches. For edge cracks, the left edge is a free surface; i.e., the surface shear and normal stresses vanish and the total sample length is L = 2 inches.

Two different vertical locations for the crack are considered: a centered crack, b = H/2 = 1 inch, and a near-grip crack, b = H/10 = 0.2 inch. In the latter case, the three-dimensional model (Figure 41) employs four rows of elements above the crack plane (as shown) and two rows below this plane.

Loading is imposed through specified upward vertical and rightward horizontal grip displacements, with the bottom grip fixed. The amount of displacement is normalized by specimen height, so that the extension or average tensile strain is one input,

$$\bar{\epsilon}_z \equiv \text{vertical displacement}/H$$

and the shear or average shearing strain is a second input,

$$\bar{\gamma}_{yz} \equiv \text{horizontal displacement}/H$$

These are applied separately, as the stress and displacement solutions for combined inputs can be readily obtained by addition of the individual results. In all cases the Poisson's ratio $\nu = 1/2$.

As a final matter before presenting results, it is to be noted that the symbol "a" represents the full crack length for an edge crack and one-half the length of a central crack. In the section on J integral theory, a' was used to denote a half-crack length, but for notational convenience the prime is now omitted.

Representative results from the stress analyses of two-dimensional problems are shown in Figures 43-49; for comparison purposes, some stress distributions in specimens without cracks are drawn. In all cases the stresses are divided by $E\bar{\epsilon}_z$ or $E\bar{\gamma}_{yz}$; since linear elasticity theory is used and the grips are rigid, these normalized stresses are, of course, independent of the input, $\bar{\epsilon}_z$ or $\bar{\gamma}_{yz}$, and the modulus, E.

It is to be observed that the stress distributions for plane strain and plane stress in Figure 43 are qualitatively the same; the amplitude difference is due to the difference in constraint and the fact that axial deformation, rather than load, is the same for both cases. The remaining plots of stresses are for plane strain, as it is believed to be a more appropriate state of strain for predicting shapes of the stress distributions associated with cracks adjacent to a grip. For comparison, however, some stress distributions in samples with vertically centered cracks are drawn.

In the next section many results directly applicable to fracture analysis are given for plane stress, plane strain, and three-dimensional problems. First, however, it is of interest to refer to Figure 50, which is a plot of the normalized contraction of the free surface, $x = B/2 = 0.5$ inches; along the plane of the crack, $z' = 0$ (Figure 41). This normalized contraction is $-U_x/E\bar{\epsilon}_z$, where U_x is the displacement in the x-direction. Figure 50 shows the characteristic dimple just ahead of the crack tip (which is easily seen on samples of rubber at high elongations). Also, the formation of lips (local thickening of the sample near the crack surfaces) is predicted, and is represented by the small positive and negative values of contraction for $y < a$. Notice further that the contraction, a short distance ahead of the crack tip, is essentially the same as without a crack. These results provide some indication of how complex the three-dimensional problem is and also lend some support to the validity of the analysis.
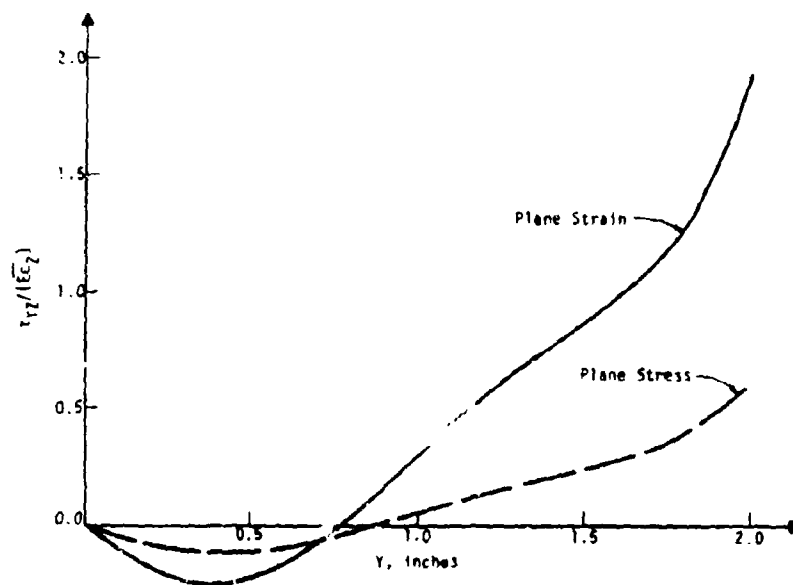
Figure 43. Distribution of Normalized Shear Stress, at $Z = 2$ in. (Top grip edge) $2a = 1.0$ in., $b = 1.0$ in., $\overline{\epsilon}_z$ Applied, Central Crack
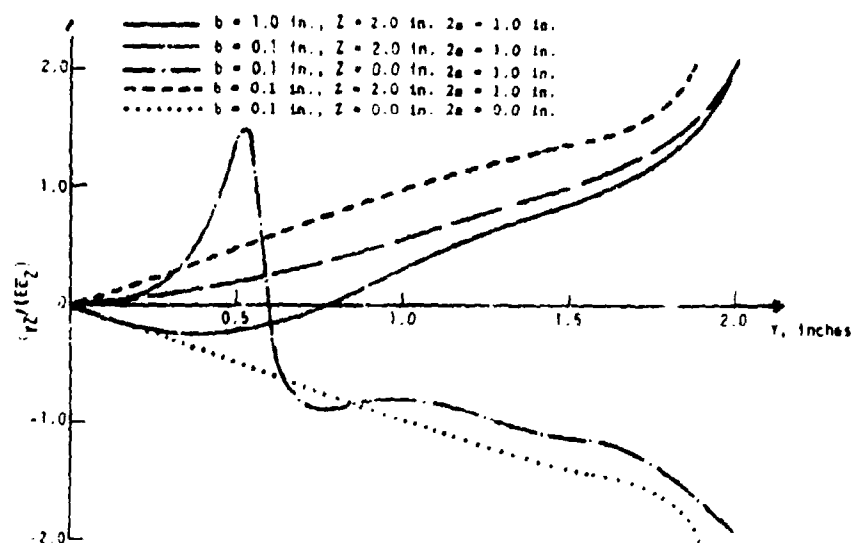
Figure 44. Distribution of Normalized Shear Stress $2a = 1.0$ in., Plane Strain, $\overline{\epsilon}_z$ Applied, Central Crack
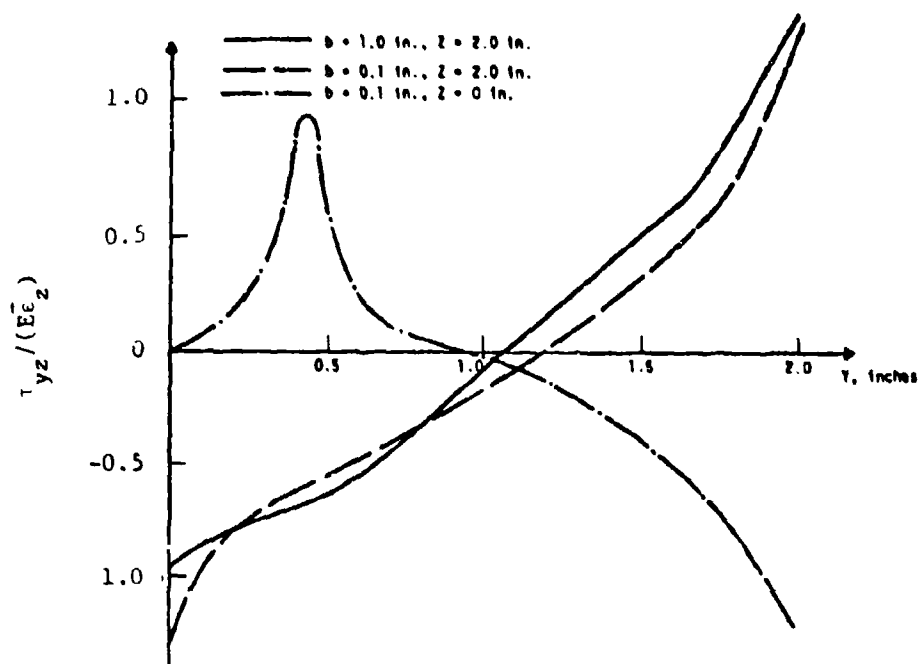
Figure 45. Distribution of Normalized Shear Stress at
a = 0.5 in., Plane Strain, $\bar{\epsilon}_z$ Applied
(Edge Crack)
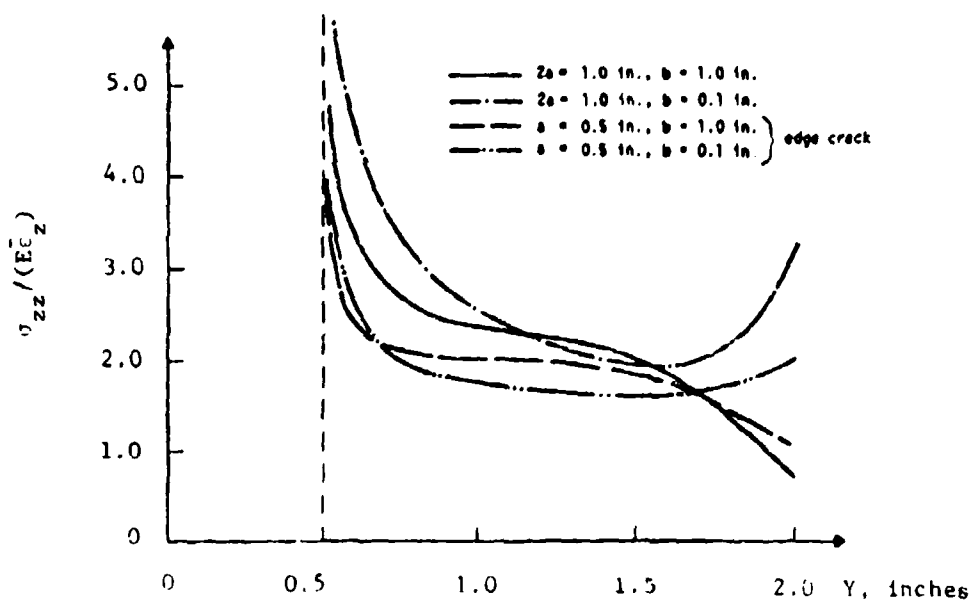
Figure 46. Distribution of Normalized Axial Stress at
z = b, (Along Crack Plane), Plane Strain,
$\bar{\epsilon}_z$ Applied
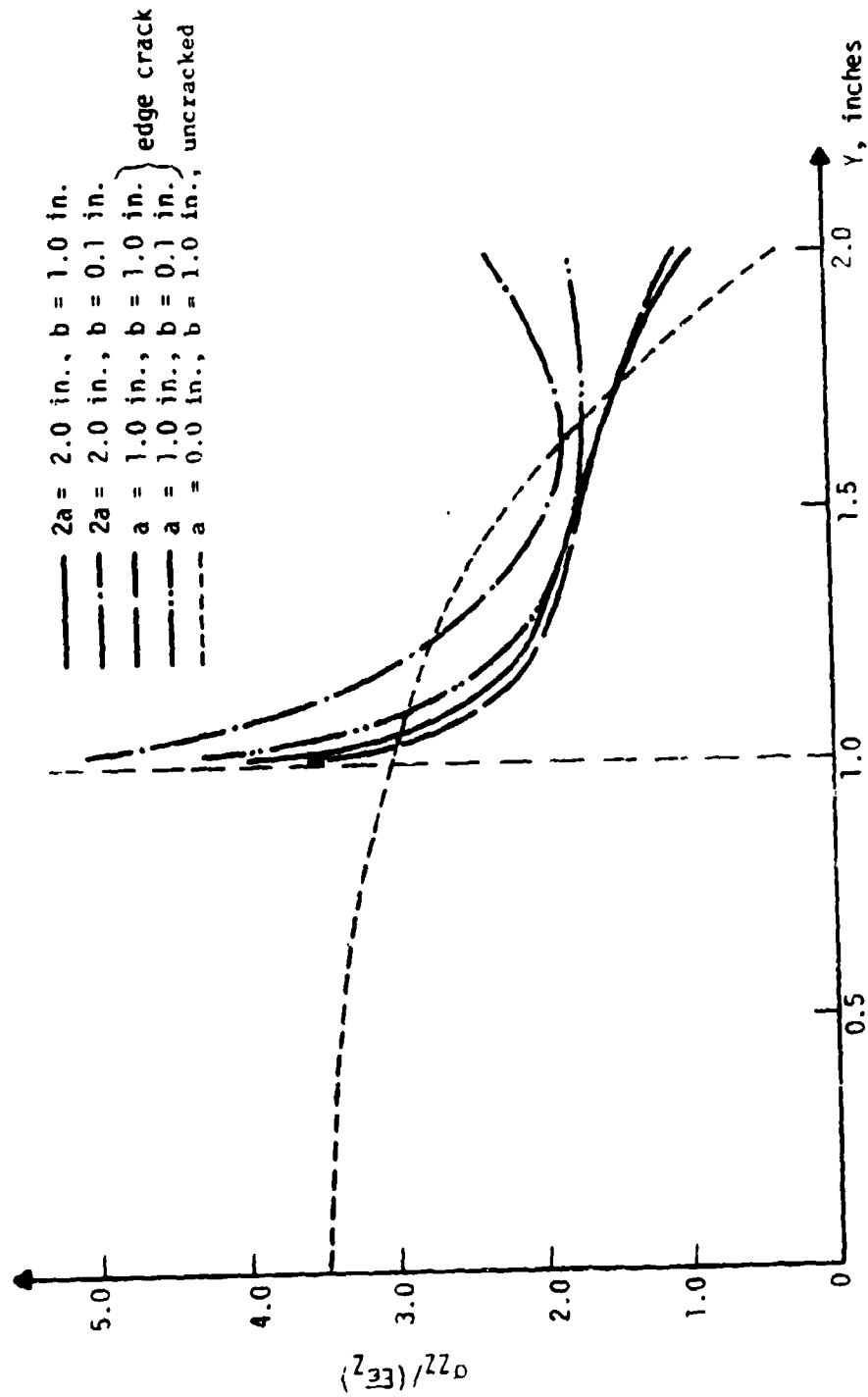
Figure 47. Distribution of Normalized Axial Stress at
Z = b (Along Crack Tip Front), $\bar{\epsilon}_Z$ Applied
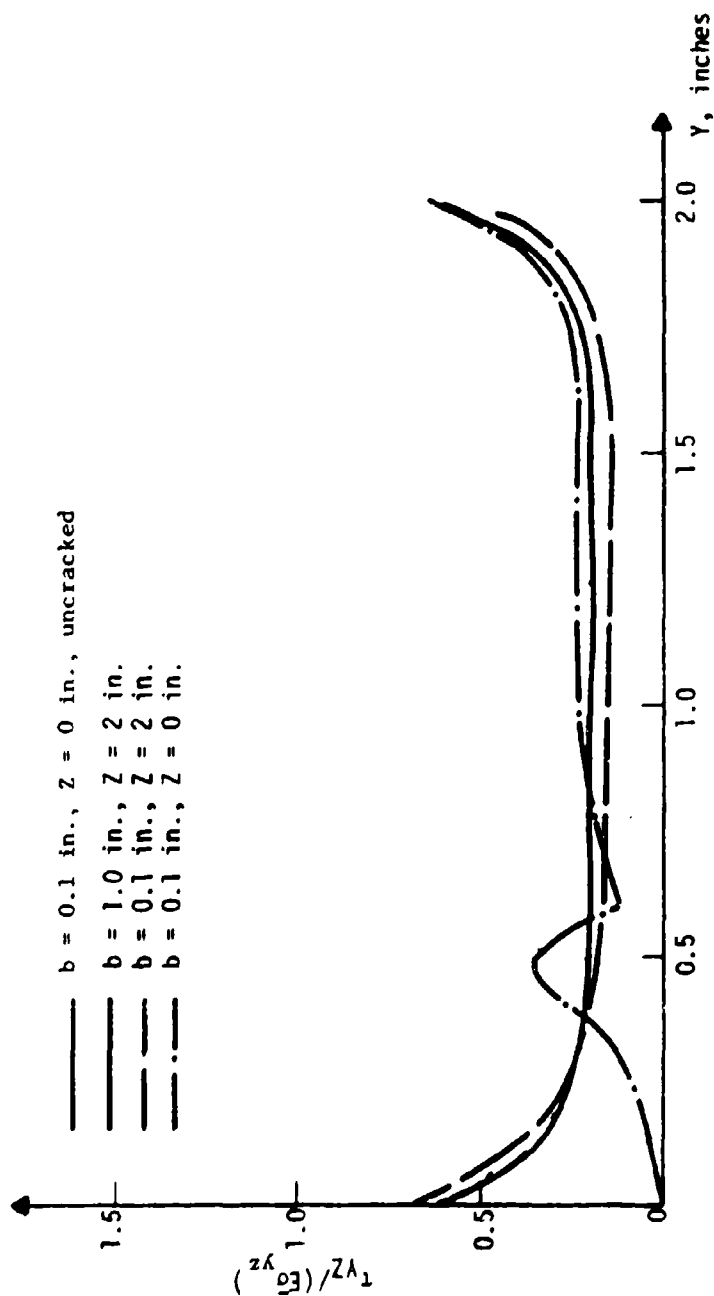
Figure 48. Distribution of Normalized Shear Stress at
a = 0.5 in., Plane Strain,
$\bar{\sigma}_{yz}$ Applied, Edge Crack
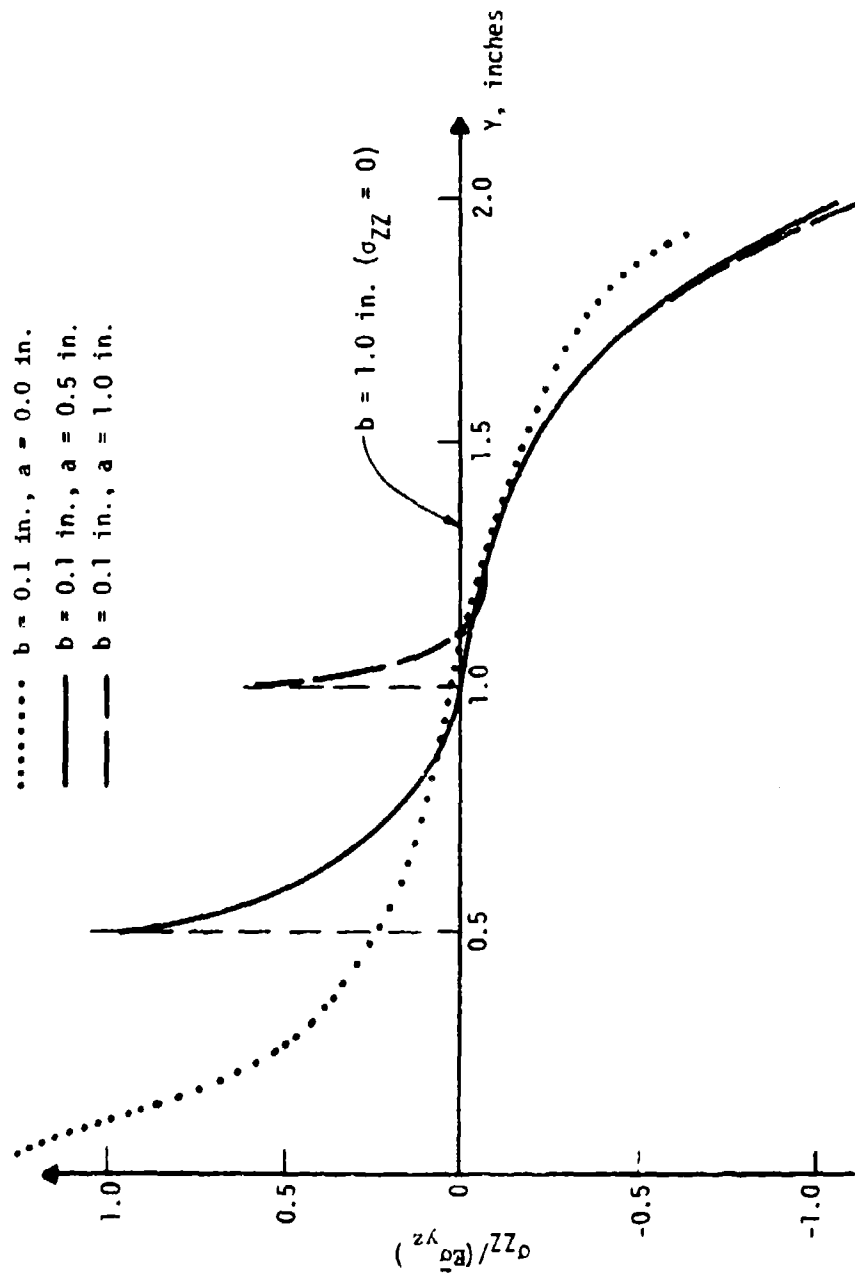
Figure 49. Distribution of Normalized Axial Stress at
Z = b (Along Crack Plane), Plane Strain
$\bar{\sigma}_{yz}$ Applied, Edge Crack
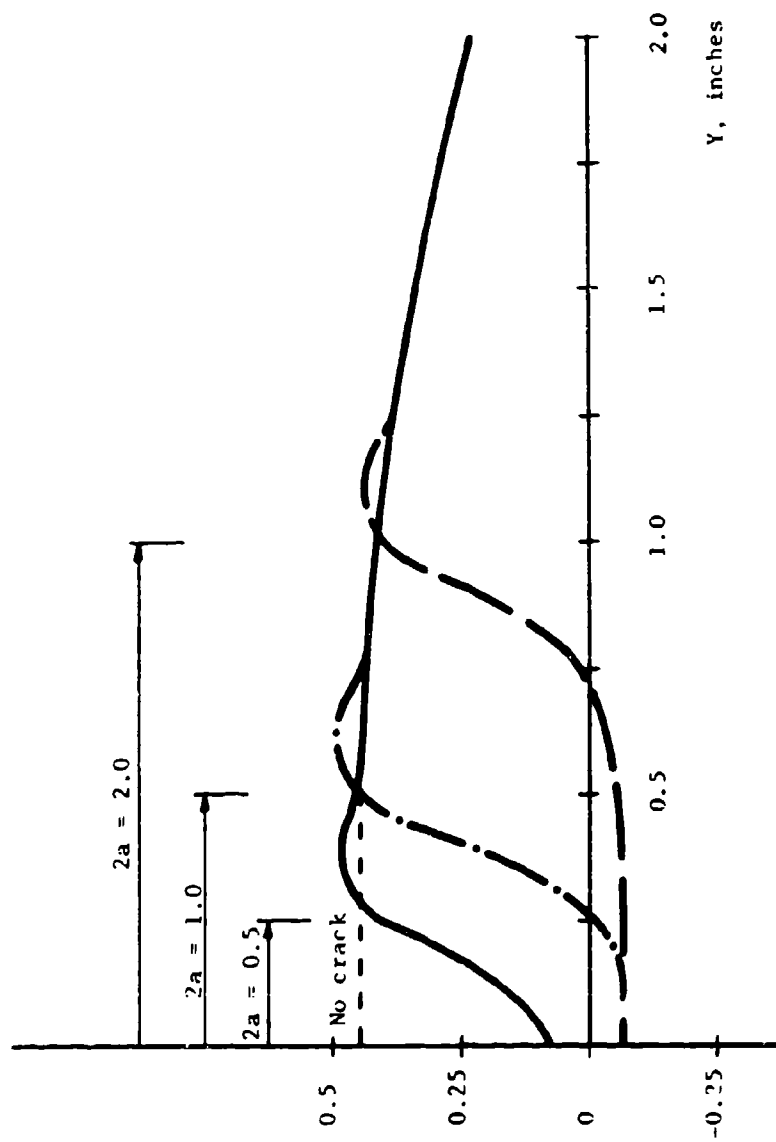
Figure 50. Normalized Surface Contraction Along the Plane of a Three-Dimensional, Central Crack for Three Crack Lengths

Normalized Contraction at Free Surface, X = B/2

4.4 PARAMETERS RELATED TO FRACTURE IN SCARF-JOINT SPECIMENS

The J integral theory does not necessarily depend on a specimen stress analysis to quantitatively characterize fracture behavior. Rather, as noted in the section on the J integral, one can determine values of J up to initiation of crack growth directly from experimental force-displacement curves together with application of Equation (7) for elastic materials or Equation (10) for viscoelastic materials. However, some specimen analysis may be useful to reduce the amount of experimental work that would otherwise be needed and to aid in selecting test specimen geometry and initial crack length. This section is concerned specifically with these two uses. Results from the linear elastic finite element analyses are employed to illustrate the methods and draw practical conclusions, although the analyses are not for nonlinear viscoelastic specimens, it is believed they provide helpful guidelines.

For a three-dimensional specimen, in general, the force-displacement relation is

$$F = SU \tag{61}$$

where S is the specimen's stiffness, which is a function of crack length. As a matter of notation, we shall suppose the pair (F, U) represents either a normal force and displacement (F_z, U_z) or a shear force and displacement (F_y, U_y). Also, in order to treat both central and edge cracks with the same notation, F is to be interpreted as one-half the total load on a specimen with a horizontally centered crack and as the total load with an edge crack.

Equation (7) in Section 2.1 becomes

$$J = \frac{1}{B} \frac{\partial}{\partial a} \left(\frac{1}{2} SU^2 \right) = -\frac{U^2}{2B} \frac{\partial S}{\partial a} \tag{62}$$

-85-

It will be helpful to rewrite this equation in terms of effective specimen moduli.

By definition,

$$E_{eff} \equiv \frac{(F_z/BL')}{(U_z/H)} \tag{63}$$

$$G_{eff} \equiv \frac{(F_y/BL')}{(U_y/H)} \tag{64}$$

where $L' = L/2$ in the case of a central crack and $L' = L$ with an edge crack. The symbols E_o and G_o denote these effective moduli, respectively, in specimens without cracks.

Equations (62) and (63) yield the expression for J under normal displacement U_z (assumed positive),

$$J_z = -\frac{1}{2} E_o HL' \bar{\epsilon}_z^2 \frac{\partial(E_{eff}/E_o)}{\partial a} \tag{65}$$

and under shear displacement U_y,

$$J_y = -\frac{1}{2} G_o HL' \frac{\bar{\gamma}_{yz}^2 \partial(G_{eff}/G_o)}{\partial a} \tag{66}$$

where, as introduced previously, $\bar{\epsilon}_z \equiv U_z/H$ and $\bar{\gamma}_{yz} \equiv U_y/H$. Equations (65) and (66) apply to three-dimensional geometries, and thus contain as special cases both plane stress and plane strain.

The effective moduli ratios E_{eff}/E_o and G_{eff}/G_o are plotted in Figures 51-58 for several two-and three-dimensional problems. According to Equations (65) and (66), the J integral is proportional to the slope of these curves. Thus, if the slope is essentially constant over a range of crack lengths, the value of J is independent of crack length over this range. For a linear or nonlinear material, experimental work and data analysis
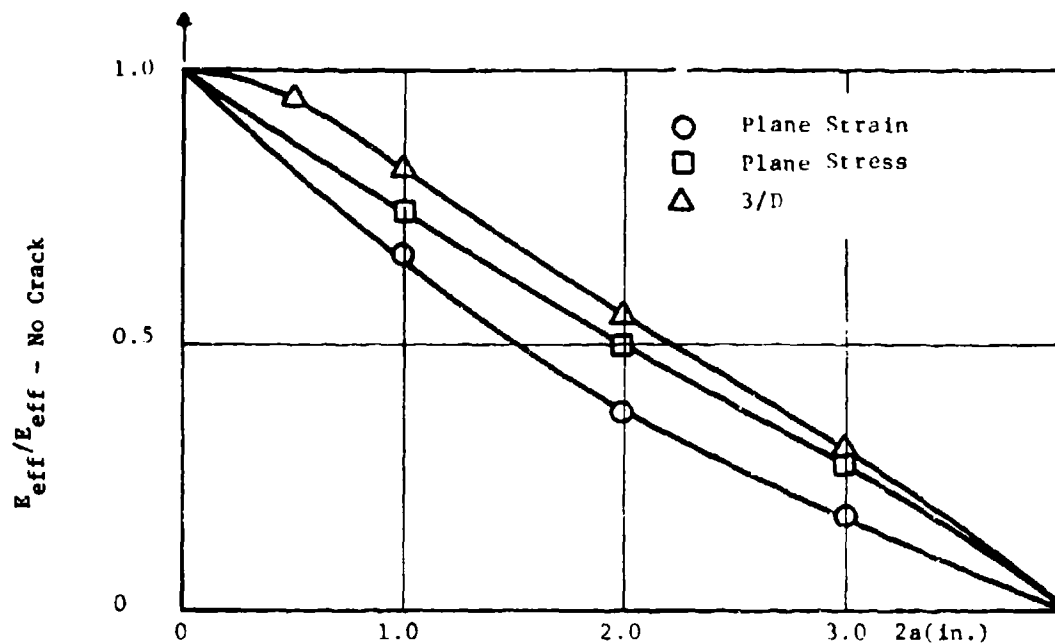
Figure 51. Effective Stiffness Ratio vs. Crack Length,
b = 1.0 inch (Central Crack), $\bar{\epsilon}_z$ Applied
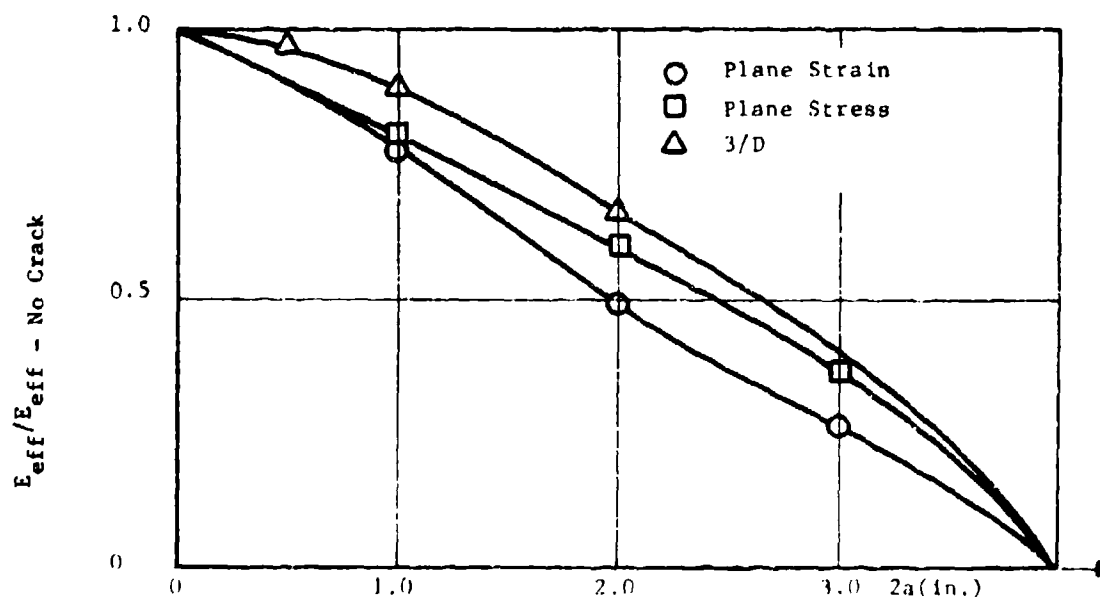
Figure 52. Effective Stiffness Ratio vs. Crack Length,
b = 0.1 inch (Central Crack), $\bar{\epsilon}_z$ Applied
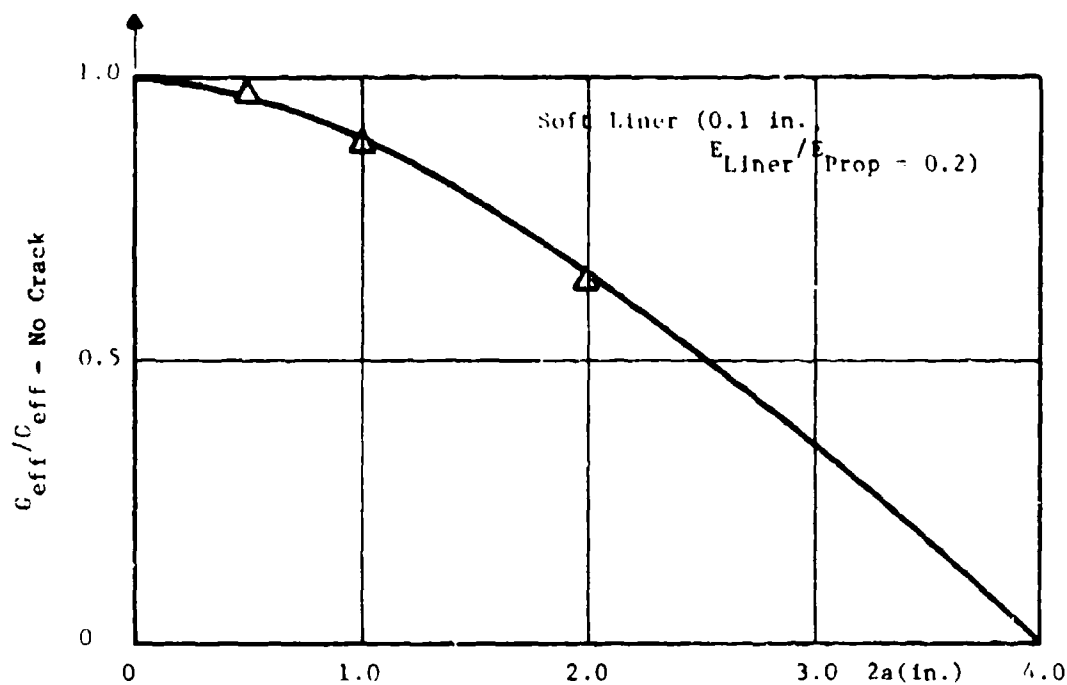
Figure 53. Effective Stiffness Ratio vs. Crack Length,
Soft Liner, b = 0.1 inch (Central Crack),
$\bar{\varepsilon}_z$ Applied, Three Dimensional Analysis
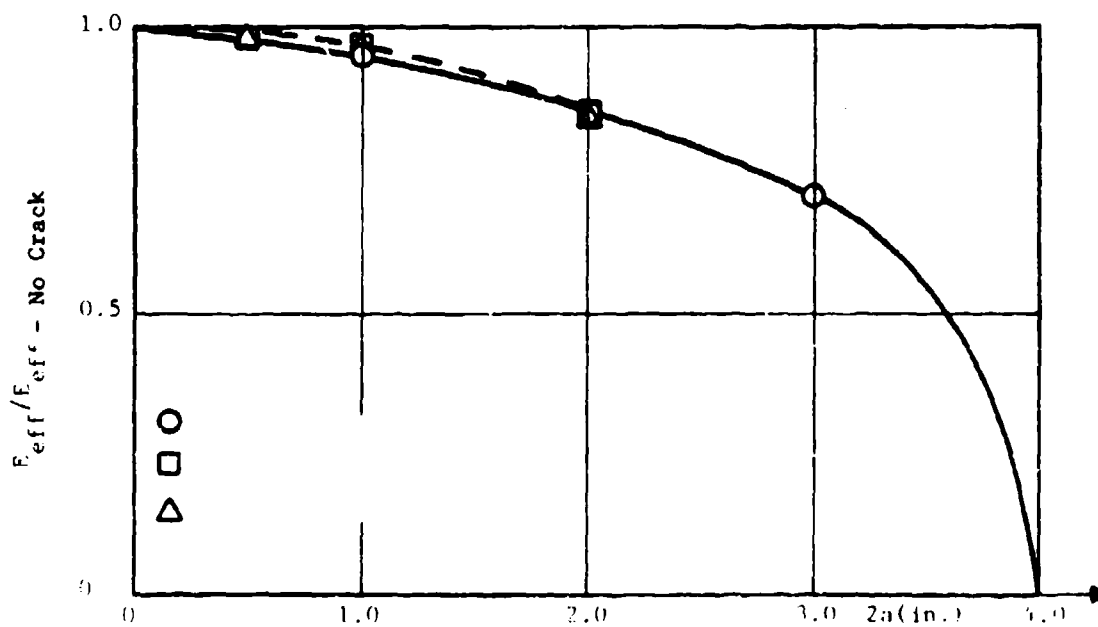
Figure 54. Effective Stiffness Ratio vs. Crack Length,
b = 0.1 inch (Central Crack), $\bar{\gamma}_{yz}$ Applied
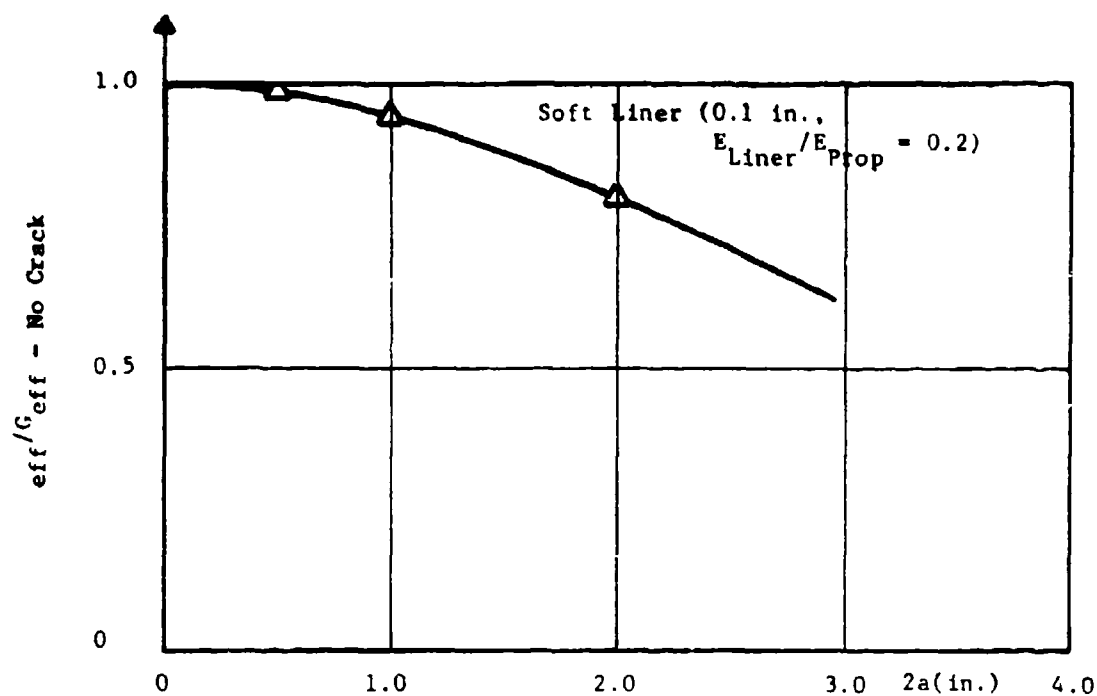
Figure 55. Effective Stiffness vs. Crack Length,
Soft Liner, b = 0.1 Inch (Central Crack),
$\bar{\gamma}_{yz}$ Applied Three Dimensional Analyses
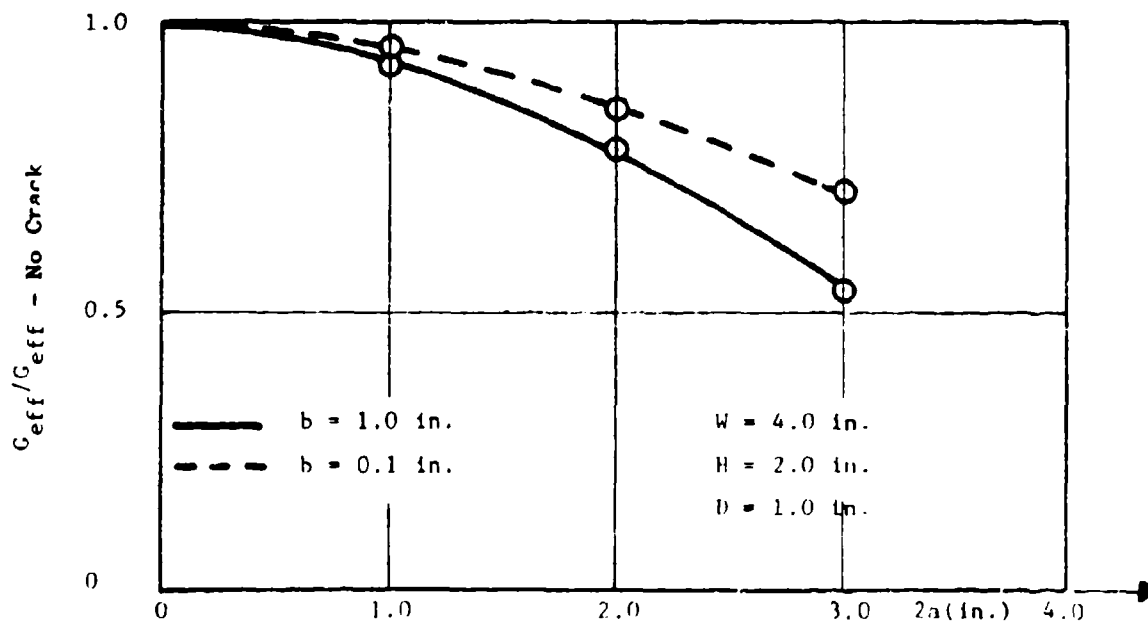
Figure 56. Effective Shear Moduli for Centered
Cracks under Shear Displacement
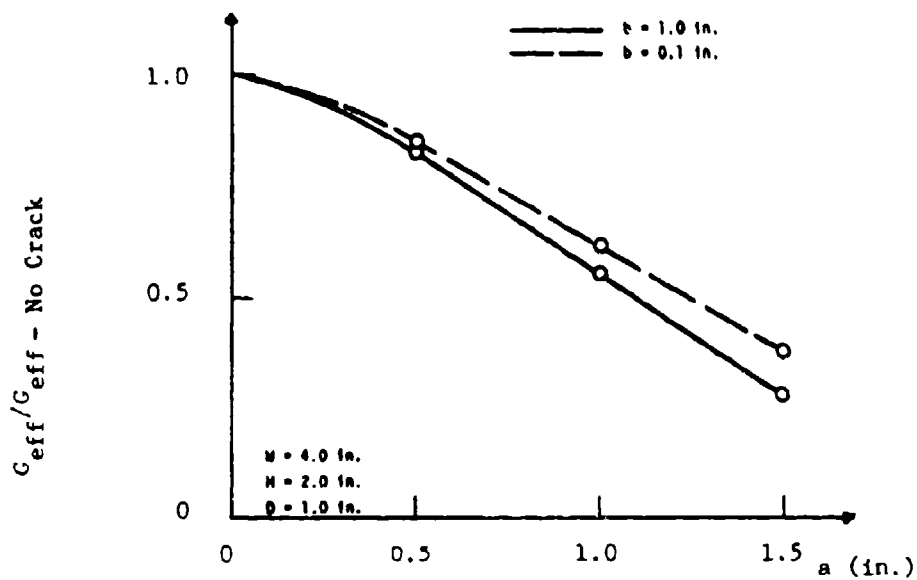
Figure 57. Effective Stiffness Ratio vs. Crack Length,
Plane Strain (Edge Crack), $\bar{\epsilon}_z$ Applied
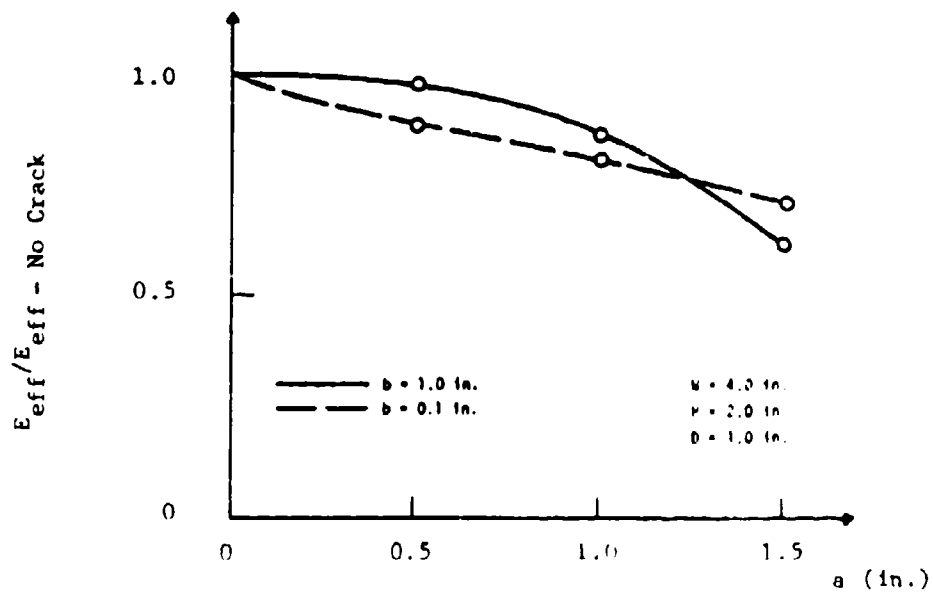
Figure 58. Effective Stiffness Ratio vs. Crack Length,
Plane Strain (Edge Crack), $\bar{\sigma}_{yz}$ Applied

are minimized whenever it is known J is independent of crack length. For horizontally centered cracks and edge cracks, it is seen that the slope is essentially constant if $0.5 \lesssim a \lesssim 1$ inches for several of the cases in Figures 51, 52, 55, 57 and 58. For shear loading, the value of J appears to be more sensitive to crack length; indeed only for an edge crack with $b = 0.1$, Figure 58, is there a range of crack lengths for which J is nearly constant.

These results indicate that for a horizontally centered crack, the best choice for initial length is $2a \approx 1$ inch, and for an edge crack one should use an initial length of $a \approx 0.5$ inch. Once a crack starts to propagate, the rate of propagation may be different through the specimen thickness, resulting in a curved crack front or tip even if the front is initially straight. Table 4 shows normalized normal forces at nodal points along the tip for tensile loading; the area over which each force acts is the same. In both cases, the crack is close to the grip, $b = 0.1$ inch; the specimen is homogeneous in the first case, while there is a 0.1 inch thick soft liner in the second case. With the soft liner, a tendency for tunneling is predicted because the forces increase with distance from the free surfaces. However, for a homogeneous specimen, outer and central forces are about equal, with a slightly reduced force at 0.25 inch from the free surface; in this case, the crack front could be expected to remain relatively straight, which is substantiated by experimental observations.

Let us now return to Equations (65) and (66) and rewrite them so that results for plane stress, plane strain, and the three-dimensional state can be compared. Clearly, it is not particularly meaningful to compare energy release rates for equal values of applied deformation because of the large difference in the global effect of thickness constraint (especially with tensile loading). Instead, let us suppose the applied deformation is such that the total strain energy for each of these three states is the same without a crack. Denote this strain energy by W_{TO}; then Equations (65) and (66) become respectively,

TABLE 4

NORMALIZED NODAL POINT FORCES ALONG CRACK
EDGE UNDER TENSILE LOADING,
CENTRAL CRACK, $2a = 1$ INCH, $b = 0.1$ INCH

	x (Inches)	$F_z/E\bar{\epsilon}_z$ (Homogeneous Specimens)	$F_z/E\bar{\epsilon}_z$ (0.1 Inch Soft Liner $E_{liner}/E_{prop} = 0.2$)
(Center Plane)	0	.00530	.01123
	0.25	.00478	.00783
(Free Surface)	0.50	.00526	.00705

$$J_z = -\frac{W_{TO}}{B'} \frac{\partial(E_{eff}/E_o)}{\partial a} \tag{67}$$

$$J_y = -\frac{W_{TO}}{B'} \frac{\partial(G_{eff}/G_o)}{\partial a} \tag{68}$$

where $B' = 2B$ for specimens with central cracks and $B' = B$ for the edge cracks. Thus, with this method of selecting the deformation, the energy release rate for each state of stress can be compared by simply comparing the appropriate slopes in Figures 51 - 56. For cracks in the range $1 < 2a < 2$ inches, Figures 51 and 52 show that the energy release rate decreases in the order plane strain, three-dimensions, plane stress, as one might anticipate from the effect of thickness constraint. By contrast, on shear loading, as Figure 54 indicates, there is almost no difference over practically the entire range of possible crack lengths.

Normalized effective moduli are given in Table 5 for some three-dimensional and plane stress cases. These moduli are equal to total load divided by cross-sectional area, Young's modulus, and the average strain, $\bar{\varepsilon}_z$ or $\bar{\gamma}_{yz}$. Thus, these results serve to show how close the actual three-dimensional specimens are to a state of plane stress for the same applied deformation. Notice, for example, that without a crack the ratio of plane stress to three-dimensional sample stiffness is $1.25/1.29 = 0.97$. In contrast, the stiffness for plane strain is relatively very high because $\nu = 1/2$.

The effect of a soft liner on sample stiffness is also indicated in Table 5. These three-dimensional results show there is a small, but not negligible, decrease in sample stiffness with a liner, compared to the stiffness of a homogeneous sample. The effective moduli which are given enable one to estimate energy release rate from Equations (65) and (66).

TABLE 5

NORMALIZED EFFECTIVE MODULI
FOR THREE-DIMENSIONAL AND PLANE
STRESS STATES

Crack Length 2a (Central Crack)	b = 1 Inch Homogenous E_{eff}/E		b = 0.1 Inch Homogeneous E_{eff}/E		b = 0.1 Inch 0.1 In. Soft Liner, $E_{liner}/E_{prop} = .2$ E_{eff}/E
	3-D	Plane σ	3-D	Plane σ	3-D
0	1.290	1.250	1.290	1.250	1.190
0.5	1.224		1.249		1.149
1.0	1.059	0.939	1.152	1.014	1.051
2.0	0.706	0.623	0.848	.748	0.767
3.0	0.389	0.341	-	0.460	
			G_{eff}/E		G_{eff}/E
			3-D		3-D
0			0.292		0.245
0.5			0.291		0.242
1.0			0.282		0.231
2.0			0.251		0.195

Table 6 gives stress intensity factors for several cases of plane stress and strain. The skew-symmetric shear mode factor, K_{II}, can have significant effect on the trajectory of crack growth. For edge cracks, it is to be observed that the dependence of K_{II} on crack length is quite irregular; this behavior is a result of the high corner shear stresses which interact with the shear stresses due to the crack itself. Interpretation of data from near-grip edge cracks therefore will be difficult because of this behavior. It is noted for these 2-D problems that where a soft liner is used, the crack is not at the interface; but, instead it is a small distance into the propellant.

The energy release rate is readily predicted from these stress-intensity factors (e.g., Equation (37)) in Section 2. Specifically,

$$J = \frac{C}{E} (K_I^2 + K_{II}^2) \tag{69}$$

where $C = 1$ for plane stress and $C = 1 - \nu^2 = 0.75$ for plane strain; E is Young's modulus of the propellant.

As a final matter, it will be shown that the results in this section for central cracks can be used to predict energy release rate for mixed tensile and shear loading. Specifically, the upper grip displacement amplitude, U, and orientation, θ, (relative to the lower grip) are given by

$$U = \sqrt{U_z^2 + U_y^2} \tag{70}$$

$$\theta = \tan^{-1} U_y/U_z \tag{71}$$

As linearity is assumed,

$$F_y = S_y U_y + S_{yz} U_z \tag{72}$$

$$F_z = S_{yz} U_y + S_z U_z \tag{73}$$

TABLE 6   Page 1 of 2

NORMALIZED TWO-DIMENSIONAL
STRESS INTENSITY FACTORS*

			Plane Strain		Plane Stress	
			K_1	K_2	K_1	K_2
I.	Central Crack, $\bar{\epsilon}_z$ Applied					
	b = 1.0,	2a = 1.0	2.28	0	1.11	0
	b = 1.0,	2a = 2.0	1.76	0	1.08	0
	b = 1.0,	2a = 3.0	1.50	0	1.04	0
	b = 0.1,	2a = 1.0	2.11	-0.42	0.94	-0.21
	b = 0.1,	2a = 2.0	1.85	-0.49	1.02	-0.32
	b = 0.1,	2a = 3.0	1.56	-0.55	1.01	-0.37
II.	Edge Crack, $\bar{\epsilon}_z$ Applied					
	b = 1.0,	a = 0.5	1.55	0	1.02	0
	b = 1.0,	a = 1.0	1.66	0	1.07	0
	b = 1.0,	a = 1.5	1.50	0	1.04	0
	b = 0.1,	a = 0.5	1.40	0.20	0.89	-0.07
	b = 0.1,	a = 1.0	1.49	-0.05	0.97	-0.21
	b = 0.1,	a = 1.5	1.47	-0.33	0.99	-0.33
III.	Edge Crack, $\bar{\sigma}_{yz}$ Applied					
	b = 1.0,	a = 0.5	0	0.25	0	0.23
	b = 1.0,	a = 1.0	0	0.12	0	0.45
	b = 1.0,	a = 1.5	0	0.63	0	0.52
	b = 0.1,	a = 0.5	0.31	0.14	0.30	0.10
	b = 0.1,	a = 1.0	0.12	0.28	0.15	0.24
	b = 0.1,	a = 1.5	0.02	0.47	0.04	0.40

TABLE 6 (Continued)   Page 2 of 2

NORMALIZED TWO-DIMENSIONAL
STRESS INTENSITY FACTORS*

		Plane Strain		Plane Stress	
		K_1	K_2	K_1	K_2
IV.	Central Crack, $\bar{\sigma}_{yz}$ Applied				
	b = 1.0, 2a = 1.0	0	0.41	0	0.40
	b = 1.0, 2a = 2.0	0	0.55	0	0.50
	b = 1.0, 2a = 3.0	0	0.64	0	0.54
	b = 0.1, 2a = 1.0	0.04	0.32	0.06	0.30
	b = 0.1, 2a = 2.0	0.02	0.43	0.07	0.40
	b = 0.1, 2a = 3.0	-0.03	0.57	0.03	0.50
V.*	Central Crack, $\bar{\epsilon}_z$ Applied, 0.05 Inch Soft Liner (E_{liner}/E_{prop} = 0.2)				
		1.91	-0.35	0.91	-0.10
		1.71	-0.43	0.98	-0.19
		1.47	-0.43	0.97	-0.19
VI.*	Edge Crack, $\bar{\epsilon}_z$ Applied, 0.05 Inch Soft Liner (E_{liner}/E_{prop} = 0.2)				
		1.40	0.20	0.89	-0.07
		1.44	-0.12	0.94	-0.13
		1.41	-0.34	0.95	-0.19

*   Crack Tip Detail for Cases V and VI

Let

$$\lambda = U_y/U_z \qquad (74)$$

and

$$F = \sqrt{F_z^2 + F_y^2} \qquad (75)$$

Assume λ is constant during actual or virtual crack growth. Then, Equation (62) may be used, where S is the ratio of force to displacement amplitudes. For those cases in which $S_{yz} = 0$, we obtain from Equations (70) - (75),

$$S = \left[\frac{S_z^2 + S_y^2 \lambda^2}{1 + \lambda^2} \right]^{1/2} \qquad (76)$$

Also, from Equations (63) and (64),

$$S_z = \frac{BL'}{H} E_{eff} \quad , \quad S_y = \frac{BL'}{H} G_{eff} \qquad (77)$$

The stiffness associated with tensile-shear coupling, S_{yz}, vanishes for all scarf-joint specimens without a crack and with a horizontally centered crack. This observation can be proved by referring to Equation (73), and considering only shear displacement ($U_z = 0$). If $S_{yz} \neq 0$, and we change the sign of U_y, F_z changes sign. However, except for samples with edge cracks, the specimens are symmetric with respect to the x-z plane, and therefore the induced force F_z cannot change sign. Thus, we must conclude $S_{yz} = 0$.

Consequently, Equations (76) and (77) and (62) can be used to predict sample stiffness and energy release rate for mixed-mode loading. This observation, together with the complex variation of K_{II} with near-grip edge cracks, makes samples with horizontally centered cracks more desirable than those with edge cracks. Two additional reasons for using centered cracks are:

-98-

- With axial loading there is a high tensile stress
  acting along the grip near the central region for a
  sample without a crack or with a short edge crack;
  this high stress may lead to premature failure at
  the bondline. In contrast, this stress is relieved
  in a specimen with a central crack.

- The opening-mode stress intensity factor, K_I,
  under shear loading is very small compared to the
  anti-symmetric stress intensity factor, K_{II}; for
  an edge crack the value of K_I is comparable to that
  of K_{II}, making interpretation of the data more difficult.

5.0 STANDARDIZATION OF PREPARATION AND TEST PROCEDURES

A specific set of preparation and test procedures evolved over the course of the experimental program. The resulting procedures are rather complex and are presented in detail in Appendix A.

Many of the features of this test are unique and are described below. A few special items are described later in conjunction with the particular tests to which they apply. The unique features described here include the following categories:

- Refinements in specimen design

- Crack detection and displacement measurements

- Data Acquisition System

- Toes and holes

- Data Reduction Methods

The experimental procedures were developed in the course of actual laboratory tests, the J integrals of which are presented in Section 6.0.

5.1 EMPIRICAL REFINEMENTS TO SPECIMEN DESIGN

Three design modifications to the scarf-joint specimen were derived from the experimental results. The first involved stress relief of the specimen ends to prevent premature failures there. The second modification had to do with the maximum tolerable crack length while the third considered further the effects of specimen size. These three modifications are described below.

5.1.1   Edge Stress Relief

Three designs of edge stress relief were considered. These are shown in Figure 59. Design 1 worked well and was easier to prepare

End Plate

Design 2

End Plate

Design 3

Through Cuts

End Plate
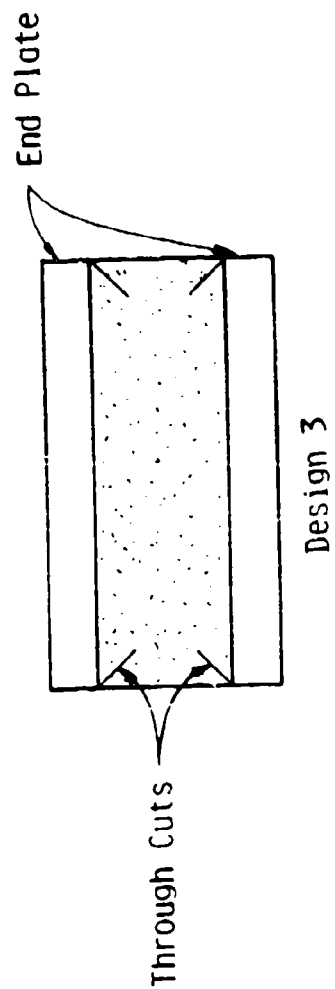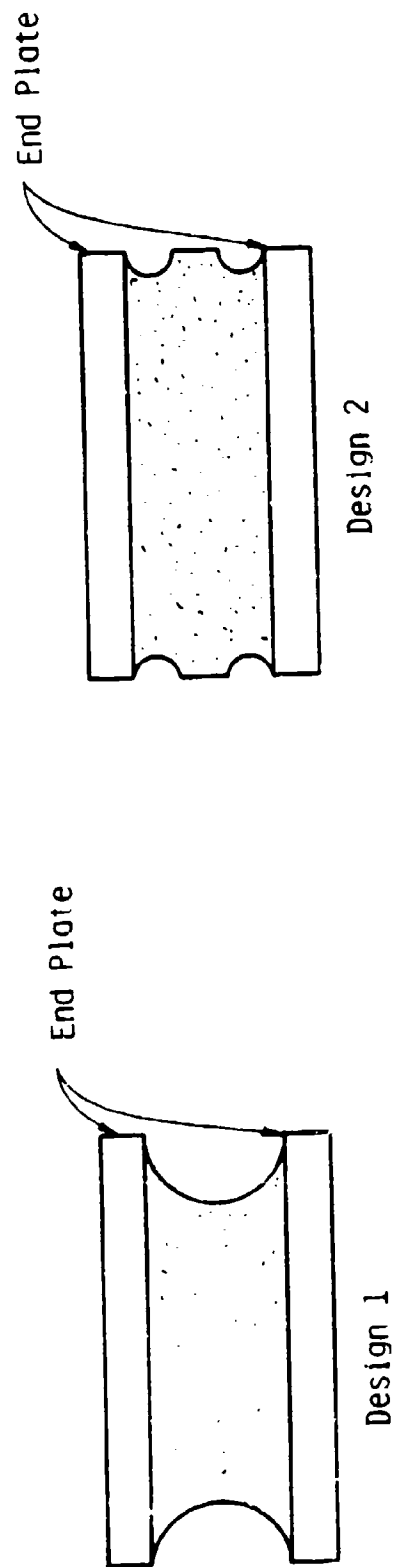
Design 1

Figure 59. Candidate Designs for Edge Stress Relief

than Design 2. Design 3 (45° angle cuts) is the least expensive to make and is convenient to manufacture in the laboratory. However, in some of the later tests at 0°F some cracking was observed at the tips of the cuts. Design 1 was finally selected as the standard and was used in most of the testing.

5.1.2   Optimization of Initial Crack Length

A large shear component is known to exist in specimens with long cracks (Section 4.0) Besides complicating the data analysis, this component also contributes to the nonlinearity of the force-time traces.

A special set of tests was performed to evaluate crack-length dependency in the scarf-joint test. These tests were conducted on Minuteman propellant-liner bond specimens with initial crack sizes, 2a', varying from 0 to 2 inches and crosshead speeds of 0.02, 0.10 and 0.50 inch per minute.

The analytical relation for deriving the J integral from the test data is:

$$J = -\frac{1}{t^m} \frac{\partial}{\partial a} \int_0^U c(a,U) \ U^m dU \qquad (78)$$

where: J is the J integral

U is the point load tensile displacement of the test specimen

t is the testing time

m is an empirical constant

The values of c(a,U) and m are obtained from crossplots at constant a and U according to the following relationship:

$$f = c(a,U)R^m \qquad (79)$$

where f is a normalized pulling force and R is the crosshead speed.

The values of m were obtained from linear regression analyses of log f versus log R.

The nonlinearities due to crack size were found to affect primarily the integral term in Equation (78). Plots of that integral versus crack length 2a', are given in Figure 60.

The integral for the 2-inch crack falls below the straight line projected from the values at smaller crack sizes. Considering the curves in Figure 60, the largest crack size, 2a', that would fit a straight line projection is 1.6 inches. That upper limit was used for the remainder of the experimental program.

5.1.3 Further Considerations of Specimen Size

The earlier experimental considerations (Section 3.4.2) indicated the optimum specimen dimensions to be roughly L = 4 in., H = 2 in., and B = 1 in. This specimen size was used as the basic design for the analysis in Section 4.0. As the experimental efforts continued there were indications that larger specimens would give higher load readings and, possibly, more sensitivity to crack size changes.

The height of the specimen, as originally observed, was dictated by the method for detecting crack initiation (see below). Thus, the length, L, and breadth, B, of the specimen were the only parameters amenable to further investigation. To simplify the plan, considerations were limited to the simple grid shown in Table 7, where the behavior of the base specimen design (4 x 2 x 1-in.) is compared with that of a two-inch longer (L = 6 in.) specimen and of a specimen that is one-inch broader (B = 2 in.). These specimens used the earlier, edge stress relief design; design 3 in Figure 59.
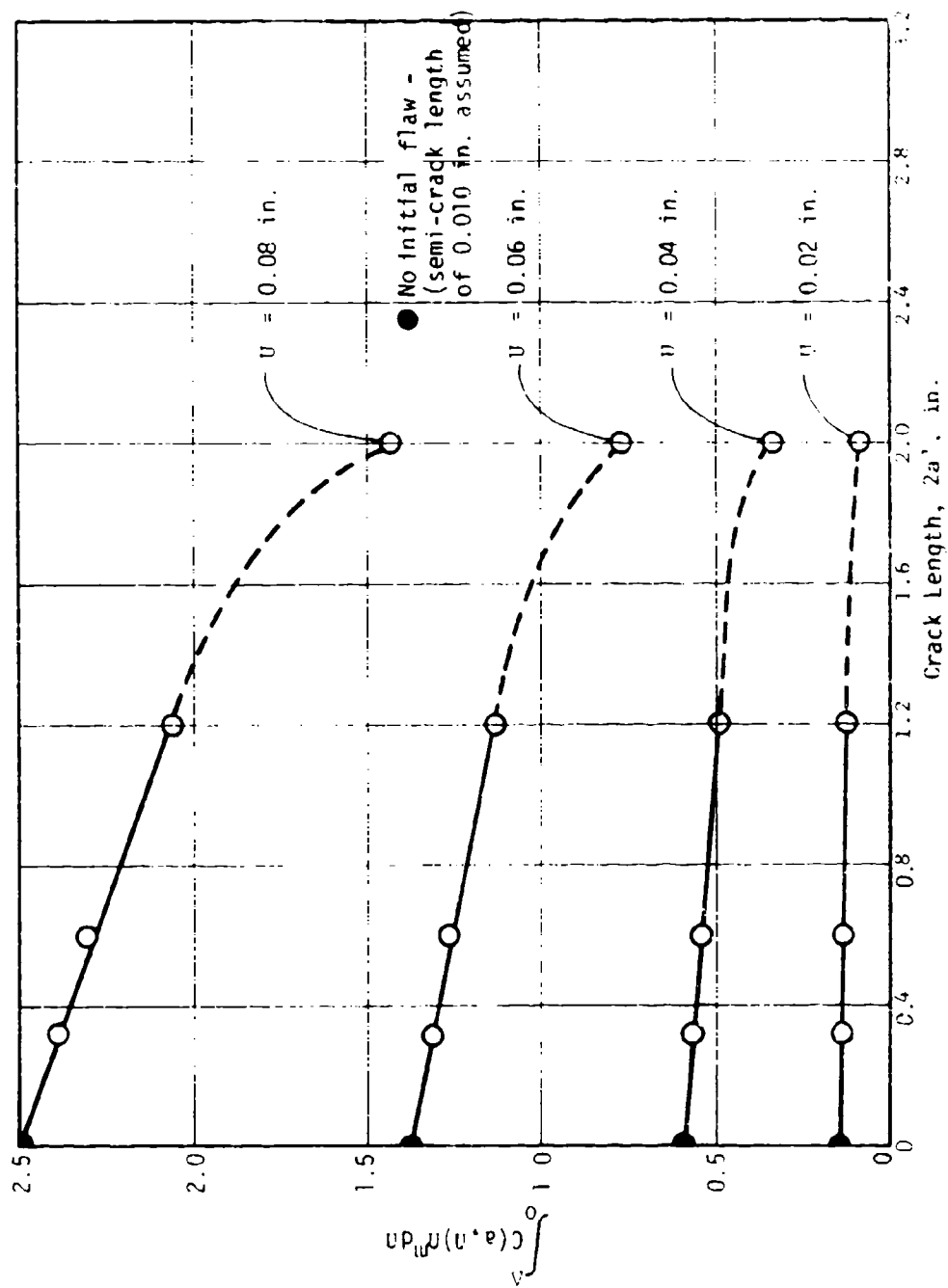
Figure 60. Plot of Integral of $C L^m$ versus $2a'$

TABLE 7. EXPERIMENTAL ASSESSMENTS OF DIMENSIONAL VARIATIONS
(H = 2 in.) USING ANB-3066/SD-851-2/V-45

L, in.	B, in.	Crosshead Speed, in./min	2a'/L=0.8	Test Matrices at 77°F		
				0.3	0.5	0.7
4.0	1.0	0.02		xx	x	x
		0.10		x	x	x
		0.50		x	xx	
4.0	2.0	0.02		xx	xx	x
		0.10		x	x	x
		0.50		xx	xx	
6.0	1.0	0.02	x	x	x	x
		0.10		xx	x	x
		0.50		xx	xx	x

x indicates test conducted.

-105-

Both of the bigger specimens developed large shear and normal stresses along the edges at the propellant-liner bond. As shown in Figure 61, the broader specimen curled along the sides of the specimen while the long one curled in along the sides and at the outside edges. These curling effects caused sufficient stress relief at the crack tips so that secondary bond failures occurred instead of crack initiation. The secondary bond failures took place between the insulation and the supporting end plate. The curling effects also greatly modified the force-deformation traces so that they markedly departed from the power-law relation that was found applicable to data from the basic design (see Section 5.5).

The three effects of the curling (non-uniform crack propagation, secondary bond failures and deviations from the power-law relation) precluded using the larger specimens for this testing. Occasionally, these effects are seen in small degrees in tests of the basic specimen, making this design the largest size that should be used. Thus, the basic specimen design, within the many constraints imposed upon it, is reasonably close to the optimum dimensions.

5.2 CRACK DETECTION AND DISPLACEMENT MEASUREMENTS

The primary measurements in the J integral test involve methods for:

1. Measuring the applied force

2. Proving measures of point load displacement

3. Defining initiation of the crack

The force measurements are obtained using well qualified commercial load cells, and need no further description here. The latter two measurements have some unique characteristics and are described below.

-106-
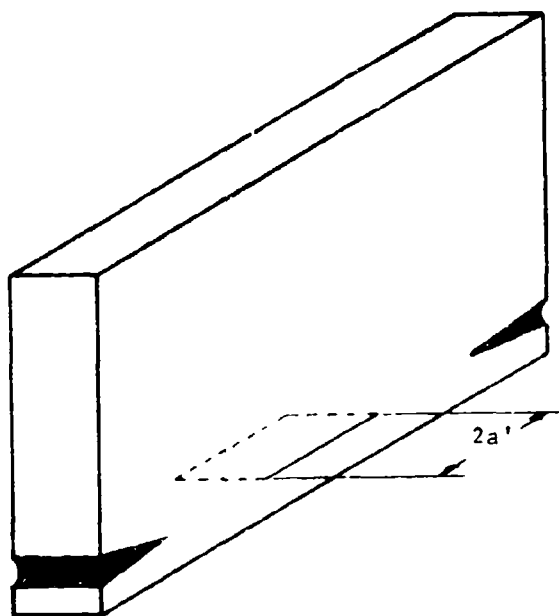
a. One-Inch by Six-Inch Long Specimen
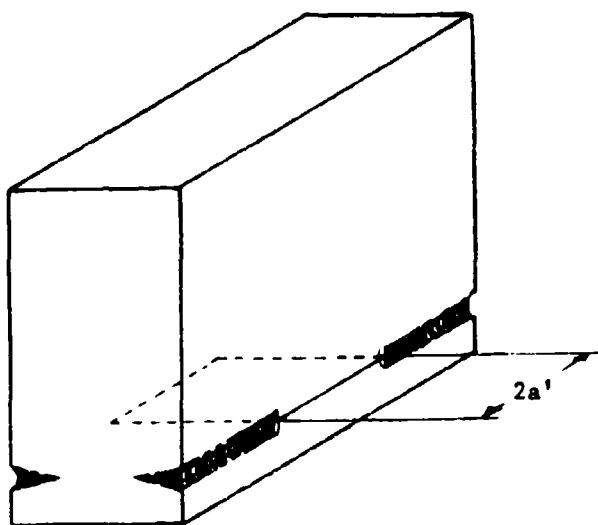
b. Four-Inch by Two-Inch Wide Specimen

Figure 61. Curling Along Sides and at
Ends of Oversized Scarf-Joint
Test Specimens

5.2.1   Specimen Displacement Measurements

To verify that the scarf-joint bond specimen has been
uniformly extended (the end plates remaining parallel to each other) an ex-
tension monitoring unit was devised. This unit consists of four extensometers
mounted on a flat plate which, in turn, is attached to the upper end-plate of
the test specimen, Figure 62. A second flat plate is mounted to the lower end-
plate of the specimen. The four extensometers are designed to measure the
displacements at the four corners of the test specimens.

For most carefully conducted tests, the end-plates remained
parallel within an angular deflection of 0.2°. Although we would prefer a narrower
limit, this appears to be reasonable and is within the expected reproducibility
(statistical effects due primarily to liner thickness variations in specimen
preparation).

To maintain the parallel displacement of the scarf-joint
bond specimen, it was necessary to couple the two end-plates rigidly to the
tensile tester. This required replacement of the standard univeral joint with
a short rigid bar. For the Instron Tensile Testers this also meant a change in
the load cell to one that would allow rigid coupling. A Lebow Model 3169-104
load cell was used for these tests.

5.2.2   Detection of Crack Initiation

5.2.2.1   Concept

The method selected for this measurement is
called acoustic profilography, which was developed at Aerojet in 1973 [18].
In this approach a sound wave is pulse-generated in a PZT transducer and
transmitted through the test specimen. The key measurement is the time required
for the ultrasonic pulse to traverse the specimen after diffracting around the
crack tip, a longer traverse time being required after the crack has propagated.

Specimen

Extensometer
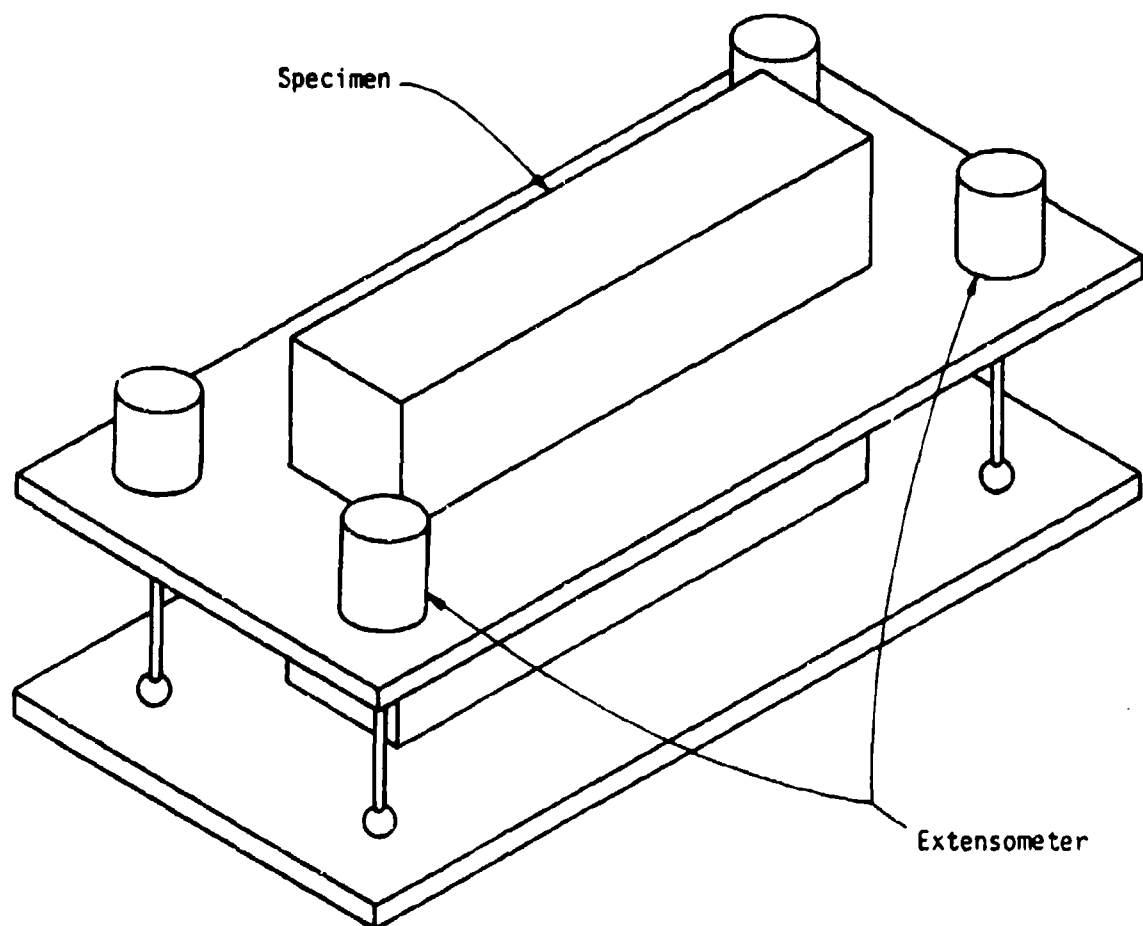
Figure 62. Parallel Displacement Monitoring Fixture for
the Scarf-Joint Specimen

-109-

Figure 63 illustrates the relative placements of
the transmitting and receiving PZT crystals and the interposed crack. Since
the path also increases as the specimen is stretched there will be a linear
continuously increasing traverse time, as illustrated in Figure 64. Upon crack
initiation and growth, the traverse time suddenly jumps and changes slope,
leaving a clearly identifiable initiation point (also shown in Figure 64).

Using this technique, a propagation of the crack
tip of as little as six mils can be detected with state-of-the-art data acqui-
sition equipment. However, the very soft liner used in this study produced
poker-chip type fractures that sometimes interfered with the acoustic signal
giving anomalous results. This behavior and a corrective technique are dis-
cussed later in the report.

A specially modified data acquisition system was
used for the ultrasonic measurements, in addition to the collection of other
relevant test data. As part of the background data needed to design that
system, preliminary tests were conducted as discussed below.

5.2.2.2   Tests on Specimens Cut from Motors

To demonstrate the applicability of acoustic
profilography to dissected motor samples, we conducted sound transmission tests
through an insulated titanium case section. The sound was sent through a
two-inch layer of propellant, plus the liner, insulation and case. A small
hole was cut through the case to permit direct access to the insulation in
order to make comparative measurements of signal strengths with and without
the case.

As illustrated by the oscilloscope traces in
Figure 65, the magnitude of the leading edge* of the received pulse was the
same whether through the case (Figure 65b) or just to the insulation surface
(Figure 65a). This result should greatly simplify those tests where the case
materials must remain attached to the test specimens.

---

* This is the reference point for the traverse time measurements.

Figure 64. Detection of Crack Initiation

Figure 63. Crack Detection by
Acoustic Profilography

-111-

Pulse
front

b. Through Sample and Titanium Case

Pulse
front

a. Through Sample without the Case

Figure 65. Acoustic Transmission Output Through Sample
With and Without the Titanium Case

5.2.2.3 Operating Frequency

The necessary exposure of some lead wires in the scarf-joint tests causes interference and noise, so the received signals have to be enhanced by the use of filters. To aid filtering, the natural frequency of the transmitting crystal has to be as high as possible, where removal of low frequency interference is easier.

The commercially available PZT crystals in the preferred one-inch diameter had thicknesses of 0.035 and 0.10 inches. When driven with 175 volt transmit pulses, both of these crystals gave strong signals across slabs of solid propellant. The measured frequencies and the magnitudes of the leading edge of the received pulse, in volts, are listed below.

Transmitter Thickness, in.	Natural Frequency	Thickness of Propellant, in.	Received Pulse, Volts
0.035	2.25 MHz	1.50	0.15
		3.20	0.06
0.10	780 KHz	1.50	0.075
		3.20	0.025

The 2.25 MHz transmitter (0.035 in. thick by one-inch diameter PZT crystal) is indicated as the proper choice for the filtering.

5.2.2.4 Optimum Placement of PZT Crystals Relative to the Crack Tip

In a series of experiments, the receiver PZT was placed at various positions relative to the crack tip, using the centerpoint of the crystal as the reference. This experiment is illustrated in Figure 66. The strength of the received signal, measured at each position, is plotted in Figure 67. The placement of the crack edge at 0.5 inch, is also shown. The resulting parabolically shaped curve clearly indicates that the best placement

-113-
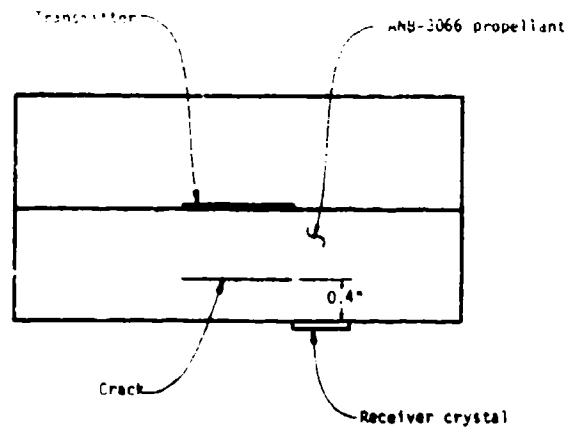
Figure 66.   Set-up of Test for Evaluating the Optimum
Placement of Receiver Crystal
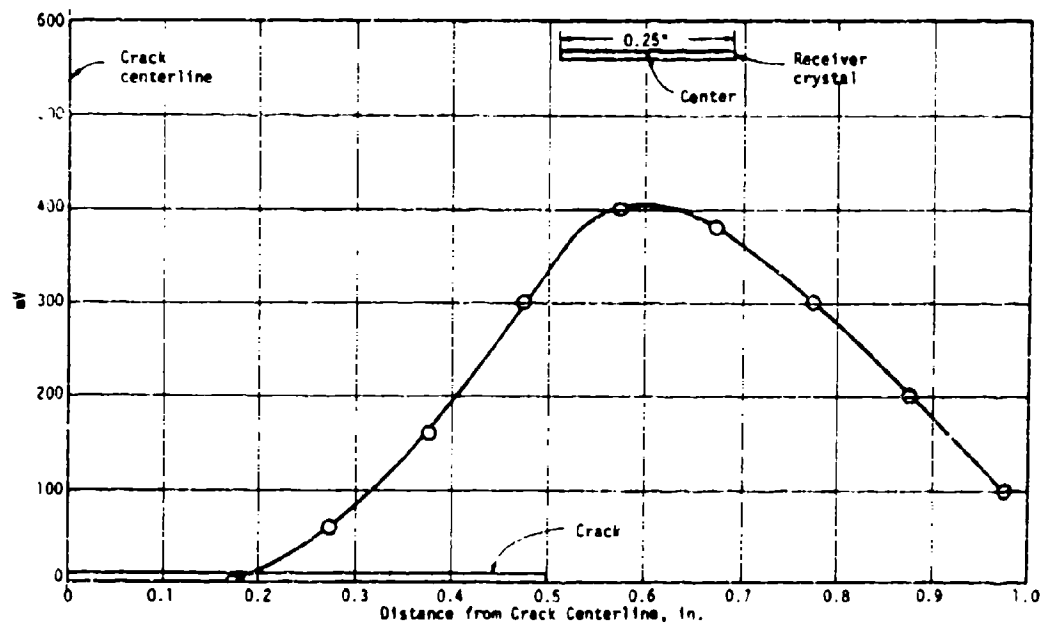
Figure 67.   Test to Determine Optimum Placement
of PZT Receiver Crystals

of the crystal is with its centerpoint placed over the edge of the crack. At
that location the rate of change of the received signal should be greatest,
hence the test would be the most sensitive.

5.2.2.5 Final Design of the Scarf-Joint Specimen with Acoustic Profilography

The final design of this specimen is shown in
Figure 68. The PZT transmitting crystal is potted with epoxy into a hole cut
into the center of the top plate. The PZT receivers are potted into holes cut
in the lower end-plate. The holes are centered under the ends of the crack and
half-way between the front and back faces of the lower plate.

5.3 DATA ACQUISITION SYSTEM

The data acquisition system used for these tests was programmed
for system calibrations, to acquire data, to perform the appropriate calculations,
and then to printout and/or plot the test results. Fourteen functions were
designated for this monitoring; they are:

1. Environmental temperature
2. Specimen temperature
3. Environmental pressure
4. Time in testing
5. Crosshead displacement
6. Tensile component of crack displacement
7. Shear component of crack displacement
8. Load cell force
9. Δt_1 (Time interval for ultrasonic pulse to traverse specimen)
10. Δt_2 (Time interval for ultrasonic pulse to traverse specimen)
11. Δt_3 (Time interval for ultrasonic pulse to traverse specimen)
12. Δt_4 (Time interval for ultrasonic pulse to traverse specimen)
13. Δt_5 (Time interval for ultrasonic pulse to traverse specimen)
14. Δt_6 (Time interval for ultrasonic pulse to traverse specimen)

-115-
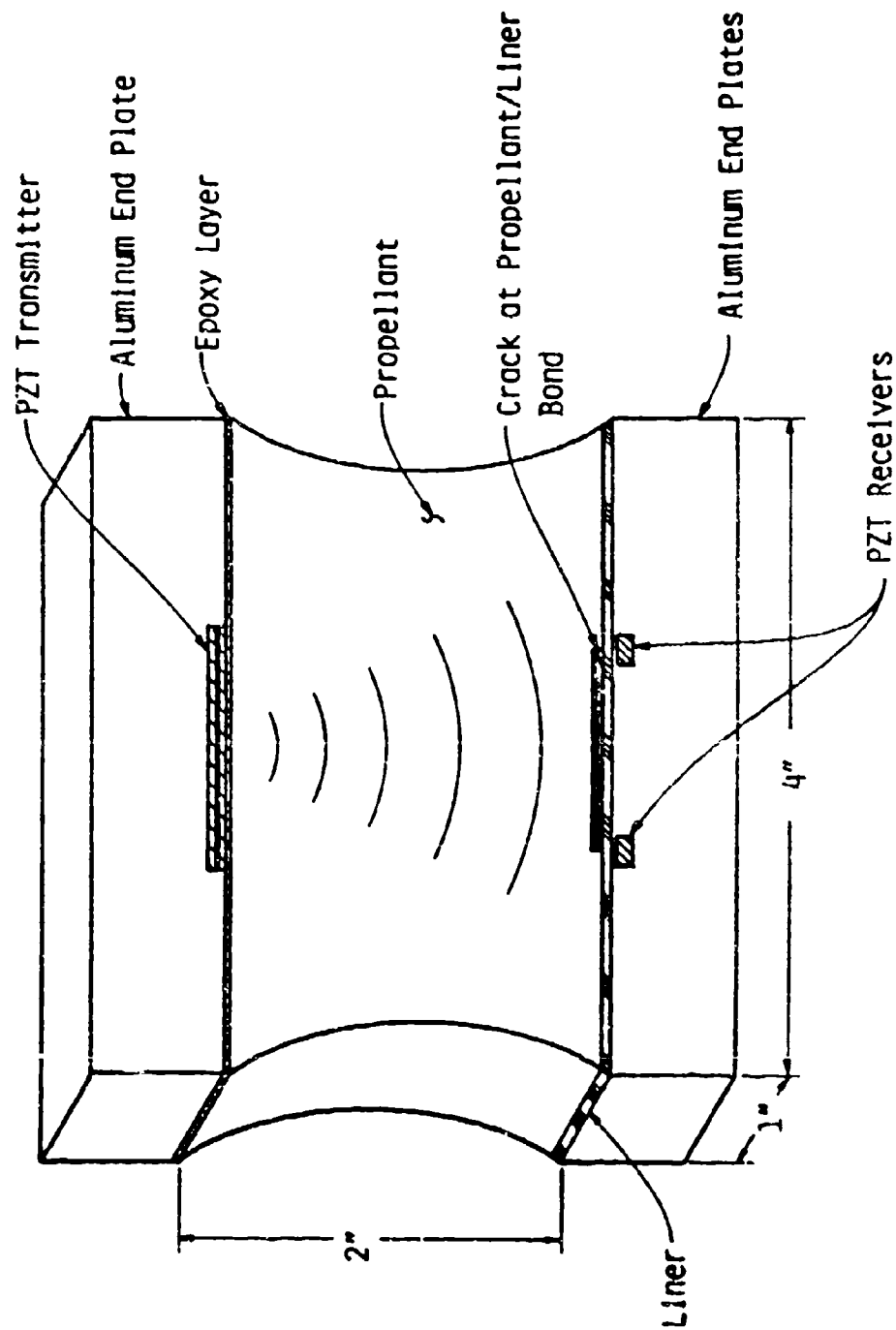
Figure 68. Scarf-Joint Specimen with Acoustic Profilography

116

Channels 9 through 14 were designated to monitor crack initiation times and crack propagation. These latter measurements were not made on this program.

5.4 TOES AND HOLES

Two testing anomalies that affected the test development efforts are:

1. "Toes" in the force-time trace
2. Microscopic holes formed in the liner at the crack front.

Special development efforts were required to solve each of these problems. The problems and their solutions are summarized below.

5.4.1   Toes in Force-Time Trace

The initial portion of the force-time trace has a different curvature from that of the remainder of the curve. Figure 69 gives sketches of three different toe shapes observed in this testing. The difference in the strain energy between the curves represents less than 2% of that required to fail the specimen, so that feature is not considered to be important.

Since the toe represents the point of reference for the displacement measurements, there can be a sizeable effect between the different toes. Differences of more than 15% of the critical displacement have been observed. This is clearly a significant effect and required resolution in order to give a proper measure of the critical displacement of the test specimen.

The toe marked "loose assembly" in Figure 69 indicates the curve shape when the effect was initially observed. As techniques were improved in

-117-
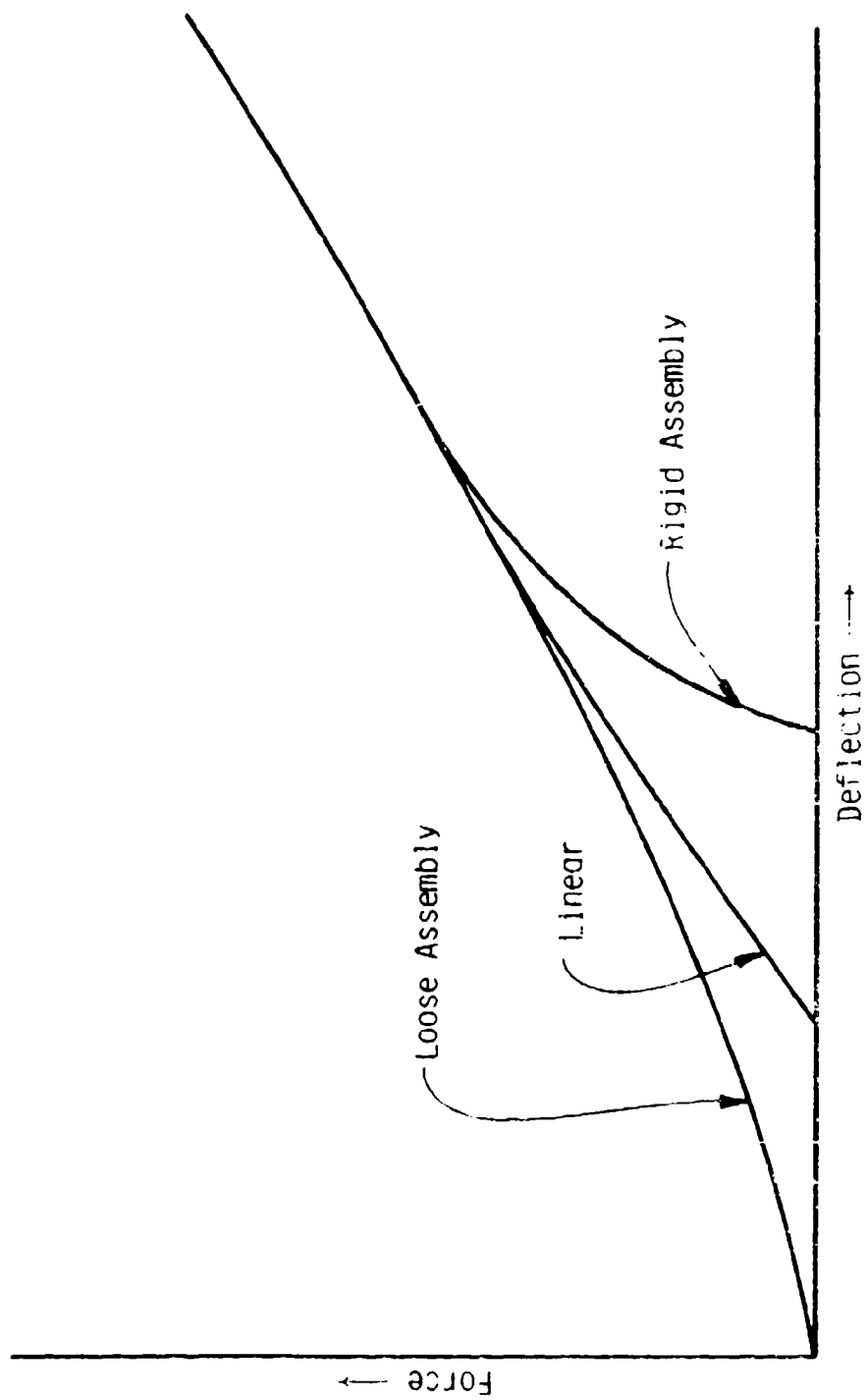
Figure 69. Improvements in "Toe" of the Force-Time Trace

specimen preparation and test alignment, the curve changed to that marked
"linear", then to the "rigid assembly" curve. Later the quality of a test
set-up could often be evaluated by comparison of its toe with the rigid
assembly curve in Figure 69.

5.4.2 Liner Fractures in Advance of Crack Propagation

Micro-fractures* within the weak SD-851-2 liner have been
observed to occur in some specimens prior to the onset of crack propagation.
The microfractures were observed microscopically and found to be of two types;
"tunnels" and "cones". The tunnels were small holes emanating from the edge
of the crack and running perpendicular to the edge (Figure 70b). No attempt
was made to determine the length of the tunnels.

The cones appear to have originated at interior three-
dimensional fractures of the poker-chip type. Then, they propagated to the
propellant-liner interface giving the appearance of an expanding cone.
Figure 70a illustrates this cone, the mechanism of propagation from the three-
dimensional crack is conjectured.

The impact of these microscopic holes upon the strain
energy was negligible, Figure 71. But, the holes did absorb the transmitted
ultrasound and gave an early indication of crack initiation (a large increase
in transit time is suddenly observed).

A correction technique to define the true crack
initiation was devised. It involved looking for a second step in the transit
time. If the transit time step caused by the holes is not large, this second
step is a reasonable indicator of crack initiation. If the first step is
large, then the transit time associated with crack initiation is hidden in the
noise of the data, and no measure of the critical point can be made.

---

* The local three-dimensional stress condition at the crack front and the
  low modulus of liner are blamed for these fractures.

-119-
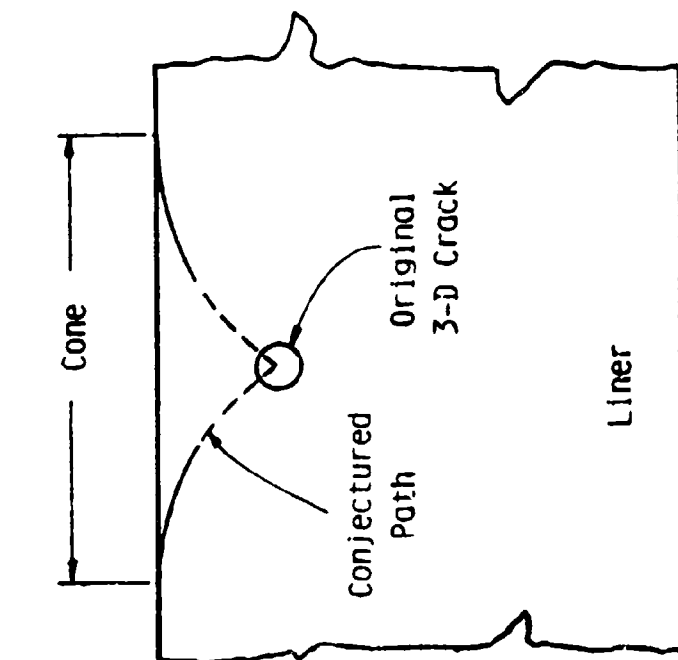
b. Tunnel Fractures

a. Cone Fractures

Figure 70. Tunnel and Cone Fractures in Liner Near the Crack Front

-120-
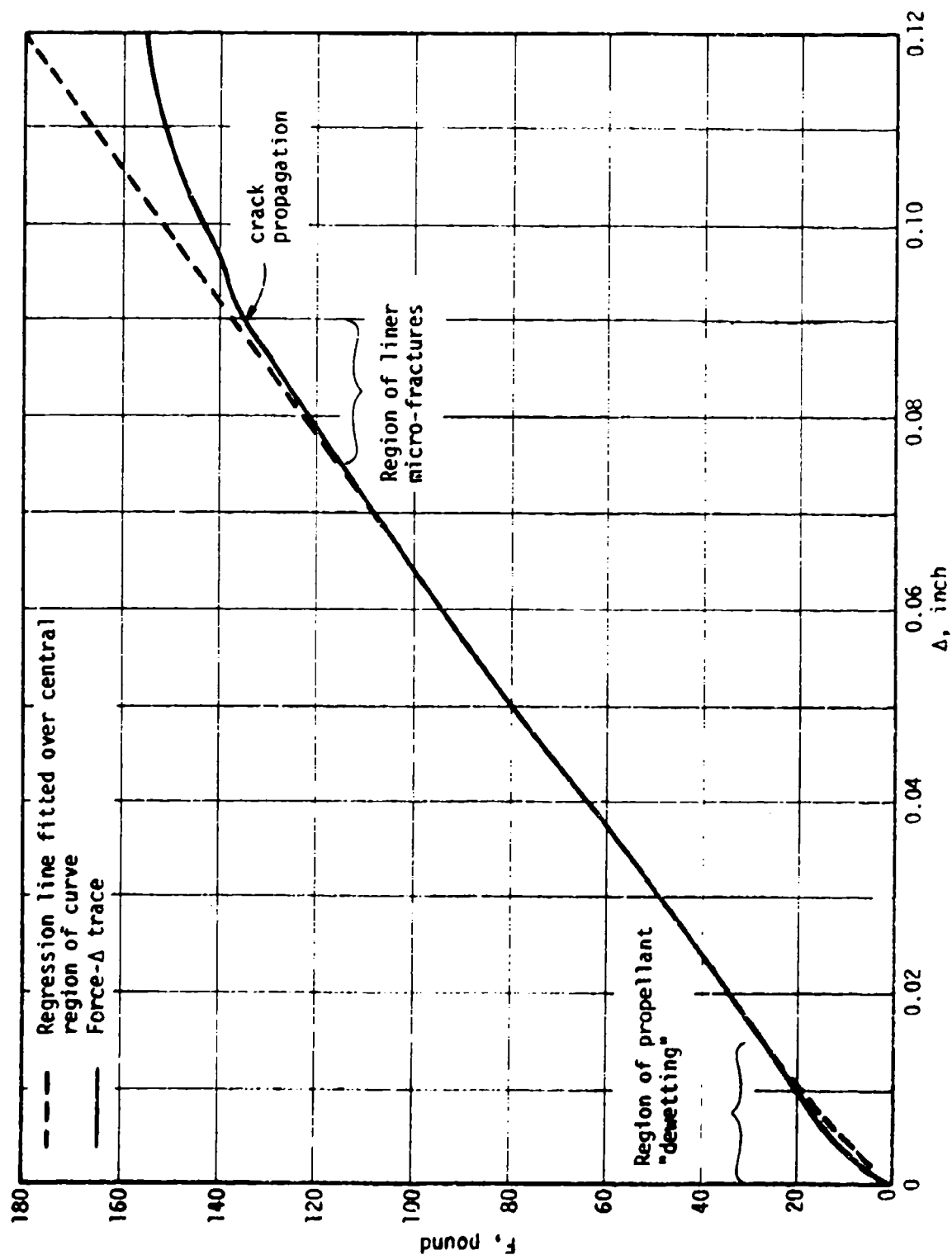
Figure 71. Micro-fracturing and Response Behaviors of Propellant-Liner Bond Specimen. Comparison with Optimum Regression Line

When the acoustic measure does not work, then crack initiation is taken as the point where the curve deviates from a straight line in a log-log plot of F versus U.

5.5 DATA REDUCTION METHODS

There are two methods worth considering. The first is a general method that allows for highly nonlinear behavior. The second is a relatively easier method to use and is based upon the power law relationship. These data reduction methods, together with laboratory observations, lead to a recommended pattern for the testing.

5.5.1 General Method of Data Reduction

This method permits the use of both linear and nonlinear behaviors, as described in Section 2. The J integral is derived from the test data using the following equations:

$$J = -2t^{-m} \frac{\partial}{\partial 2a'} \int_0^U c(2a',U)U^m dU \qquad (80)$$

where: U is the point load tensile displacement of the test specimen
t is the testing time

The values of $c(a,U)$ and m are obtained from crossplots at constant a and U according to the following relationship.

$$f = c(a,U)R^m \qquad (81)$$

where f is a normalized pulling force and R is the crosshead speed

$$f = F/2B \qquad (82)$$

The values of m and $c(a,U)$ were obtained from linear regression analyses of log f versus log R, where R is limited to a narrow range (a factor of 25). Then, integration at constant time is followed by partial differentiation with respect to crack size to obtain J.

-122-

Hand-trimmed specimens of ANB-3066/SD-851-2 propellant-liner
bond (numbered J-71 through J-82) were used to evaluate this method early in
the program. These specimens were tested at 77°F at three crosshead speeds and
five crack sizes.

Table 8 contains a tabulation of the integral $\int_0^U c(a,U)U^m dU$
as a function of U for the five test crack lengths. The partial derivative
of that integral is also tabulated in Table 8 along with the calculated J integral
values, which are also plotted in Figure 72.

To complete the analyses of these specimens, the observed crit-
ical displacements, U_c, are provided in Table 9 along with the corresponding values
of J_{Ic}. The test results are consistent, but are not considered to be accurate
considering the preliminary nature of the specimen preparation and testing
procedures.

5.5.2 Power-Law Approach

This approach is more convenient to use and may be treated
graphically or on a computer. It is an extension of Equation (81) and assumes
a further separation of the variables to give the following power-law relation.

$$f = K(a)\ R^m U^n \tag{83}$$

where K(a) is constant for any given test, but is a function of crack size, a,
while n is an empirical constant. The parameters R, U and m are defined as before.

Table 8. J Integral Values Following the General Method of Analysis*

U, in.	$\int_0^U c(a,U) U^m du$, in.-lb/in.					$-\frac{2a}{\partial 2c^2}\int_0^U c(a,U) U^m du$	J in. - lb/in.²		
	2a' = 0.00 in.	2a' = 0.32 in.	2a' = 0.60 in.	2a' = 1.2 in.	2a' = 2.0 in.		R = 0.02 in./min	R = 0.10 in./min	R = 0.50 in./min
0	0	0	0	0	0	0	0	0	0
0.01	0.032	0.033	0.031	0.028	0.021	.018	.020	.022	.026
0.02	0.135	0.134	0.128	0.117	0.083	.080	.080	.090	.104
0.03	0.316	0.311	0.297	0.270	0.186	.190	.184	.210	.242
0.04	0.579	0.566	0.542	0.489	0.334	.354	.334	.382	.442
0.05	0.927	0.901	0.864	0.775	0.529	.574	.530	.610	.702
0.06	1.363	1.317	1.265	1.131	0.777	.854	.776	.892	1.024
0.07	1.889	1.817	1.747	1.557	1.078	1.194	1.072	1.232	1.418
0.08	2.506	2.400	2.310	2.054	1.430	1.596	1.416	1.626	1.870
0.09	3.216	3.069	2.957	2.622	1.834	2.062	1.810	2.080	2.392
0.10	4.019	3.823	3.687	3.263	2.283	2.592	2.256	2.592	2.978
0.11	4.919	4.664	4.502	3.976	2.783	3.188	2.752	3.162	3.634

* m = 0.163
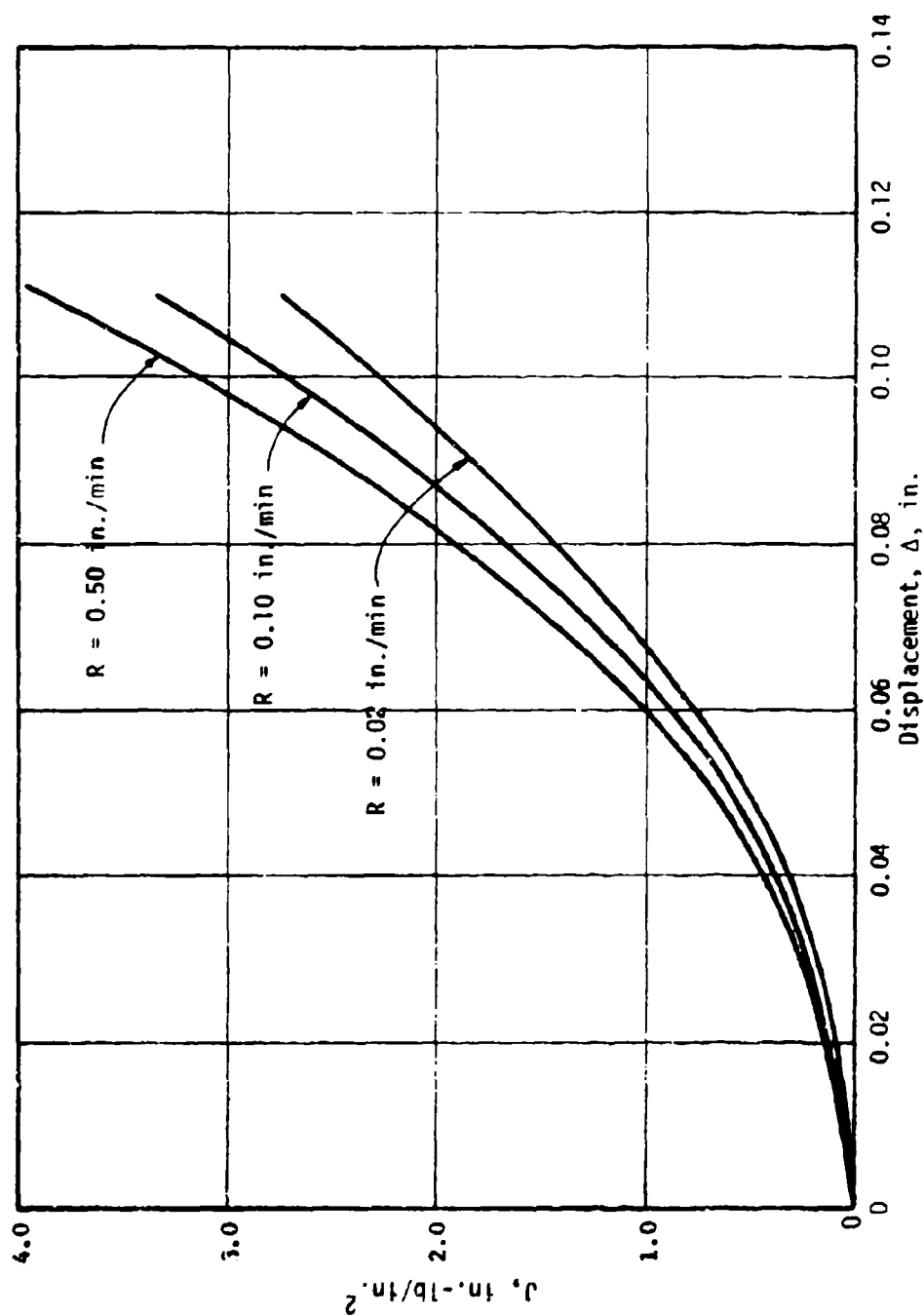
Figure 72. J Integral versus U as Determined by General Method

TABLE 9

CRITICAL VALUES OF THE J INTEGRAL

Specimen No.	Crosshead Speed, R, in./min	Crack Length, 2a', in.	U_c, in.		J_{Ic}, lb/in.
J-75	0.02	0.32	0.107		2.3
J-74	0.10	0.32	0.116		3.5
J-76	0.50	0.32	0.108		3.1
				mean	3.0
J-71	0.02	0.60	0.123		3.5
J-72	0.10	0.60	0.108		2.7
J-73	0.50	0.60	0.109		3.1
				mean	3.1
J-77	0.02	1.2	0.098		2.2
J-78	0.10	1.2	0.118		3.7
J-79	0.50	1.2	0.107		3.1
				mean	3.0
J-80	0.02	2.0	0.110		2.8
J-81	0.10	2.0	0.093		2.6
J-82	0.50	2.0	0.089		2.3
				mean	2.6

The J integral derived from the power-law relation can be of either of the following forms:

$$J = \psi \; t^{-m} U^{1+m+n} \tag{84}$$

or, for constant crosshead speed, R,

$$J = \psi \; R^{m} U^{1+n} \tag{85}$$

where

$$\psi = -\frac{2}{1+m+n} \left(\frac{\partial K(a)}{\partial 2a} \right)_{U,t} \tag{86}$$

Tables 10 through 13 illustrate this data reduction procedure for a set of tests conducted at $0°F$. In this illustration there were 13 specimens tested at five different crack sizes and three crosshead speeds. With this number of specimens the results are reasonable.

The individual values of n were obtained from separate regression analyses of log f versus log U, which usually has correlation coefficients between 0.999 and 0.9999. Typical data are given in Table 10. These values are averaged (a mean of 0.787 is illustrated) then used to force parallel curves through the data to obtain the individual A_o values. The quantity A_o is obtained from the relation

$$f = A_o U^{n} \tag{87}$$

Thus, from Equation (83), we have

$$A_o = K(a) R^{m} \tag{88}$$

The A_o values given in Table 11 are used in regression analyses at constant crack size to obtain the separate values of m, which are also listed in Table 11. These values of m are averaged (a mean of 0.163 is shown), then used to give parallel curves to obtain the individual values of K(a).

-127-

TABLE 10

DETERMINATION OF (n) FROM SPECIMENS
TESTED AT 0°F AT ATMOSPHERIC PRESSURE

Specimen No.	2a, inch	R, in./min	n
5-10	0.2	0.10	0.817
5-12	0.4	0.02	0.773
5-12	0.4	0.10	0.838
5-50	0.4	0.50	0.805
5-30	0.8	0.02	0.840
5-11	0.8	0.10	0.781
5-29	0.8	0.50	0.784
5-31	1.2	0.02	0.772
5-26	1.2	0.10	0.780
5-28	1.2	0.50	0.770
5-49	1.6	0.02	0.740
5-27	1.6	0.10	0.776
5-56	1.6	0.50	0.756

mean = 0.787

TABLE 11

DETERMINATION OF (m) FROM A_o VALUES TAKEN ON SPECIMENS
TESTED AT 0°F AT ATMOSPHERIC PRESSURE

Specimen No.	2a, inch	R, in./min	A_o	m
5-52	0.4	0.02	1108	0.136
5-12	0.4	0.10	1436	
5-50	0.4	0.50	1715	
5-30	0.8	0.02	913.7	0.157
5-11	0.8	0.10	1195	
5-29	0.8	0.50	1513	
5-31	1.2	0.02	872.5	0.157
5-26	1.2	0.10	1070	
5-28	1.2	0.50	1448	
5-49	1.6	0.02	659.3	0.203
5-27	1.6	0.10	940.8	
5-56	1.6	0.50	1267	

mean = 0.163

Then, all of the K(a) values reported in Table 12 are used in
a further regression analysis versus crack size (2a') to obtain the
$\left(\dfrac{\partial K(a)}{\partial 2a'} \right)_{R,U}$ value which equals -590 in this case.

Inserting the constants obtained above into Equation (84)
gives

$$J = 605t^{-0.163}U^{1.95} \qquad (89)$$

The exponent on U is very close to the ideal value of 2, which theoretically
applies to elastic materials.

The constant rate form of the J integral is

$$J = 605R^{0.163}U^{1.79} \qquad (90)$$

As in the general method, J-critical is obtained from U_c. The
J values of this test are given in Table 13, and yield an average value of
$3.56 \dfrac{in.-lb}{in.^2}$.

Fracture Approach

Combining Equations (83) and (85) and taking the
values at the critical point gives the following interesting relation for J_{IC}.

$$J_{IC} = \Psi \left[\frac{f_c U_c}{K(a)} \right] \qquad (91)$$

Within experiment error the quantity inside the
bracket is a constant over the test matrix. S. Ψ is a constant then
J_{IC} is also.

The constancy of $f_c U_c / K(a)$ is illustrated in Table 14:
there the mean value is 5.96×10^{-3}. Inserting this quantity into Equation (91),
and taking the previously used value of $\Psi = 605$, gave $J_{IC} = 3.61$ in.-lb/in.^{2}. This
value is almost identical to that given in Table 13.

TABLE 12

DETERMINATION OF $(\partial K(a)/\partial 2a')_{R,U}$
FROM SPECIMENS TESTED AT 0°F
AT ATMOSPHERIC PRESSURE

Specimen No.	R, in./min	2a', in.	K(a)	$[\partial K(a)/\partial 2a']_{R,U}$
5-52	0.02	0.4	2099	
5-30	0.02	0.8	1729	
5-31	0.02	1.2	1652	-657.5
5-49	0.02	1.6	1248	
5-10	0.10	0.2	2293	
5-12	0.10	0.4	2091	
5-11	0.10	0.8	1739	-652.0
5-26	0.10	1.2	1557	
5-27	0.10	1.6	1370	
5-50	0.50	0.4	1920	
5-29	0.50	0.8	1694	
5-28	0.50	1.2	1622	-393.8
5-56	0.50	1.6	1419	

overall value = -590.1

TABLE 13

DETERMINATION OF J_{1c} CRITICAL FROM SPECIMENS TESTED AT 0°F AT ATMOSPHERIC PRESSURE

Specimen No.	R, in./min	2a, inch	U_c, inch	$J_{1c} = \dfrac{605_t{}^{-0.163}U_c{}^{1.95}}{}$, $\dfrac{in.-lb}{in.^2}$
5-52	0.02	0.4	–	
5-30	0.02	0.8	0.093	
5-31	0.02	1.2	0.087	
5-49	0.02	1.6	0.073	
			mean = 3.82	
5-10	0.10	0.2	–	
5-12	0.10	0.4	–	
5-11	0.10	0.6	0.073	
5-26	0.10	1.2	0.073	
5-27	0.10	1.6	0.063	
			3.59	
5-50	0.50	0.4	–	
5-29	0.50	0.8	0.050	
5-28	0.50	1.2	0.068	
5-56	0.50	1.6	0.053	
			mean = 3.23	
			mean = 3.56	

-122-

TABLE 14

Determination of the Constancy of Critical Ratio $f_c U_c/K(a)$

from Specimens Tested at 0°F at Atmospheric Pressure

Specimen No.	2a', in.	R, in./min	K(a)	f_c	U_c	$f_c U_c/K(a)$
5-10	0.2	0.10	2293	-------	-------	------- SBF -------
5-52	0.4	0.02	2099	-------	-------	------- SBF -------
5-12	0.4	0.10	2091	-------	-------	------- SBF -------
5-50	0.4	0.50	1921	-------	-------	------- SBF -------
5-30	0.8	0.02	1729	142.4	0.093	7.66×10^{-3}
5-11	0.8	0.10	1739	153.1	0.073	6.43×10^{-3}
5-29	0.8	0.50	1694	151.4	0.05	4.47×10^{-3}
5-31	1.2	0.02	1652	123.5	0.087	6.50×10^{-3}
5-26	1.2	0.10	1557	135.1	0.073	6.33×10^{-3}
5-28	1.2	0.50	1622	173.4	0.068	7.27×10^{-3}
5-49	1.6	0.02	1248	81.8	0.073	4.78×10^{-3}
5-27	1.6	0.10	1370	107.8	0.063	5.35×10^{-3}
5-56	1.6	0.50	1419	130.0	0.053	4.86×10^{-3}
					Mean	5.96×10^{-3}

SBF: Secondary Bond Failure

The real value of Equation (91) is that it provides an internal check on the critical value determinations.

5.5.3 Preferred Test Matrix

Analyses of various test results using the power-law method have demonstrated the need for:

- Test replications sufficient to eliminate or minimize the effects of bad data
- As wide a range as possible for the crack sizes (an upper limit of 1.6-inches was previously established)
- At least three deformation rates

A test pattern like the following is recommended as a minimum effort. A reduced test matrix with half this number of tests was followed on this program.

Crosshead Speed in./min	Tests at Crack Size 2a', in.			
	0.4	0.8	1.2	1.6
0.01	X	XX	XX	X
0.10	X	XX	XX	X
1.00	X	XX	XX	X

X indicates a single test to be performed under the indicated conditions.

6.0   EVALUATIONS UNDER STRESS CONDITIONS THAT DUPLICATE THOSE 1 . MOTOR

The goal here is to evaluate the J integral under typical motor loading
conditions, then compare the results to find the extent of the change. Only
three sets of tests were conducted. The first provided measures of the J
integral under superimposed pressures. The second was a series of tests under
combined tension and shear, while the third evaluated the effects of simultaneous
cooling and deformation.

All of the force-displacement data for these tests are reported in
Appendix B. The tests were all performed on bond specimens of ANB-3066/SD-851-2/
V-45, propellant/liner/insulation. Different propellant batches were used in
each test matrix so the results may not correlate. Also, variations in some
experimental procedures did occur because of attempts to improve them.

6.1   EFFECTS OF SUPERIMPOSED PRESSURES

This testing involved measurements at three superimposed pressures
(atmospheric, 500 and 1000 psig) at two test temperatures, 0 and 77°F. They
were the first tests to be conducted in the MTS hydraulic tester, which
is a low compliance system that allowed a rigid connection to the load cell.
When this work was conducted the test methods were still in development, so
some variations in testing sequences occurred. The test matrix conducted
in this effort are provided in Table 15, while the individual test results
are given in Appendix B, Tables B-5-1 through B-5-6.

The data reduction followed the procedures described in Section 5
for the power-law relation. The key parameters derived from the raw data
are tabulated in Tables 16 through 21. Ideally, in each test matrix the
values of n should be the same for all of the tests, while the values of
m (calculated at each crack size) should be the same over the test matrix.
The K(a) values should be independent of crosshead rate, but vary with crack
size. These generalizations seem to be supported in each of the derived data
tabulations (Tables 16 through 21).

TABLE 15

TESTS CONDUCTED UNDER SUPERIMPOSED PRESSURES USING THE STANDARD SPECIMEN WITH ANB-3066/SD-851-2/V-45

Temp., °F	Superimposed Pressure, psi	Crosshead Speed, in./min	2a', in. =	Test Matrices				
				0.2	0.4	0.8	1.2	1.6
0	0	0.02			X	X	X	X
		0.10		X	X	X	X	X
		0.50			X	X	X	X
	500	0.02			X		X	X
		0.10			X		X	X
		0.50			X		X	
	1000	0.02			X		XX	
		0.10			X		X	XX
		0.50			X		XX	
77	0	0.02			X	X	X	X
		0.10		X	XX	X	X	X
		0.50			X	X	X	
	500	0.02			X	X	X	X
		0.10			X	X	X	X
		0.50			X		X	
	1000	0.02			X		XX	
		0.10			X		X	XX
		0.50			X		XX	

X indicates test conducted.

TABLE 16

DERIVED VALUES FROM TESTS OF ANB-3066/SD-851-2 PROPELLANT/LINER BOND AT ATMOSPHERIC PRESSURE AND 0°F

Specimen No.	$2a'$, in.	$\dot{R}$, in./min	a	m	$K(a)$	$(\partial K(a)/\partial 2a')_{\dot{R},U}$	U_c, in.
5-10	0.2	0.10	0.817	0.136	2293	-590.1	*SBF
5-57	0.4	0.02	0.773		2098		SBF
5-12	0.4	0.10	0.838		2091		SBF
5-50	0.4	0.50	0.805		1920		SBF
5-30	0.8	0.02	0.840	0.157	1729		0.093
5-11	0.8	0.10	0.781		1739		0.073
5-29	0.8	0.50	0.784		1594		0.050
5-31	1.2	0.02	0.772	0.157	1652		0.087
5-26	1.2	0.10	0.780		1557		0.073
5-28	1.2	0.50	0.770		1622		0.068
5-49	1.6	0.02	0.740	0.203	1248		0.073
5-27	1.6	0.10	0.776		1370		0.063
5-56	1.6	0.50	0.758		1419		0.053
			mean = 0.787	mean = 0.163			

* SBF : Secondary Bond Failure

-137-

TABLE 17

DERIVED VALUES FROM TESTS OF ANB-3066/SD-851-2 PROPELLANT/LINER BOND UNDER A SUPERIMPOSED PRESSURE OF 500 PSIG AT 0°F

Specimen No.	2a', in.	R, in./min	n	m	K(a)	$(\partial K(a)/\partial 2a')_{R,U}$	U_c, in.
5-41	0.4	0.02	0.857	0.1189	2106	-478	*SBF
5-41	0.4	0.10	0.804		2509		SBF
5-40	0.4	0.50	0.815		2184		SBF
5-34	1.2	0.02	0.826	0.1083	2047		0.138
5-39	1.2	0.10	0.841		1720		0.121
5-38	1.2	0.50	0.839		2071		0.108
5-47	1.6	0.02	0.803	0.0960	1681		0.118
5-46	1.6	0.10	0.777		1649		0.097
			mean = 0.820	mean = 0.108			

* SBF = Secondary Bond Failure

-138-

TABLE 18

DERIVED VALUES FROM TESTS OF ANB-3066/SD-851-2 PROPELLANT/LINER BOND UNDER A SUPERIMPOSED PRESSURE OF 1000 PSIG AT 0°F

Specimen No.	2a', in.	R, in./min	a	m	E(o)	$(\partial K(o)/\partial 2a')_{R,U}$	U_c, in.
5-51	0.4	0.02	.8233		3314		*SBF
5-57	0.4	0.10	.8018	0.1259	3329	-1180	SBF
5-58*	0.4	0.50	.8103		2704		SBF
5-65	1.2	0.02	.8531		2225		0.148
5-113	1.2	0.02	.8448		1908		0.118
5-48	1.2	0.10	.8267		2155		0.118
5-53	1.2	0.50	.7702		2161		0.138
5-119	1.2	0.50	.8087		2182		0.108
5-116	1.6	0.10	.8027		1829		0.108
5-117	1.6	0.10	.8587		1640		0.108
			mean = .820	mean = 0.142			

* Outlier, excluded from further analyses
** Secondary Bond Failure

TABLE 19

DERIVED VALUES FROM TESTS OF ANB-3066/SD-851-2 PROPELLANT/LINER BOND AT ATMOSPHERIC PRESSURE AND 77°F

Specimen No.	$2a'$, in.	R, in./min	n	m	$K(a)$	$\left(\dfrac{\partial K(a)}{\partial 2a'}\right)_{R,U}$	U_c, in.
5-9	0.2	0.10	0.89	0.1763	1054	-204.3	*SBF
5-32	0.4	0.02	0.951		945**		SBF
5-1	0.4	0.10	0.940		1248		SBF
5-33	0.4	0.10	0.954		1027		SBF
5-25	0.4	0.50	0.911		1071		SBF
5-6	0.8	0.02	0.921	0.1567	977		0.105
5-7	0.8	0.10	0.941		1037		0.099
5-8	0.8	0.50	0.899		1040		0.096
5-3	1.2	0.02	0.932	0.0894	1036		0.094
5-4	1.2	0.10	0.803		893		0.090
5-5	1.2	0.50	0.84		888		0.093
5-42	1.6	0.02	0.946	0.1269	893		0.093
5-2	1.6	0.10	0.958		877		0.084
			mean = 0.911	mean = 0.137			

* SBF - Secondary Bond Failure
** Outlier, excluded from subsequent analyses

-140-

TABLE 20

DERIVED VALUES FROM TESTS OF ANB-3066/SD-851-2 PROPELLANT/LINER BOND UNDER A SUPERIMPOSED PRESSURE OF 500 PSIG AT 77°F

Specimen No.	$2a'$, in.	R, in./min	n	a	$K(a)$	$\partial K(a)/\partial 2a')_{R,U}$	U_c, in.
5-15	0.4	0.02	0.940	0.1165	1109	-272.6	a SBF
5-21	0.4	0.10	0.976		1262		SBF
5-13	0.4	0.50	0.944		1090		SBF
5-24	0.8	0.02	0.917		1034		0.123
5-20	0.8	0.10	0.892		941		0.118
5-34	1.2	0.02	0.967	0.1275	942		0.108
5-23	1.2	0.10	0.936		926		0.123
5-18	1.7	0.50	0.907		959		0.098
5-36	1.6	0.10	0.934		757		0.098
5-19	1.6	0.50	0.869		859		0.118
			mean = 0.928	mean = 0.122			

a SBF - Secondary Bond Failure

TABLE 21

DERIVED VALUES FROM TESTS OF ANB-3066/SD-851-2 PROPELLANT/LINER BOND UNDER A SUPERIMPOSED PRESSURE OF 1000 PSIG AT 77°F

Specimen No.	$2a'$, in.	R, in./min	$\bar{a}$	$\bar{m}$	$K(a)$	$(\partial K(a)/\partial 2a')_{R,U}$	U_c, in.
5-15	0.4	0.02	0.913	0.0689*	1067	214.5	***SBF
5-14	0.4	0.10	0.945		1070		SBF
5-17	0.4	0.50	0.865		985		SBF
5-109	1.2	0.02	0.910	0.938	892		.103
5-22	1.2	0.02	0.933		941		.133
5-37	1.2	0.10	0.939		759**		.131
5-16	1.2	0.50	0.923		980		.130
5-114	1.2	0.50	0.916		857		.120
5-107	1.6	0.10	0.873		778		.104
5-112	1.6	0.10	0.894		765		.108
			mean = 0.914	mean = 0.094			

* low values of a, the largest used in analyses

** Outlier, not used in subsequent analyses

*** SBF - Secondary Bond Failure

For convenience, the final parameters are summarized in Table 22, along with the critical values of the J integral, J_{1c}. The key feature of these data is that the quantity $1+m+n$ is nearly equal to 2 and varies little with the test conditions. The variations in Ψ (hence of J_{1c} stem directly from those in $\left(\frac{\partial K(a)}{\partial 2a'}\right)_{R,U}$ as given in Equation (86).

$$\Psi = \frac{-2}{1+m+n}\left(\frac{\partial K(a)}{\partial 2a'}\right)_{R,U} \tag{86}$$

The parameter $K(a)$ depends somewhat upon specimen stiffness, so we should expect it to be significantly affected by temperature and super-imposed pressure as well as crack size. Thus, temperature and pressure dependencies are to be expected for the J integral. The results in Table 22 exhibit a small pressure dependence at 77°F and a large effect at 0°F. At atmospheric pressure, the J_{1c} value at 0°F is more than twice that at 77°F.

The statistical variations of the data in Table 22 stem from variabilities of specimen dimensions and liner thicknesses (typically, 0.02 to 0.06 in. within a single specimen) plus errors in defining fracture initiations. Some of these effects were corrected by improved techniques, others can only be handled by replicate testing of a larger number of test specimens.

6.2   TESTS UNDER COMBINED TENSION AND SHEAR

In case-bonded grains near grain ends or boot release points, there are several loading conditions that produce axial shear stresses combined with radial normal stresses. When the loading condition is due to low temperature cooling the normal stress is tensile. This combined stress condition can be approximately duplicated in the scarf-joint specimen upon pulling it at an angle as illustrated in Figure 73. When pulled in this fashion the specimen bondline experiences both shear and tensile force components.

TABLE 22

SUMMARY OF REDUCED TEST PARAMETERS FOR THE SUPERIMPOSED PRESSURE TESTS OF ANB-3066/SD-851-2 PROPELLANT/LINER BOND AT 0 AND 77°F

Test Temperature °F	Superimposed Pressure psig	m	n	1+m+n	P	J_{IC}, in.-lb/in.^{2}
77	0	0.137	0.911	2.048	199.5	1.53
	500	0.122	0.928	2.050	266	3.00
	1000	0.094	0.914	2.008	214	2.99
0	0	0.163	0.787	1.950	605	3.75
	500	0.108	0.820	1.928	496	6.44
	1000	0.142	0.820	1.962	1200	18.4
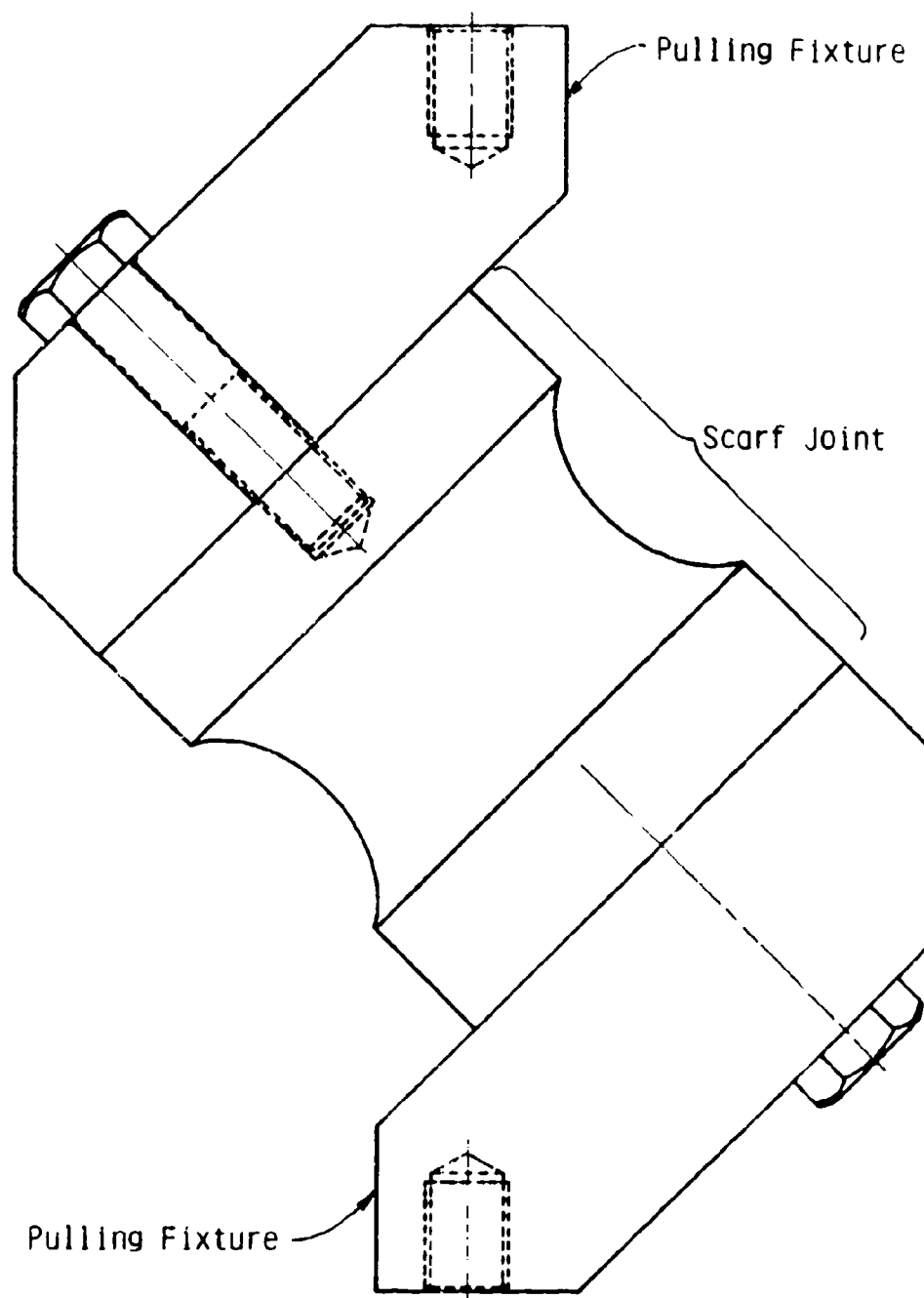
Figure 73. Fixtures for Testing the Scarf-Joint Specimen in Combined
Tension and Shear

The normal component of the deformation was measured by four extensometers, shown in the photograph of Figure 74. There was, in addition, one extensometer which measured the shear component of the deformation (also shown in Figure 74). A sketch of the shear component extensometer is given in Figure 75. Excellent comparisons were obtained between these measurements and the corresponding components calculated from the crosshead movement. These latter measurements, therefore, were used in all of the data analyses.

The normal and shear components are rectified upon considering that the specimen in its usual tensile test mode is at an angle of 0°. Rotating the specimen to some angle θ like that in Figure 73 produces at the bondline a shear force component, f_τ, and a normal force component, f_n, defined by

$$f_\tau = f \sin \theta \qquad (92)$$

$$f_n = f \cos \theta \qquad (93)$$

where f is the overall pulling force.

Similar shear and normal components* are needed for the crosshead rate (R_τ and R_n), displacement (U_τ and U_n), and the intercept constant $[K_\tau(a)$ and $K_n(a)]$. Thus, the power-law relations (see Equation (85)) become

$$f_\tau = K_\tau(a) \, R_\tau^{\,m} \, U_\tau^{\,n} \qquad (94)$$

$$f_n = K_n(a) \, R_n^{\,m} \, U_\tau^{\,n} \qquad (95)$$

---

* R_τ	=	$R \sin \theta$
R_n	=	$R \cos \theta$
U_τ	=	$U \sin \theta$
U_n	=	$U \cos \theta$
$K_\tau(a)$	=	$K(a) \sin \theta$
$K_n(a)$	=	$K(a) \cos \theta$
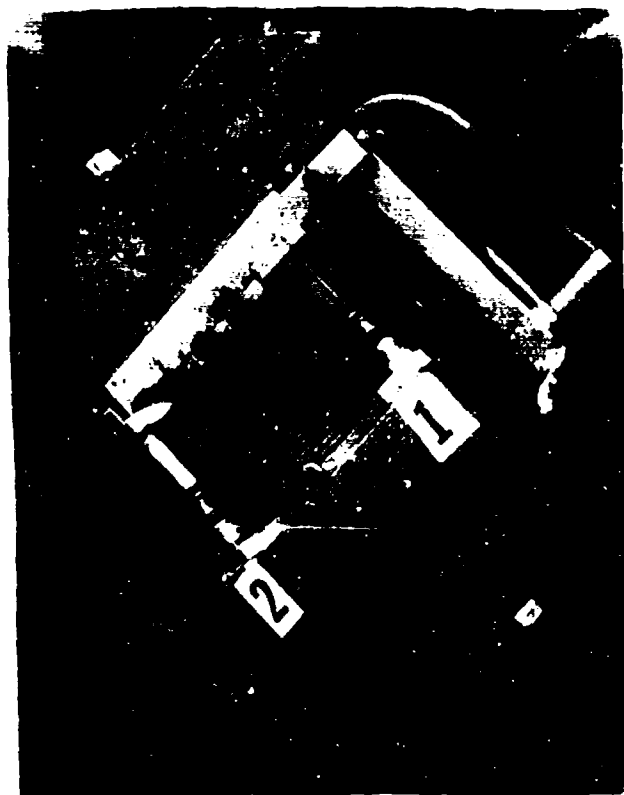
Figure 74.   Scarf-Joint Specimen with
Extensometers Mounted for the
Measurement of Shear and Normal
Components of the Deformation

Top View

"Over-Bite" Clamp

Linear Potentiometer
(One Channel Extensometer)

Side View

Thumb Screws
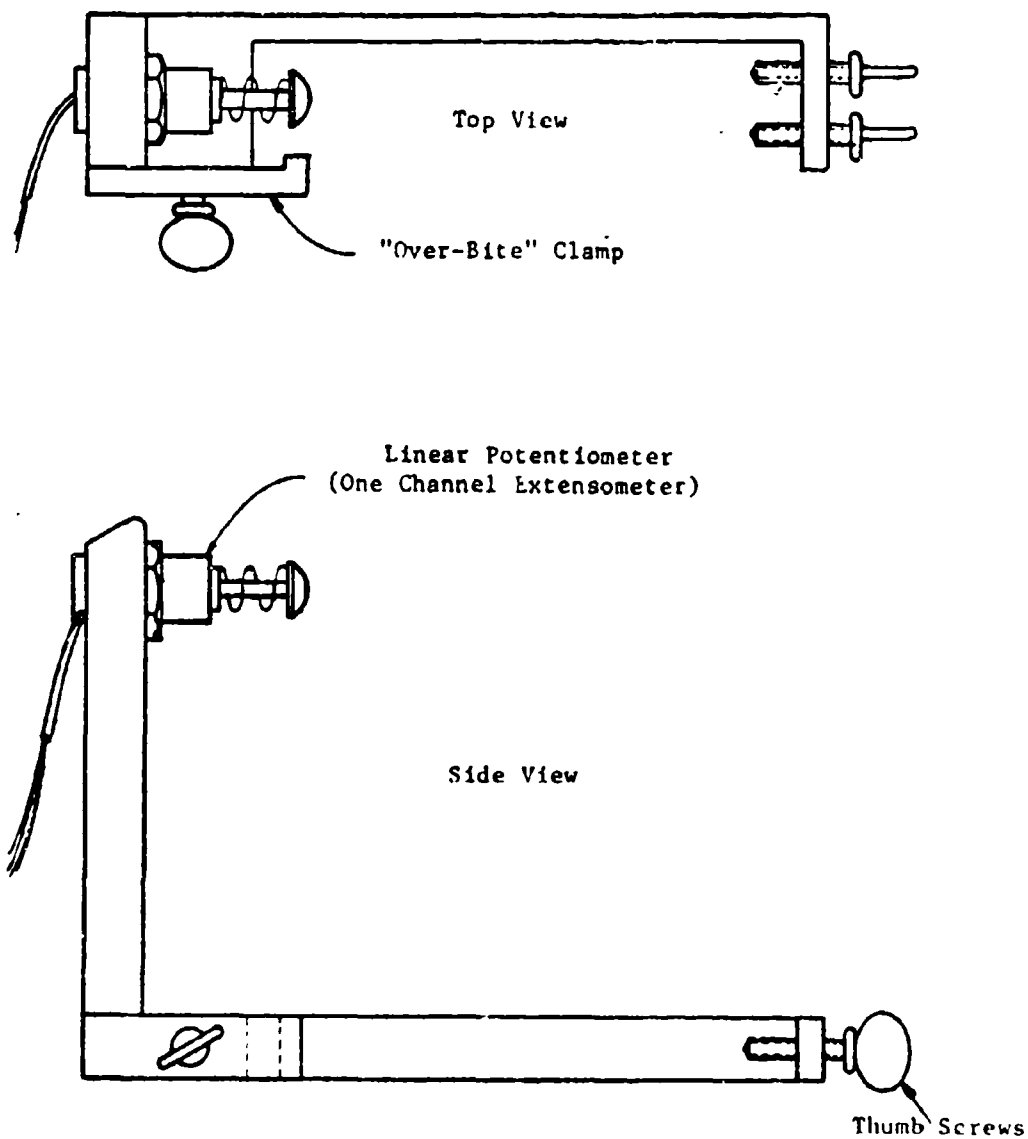
Figure 75.   Shear Component Extensometer

(Used in measuring shear deformation in
combined tension/shear test configuration)

The exponents m and n are not affected by the component rectification.

The J integral relation, Equation (84), becomes for the normal component, J_I,

$$J_I = \Psi_n t^{-m} U_t^{1+m+n} \qquad (96)$$

and the shear component, J_τ.

$$J_{II} = \Psi_\tau t^{-m} U_\tau^{1+m+n} \qquad (97)$$

The total J integral, J, is given by

$$J = J_I + J_{II} \qquad (98)$$

Observations of thermal stress analyses of motors show that the shear component never exceeds the normal component; that is, $\theta \leq 45°$. Also, at the grain ends or boot release points, a typical value for the scarf angle, θ, is about 30°. The test plan in Table 23 was devised in terms of these two scarf angles, 30 and 45°. It provides for tests at 0 and 77°F, with two scarf angles, three crosshead speeds and three crack sizes.

The test results are given as force versus displacement data in Appendix B in Tables B-6-1 through B-6-4. Tables 24 through 27 contain the derived values of m and n and the normal and shear components of R, K(a), $(\partial K(a)/\partial 2a')_{R,U}$ and U_c. Table 28 summarizes the key parameters and gives the average values of J_{Ic}, J_{IIc} and the Total J_c.

The J_c values at 0°F are 2.65 and 3.90 $\frac{in.-lb}{in.^2}$ for the 30 and 45° scarf angles, respectively. Better agreement between the two scarf angles was obtained at 77°F, with J_c equal to 1.08 and 1.10 $\frac{in.-lb}{in.^2}$. The standard angle scarf-joint test data (see Table 22) gave J_{Ic} values (equal to J_c for this case) of 3.75 and 1.53 $\frac{in.-lb}{in.^2}$ for 0 and 77°F tests, respectively, which are in good agreement with the above data.

-149-

TABLE 23

TESTS UNDER COMBINED TENSION AND SHEAR USING THE STANDARD
SPECIMEN WITH ANB-3066/SD-851-2/V-45,
PROPELLANT/LINER/INSULATION

Temp., °F	Loading Angle	Crosshead Rate, in./min	2a', in. =	Test Matrices				
				0.2	0.4	0.8	1.2	1.6
0	30°	0.02			X		X	X
		0.10			X		X	X
		0.50			X		X	X
	45°	0.02					X	XX
		0.10					X	X
		0.50			X		X	
77	30°	0.02			X		X	X
		0.10			XX		X	X
		0.50			XX		XX	X
	45°	0.02			X		X	X
		0.10			X		X	
		0.20			X		X	X
		0.50			X		X	X

X indicates test conducted.

TABLE 24

DERIVED VALUES FROM BONDLINE TESTS AT A SCARF ANGLE OF 30°F AT 0°F. TESTS OF ANB-3066/SD-851-2 PROPELLANT/LINER BOND

Specimen No.	$2a'$, in.	R_o, in./min	R_T, in./min	$\bar{m}$	m	$K_m(a)$	$K_T(a)$	$(X_m(a)/2a')_{R,U}$	$(X_T(a)/2a')_{R,U}$	U_{ac}, in.	U_{tc}, in.
6-56	0.4	0.01732	0.01	0.9046	0.0971	893.6	995.3		-149.2	**SBF	SBF
6-113	0.4	0.08660	0.05	0.8235		961.4	1021.2	-153.4		SBF	SBF
6-82	0.4	0.43301	0.25	0.8829		873.2	884.7			SBF	SBF
6-92	1.2	0.01732	0.01	1.0800	0.1002	612.9	682.6*			0.086	0.050
6-93	1.2	0.08660	0.05	0.6622		808.9	859.3			0.095	0.055
6-87	1.2	0.43301	0.25	0.8384		803.7	814.2			0.129	0.074
6-110	1.6	0.01732	0.01	0.8472	0.1155	697.7	777.1			0.110	0.063
6-84	1.6	0.08660	0.05	0.8122		744.1	790.4			0.105	0.060
6-61	1.6	0.43301	0.25	0.7811		723.4	733.0			0.105	0.060

mean = 0.845   mean = 0.104

* Outlier, not used in subsequent analysis

** SBF - Secondary Bond Failure

TABLE 25

DERIVED VALUES FROM BONDLINE TESTS AT A SCARF ANGLE OF 45°F AT 0°F. TESTS OF ANB-3066/SD-851-2 PROPELLANT/LINER BOND

Specimen No.	(a'), in.	$R_n = R_T$, in./min	n	$R_n(\sigma) = R_T(\pi)$	$K_n(\sigma) - K_T(\pi)$	$(2K_n(\sigma)/2\pi a')_{R_1 U} = (2K_T(\sigma)/2a')_{R_1 U}$	$U_{oc} = U_{tc}$, in.
6-59	0.4	0.3536	0.8802		689.3	-173.3	0.095
6-76	1.2	0.0141	0.8012	0.0652	605.0		0.071
6-77	1.2	0.0707	0.8784		505.3		0.110
6-89	1.2	0.3536	0.9619		551.2		0.117
6-80	1.6	0.0141	0.9266	0.1231	406.3*		0.113
6-83	1.6	0.0141	0.7450		493.5		0.074
6-62	1.6	0.0707	0.8667		469.2		0.132

mean = 0.8689 mean = 0.0942

* Excluded from subsequent analysis.

-152-

TABLE 26

DERIVED VALUES FROM BONDLINE TESTS AT A SCARP ANGLE OF 30° AT 77°F. TESTS OF ANB-3066/SD-851-2 PROPELLANT/LINER BOND

Specimen No.	$2a'$, in.	R_n, in./min	R_v, in./min	a	a	$K_a(a)$	$K_v(a)$	$(\partial K_a(a)/\partial 2a')_{R,U}$	$(\partial K_v(a)/\partial 2a')_{R,U}$	U_{mc}, in.	U_{tc}, in.
6-61	0.4	.01732	0.01	.9089	.0763	596.4	613.9			**SBF	SBF
6-59	0.4	.0866	0.05	.9807		547.6	560.0	-65.82	-67.68	SBF	SBF
6-85	0.4	.0866	0.05	.9871		520.4	532.1			SBF	SBF
6-62	0.4	.4330	0.25	.8692		573.1	582.2			SBF	SBF
6-914	0.4	.4330	0.25	1.0092		466.6	507.7			SBF	SBF
6-68	1.2	.01732	0.01	.9439	.1002	510.6	525.5			0.095	0.055
6-63	1.2	.0866	0.05	.9488		509.6	521.1			0.126	0.073
6-60	1.2	.4330	0.25	.9388		522.5	530.8			0.115	0.064
6-65		.4330	0.25	.8715		533.5	541.5			0.120	0.070
6-64	1.6	.01732	0.01	.9560	.1181	453.4	466.6			0.108	0.063
6-55	1.6	.0866	0.05	.8943		474.0	484.7			0.121	0.070
6-56	1.6	.4330	0.25	.8503		490.4	506.3			0.133	0.065

mean = .9297   mean = .0982

* Excluded from subsequent analysis.

** SBF - Secondary Bond Failure

-153-

TABLE 27

DERIVED VALUES FROM BONDLINE TESTS AT A SCARF ANGEL OF
45°F AT 77°F. TESTS OF ANB-3066/SD-851-2
PROPELLANT/LINER BOND

Specimen t.	±a', in.	$R = R_T$, in./min	n	m	$K_n(a) - K_T(a)$	$(\partial K_n(a)/\partial 2a')_{R,U}$ &	$(\partial K_T(a)/2a')_{R,U}$	$U_{oc} - U_{fc}$, in.
6-98	0.4	0.0141	1.0201	-	353.3			SBF
6-74	0.4	0.0707	0.9367		343.9	-47.11		0.124
6-66	0.4	0.1414	0.9214		297.9			SBF
6-75	0.4	0.3536	0.9817		291.3			SBF
6-71	1.2	0.0141	1.0028	0.0926	262.6			0.106
6-70	1.2	0.0707	0.9474		297.7			0.120
6-67	1.2	0.1414	0.8769		335.6a			0.113
6-73	1.2	0.3536	0.9397		276.2			0.126
6-90	1.6	0.0141	1.0033	0.0283	283.7			0.092
6-78	1.6	0.1414	0.8343		259.6			0.120
6-72	1.6	0.3536	0.9997		257.0			0.095
			mean = 0.951	mean = 0.0605				

* Outlier, not used in subsequent analysis.

TABLE 28

SUMMARY OF COMBINED TENSION AND SHEAR TESTS
OF ANB-3066/SD-851-2 PROPELLANT/LINER BOND

Temp. °F	Scarf Angle	n	m	1+m+n	Ψ_n	Ψ_τ	J_{Ic}	J_{IIc}	J_c, $\dfrac{\text{in.-lb}}{\text{in.}^2}$
0	30°	0.845	0.104	1.949	157.4	153.1	1.99	0.66	2.65
	45°	0.869	0.094	1.963	176.6	176.6	1.95	1.95	3.90
77	30°	0.930	0.098	2.028	64.91	66.75	0.81	0.27	1.08
	45°	0.951	0.061	2.012	46.83	46.83	0.55	0.55	1.10

6.3 SIMULTANEOUS COOLING AND STRAINING TESTS

The condition of temperature cycling in a case-bonded propellant
grain involves simultaneous cooling and straining as an important loading
mode. The testing planned here is an attempt to duplicate that loading in
the scarf-joint specimen.

The test plan was developed after thermal analyses (given in
Appendix C) of the scarf-joint specimen predicted that at 47°F/hr rate of
temperature change a maximum thermal gradient of 5°F would be obtained. This
was considered to be the maximum tolerable thermal gradient for the test.

The actual matrices completed in the program are listed in
Table 29. There were three temperatule ranges (125 to 70°F, 125 to 40°F and
125 to 0°F), three temperature change rates and four crack sizes. The tests
to 0°F were originally planned, while those to 70°F were not. The test
matrices are incomplete due to a loss of test specimens during the preliminary
check-out of the equipment and test procedures. The tests from 125 to 0°F
were stopped after a few tests because of temperature control problems below
40°F. This test matrix was then replaced by that for the 125 to 70"F
test plan.

Another test anomaly was encountered and not solved until most of
the testing was complete. The tests were conducted on an MTS hydraulic tester
the piston of which produced a small torsional moment in the test specimen.
The moments would accumulate then release in a stick-slip fashion that yielded
a slightly jagged force-time trace.   Occasionally, a large moment would
accumulate and release making the force-deformation trace unusable. The loss
of the test data further reduced the test matrices.

The available data (tabulated in Appendix B, Tables B-7-1, B-7-2
and B-7-3) were evaluated as well as possible considering their incomplete
nature. The derived values are provided in Tables 30, 31 and 32 and the
results summarized in Table 33. The test results must be considered to be
crude in spice of the apparently good agreement of the J_{1c} values (0.46 to

$$0.59 \; \frac{\text{in.-lb}}{\text{in.}^2}.$$

The test data were reduced assuming temperature independence* of the J integral and applicability of the power-law relation. This is a reasonable assumption for the temperature ranges used because of the very low deformation rates and the low temperature dependence of the ANB-3066 propellant, which uses a CTPB polymeric binder.

(

---

* A theoretical method was developed by Shapery to do this, but requires parallel tests on uncracked test specimens. This procedure was not known at the time the tests were conducted.

TABLE 29

TEST PLAN FOR SIMULTANEOUS
COOLING AND STRAINING MEASUREMENTS
OF ANB-3066/SD-851-2/V-45

Temperature Range	Duration Hr.	Cooling Rate °F/Hr	Test Matrices			
			0.4	0.8	1.2	1.6
125 to 70°F	2.66	20.7		XX		
	8.33	6.6		X	XX	X
	27.5	2.0		XX		
125 to 40°F	2.66	32.0		XXX		
	8.33	10.2	X	XX	X	X
	27.5	3.09		XX		
125 to 0°F	2.66	47.0		XX		
	8.33	15.0		XX		
	27.5	4.55	X			X

TABLE 30

DERIVED VALUES FROM SIMULTANEOUS COOLING AND STRAINING
TESTS OF THE ANB-3066/SD-851-2 PROPELLANT/LINER
BOND (COOLING FROM 125 TO 70°F)

Specimen No.	$2a'$, in.	Cooling Rate °F/Hr	R, in./min	n	m	$K(a)$	$(\partial K(a)/\partial 2a')_{R,U}$	U_c, in.
7-122	0.8	20.7	9.38×10^{-6}	1.0554	0.1422	2217	-340.2	0.10
7-123	0.8	20.7	9.38×10^{-6}	1.2181		2166		0.10
7-121	0.8	6.6	3.0×10^{-4}	1.2101		1981		0.10
7-125	0.8	2.0	9.09×10^{-5}	1.4490		2233		0.08
7-128	0.8	2.0	9.09×10^{-5}	1.0759		3041		0.075
7-126	1.2	6.6	3.0×10^{-4}	1.1909		2344		0.08
7-133	1.2	6.6	3.0×10^{-4}	1.1540		2010		0.08
7-120	1.6	6.6	3.0×10^{-4}	1.0711		2065		0.07

mean = 1.178   mean = 0.142

TABLE 31

DERIVED VALUES FROM SIMULTANEOUS COOLING AND STRAINING TESTS OF THE ANB-3066/SD-851-2 PROPELLANT/LINER BOND (COOLING FROM 125 TO 40°F)

Specimen No.	$2a'$, in.	Cooling Rate °F/Hr	R, in./min	n	m	K(m)	$(\partial K(m)/\partial 2a')_{R,U}$	U_c, in.
7-105	0.4	10.2	3×10^{-4}	1.1631	-	4514*	-388	0.115
7-99	0.8	32.0	1.25×10^{-3}	1.1024	0.1580	2830		0.11
7-100	0.8	32.0	1.25×10^{-3}	1.0190		2852		0.11
7-101	0.8	32.0	1.25×10^{-3}	1.0506		3200		0.105
7-98	0.8	10.2	3×10^{-4}	1.4273		3104		0.09
7-106	0.8	10.2	3×10^{-4}	1.4859		2510		0.085
7-130	0.8	3.09	9.09×10^{-5}	1.4031		3330		** -
7-131	0.8	3.09	9.09×10^{-5}	1.3759		2680		0.15
7-108	1.2	10.2	3×10^{-4}	1.3241	-	4100*		0.08
7-118	1.6	10.2	3×10^{-4}	1.0737	-	4073*		** -

mean = 1.243   mean = 0.158

* Derivative limited to these specimens.
** Experimental anomaly.

-160-

TABLE 40

DERIVED VALUES FROM CYLINDRICAL PEEL TESTS OF ANB-3600/SD-851-2 PROPELLANT/LINER 30°F AT 0°F

Specimen No.	$2a'$, in.	Cooling Rate °F/Hr	$\dot{R}$, in./min	$\dot{n}$	m	$K(a)$	$\left(\partial K(a)/\partial 2a'\right)_{\dot{R},u}$	U_c, in.
7-104	0.4	15.0	4.29×10^{-4}	1.2234	-	5441	-354	0.115
7-96	0.8	47.0	9.38×10^{-4}	1.3135	-	3189**		0.10
7-98	0.8	47.0	9.38×10^{-4}	-				SBF
7-102	0.8	47.0	6.25×10^{-4}	1.3929		4875		0.10
7-101	0.8	47.0	6.25×10^{-6}	1.3797		5337		0.105
7-97	1.6	15.0	3×10^{-4}	1.2427	-	4961		**

mean = 1.31C   mean = 0.15*

* Estimate from average of Tables 30 and 31.
** Omitted from analysis.

TABLE 33

SUMMARY OF SIMULTANEOUS COOLING AND STRAINING
TESTS OF ANB-3066/SD-851-2 PROPELLANT/LINER BOND

Temperature Range	n	m	$1+m+n$	ψ	J_{Ic}, $\frac{in.-lb}{in.^2}$
125 to 70°F	1.178	0.142	2.320	293	0.46
125 to 40°F	1.243	0.158	2.401	323	0.59
125 to 0°F	1.310	0.15 (est.)	2.46	288	0.52

7.0   J INTEGRAL EVALUATIONS BY OTHER TEST METHODS

One of the objectives of this program was to demonstrate that the J in-
tegral at the propellant-liner bond can be measured using other test methods.
For this demonstration it was necessary to measure only the opening mode J
integral, J_I. These measurements were made on the strip biaxial tensile and
cylindrical peel tests.

All of the tests were performed on specimens consisting of
ANB-3066/SD-851-2/V-45 propellant/liner/insulation bonds.

7.1 STRIP BIAXIAL TENSILE TESTS

This testing involved specimens that were similar in general design
to the scarf-joint specimen (Figure 69), except that the dimensions are 7-in.
long by 1-in. high by 1/4-in. thick. The ends had a circular end relief of
1.625-in. radius that extended 0.2-in. into the specimen.

The test matrices for the strip-biaxial tensile tests are given
in Table 34. They include testing at 0 and 77°F with limited testing at three
crosshead rates and four initial flaw sizes. The raw data from each test are
provided in Appendix B, Tables B-4-1 and B-4-2.

The power-law data analysis was found to be adequate for these
tests. The derived values in the analysis are listed in Tables 35 and 36, and
the final results summarized in Table 37.

The 77°F test data were found to fit the relation

$$J = 1031 \ t^{-0.117} \ u^{2.11} \tag{99}$$

This should be compared with the scarf-joint results which obeyed the
following equation

$$J = 199.5 \ t^{-0.137} \ u^{2.048} \tag{100}$$

TABLE 34

TESTS CONDUCTED ON STRIP BIAXIAL
TENSILE SPECIMENS WITH ANB-3066/
SD-851-2/V-45

Temperature °F	Crosshead Speed, in./min.	Test Matrices			
		2a', in. = 0.4	0.8	1.2	1.6
77	0.02	XX			
	0.10	X	X	XX	X
	0.50	XX			
0	0.02	XX			
	0.10	X	X	XX	X
	0.50	XX			

X indicates test conducted

TABLE 35

DERIVED VALUES FROM STRIP BIAXIAL TENSILE TESTS OF ANB-3066/SD-851-2 PROPELLANT/LINER BOND AT 77°F

Specimen No.	$2a'$, in.	R, in./min	$\underline{a}$	$\underline{m}$	$E(a)$	$(\partial K(a)/\partial 2a')_{R,U}$	U_c, in.
4-1	0.4	0.02	0.9865	0.1173	5184	-1088	0.055
4-2	0.4	0.02	1.0007		6397		0.046
4-3	0.4	0.10	0.9595		6055		0.050
4-4	0.4	0.50	0.9749		5472		0.053
4-5	0.4	0.50	0.9643		6063		0.048
4-6	0.8	0.10	0.980?	-	5326		0.051
4-7	1.2	0.10	0.9996	-	4911		0.054
4-8	1.2	0.10	1.0183	-	4953		0.053
4-9	1.6	0.10	1.0494	-	4565		0.053
			mean = 0.993	mean = 0.117			

TABLE 36

DERIVED VALUES FROM STRIP BIAXIAL TENSILE TESTS OF ANB-3066/SD-851-2 PROPELLANT/LINER BOND AT 0°F

Specimen No.	$2a'$, in.	R, in./min	n	m	$K(a)$	$(\partial K(a)/\partial 2a')_{R,U}$	U_c, in.
4-10	0.4	0.02	1.0000	0.1123	8617	+602.4*	0.045
4-11	0.4	0.02	1.0002	-	9142		0.040
4-12	0.4	0.10	0.9800	-	8625		0.043
4-13	0.4	0.50	0.9750	-	9159		0.041
4-14	0.4	0.50	0.9550	-	8603		0.044
4-15	0.8	0.10	0.9555	-	8778		0.040
4-16	1.2	0.10	0.9018	-	9788		0.038
4-17	1.2	0.10	0.8922	-	9165		0.038
4-18	1.6	0.10	0.8746	-	9393		0.038

mean = 0.948   mean = 0.112

* Wrong sign, leads to negative fracture energies.

-166-

TABLE 37

SUMMARY OF REDUCED TEST PARAMETERS FOR
THE STRIP-BIAXIAL TENSILE TESTS OF ANB-3066/SD-851-2
PROPELLANT/LINER BOND AT 0 AND 77°F

Test Temperature °F	n	m	$\frac{1+m+n}{}$	Ψ	$J_{Ic}, \frac{in.-lb}{in.^2}$
77	0.993	0.117	2.110	1031	2.18
0	0.948	0.112	2.06	- 585*	-

* Wrong sign, leads to negative fracture energies

The primary difference in the 77°F data is in the constant Ψ, which in the strip biaxial tests is about 5.2 times larger than that of the scarf-joint tests. The deformations at crack initiation, U_c, are on the other hand larger in the scarf-joint test (by a factor of about two) as seen upon comparison of Tables 19 and 35. These two differences appear to be offsetting in the final calculations (Tables 22 and 37) which yield a value for J_{Ic} of $1.53 \frac{in.-lb}{in.^2}$ for the scarf-joint test and $2.18 \frac{in.-lb}{in.^2}$ for the strip biaxial test . This difference is attributed to batch-to-batch effects of the propellant and liner and to differences in the test specimens.

There is an inexplicably large propellant stiffness in the strip-biaxial specimen as compared with the scarf-joint specimen. This is illustrated below for the force per unit width on specimens deformed to 0.05 in. at 0.10 in./min crosshead rate. The initial flaw sizes are also roughly adjusted upon division by specimen length, L.

Scarf-Joint			Strip Biaxial		
Crack Size 2a', in.	2a'/L	f,lb/in.	Initial Flaw Size, 2a', in.	2a'/L	f,lb/in.
0.04	0.10	48.2	0.8	0.114	207
0.04	0.10	58.6			
0.8	0.20	49.0	1.2	0.17	192
			1.2	0.17	197

Clearly, the strip biaxial specimens exhibit about four times the stiffness of the scarf-joint specimens.

The testing at 0°F was disappointing. Again, the deformations were relatively small (less than one-half those of the scarf-joint test). But, the specimen stiffnesses were even greater, as illustrated by comparisons of the K(a) values in Tables 16 and 36. An impact of these large stiffnesses was to reverse the sign on the slope of the K(a) versus 2a' plots. This leads to negative fracture surface energies, which has no physical meaning. Attempts

-168-

to use the general method of analysis led to similar negative result.

It is not known if this behavior is typical of other strip biaxial specimen designs and testing procedures. However, the one good result at 77°F suggests that the strip biaxial test can provide similar J_{Ic} values. Some further testing design would be required, before the test could be used routinely.

7.2 CYLINDRICAL PEEL TESTS

This test was conceived and developed at Thiokol (see Ref. 19). The testing and the specimens designs used on this current effort followed those given in Ref. 19 except for the specific requirements of the J integral.

The matrices for these tests are given in Table 38, which required 21 cylindrical peel test specimens. This plan involved tests at two temperatures (0 and 77°F), four pressurization rates and three crack sizes.

The test specimens were prepared in the configuration given in Figure 76, which illustrates the adhesive bond design. The original specimen design had an outside diameter of 1.00 in. to permit the use of three different initial flaw sizes and to reduce the relative size of the largest flaw. This testing was performed early in the program before it was learned that there was a maximum acceptable size for the initial flaws. If this had been known earlier the specimen outside diameter would have been increased to 2.0 in. with the initial flaw sizes remaining the same (0.55, 0.7 and 0.8 in. diameter). The minimum flaw size, 0.55 in. diameter, was set by the center drill hole (0.375 in.) plus a cut depth sufficient to give reproducible effects.

The test data were recorded on a two-pen strip-chart recorder. The driving force to open the crack was the internally applied pressure P which was recorded as a function of time. The axial deformation, U, was measured using an extensometer that was gravity loaded against the top of

-169-

TABLE 38

CYLINDRICAL PEEL TESTS OF SPECIMENS WITH ANB-3066/SD-851-2/V-45
PROPELLANT/LINER/INSULATION

Temp., °F	Pressurization Rate	$2a'$, in. =	Planned Tests 0.55	0.70	0.80
0	$\dot{P}_1$		x	x	x
	$\dot{P}_2$				x
	$\dot{P}_3$			x	x
	$\dot{P}_4$		x	x	x
77	$\dot{P}_1$		x	x	x
	$\dot{P}_2$		x		x
	$\dot{P}_3$		xx	x	x
	$\dot{P}_4$		x	x	x

x   indicates test to be conducted.

ANB-3066 PROPELLANT

INITIAL FLAW

SD-851-2 LINER

V-45 INSULATION

STEEL DISK

118 Deg

PRESSURIZATION INLET
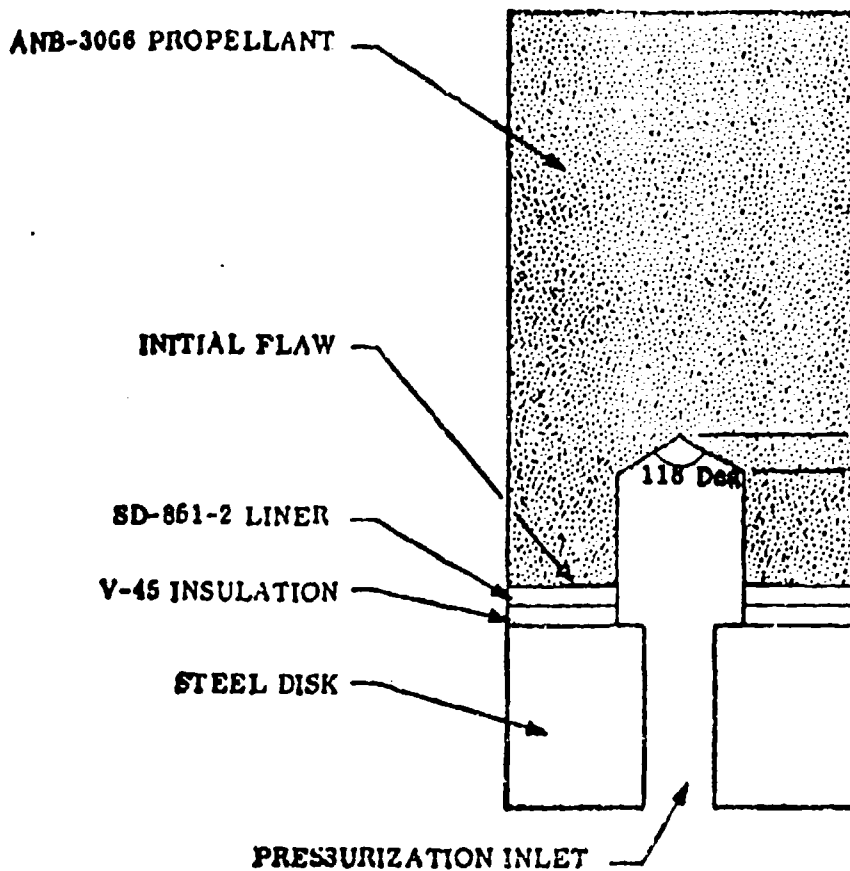
Figure 76. Cylindrical Peel Specimen

-171-

the specimen. The internal pressure and deformation data for this testing
are tabulated in Appendix B, Tables B-3-1 and B-3-2.

The data reduction procedure assumed a power-law approach like
that used for the scarf-joint specimen, Equations (83) through (88). There
is a difference, however, in that the cylindrical peel test results require
an inversion of the independent and dependent variables (force and displacement).
This inversion leads to the following power-law relation for the axial
deformation, U.

$$U = k(a) \; \dot{p}^{\mu} \; P^{\nu} \qquad\qquad (101)$$

where

    P   is the internal pressure, psig

    $\dot{p}$ is the rate of pressurization (a constant for any given
          test), psig/min.

    k(a) is a parameter that is constant for any given test and
          varies only with crack size.

    μ and ν are empirical constants.

The basic J integral analysis for this test, however, is based
upon the volume change associated with the opening of the crack. However,
this parameter was not measured in these tests for three reasons.
First, the axial opening of the initial flaw was very small (less than 0.007 in.
at crack initiation). Second, hydrostatic pressurization of the internal
cavity would produce a marked volume change in addition to that for the
opening of the crack. Third, volume change measurements at these levels
would require highly accurate, carefully designed equipment, which was not
available. For these reasons, we chose the axial extension measurement method.

The data reduction method selected was to relate the volume change
to the axial extension then treat the data as if they were dilatometric. For
this purpose, the initial flaw is assumed to be penny-shaped and does not
propagate. The tip of the crack is assumed to deform extensively, so that

the crack faces can move essentially parallel to each other. Thus, the relation between the volume change, V, of the crack and the axial separation, U, of the crack faces is given by

$$V = \frac{\Pi(2a')^2}{4} U \tag{102}$$

where 2a' is the diameter of the initial flaw.

Combining Equations (101) and (102) gives

$$V = \frac{\Pi(2a')^2}{4} \ k(a) \ \dot{p}^\mu P^\nu \tag{103}$$

The pressure is related to the time, t, in the test by the relation

$$P = \dot{p} \ t \tag{104}$$

Combining Equations (103) and (104) yields

$$V = \frac{\Pi(2a')^2}{4} \ k(a) \ t^{-\mu} \ P^{\mu+\nu} \tag{105}$$

The complimentary energy, W_c, calculated at constant time and crack size is given by

$$W_c = \int_0^P V dP \tag{106}$$

Inserting Equation (105) into (106) and completing the integration gives

$$W_c = \frac{\Pi(2a')^2}{4(1+\mu+\nu)} \ k(a) \ t^{-\mu} P^{1+\mu+\nu} \tag{107}$$

According to theory, the J integral can be written as follows (the negative sign is not used in evaluating the compliment)

$$J = \frac{2}{B} \ \frac{\partial W_c}{\partial 2a'} \tag{108}$$

where B is the circumferential length of the intial crack tip, in.

2a' is the diameter of the internal initial crack, in.

For the circular flaw the relationship for B is

$$B = 2\Pi a' \tag{109}$$

The resulting J integral relationship is

$$J = (2a') \, \phi \, t^{-\mu} \, P^{1+\mu+\nu} \tag{110}$$

where

$$\phi = \frac{1}{2(1+m+\nu)} \left(\frac{\partial k(a)}{\partial (2a')} \right)_{\dot{p},P} \tag{111}$$

The constant pressurization rate relation becomes rate

$$J = (2a') \, \phi \, \dot{p}^{\mu} \, P^{1+\nu} \tag{112}$$

This latter relationship was used in the data analysis.

The nature of the power-law relation, Equation (101), is that k(a) is related to specimen compliance, so the parameter $(\partial k(a)/\partial 2a')_{\dot{p},P}$ is positive, while μ is negative.

The data analysis led to the derived values listed in Tables 39 and 40, with the final results summarized in Table 41. The J_{Ic} values, $0.30 \, \frac{in-lb}{in^2}$ at 77°F and $0.57 \, \frac{in.-lb}{in.^2}$ at 0°F, may be compared with those for the scarf-joint test in Table 22 (1.53 and 3.75 $\frac{in.-lb}{in.^2}$, respectively).

The J_{Ic} values for the cylindrical peel test are between 15 and 20% of those for the scarf-joint test. The consistency between the two tests suggests that the cylindrical peel test can be developed to give a good measure of the J integral, but the present design and test procedures need improvement.

TABLE 39

DERIVED VALUES FROM CYLINDRICAL PEEL TESTS OF ANB-3066/SD-851-2 PROPELLANT/LINER BOND AT 77°F

Specimen No.	2a', in.	$\dot{P}$, psig/min	ν	m	$k(a)$	$\left(\frac{\partial K(a)}{\partial 2a'}\right)_{P,\dot{P}}$	P_c, psig
3-12	0.55	3.73	1.477	-0.1087	1.212×10^{-5}	6.296×10^{-5}	70
3-11	0.55	11.62	1.476		1.359×10^{-5}		61
3-10	0.55	182.6	1.429		1.686×10^{-5}		90
3-27	0.55	265	1.357		1.078×10^{-5}		95
3-9	0.55	766	1.640		1.566×10^{-5}		100
3-5*	0.70	3.98	1.383	-0.1322	2.55×10^{-5}		N.F.*
3-3	0.70	170	1.397		2.831×10^{-5}		59
3-2	0.70	800	1.596		2.547×10^{-5}		58
3-21*	0.80	3.58	1.633	-0.1703	2.476×10^{-5}		N.F.*
3-20*	0.80	11.24	1.246		3.926×10^{-5}		N.F.*
3-19	0.80	356	1.434		2.958×10^{-5}		57
3-18	0.80	686	1.614		2.243×10^{-5}		67.5

mean = 1.47   mean = -0.137

---

* No failure data, N.F.

TABLE 40

DERIVED VALUES FROM CYLINDRICAL PEEL TESTS OF ANB-3600/SD-851-2 PROPELLANT/LINER BOND AT 0°F

Specimen No.	2a', in.	$\dot{\rho}$, psig/min	ν	m	k(a)	$(\partial K(a)/\partial 2a')_{\dot{\rho},p}$	P_c, psig
3-16	0.55	3.44	1.764	-0.0621	1.451×10^{-6}	8.373×10^{-6}	128
3-13	0.55	570	1.766		1.578×10^{-6}		116.3
3-17	0.70	3.74	1.660	-0.1086	2.60×10^{-6}		67
3-7	0.70	218	1.638		2.321×10^{-6}		97.5
3-6	0.70	632	1.745		2.227×10^{-6}		97.5
3-25*	0.80	3.55	2.046	-.0651	4.050×10^{-6}		75
3-24	0.80	3.55	1.788		1.965×10^{-6}		67.5
3-23*	0.80	254	1.756		6.146×10^{-6}		75
3-22	0.80	492	1.674		2.126×10^{-6}		120
			mean = 1.76	mean = 0.0786			

* Probably in error, but used in analysis.

TABLE 41

SUMMARY OF REDUCED TEST PARAMETERS FOR
THE CYLINDRICAL PEEL TESTS OF ANB-3066/SD-851-2
PROPELLANT/LINER BONDS AT 0 AND 77°F

Test Temperature °F	ν	μ	$1+\mu+\nu$	Φ	J_{Ic}, $\dfrac{\text{in.-lb}}{\text{in.}^2}$
77	1.47	-0.137	2.333	1.350×10^{-5}	0.30
0	1.76	-0.0786	2.681	1.504×10^{-6}	0.57

8.0 TESTING OF DISSECTED MOTOR SPECIMENS AND EVALUATIONS OF TEST REPEATABILITY

The primary goals of this testing were; to apply the J integral measurements to other well characterized propellant/liner/insulation bond systems, then to measure the level of the experimental error in the scarf-joint test. The first objective was combined with a desire to know the applicability of this test to specimens dissected from motors. Two well characterized bond systems were chosen for this, the Polaris A-3 Stage 2 motor and the Minuteman III Stage 2 motor. The first motor involves ANP-2969 propellant, with no liner, bonded to V-52 insulation and a fiberglass case. The Minuteman motor used ANB-3066 propellant, SD-851-2 liner, V-45 insulation and a titanium metal case.

The statistical measurements were conducted on an MX Stage II candidate bond system ANB-3600 propellant, SD-923 liner and WS-15353 insulation. In addition to defining the level of the experimental error, this testing gives more assurance of the applicability of the J integral method to different propellant/bond systems.

The following subsections describe first evaluations of the motor bond systems then the determinations of the level of experimental error.

8.1 EVALUATIONS OF MOTOR BOND SYSTEMS

This testing involved the adhesive bonds of specimens which had been obtained from full-scale motors by dissection. Initially, the motor case portion of the specimen was cut to size, while the propellant, liner and insulation were left oversized. The final milling of the propellant and liner (the insulation was left oversized for purposes of safety in milling) brought the specimens to the desired dimensions and alignment with the case.

During initial trials the upper end plate-to-propellant interface was kept flat, ignoring the small curvature (23 and 26 inches) of the two motors. However, the testing indicated crack initiation along the sides of the specimen. A satisfactory correction was to change the curvature of the upper end plate-to-propellant interface to match that of the motor case. Careful observation of the crack tip showed essentially uniform initiation and propagation for the corrected specimens.

Alignment of the specimen while bonding to the end plates required special techniques. The upper end plate was easily aligned and bonded (even with interface curvature) by placing them on a flat surface. The case-to-end plate interface, however, required the use of the alignment fixture illustrated in Figure 77.

The initial flaw is cut in these specimens using a special, very long cutting blade, Figure 78a. The blade is aligned between the blocks of a cutting guide on one side and held against a single block on the exit side, Figure 78b. The cutting blade is made of spring steel and holds the curvature of the guides across the specimen. A small hole is drilled through the scarf-joint specimen at the propellant/liner bond, the piano wire part of the cutting blade is pushed through the hole, then the blade is pulled through the specimen. In the case of a gummy liner it is better to start with a small blade, since the first cut is often rough. The second blade usually gives a smooth cut and minimizes the damage at the crack tip.

Further details on the specimen and cutting alignment fixtures and the cutting blade are provided in Appendix A, Figures A-2, A-3 and A-4.

Tests of the specimens dissected from the Polaris A-3 Stage 2 and Minuteman III Stage 2 motors are given next.

Fixture

Scarf-
Joint
Specimen

PROPELLANT

LINER
INSULATION
CASE
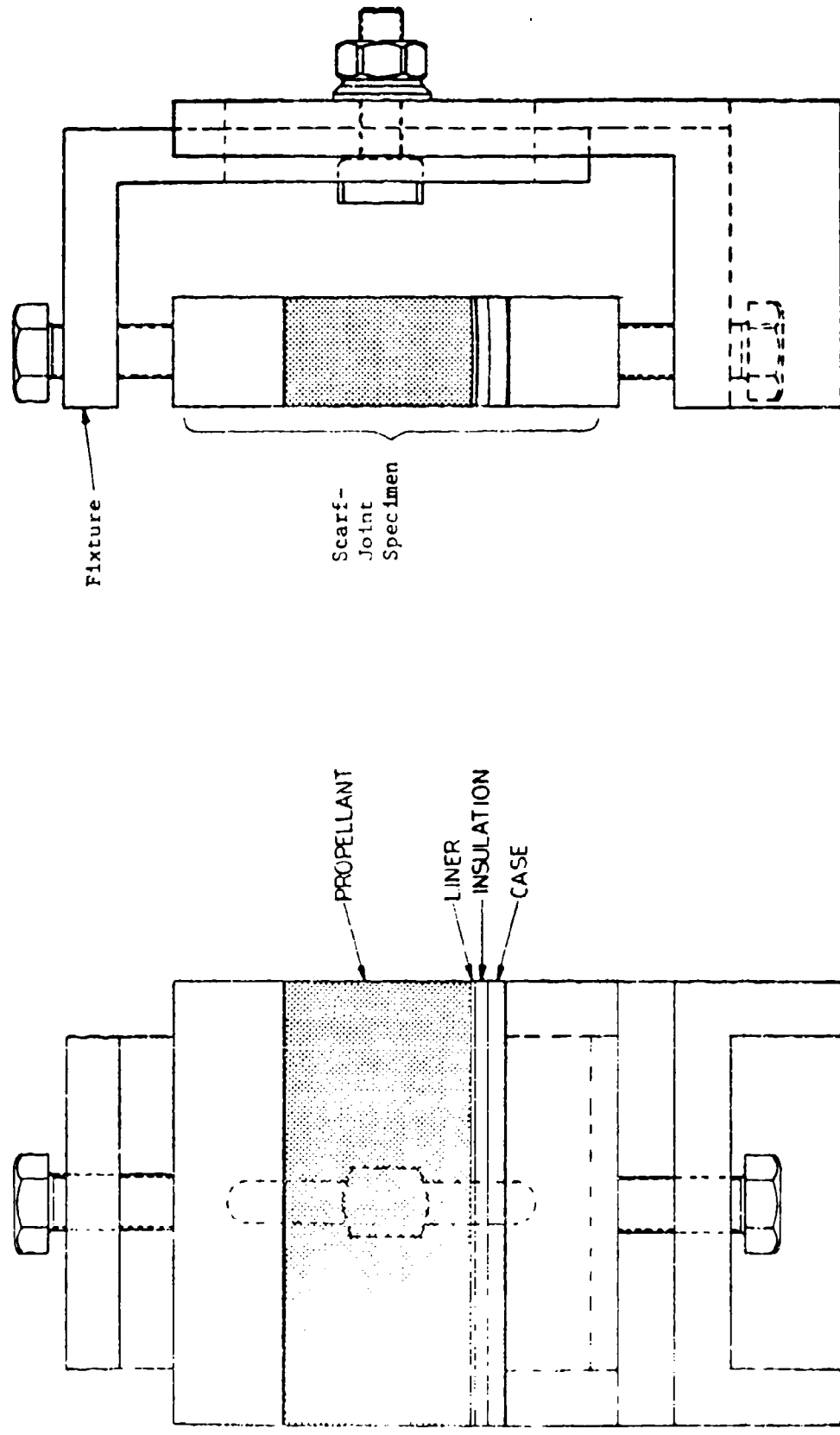
Figure 77. Bond Alignment Fixture

Music Wire

A. Cutting Blade

Scarf-Joint
Specimen

Cutting
Slot

Cutting
Guide

Cutting
Guide

B. Bonding and Cutting
Alignment Fixture
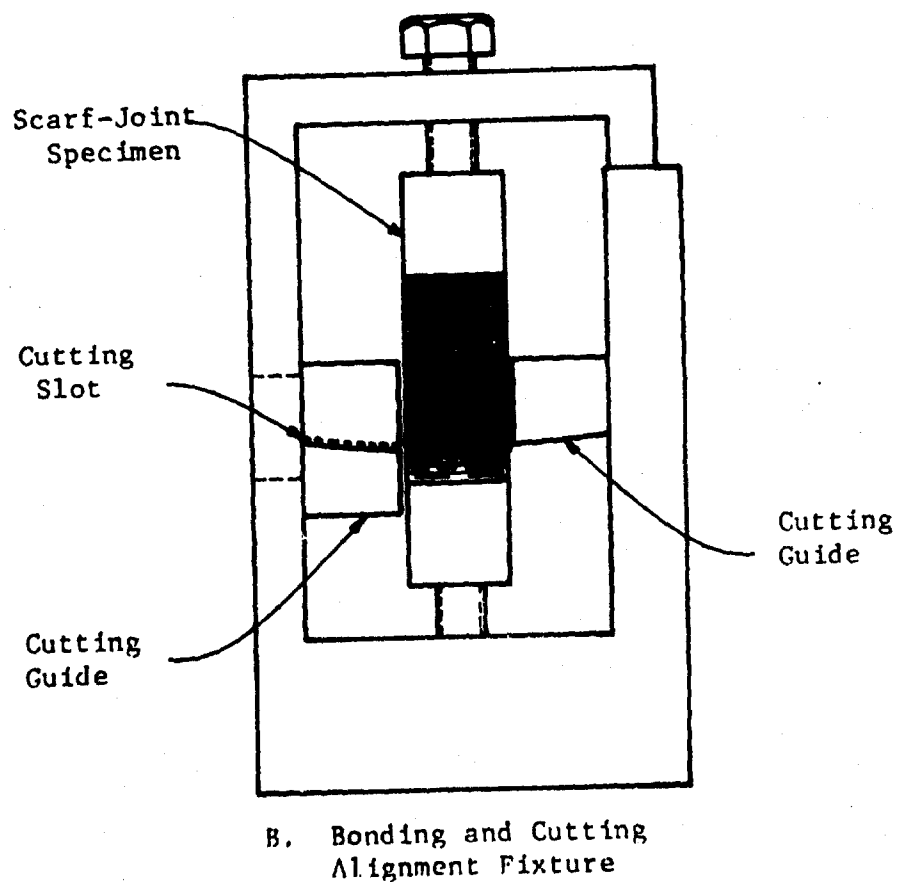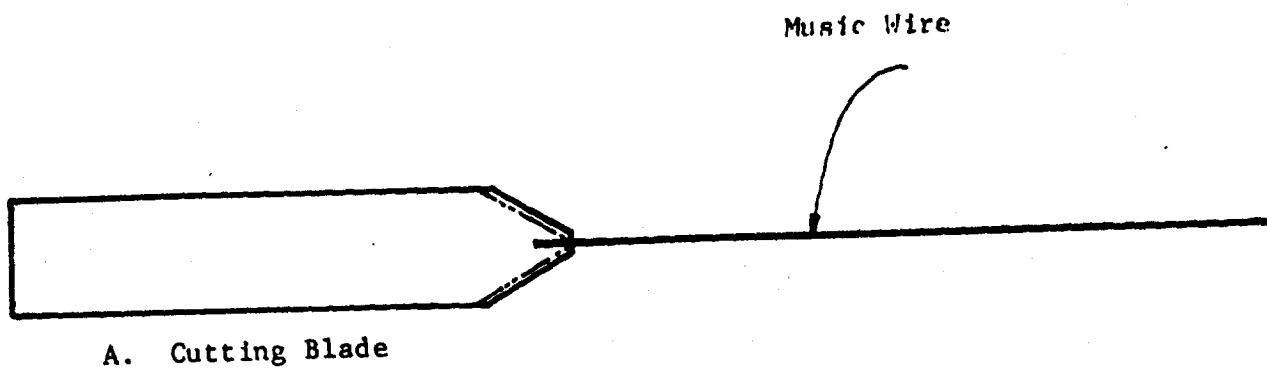
Figure 78. Bonding and Cutting Alignment Fixture and
Cutting Blade for Motor Specimens

8.2 TESTS OF SPECIMENS DISSECTED FROM POLARIS A-3 MOTOR S/N 2864

These tests were all performed on bond specimens of ANP-2969/ V-52/epoxy-fiberglass, propellant/insulation/case. The test plan for this work is given in Table 42, while the force-displacement data are tabulated in Appendix B, Tables B-10-1 and B-10-2.

The data reduction followed the procedures described in Section 5 for the power-law relation. The derived values of m, n, K(a), $(\partial K(a)/\partial 2a')_{R,U}$ and U_c are tabulated in Tables 43 and 44. Table 45 summarizes the key parameters, including Ψ and J_{Ic}.

The J_{Ic} values were found to be 1.21 and 3.06 $\frac{\text{in.-lb}}{\text{in.}^2}$ at 77 and 0°F, respectively. By comparison the J_{Ic} values for the ANB-3066/SD-851-2, propellant/liner bond (Table 22) were 1.53 and 3.75 $\frac{\text{in.-lb}}{\text{in.}^2}$ at 77 and 0°F, respectively.

The primary differences among the two bond systems are the values of Ψ, which are tabulated below.

	Ψ	
Bond System	77°F	0°F
ANP-2969/V-52	77.7	129
ANB-3066/SD-851-2	200	605

Another difference among the two bond systems was the deformation at crack initiation, U_c, which was higher for the ANP-2969/V-52 bond system; namely, 100% higher at 0°F and 25% higher at 77°F.

The ANP-2969/V-52 bond system also evinced clear characteristics of a slowly increasing crack rate (from infinitesimally low to a moderate rate). This has caused difficulty in visually defining a <u>point</u> of crack initiation, so the method was not used.

TABLE 42

TESTS OF SPECIMENS DISSECTED FROM
POLARIS A-3 MOTOR S/N 2864

Temperature °F	Crosshead Rate, in./min	2a' =	Test Matrices 0.4	0.8	1.2	1.6
77	0.02			XX		
	0.10		X	X	XX	X
	0.50			XX		
0	0.02			XX		
	0.10		X	X	XX	X
	0.50			XX		

X indicates test performed.

TABLE 43

DERIVED VALUES FROM SCARF-JOINT TESTS AT 77°F OF SPECIMENS DISSECTED FROM POLARIS A-3 MOTOR SN 2864

Specimen No.	$2a'$, in.	R_1, in./min	n	m	$K(a)$	$\partial K(a)/\partial 2a')_{R,U}$	c_L, in.
10-1	0.4	0.10	0.9519	-	396.0	-77.0	0.10
10-2	0.8	0.02	0.9467	0.0747	364.8		0.13
10-3	0.8	0.02	0.8994		395.7		0.14
10-4	0.8	0.10	0.8055		278.0*		0.12
10-5	0.8	0.50	0.9093		380.0		0.125
10-6	0.8	0.50	0.9330		379.9		0.125
10-7	1.2	0.10	0.8853		377.3		0.13
10-8	1.2	0.10	0.9224		327.8		0.13
10-9	1.6	0.10	0.8898	-	303.4		0.105
			mean = 0.906	mean = 0.0747			

* Excluded from analysis.

TABLE 44

DERIVED VALUES FROM SCARF-JOINT TESTS AT 0°F OF SPECIMENS DISSECTED FROM POLARIS A-3 MOTOR SN 2864

Specimen No.	$2a'$, in.	R, in./min	p	m	$K(m)$	$(\partial K(m)/\partial 2a')_{R,U}$	U_{c}, in.
10-10	0.4	0.10	0.7199		705	-120.8	0.145
10-11	0.8	0.02	0.7978	0.1634	669		0.15
10-12	0.8	0.02	0.7900		630		0.135
10-13	0.8	0.10	0.7167		583		0.16
10-14	0.8	0.50	0.6483		653		0.135
10-15	0.8	0.50	0.6893		646		0.105
10-16	1.2	0.10	0.6936	-	610		0.145
10-17	1.2	0.10	0.6948	-	601		0.14
10-18	1.6	0.10	0.6979		541		0.15

mean = 0.716   mean = 0.163

TABLE 45

SUMMARY OF REDUCED PARAMETERS FROM SCARF-JOINT
TESTS OF SPECIMENS DISSECTED FROM POLARIS A-3 MOTOR S/N 2864

Temperature $^\circ F$	m	n	$1+m+n$	ψ	$J_{Ic}, \dfrac{\text{in.-lb}}{\text{in.}^2}$
77	0.0747	0.906	1.981	77.74	1.21
0	0.163	0.716	1.879	128.6	3.06

8.3 TESTS OF SPECIMENS DISSECTED FROM MINUTEMAN III MOTOR S/N AA20147

These tests were all performed on bond specimens of ANB-3066/SD-851-2/ V-45/Titanium Metal, propellant/liner/insulation case. The initial test plan for this work is given in Table 46. The plan was completed, but surface hardening of the propellant(clearly apparent in Shore A hardness tests) caused early crack initiation at the outside edges of the cracks. This was detected visually in some of the test specimens.

The effects of surface hardening of the propellant are best illustrated in terms of the deformation at crack initiation, U_c. The reduction in this parameter is seen in Table 47, which compares the U_c values at 77 and 0°F for the motor specimens with previously measured scarf-joint specimens (Tables 16 and 19). Also included are data from repeat tests where surface hardening was minimized. At 0°F there is a marked difference (by a ratio of more than 3) among the standard specimen and the surface hardened motor specimen.

At 77°F there is only a small difference among the U_c values for the hardened motor specimen and the repeat tests. The latter tests were carefully observed to assure uniform crack initiation and propagation along the crack tip. The clear difference among the U_c values for the standard scarf-joint tests and those for the repeat motor specimens is attributed primarily to batch-to-batch and carton-to-motor effects.

For the dissected motor specimens, the only complete set of data analyses were those performed on the repeat tests at 77°F. The plan for this testing is given in Table 48, while the force-displacement data are tabulated in Appendix B, Table B-8-1.

The data reduction followed the procedures in Section 5 for the power-law relation. The values of the derived parameters are tabulated in Table 49, while Table 50 summarizes the key parameters.

TABLE 46

INITIAL TESTS OF SPECIMENS DISSECTED FROM
MINUTEMAN III STAGE 2 MOTOR S/N AA20147

Temperature °F	Crosshead Rate in./min	2a', in. =	Test Matrices			
			0.4	0.8	1.2	1.6
77	0.02			XX		
	0.10		X	XX	XX	X
	0.50			XX		
0	0.02			XX		
	0.10		X	X	XX	X
	0.50			X		

X   indicates test performed.

TABLE 47

COMPARISONS OF DEFORMATION BEHAVIORS OF SPECIMENS
PREPARED FROM CARTONS AND FROM MOTORS WITH AND WITHOUT SURFACE HARDENING

$2a$, in.	R, in./min	U_c, in. at 77°F			U_c, in. at 0°F	
		Standard Specimens	Hardened Motor Specimens	Repeat Motor Specimens	Standard Specimens	Hardened Motor Specimens
0.4	0.10	SBF	0.083	0.076	SBF	0.05
0.8	0.02	0.105	0.072 0.068	0.087 0.083	0.093	0.036 0.024
	0.10	0.099	0.074	0.081 0.076	0.073	0.022
	0.50	0.096	0.049 0.050	0.069 0.076	0.050	0.018
1.2	0.02	0.094	-	-	0.087	-
	0.10	0.090	0.068 0.057	0.074 0.067	0.073	0.035 0.026
	0.50	0.093	-	-	0.068	-
1.6	0.10	0.084	0.073	0.081	0.063	0.022

TABLE 48

REPEAT TESTS AT 77°F OF SPECIMENS DISSECTED
FROM MINUTEMAN III STAGE 2
MOTOR S/N AA20147

Crosshead Rate in./min	2a', in. =	Tests 0.4	0.8	1.2	1.6
0.02			XX		
0.10		X	XX	XX	X
0.50			XX		

X indates test performed.

TABLE 49

DERIVED VALUES FROM SCARF-JOINT TESTS AT 77°F OF
SPECIMENS DISSECTED FROM MINUTEMAN III STAGE 2
MOTOR SN AA20147

Specimen No.	$2a'$, in.	R, in./min	n	m	K(e)	$(\partial K(e)/\partial 2a')_{R,U}$	U_c, in.
8-1	0.4	0.10	0.9898	-	1369	-344.7	0.076
8-2	0.8	0.02	0.9423	0.08639	1273		0.087
8-3	0.8	0.02	0.9972		1215		0.083
8-4	0.8	0.10	0.9442		1255		0.081
8-5	0.8	0.10	0.9685		1195		0.082
8-6	0.8	0.50	0.9361		1269		0.069
8-7	0.8	0.50	0.9434		1218		0.076
8-8	1.2	0.10	0.9653	-	1104		0.074
8-9	1.2	0.10	0.9339		1123		0.067
8-10	1.6	0.10	0.8946	-	945		0.081
			mean = 0.952	mean = 0.0864			

TABLE 50

SUMMARY OF REDUCED PARAMETERS FROM SCARF-JOINT
TESTS OF SPECIMENS DISSECTED FROM MINUTEMAN III STAGE 2
MOTOR S/N AA20147

Temperature °F	m	n	$1+m+n$	$\frac{\psi}{1}$	$J_{Ic}, \frac{in.-lb}{in.^2}$
77	0.0864	0.952	2.038	338.2	1.89

The J_{Ic} value of 1.89 $\frac{in.-lb}{in.^2}$ is in good agreement with the standard scarf-joint test value of 1.53 $\frac{in.-lb}{in.^2}$ that was previously given in Table 22. Since the standard scarf-joint specimens and the dissected motor specimens were prepared from separate propellant and liner batches, a larger difference among the two test results might have occurred.

The good agreement between the two specimen types does not prove that the two tests give the same results. But, the two tests yielded similar force-deformation profiles and both followed the power-law relation in data analysis. The observed uniform propagation of the crack front in both specimens further indicates no special stress concentration problems.

In summary, the test results are satisfactory and they, most certainly, indicate that the testing of specimens obtained from large motors is practical. Tests on specimens from smaller motors should be attempted as soon as possible.

8.4 MEASUREMENT OF LEVEL OF EXPERIMENTAL ERROR IN SCARF-JOINT TEST

This objective was met using a method of experimentation which can quickly and efficiently evaluate a number of factors all at one time. In this method, all factors are varied for each experiment according to a "Graeco-Latin square" experimental design[20]. Originally, the plan was designed to use a 4 x 4 Graeco-Latin square which would permit the evaluation of four test variables (at four levels each) plus an estimate of the experimental error (inherent variation of the test). A program revision forced a reduction of the effort, so a 2 x 2 Graeco-Latin square was devised.

The selected 2 x 2 Graeco-Latin square experimental design is given below

A	A	A	B
	A		B
B	B	B	A
	A		B

This square gives the design for a series of four experiments for evaluating up to three factors at two levels each. Each sub-square represents the plan for one J integral determination (10 scarf-joint tests). Each of the three letter positions (top left, to right and bottom center) within a sub-square is allocated to one of the factors being studied.

In this testing there were three factors of primary concern; the experimental error, and operator-to-operator and batch-to-batch differences. Specimens of different crack length and crosshead speed were evaluated as part of the J_{Ic} determination, so those factors were not a consideration. All other factors were held constant.

The specific Graeco-Latin square test plan is given in Table 51. Here, the operators and batches for each test were specifically assigned.

The test matrices for the J_{Ic} determinations listed in Table 52 required 40 standard specimens. Each operator prepared the test specimens that he was to test. The tests were conducted one set at a time, with the operators alternating after each set.

The testing was performed on an MX candidate propellant/liner/ insulation bond system, ANB-3600/SD-923/WS-15353. All of the testing was performed at 77°F.

The data analysis followed the power-law relation given in Section 5.5.2. The raw test data (digitized) are tabulated in Appendix B, Tables B-11, B-12, B-21 and B-22. The derived values of the parameters are listed in Tables 53-56, while the final results of all four data sets are given in Table 57. The J_{Ic} values varied from 2.37 to 4.23 $\frac{in.-lb}{in.^2}$ (Table 57).

The initial data analysis gave the following average values of J_{Ic}, which is provided to illustrate the effects.

TABLE 51

TESTS TO MEASURE THE LEVEL OF THE EXPERIMENTAL ERROR
(STANDARD SPECIMEN WITH ANB-3600/SD-923/WS-15353)

● Two-by-Two Graeco-Latin Test Grid

O_1	B_1	O_1	B_2
	E_1		E_2
O_2	B_1	O_2	B_2
	E_2		E_1

● Parameters

O_1 and O_2 are the test operators

B_1 and B_2 are the material batches

E_1 and E_2 are components of the experimental error

-195-

TABLE 52

TEST MATRICES FOR DETERMINING
LEVEL OF EXPERIMENTAL ERROR AT 77°F
(STANDARD SPECIMEN WITH ANB-3600/SD-923/WS-15353)

● Operator 1, Batches 1 and 2

R, in./min	2a', in. =	Test Matrix			
		0.4	0.8	1.2	1.6
0.02			XX		
0.10		X	XX	XX	X
0.50			XX		

● Operator 2, Batches 1 and 2

R, in./min	2a', in. =	Test Matrix			
		0.4	0.8	1.2	1.6
0.02			XX		
0.10		X	XX	XX	X
0.20			XX		

X   Indicates test performed.

TABLE 53

DERIVED VALUES FROM SCARF-JOINT TESTS AT 77° OF ANB-3600/SD-923, PROPELLANT/LINER BOND (OPERATOR 1, BATCH 1)

Specimen No.	$2a'$, in.	R, in./min	a	m	$K(a)$	$(2K(a)/2a')_{R,U}$	U_c, in.
11-1	0.4	0.10	1.1022	-	1404	-332.3	0.185
11-2	0.8	0.02	1.2665	0.1008	1210		0.148
11-3	0.8	0.02	1.2961		1034		0.188
11-4	0.8	0.10	1.1329		1278		0.144
11-5	0.8	0.50	1.1693		1133		0.161
11-6	0.8	0.50	1.1821		1103		0.168
11-7	1.2	0.10	1.1659	-	1206		0.142
11-8	1.2	0.10	1.3084		937		0.147
11-9	1.6	0.10	1.2215	-	939		0.179
			Mean = 1.205	0.101			

-197-

TABLE 54

DERIVED VALUES FROM SCARF-JOINT TESTS AT 77°F OF ANB-3600/SD-923, PROPELLANT/LINER BOND (OPERATOR 1, BATCH 2)

Specimen No.	$2a'$, in.	R, in./min	n	m	$K(a)$	$(\partial K(a)/\partial 2a')_{R,U}$	H_c, in.
12-1	0.4	0.10	1.2934	-	1241	-255.9	SBF
12-2	0.8	0.02	1.2907	0.152	1119		0.158
12-3	0.8	0.02	1.3722		1120		0.194
12-4	0.8	0.10	1.2471		1025		0.204
12-5	0.8	0.10	1.2296		1135		0.17
12-6	0.8	0.50	1.2032		1134		0.168
12-7	0.8	0.50	1.1372		1106		0.165
12-8	1.2	0.10	1.2482	!	1003		0.154
12-9	1.2	0.10	1.2223		983		0.173
12-10	1.6	0.10	1.2548	-	936		0.141
		Mean =	1.251	0.152			

TABLE 55

DERIVED VALUES FROM SCARF-JOINT TESTS AT 77°F OF
ANB-3600/SD-923, PROPELLANT/LINER BOND
(OPERATOR 2, BATCH 1)

Specimen No.	$2a'$, in.	R, in./min	n	m	$K(a)$	$(\partial K(a)/\partial 2a')_{R,U}$	U_c, in.
21-11	0.4	0.10	1.3093	-	1225	-357.9	0.193
21-12	0.8	0.02	1.2596	0.1946	1242		0.175
21-13	0.8	0.02	1.2566		1252		0.179
21-14	0.8	0.10	1.1504		1357		0.153
21-15	0.8	0.10	1.0707		1376		0.153
21-16	0.8	0.20	1.1459*		912*		0.152
21-17	0.8	0.20	1.0598		1155		0.156
21-18	1.2	0.10	1.2538	-	1098		0.177
21-19	1.2	0.10	1.1665		1079		0.174
21-20	1.6	0.10	1.1040	-	870		0.16
		Mean =	1.178	0.195			

* Erratic test data excluded from final analysis.

TABLE 56

DERIVED VALUES FROM SCARF-JOINT TESTS AT 77° F OF ANB-3600/SD-923, PROPELLANT/LINER BOND (OPERATOR 2, BATCH 2)

Specimen No.	2a', in.	R, in./min	n	m	K(a)	$(\partial K(a)/\partial 2a')_{R,U}$	U_c, in.
22-11	0.4	0.1	1.2553	–	865	-146.7	0.215
22-12	0.8	0.02	1.2262	0.1220	895		0.16
22-13	0.8	0.02	1.1872		832		0.164
22-14	0.8	0.10	1.2166		815		0.182
22-14	0.8	0.10	1.2138		801		0.218
22-15	0.8	0.50	1.1850		842		0.206
22-16	0.8	0.50	1.1429		885		0.169
22-17	1.2	0.10	1.1854	–	754		0.165
22-18	1.2	0.10	1.1713		738		0.193
22-19	1.6	0.10	1.1559	–	732		0.145
22-20							
		Mean =	1.194	0.122			

-200-

TABLE 57

SUMMARY OF REDUCED PARAMETERS FROM SCARF-JOINT
TESTS AT 77°F OF ANB-3600/SD-923, PROPELLANT/LINER BOND

Operator No.	Batch I.D. No.	m	n	1+m+n	Ψ	$J_{IC}, \dfrac{\text{in.-lb}}{\text{in.}}$
1	1	0.101	1.205	2.306	288	4.23
1	2	0.152	1.251	2.403	213	2.82
2	1	0.195	1.178	2.373	302	3.74
2	2	0.122	1.194	2.316	127	2.37

	Mean J_{Ic}, $\dfrac{\text{in.-lb}}{\text{in.}^2}$	
	No. 1	No. 2
Operator	3.525	3.055
Batch	3.985	2.595
Error	3.30	3.28

Clearly, there are large between-the-mean differences for the operators and for the batches.

A simple F-ratio for the between-means source of variation was computed and gave the following results.

Source of Variation	Mean Square	F-Ratio
Operators	0.2209	552
Batches	1.9321	4,830
Experimental Error	0.0004	

The F-ratio for operator error is significant at a confidence level of 95%, while for batch-to-batch error the confidence level was 99%.

The overall experimental error was unexpectedly small, $0.02 \dfrac{\text{in.-lb}}{\text{in.}^2}$ (coefficient of variation of 0.61%). This helps to verify that it is a well designed test method.

While the batch-to-batch error is a natural variant of the material, the operator error is not. Since the test method gives only a small experimental error, we must assume that the operator error has to do with specimen preparation (each operator prepared his own test specimens as well as conducting his own tests). We placed a great emphasis upon training both operators in the conduct of the tests and apparently did not pay sufficient attention to specimen preparation.

As a final matter, the exponent l+m+n in the previous propellant/ liner bond tests have fallen near 2.0, which is near the ideal linear elastic value, Equation (62). That exponent for the ANB-3600/SD-923/WS 15353 bond system was found to fall in the range 2.3 to 2.4, which makes the behavior rather nonlinear. The test data were not otherwise affected by this nonlinearity.

9.0   ACKNOWLEDGEMENTS

The authors owe much to the many people who worked on this contract. The enthusiasm that each person brought to the effort was in itself a rewarding part of the experience.

A special thanks is given posthumously to Albert B. Curtis, Jr., for his experimental skill in getting the laboratory program off to a good start. His death in the prime of life left us all much more humble.

Mr. Thomas J. Icanberry stepped in to fill the shoes of Al Curtis. His constant drive for excellence gave success to the experimental program.

Professor Walter E. Haisler, Jr. of Texas A & M University went far beyond the call of duty in providing the many structural analyses of the scarf-joint specimen. Through him the latest methods were used to give us one-, two- and three-dimensional analyses.

Many thanks are due also to Mr. Herman P. Briar of Automation Services and to Mr. Charles C. Surland of ASPC for their able help in experimental and analytical efforts.

REFERENCES

1. W. G. Knauss, "The Mechanics of Polymer Fracture," Applied Mechanics Reviews, 26, 1973, pp. 1-17

2. W. G. Knauss, "Fracture of Solids Possessing Deformation Rate Sensitive Material Properties, A.S.M.E. - AMD No. 19, 1976, pp. 69-97.

3. R. A. Schapery, "A Theory of Crack Initiation and Growth in Viscoelastic Media. I. Theoretical Development." Int. Journal of Fracture, Vol. 3, Feb. 1975, pp. 141-159.

4. R. A. Schapery, "A Theory of Crack Initiation and Growth in Viscoelastic Media, II, No. 3, June 1975, pp. 369-388

5. R. A. Schapery, "A Theory of Crack Initiation and Growth in Viscoelastic Media, III. Analysis of Continuous Growth". Int. Journal of Fracture, Vol. 11, No. 4, Aug. 1975, pp. 549-562.

6. R. A. Schapery, "A Method for Predicting Crack Growth in Nonhomogeneous Viscoelastic Media". Int. Journal of Fracture, Vol. 14, No. 3, June 1978, pp. 293-309.

7. R. A. Schapery, "Fracture Mechanics of Solid Propellant", Fracture, H. Laboratory, Ed. (1978).

8. R. A. Schapery, "On the Analysis of Crack Initiation and Growth in Non-homogeneous Viscoelastic Media", SIAM-AMS Proceedings, Vol. 12, 1979, pp. 137-152.

9. Schapery, R. A., "Correspondence Principles and a Generalized J Integral Theory for Deformation and Fracture Analysis of Nonlinear Viscoelastic Media", In three parts. Texas A&M University Report Nos. MM 3724-81-1 through -3, 1981, College Station, TX.

10. J. R. Rice, "A Path Independent Integral and the Approximate Analysis of Strain Concentration by Notches and Cracks", J. Applied Mechanics, ASME, June 1968, pp. 379-386.

11. J. K. Knowles and E. Sternberg, "On a Class of Conservation Laws in Linearized Finite Elastostatics", Archives for Rational Mechanics and Analysis, Vol. 44, No. 3, 1972, pp. 187.

12. S. T. Rolfe and J. M. Barsom, Fracture and Fatigue Control in Structures, Prentice-Hall, Englewood Cliffs, N. J., 1977.

13. Francis, G. et al., "Predictive Techniques for Failure Mechanisms in Solid Rocket Motors", Chemical Systems Div. Report CSD 2540-FR (Air Force Rocket Propulsion Laboratory Report AFRPL-TR-79-87), January 1980.

14. Anon, "JANNAF Solid Propellant Structural Integrity Handbook, Section 5.5.3, CPIA Pub. No. 230, September 1972.

REFERENCES

15. R. C. Sampson, "Experimental Evaluation of Some Problems in Solid Propellant and Binder Deformation", Aerojet-General Corp. Technical Memorandum, May 1965.

16. R. S. Dunham and E. B. Becker, "TEXGAP - The Texas Grain Analysis Program," University of Texas Report TICOM 73-1, 1973.

17. W. E. Haisler, "AGGIE 1 - "A Finite Element Program for Nonlinear Structural Analysis," Texas A&M University Report TEES 3275-77-1, Aerospace Engineering, 1977.

18. Briar, H. P., Bills, K. W., Jr. Cribbs, R. W., and Lamb, B. L., "The Selection and Demonstration of Advanced Nondestructive Testing Techniques for On-Site Missile Inspection", AFRPL-TR-73-91 (November 1973).

19. G. P. Anderson and L. E. Jensen, "Testing for Adhesive and Cohesive Fracture," Bulletin of JANNAF Structures and Mechanical Behavior Subcommittee, 15th Meeting 1978, Vol. I, July 1978, pp. 37-52.

20. Fisher, R. A., The Design of Experiments, Oliver and Boyd, Edinburgh, Fifth Edition (1948).

APPENDIX A

PREPARATION AND TESTING PROCEDURES FOR THE
SCARF-JOINT TEST SPECIMEN

1.0 ABSTRACT

Procedures are described for the preparation and testing of propellant/liner bonds in the scarf-joint specimens. Test specimens will contain piezoelectric crack sensors for monitoring tear propagation. Calculations are made from a combination of parameters including those of force, time, deflection, temperature and the ultrasonic transit time, Δt, measurements from the PZT crystals. A DAR data recording and analysis system is employed to monitor these parameters.

2.0 EQUIPMENT AND MATERIALS

The following equipment and materials are needed to prepare and test the Scarf-Joint Specimens (Figure A-1).

a. Measuring rule (0.01 in. graduations).

b. Double-backed tape (permacel or equivalent).

c. X-acto knife with 2-1/2 in. blade No. 226.

d. Adhesive (Ren 6405) Ren plastics.

e. Adhesive (EA 901-B1) Hysol-Dexter Corp.

f. Paint or acid brush approximately 1/2 in. wide.

g. Ball-point (fine) or fine felt-tipped pen.

h. Prepared aluminum end-plates measuring 1 by 1 by 4 in. (with embedded PZT crystal transducers suitable for attachment to tester hardware).

i. ASPC developed bonding support (Figure A-2), flaw inducing fixture (Figure A-3), and cutting blades (Figure A-4).

j. Specimen preparation saw or milling machine capable of producing uniform 4 by 2 by 1 in. propellant specimens (Figure A-5).

k. Instron tensile tester with temperature environment chamber.

l. Multi-channel variable gain and zero control junction for extensometer calibration and balance.

m. DAR data recording and analysis system (Figure A-6).

n. Multi-channel time y - MV strip recorder plus 5 to minus 5 MV full-scale range.

o. Piezoelectric crystal transducers - transmitters and receivers (Figure A-1).

p. High frequency signal conditioning system (pulse genrator) for PZT crystals (Figure A-6).

q. Oscilloscope Tektronik Mod 77048 or equivalent.

r. Multimeter (VOM) Kiethley Mod 178 or equivalent.

s. Stop-watch accurate to within 0.01 sec.

t. Video recording system with closed circuit T.V.

u. Preston Mod DK variable gain amplifiers or equivalent - 1 ea. per channel of recording.

v. Copper - Constantan temperature reference junction.

w. Copper - Constantan thermocouple.

x. Shear component extensometer with attachment hardware (Figure A-7).

y. Axial displacement fixture with four extensometers and attachment hardware (Figure A-8).

z. Digital clock and frequency counter.

aa. ASPC developed programmable temperature rate controller (P.T.R.C.) (Figure A-9).

3.0 PROCEDURES

3.1 SPECIMEN PREPARATION

Machine saw scarf-joint specimens from liner box measuring 4 by 2 by 1 in. All sides must be parallel and 90 degrees from the adjacent side (Figure A-5).

a. Brush loose particles from all specimen surfaces.

b. Place strips of double-backed tape on a flat surface. Press the surfaces to be bonded to the exposed adhesive face to remove the remaining loose material. Repeat until no new material transfer is detected.

c. Mix EA 901-B1 per manufacturer's instructions.

d. Apply a thin layer of EA 901-B1 adhesive to the sand-blasted and degreased (with embedded PZT crystal) aluminum end plate.

e. Apply layer of EA 901-B1 to insulator of specimen.

f. Place end-plate and specimen on a flat nonstick (waxed paper paper) surface in preparation for bonding.

g. With the adhesive-painted surfaces opposite one another push the end-plate to the insulator of the specimen with sufficient force to produce an epoxy bead at the interface edge.

h. Cure the bond for 24 hours at 77°F.

i. Mix Ren-6405 adhesive per manufacturer's instructions and allow 10 to 15 min. before application.

j. Bolt sand-blasted and degreased, aluminum end-plate (with embedded PZT crystal transducer) to bonding support fixture (Figure A-2).

k.   Apply Ren-6405 adhesive to end-plate and propellant surfaces.

l.   Push bonding surfaces together and bolt EA 901-B1 bonded
      end-plate to bonding fixture to ensure proper contact and
      alignment (Figure A-2).

m.   Cure the bond for 24 hours at 77°F.

n.   Remove bonded specimen from fixture.

o.   Mark the flaw locations at the propellant-liner interface on
      the specimen and then carefully drill a 0.2 in. hole at the
      mid-point of the proposed flaw.

p.   Reinstall specimen in the bonding support flaw inducing fixture
      (Figure A-2) and align the flaw inducing guide slots at the
      propellant liner interface (Figure A-3).

q.   Feed the flaw-inducer blade guide tab (Figure A-4) through the
      guide slot at one side of the fixture, through the pre-drilled
      hole in the specimen and through the guide slot on the opposite
      side of the fixture. Using a firm, continuous motion, pull the
      guide tab and attached blade through the fixture and specimen.

r.   Remove the specimen from the fixture.

s.   Map and cut the stress relief configuration in the propellant
      (Figure A-10).

t.   Measure and record all specimen dimensions.

u.   Attach extensometer hardware to the specimen end plates.

3.2   TEMPERATURE CONDITIONING

      Prior to testing, condition specimen at the prescribed test
temperature as follows:

Test Temperature, °F	Conditioning Time, hours	
	Minimum	Maximum
a. Minus 75 to plus 60	1	24
b. Plus 60 to plus 80	1	-
c. Plus 80 to plus 110	1	8

3.3 TESTING PROCEDURE

a. Secure pre-drilled 1000 lb capacity load cell in place. Particular care should be taken to ensure that the cell is level and aligned with the cross-head shaft (Figure A-11).

b. Calibrate tensile tester according to Section 5.30 of the "Operating Instructions for the Instron Tensile Testing Instruments", Manual 10-29-1.

c. Calibrate the load voltage input to the DAR system using an VOM hook-up with a variable output rheostat control. Calibrate 5 volts full scale regardless of load cell or amplifier output.

d. Balance individual specimen tare weight before each test.

e. Secure specimen with jam nut to lower cross-head shaft. Remove slack with manual cross-head adjustment control while taking care not to preload specimen (watch VOM for zero, not the chart pen). Lock jam nut at the upper load cell shaft and recheck the zero manipulating the cross-head adjustment control as necessary.

f. Connect PZT and extensometer cables to DAR monitoring system.

g. Calibrate extensometers output to 5 volt DAR system using VOM hook-up with variable gain controls:

A-5

1. Set zeros for each extensometer in turn.

2. Insert spacing block of known thickness, i.e., 0.075 in. represents half-scale of 0.15 in. total displacement.

3. Adjust variable gain controls to represent the percentage of mechanical displacement in volts, i.e., using half-scale displacement adjust the VOM readout to 50% of 5 volts full-scale - 2.5 volts.

h. Switch trigger mode at pulse generator to "internal". Adjust comparator controls and amplifier settings to correct value for the test, i.e., using the oscilloscope, set the trigger level at the comparator controls to a level above the random noise of the setup and adjust the amplitude of the receiver PZT crystals to matching levels (Figure A-12).

i. Switch the trigger mode at the pulse generator back to the "external" position.

j. Address DAR and call for operator options.

k. Set test duration and time interval.

l. Calibrate analog channels.

m. Recheck settings and record test temperature for each specimen.

n. Set-up video recording equipment and position T.V. camera in such a manner that the specimens and the digital counter can both be seen on the monitor.

o. Record the test conditions and the video recorder counter number on the specimen information sheet.

p. Start the test in the following sequence as rapidly as possible:

    1. Video Recorder On

    2. DAR On

    3. Tensile Tester and Recorder Chart On

q. Observe test and record all relevant events on the strip chart.

    1. Location of fracture initiation

    2. Location of fracture propagation

    3. Flaws at tip of original crack

    4. Rotation or distortion of specimen prior to fracture initiation

    5. Separation at bondline along edge of specimen

    6. Description of failure sequence

r. When test is complete, reverse order to "p" above.

s. Address DAR to print-out data.
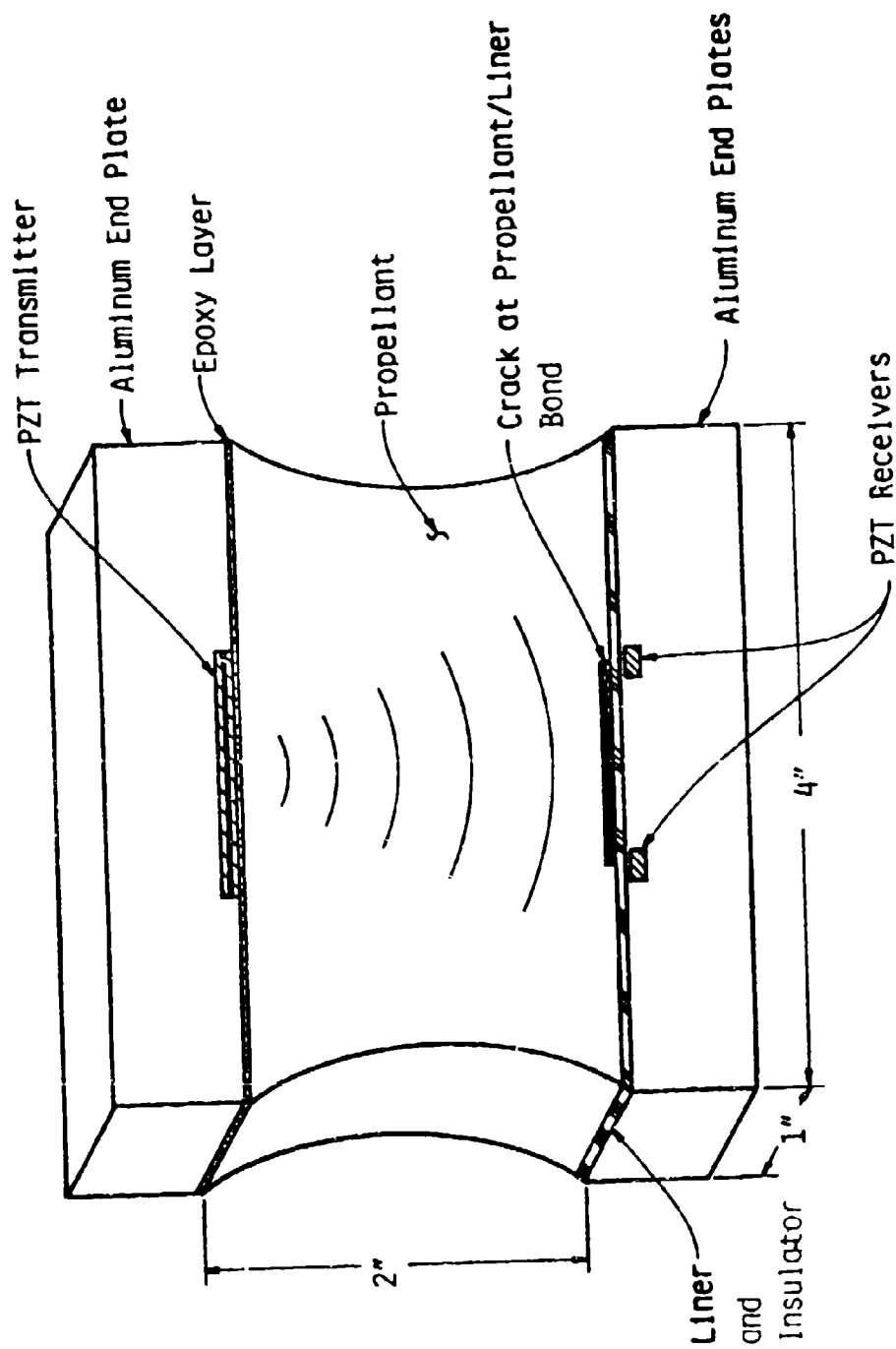
Figure A-1. Scarf-Joint Specimen with PZT Sending and Receiving Transducers

A-8

Fixture

Scarf-
Joint
Specimen

PROPELLANT

LINER
INSULATION
CASE
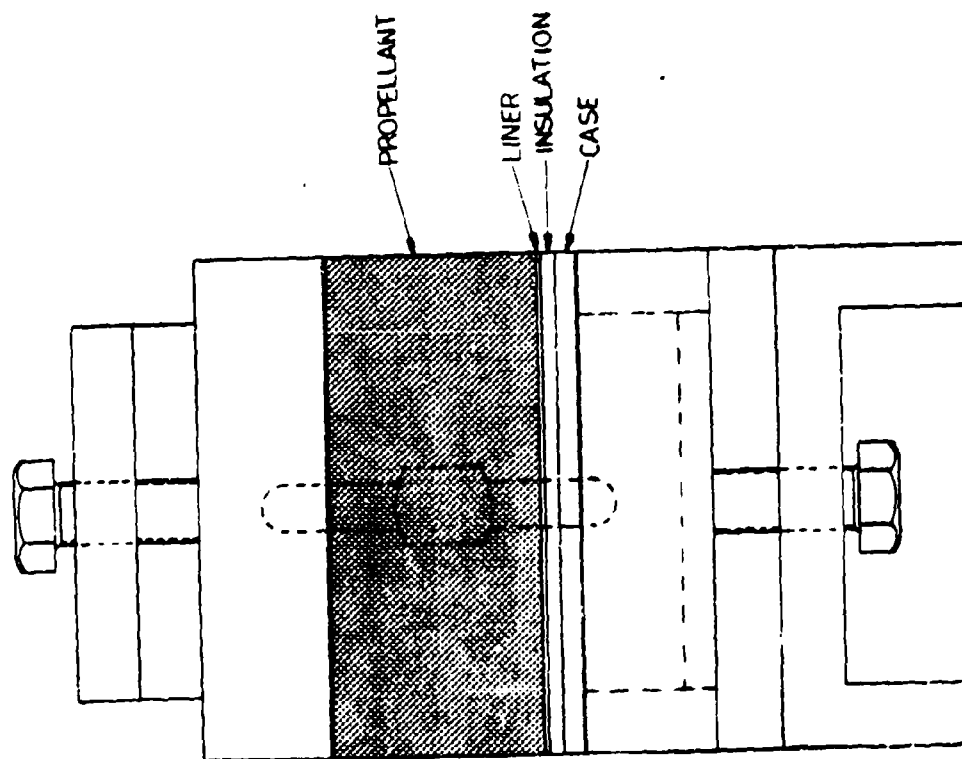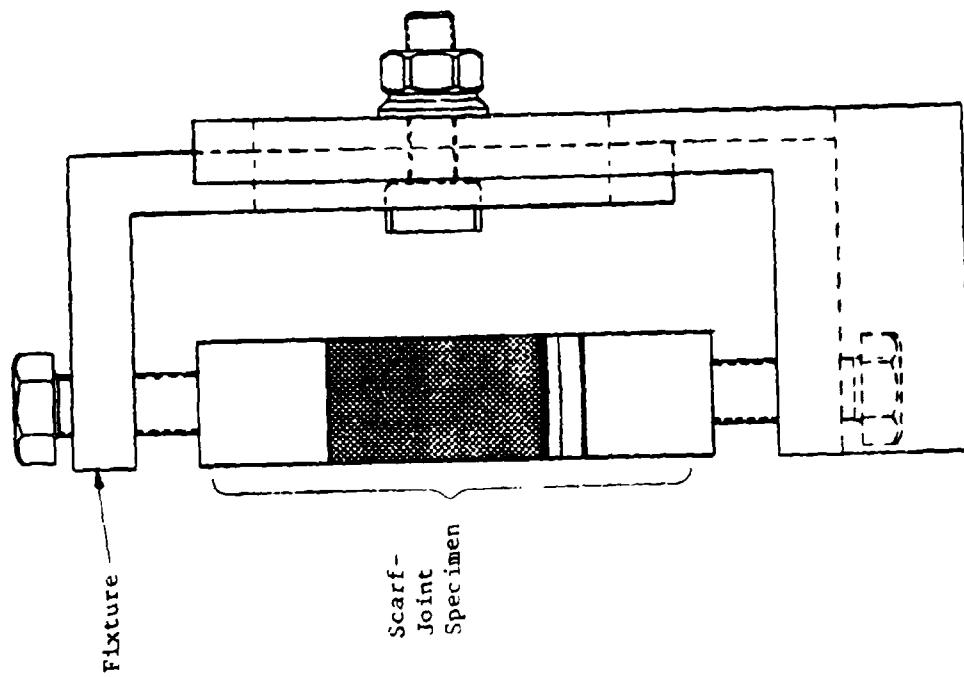
Figure A-2. Bonding Support Fixture

Alignment
and Cutting
Fixture

Bonding
Support
Fixture
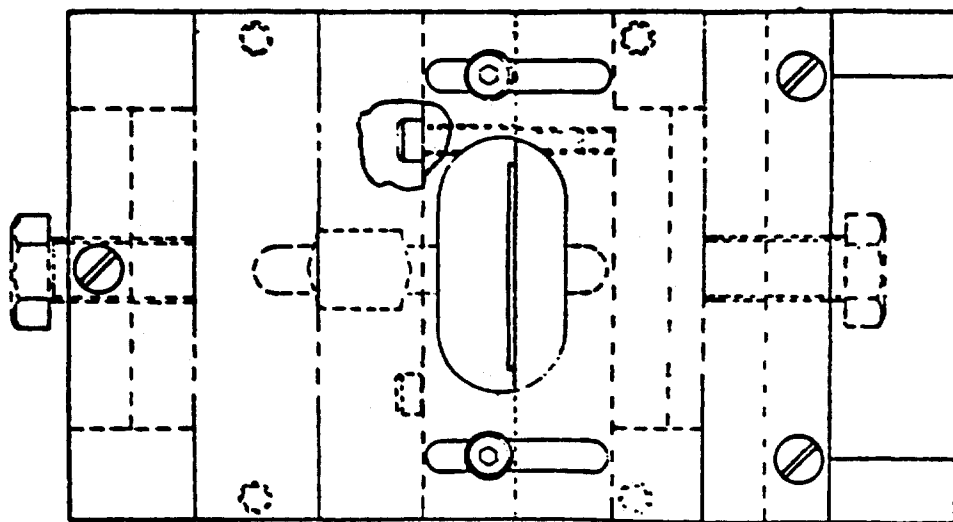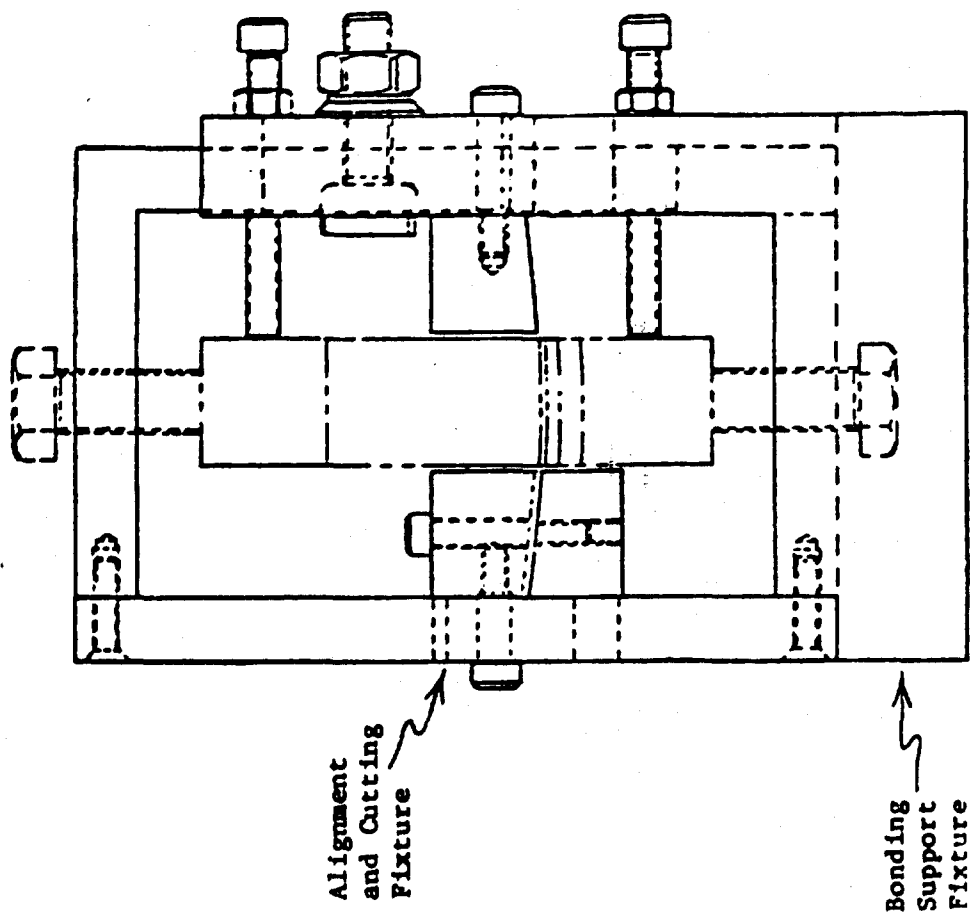
Figure A-3. Bonding Support, Alignment and
Cutting for Motor Specimens
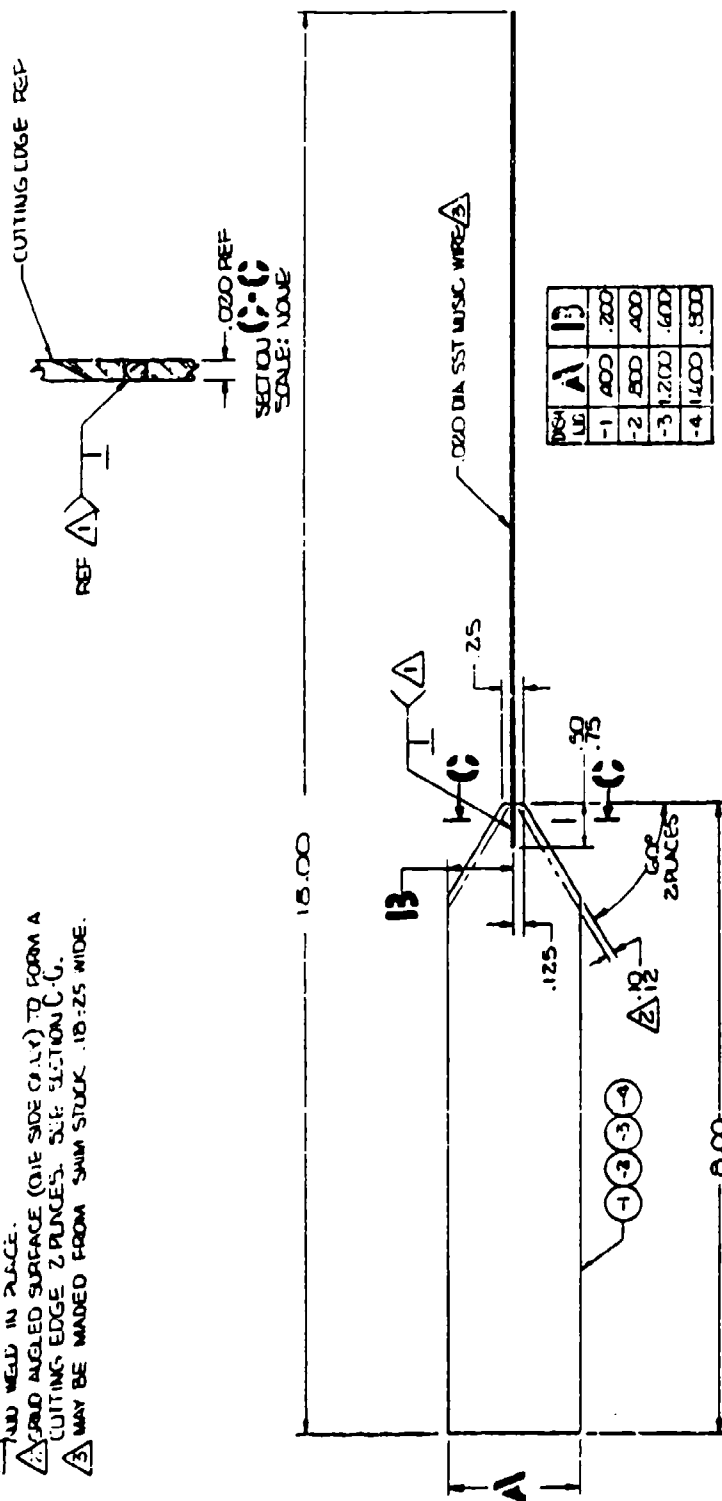
Figure A-4. Cutting Blade Designs

Propellant

Liner

Insulation

2 in.

4 in.

1 in.
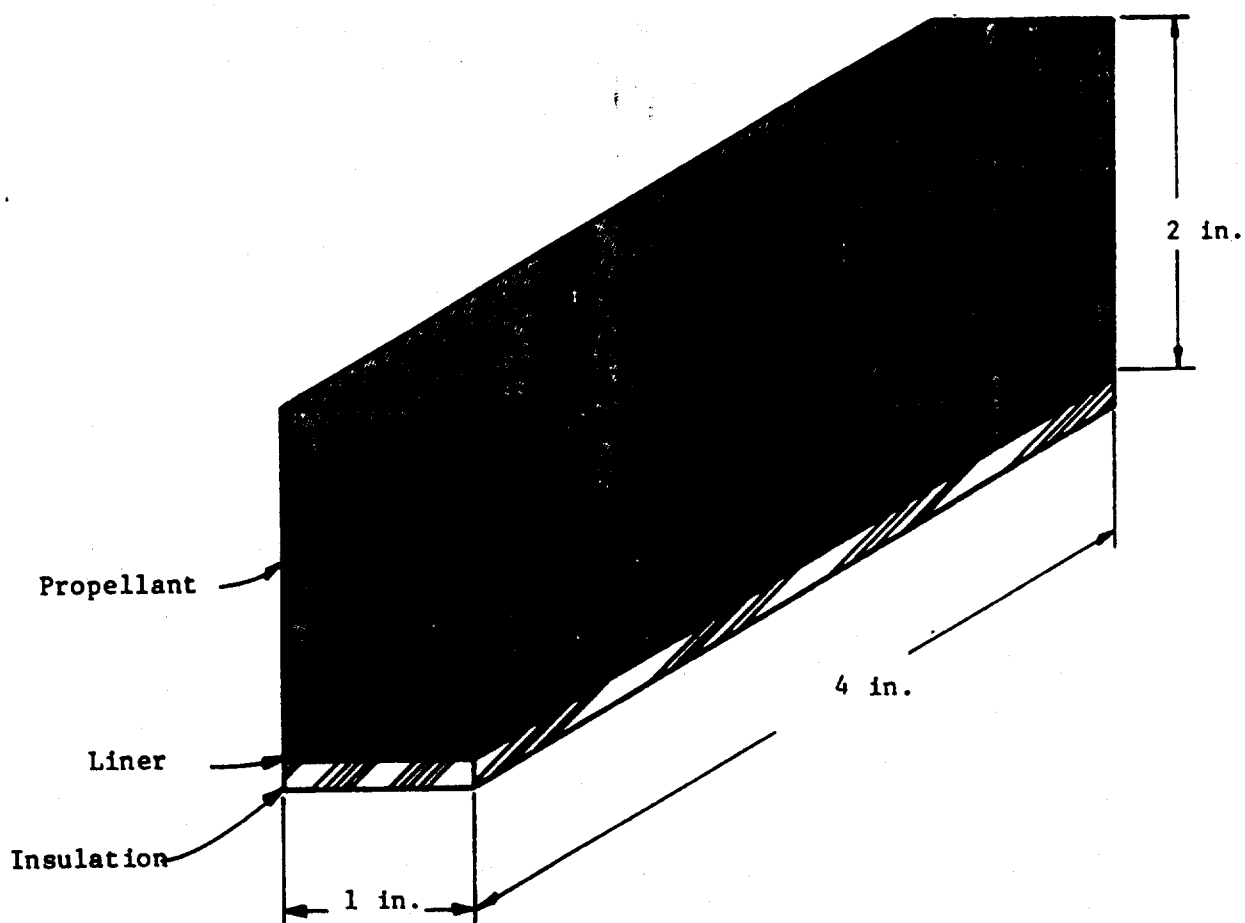
Figure A-5. Milled or Saw-Cut Scarf-Joint Specimen
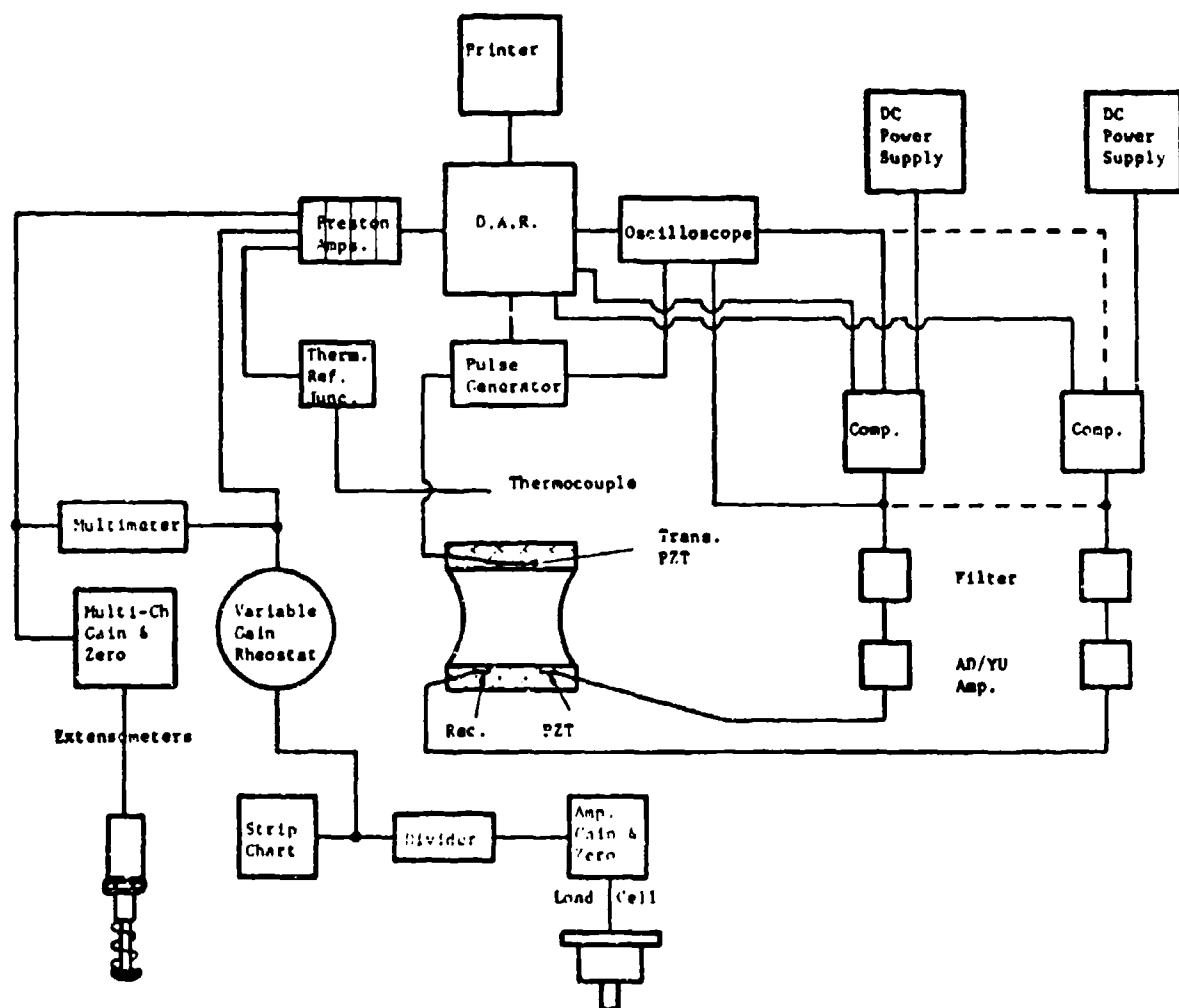
Figure A-6. D.A.R. Data Recording and Analysis System

A-13

Top View

"Over-Bite" Clamp

Linear Potentiometer
(One Channel Extensometer)

Side View

Thumb Screws
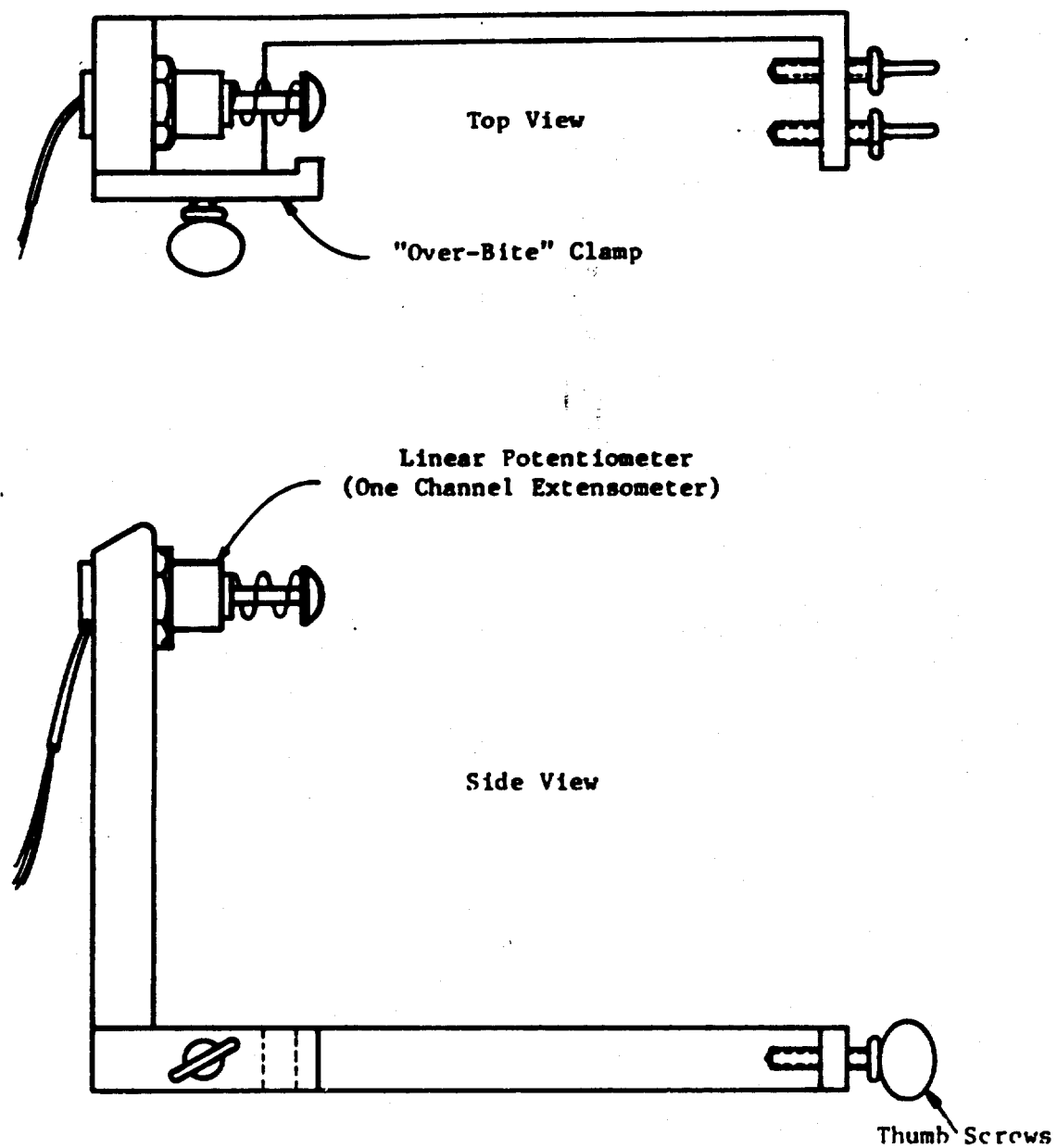
Figure A-7. Shear Component Extensometer

(Used in measuring shear deformation in combined
tension/shear test configuration)
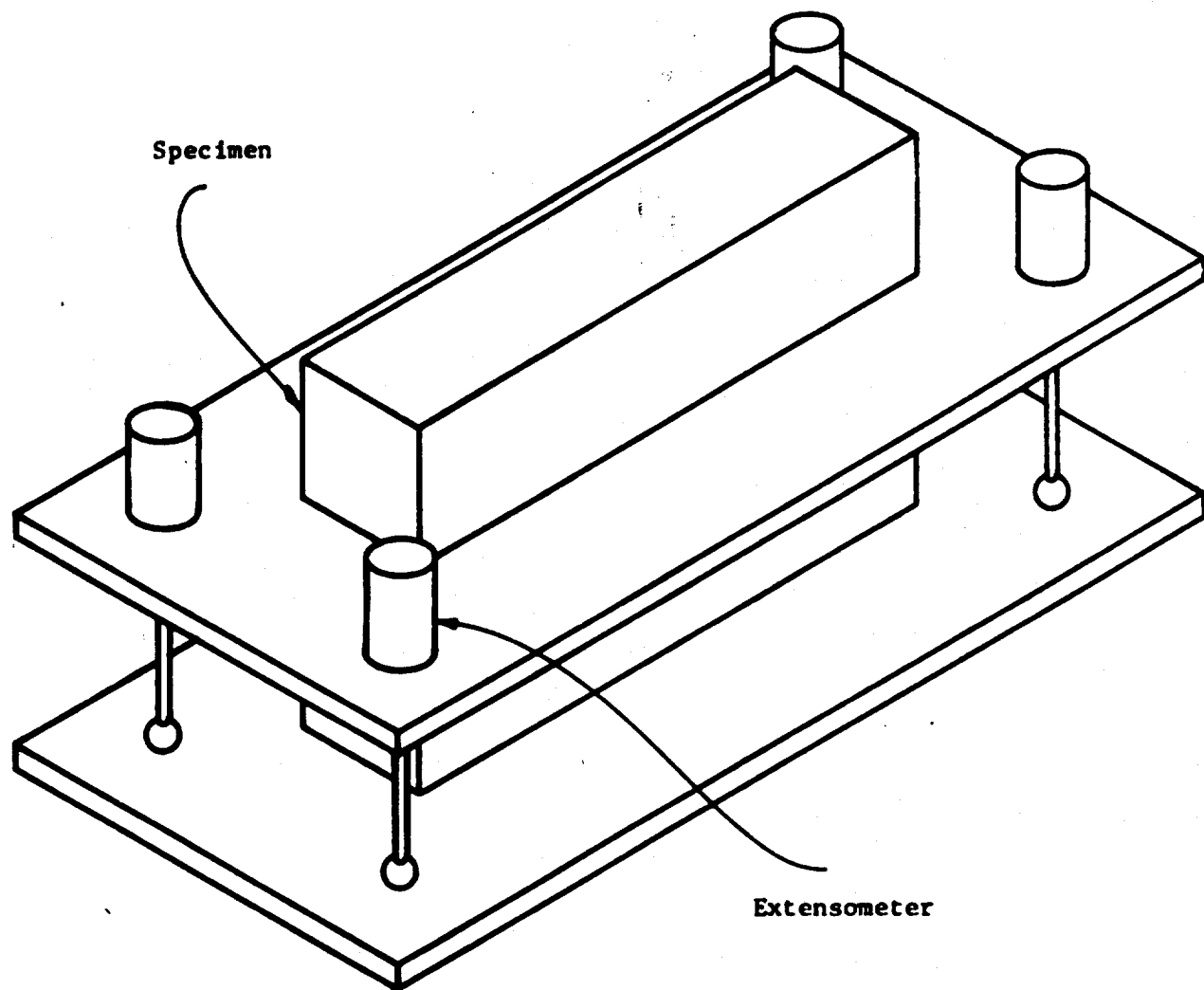
Figure A-8.   Axial Displacement Monitoring Fixture for
the Scarf-Joint Specimen

```
┌─────────────────┐
│   Oscillator    │
│     Clock       │
└────────┬────────┘
         │
┌────────┴────────┐
│  Rate Selector  │
│   Clock ÷ N     │
└────────┬────────┘
         │
┌────────┴────────┐
│ Rapid-Syn M-62  │
│   Translator    │
└────────┬────────┘
         │
┌────────┴────────┐
│    Stepping     │
│     Motor       │
└────────┬────────┘
         │
┌────────┴────────┐
│    10 Turn      │
│   1 k Ω Pot.    │
└────────┬────────┘
         │
┌────────┴────────┐
│   Honeywell     │
│   Controller    │
└────────┬────────┘
         │
┌────────┴────────┐
│    MTS High     │
│  Rate Tester    │
│  Cond. Chamber  │
└─────────────────┘
```
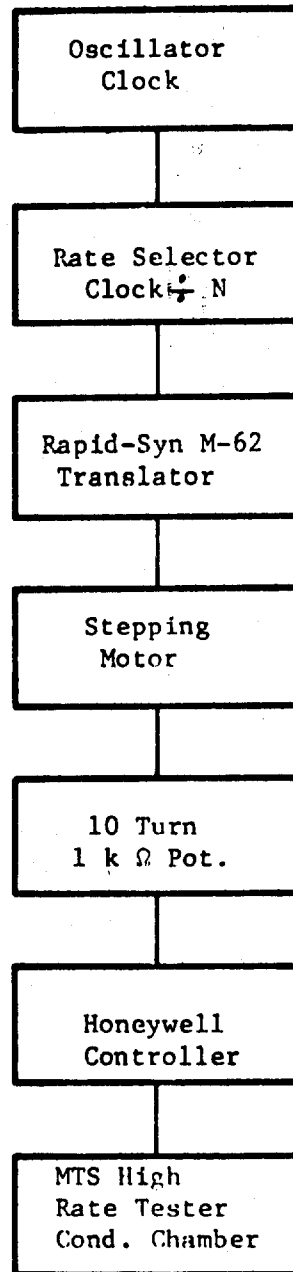
Figure A-9. Programmable Temperature Rate Controller
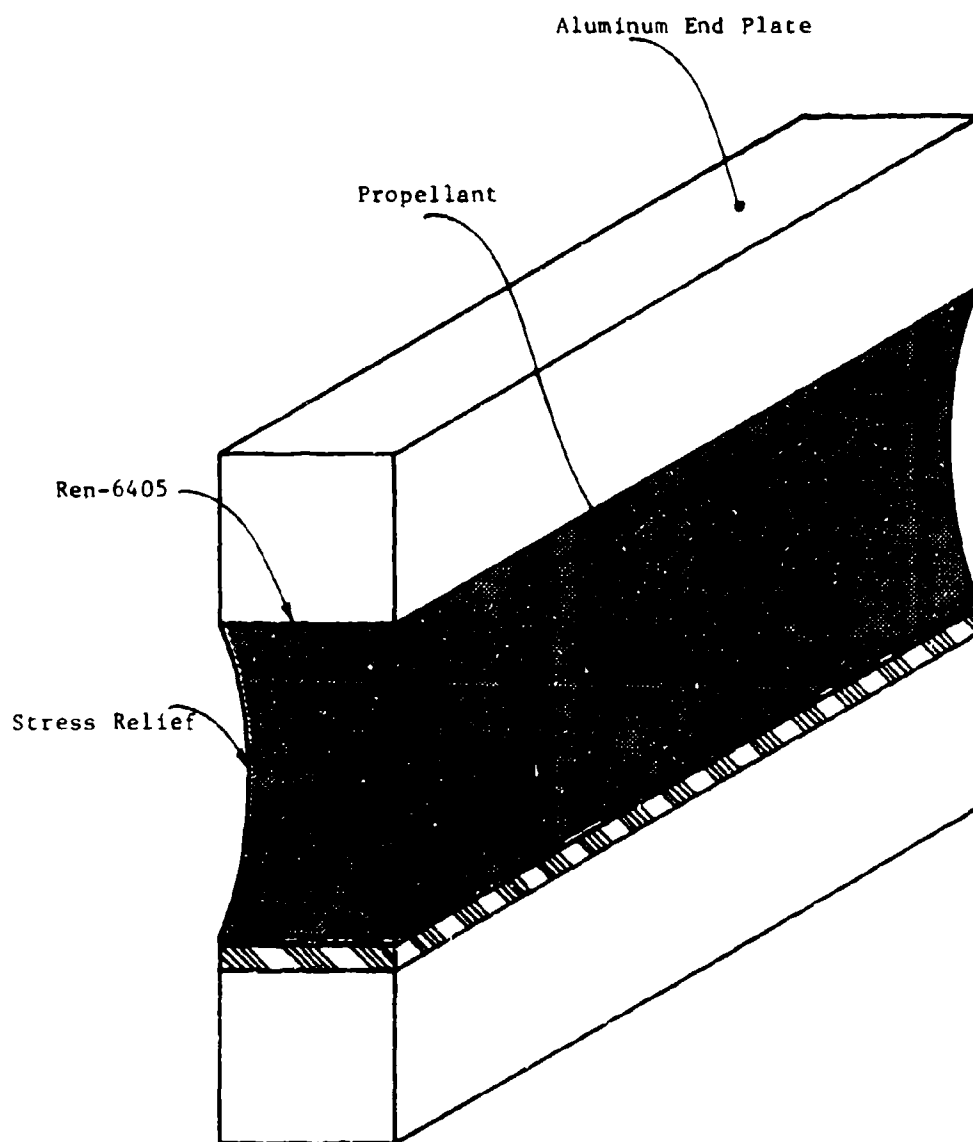
Figure A-10. Cutting End Stress Relief
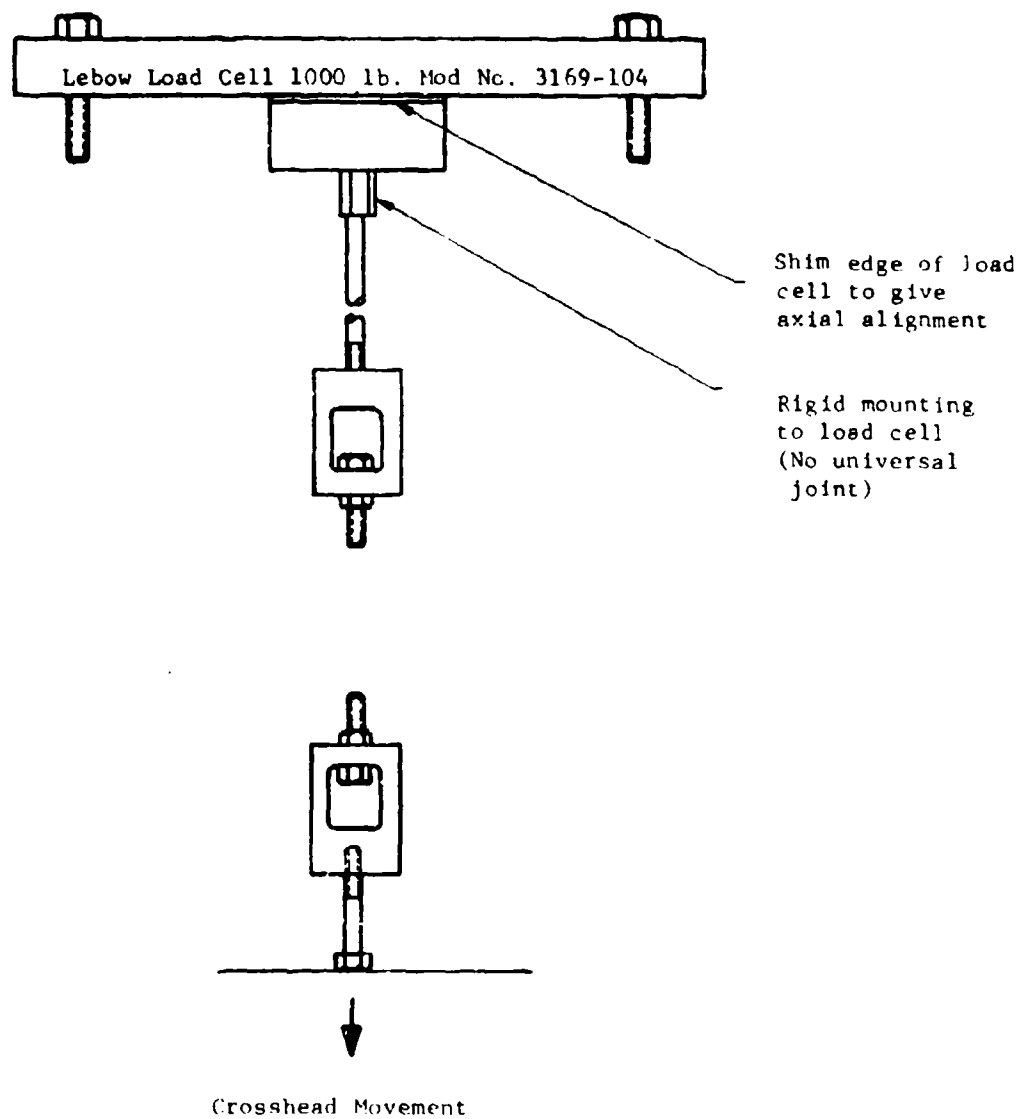
Figure A-11. Instron Tester - Typical Test Setup

A-18

Oscillograph Representation
of pulse in-put

Overlay as close to
baseline as possible

Oscillograph Representation
of Comparator in-put
(Time base delay)

Approx. 28 MS delay

st Trigger after Delay
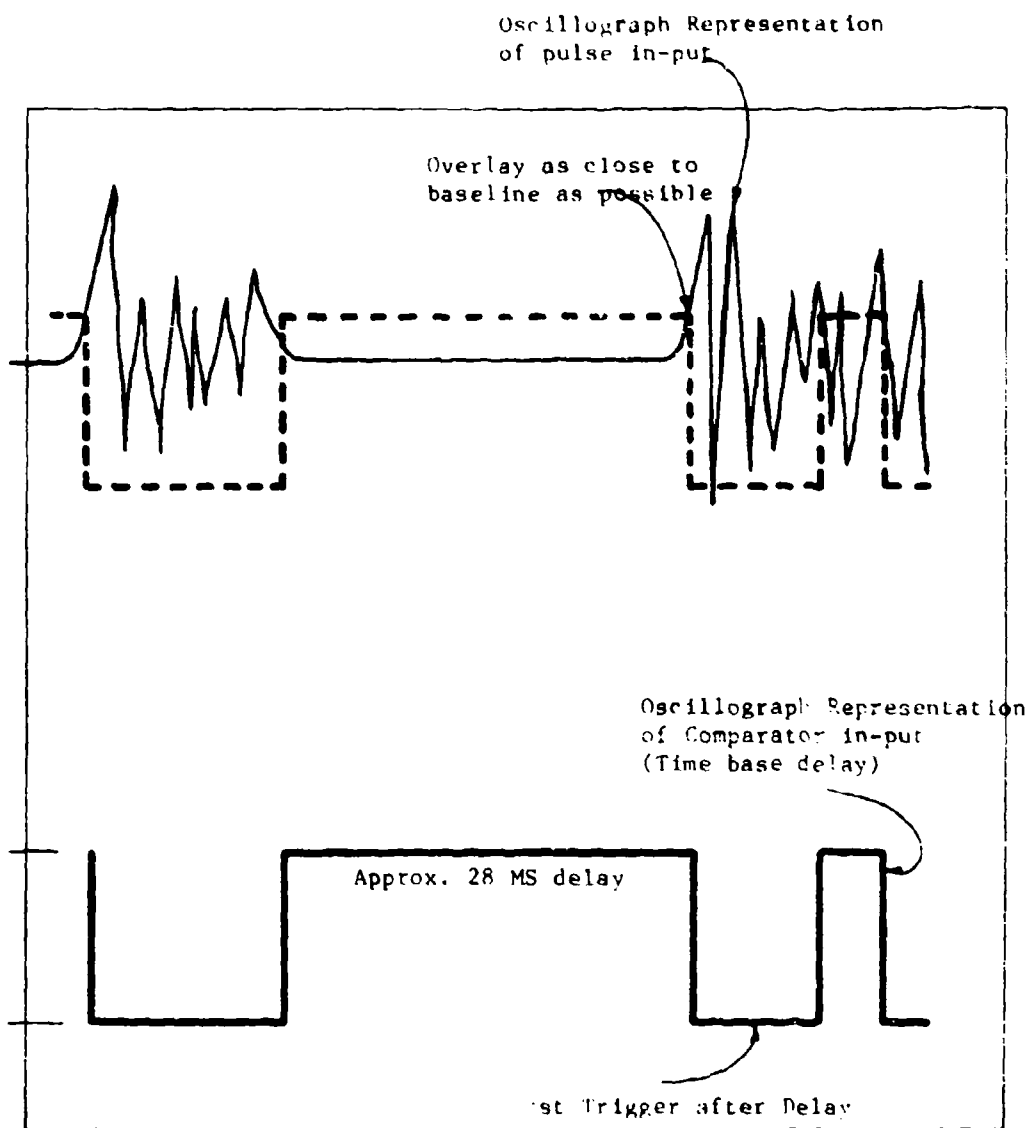
Figure A-12. Oscilloscope/Comparator Time Base Delay

A-19

APPENDIX B

TABULATIONS OF LABORATORY
TEST DATA

TABULATIONS OF LABORATORY TEST DATA

The following tabulations provide raw data taken on individual specimens in the various tests performed on this program. Only those test matrices that were appropriate for data analysis are provided; thus, some table numbers are skipped. Tables B-11, B-12, B-21 and B-22 are numbered appropriate to the parameters in the Graeco-Latin square test plan.

The data are taken at discreet intervals and in sufficient numbers to define the force-displacement curves. The data tabulations go several steps beyond the crack initiation point to illustrate the nature of the curve in this region.

The following notations are used.

2a' = length of the crack, in.

  f = force on the specimen per lineal inch of the crack tip, lb/in.

  R = crosshead rate of motion, in./min

SBF = secondary bond failure

  U = deformation of the specimen   test, in.

TABLE B-3-1

CYLINDRICAL PEEL TESTS OF ANB-3066/SD-851-2
PROPELLANT/LINER BOND AT 77°F

Spec. No.:	3-12	3-11	3-10	3-27	3-9
2a', in.	0.55	0.55	0.55	0.55	0.55
$\dot{p}$, psig/min.	3.73	11.62	183	265	766
P,psig	$U X10^3$, in.	$U X10^3$, in.	$U X10^3$, in.	$U X10^3$, in.	$U X10^3$, in.
5	0.1	0.3	0.2	0.1	0.17
10	0.3	0.5	0.4	1.5	0.35
15	0.55	0.75	0.65	0.25	0.52
20	0.9	1.0	0.85	0.35	0.58
25	1.25	1.2	1.0	0.65	0.87
30	1.6	1.25	0.8	0.8	1.05
35	2.0	1.8	1.55	1.0	1.22
40	2.4	2.15	1.95	1.1	1.4
45	2.65	2.45	2.2	1.35	1.57
50	3.2	3.0	2.65	1.6	2.0
55	3.6	3.5	2.95	1.85	2.2
60	4.05	4.1	3.3	2.0	2.6
65	4.6	5.2	3.75	2.2	2.9
70	5.3	6.9	4.1	2.35	3.25
75	6.7	9.0	4.7	2.75	3.65
80	6.7	9.0	5.2	3.0	4.0
85			5.7	3.3	4.5
90			6.2	3.65	5.0
95			6.9	4.0	5.5
100			7.6	4.3	6.1
105			8.35	4.75	6.7
110			9.2	5.3	7.55
115				6.0	8.3
120					9.4

CYLINDRICAL PEEL TESTS OF ANB-3066/SD-851-2
PROPELLANT/LINER BOND AT 77°F

Spec. No.:	3-5	3-3	3-2
2a', in.	0.70	0.70	0.70
$\dot{p}$, psig/min.	3.98	170	800
P, psig	$UX10^3$, in.	$UX10^3$, in.	$UX10^3$, in.
5	0.35	0.7	0.1
10	1.0	1.0	0.1
15	1.5	1.25	0.3
20	2.15	1.6	0.6
25	2.7	2.0	1.2
30	3.3	2.3	1.5
35	4.0	2.7	1.9
40	4.8	3.25	2.3
45	5.6	3.75	2.8
50	6.75	4.35	3.3
55		5.0	4.0
60		5.8	4.75
65		6.7	5.7
70		7.65	6.5
75		8.8	7.6
80		10.5	8.9

CYLINDRICAL PEEL TESTS OF ANB-3066/SD-851-2
PROPELLANT/LINER BOND AT 77°F

Spec. No.:	3-21	3-20	3-19	3-18
2a', in.	0.80	0.80	0.80	0.80
$\dot{p}$, psig/min.	3.58	11.24	356	686
P, psig	$U \times 10^3$, in.	$U \times 10^3$, in.	$U \times 10^3$, in.	$U \times 10^3$, in.
5	0.1	0.9	0.3	0.1
10	0.5	1.35	0.6	0.2
15	1.0	2.0	0.9	0.35
20	1.6	2.5	1.2	0.65
25	2.25	3.35	1.55	1.0
30	2.9	4.05	2.0	1.3
35	3.9	5.0	2.4	1.7
40	4.9	6.0	3.0	2.0
45	6.0	7.5	3.6	2.4
50	7.0	9.3	4.1	2.9
55		12.3	4.8	3.35
60		19.0	5.6	3.95
65			6.7	4.5
70			7.8	5.2
75			9.8	5.9
80				6.75

TABLE B-3-2

CYLINDRICAL PEEL TESTS OF ANB-3066/SD-851-2
PROPELLANT/LINER BOND AT 0°F

Spec. No.:	3-16	3-13	3-17	3-7	3-6
2a', in.	0.55	0.55	0.70	0.70	0.70
$\dot{p}$, psig/min.	3.44	570	3.74	218	632
P, psig	$U \times 10^3$, in.	$U \times 10^3$, in.	$U \times 10^3$, in.	$U \times 10^3$, in.	$U \times 10^3$, in.
7.5	0.1	0.1	0.1	0.1	0.1
15.0	0.1	0.2	0.3	0.2	0.25
22.5	0.2	0.3	0.7	0.4	0.35
30.0	0.3	0.4	1.0	0.7	0.6
37.5	0.8	0.6	1.4	0.9	0.8
45.0	1.0	0.8	1.9	1.2	1.05
52.5	1.4	1.0	2.5	1.4	1.35
60.0	1.8	1.3	3.1	1.8	1.75
67.5	2.1	1.5	3.9	2.3	2.2
75.0	2.6	1.9	4.8	2.7	2.55
82.5	3.1	2.3	5.9	3.2	3.0
90.0	3.6	2.6	7.4	3.7	3.6
97.5	4.1	3.0		4.3	4.2
105.0	4.7	3.3		5.3	4.9
112.5	5.4	3.8		6.1	5.6
120.0	6.0	4.4		7.3	6.4
127.5	6.7	5.0			
135.0	7.7	5.5			
142.5	8.7	6.39			
150.0	10.2	7.2			

CYLINDRICAL PEEL TESTS OF ANB-3066/SD-851-2
PROPELLANT/LINER BOND AT 0°F

Spec. No.:	3-25	3-24	3-23	3-22
2a', in.	0.80	0.80	0.80	0.80
$\dot{p}$, psig/min.	3.55	11.24	254	492
P, psig	$UX10^3$, in.	$UX10^3$, in.	$UX10^3$, in.	$UX10^3$, in.
7.5	0.2	0.1	0.7	0.1
15.0	0.35	0.2	1.0	0.25
22.5	0.6	0.3	1.3	0.4
30.0	1.3	0.6	1.6	0.7
37.5	2.0	1.0	2.1	0.9
45.0	2.8	1.5	2.8	1.1
52.5	3.9	2.3	3.7	1.5
60.0	5.2	2.9	4.9	1.8
67.5	6.7	3.5	6.2	2.2
75.0	9.0	4.3	7.85	2.6
82.5	12.7	5.9	10.2	3.0
90.0	41.2	17.2	13.25	3.5
97.5			18.2	4.0
105.0			28.0	4.6
112.5				5.1
120.0				5.8
127.5				6.6
135.0				7.5
142.5				8.7
150.0				11.9

STRIP BIAXIAL TENSILE TESTS OF ANB-3066/SD-851 2
PROPELLANT/LINER BOND AT 77°F

Spec. No.:	4-1	4-2	4-3	4-4	4-5
2a', in.	0.4	0.4	0.4	0.4	0.4
R, in./min.	0.02	0.02	0.10	0.50	0.50
U, in.	f, lb/in.	f, lb/in.	f, lb/in.	f, lb/in.	f, lb/in.
.005	16.7	22.2	26.0	26.0	29.6
.010	34.2	41.8	49.6	53.2	59.2
.015	51.7	61.2	71.0	78.0	88.0
.020	68.1	82.0	93.2	103.2	116.8
.025	85.0	103.0	116.8	129.2	143.2
.030	101.7	124.3	140.4	154.8	172.4
.035	118.3	145.8	163.2	180.4	200.0
.040	134.8	166.2	185.6	205.2	226.8
.045	151.3	185.8	207.0	228.8	251.2
.050	166.0	202.7	227.6	252.8	273.2
.055	180.8	215.0	244.4	274.8	292.8
.060	191.5	220.4	257.2	292.8	305.6
.065	195.8		264.0	300.4	312.0
.070			265.4		312.8

STRIP BIAXIAL TENSILE TESTS OF ANB-3066/SD-851-2
PROPELLANT/LINER BOND AT 77°F

Spec. No.:	4-6	4-7	4-8	4-9
2a', in.	0.8	1.2	1.2	1.6
R, in./min.	0.10	0.10	0.10	0.10
U, in.	f, lb/in.	f, lb/in.	f, lb/in.	f, lb/in.
.005	21.4	18.8	20.4	14.8
.010	42.3	38.8	38.3	30.4
.015	63.8	57.7	59.2	46.0
.020	84.6	76.9	79.2	62.0
.025	104.6	96.2	99.6	78.4
.030	125.4	115.8	119.6	95.6
.035	146.2	135.8	140.4	113.2
.040	166.9	155.4	160.0	130.0
.045	187.3	174.2	179.2	146.8
.050	206.5	191.9	197.1	162.4
.055	224.6	208.5	212.9	176.8
.060	238.1	221.9	225.0	189.2
.065	246.2	230.0	229.65	195.2
.070		233.5	233.4	198.8

STRIP BIAXIAL TENSILE TESTS OF ANB-3066/SD-851-2 PROPELLANT/LINER BOND AT 0°F

Spec. No.:	4-10	4-11	4-12	4-13	4-14
2a', in.	0.4	0.4	0.4	0.4	0.4
R, in./min.	0.02	0.02	0.10	0.50	0.50
U, in.	f, lb/in.	f, lb/in.	f, lb/in.	f, lb/in.	f, lb/in.
.005	36.0	35.0	40.7	53.0	50.0
.010	74.0	72.0	82.6	105.0	100.0
.015	112.5	111.4	123.7	159.0	148.0
.020	148.0	149.1	166.6	214.0	199.0
.025	173.0	183.7	208.5	266.0	246.1
.030	193.2	222.5	248.8	317.0	292.3
.035	210.0	256.2	283.7	366.0	340.3
.040	220.1	288.7	313.7	410.0	379.8
.045	234.6	315.0	333.7	449.0	417.3
.050	262.5	332.0	343.3	470.0	447.1
.055	298.0	338.3	347.0	475.0	467.3
.060	315.8				471.1

STRIP BIAXIAL TENSILE TESTS OF ANB-3066/SD-851-2
PROPELLANT/LINER BOND AT 0°F

Spec. No.:	4-15	4-16	4-17	4-18
2a', in.	0.8	1.2	1.2	1.6
R, in./min.	0.10	0.10	0.10	0.10
U, in.	f, lb/in.	f, lb/in.	f, lb/in.	f, lb/in.
.005	42.3	48.8	45.2	49.5
.010	85.5	97.6	92.0	95.8
.015	129.6	145.6	138.4	138.7
.020	172.3	192.0	174.4	180.0
.025	213.0	236.6	214.0	219.5
.030	241.5	277.6	251.2	257.0
.035	287.5	309.2	287.6	290.0
.040	321.9	334.8	318.8	319.1
.045	346.5	348.4	340.4	340.0
.050	361.5	356.8	352.0	345.4
.055	370.3		357.0	

TESTS OF ANB-3066/SD-851-2 PROPELLANT/LINER
BOND UNDER ATMOSPHERIC PRESSURE AT 77°F

Spec. No.:	5-9	5-32	5-33	5-1
2a', in.	0.2	0.4	0.4	0.4
R, in./min.	0.10	0.02	0.10	0.10
U, in.	f, lb/in.	f, lb/in.	f, lb/in.	f, lb/in.
.005	7.6	4.7	6.5	8.8
.010	12.7	8.0	11.2	14.7
.015	17.7	12.1	15.7	20.0
.020	22.5	15.4	20.5	25.7
.025	27.1	16.9	25.0	30.8
.030	31.7	23.0	30.0	36.6
.035	36.5	26.1	34.7	42.0
0.40	41.1	29.2	39.5	47.6
.045	45.4	32.9	44.2	53.5
.050	50.0	36.1	48.2	58.6
.055	54.8	40.0	53.5	64.7
.060	59.3	42.8	57.5	70.3
.065	63.2	45.9	62.7	75.4
.070	67.7	49.2	67.5	81.3
.075	72.1	52.3	72.0	86.9
.080	76.2	55.2	76.7	91.8
.085	80.5	58.8	81.2	97.1
.090	84.8	62.1	85.7	102.3
.095	88.4	65.0	80.0	105.3
.100	92.7	68.0	94.0	107.0
.105	96.3	71.1	98.2	
.110	100.0	73.8	102.2	
.115	103.8	76.9	106.5	
.120	107.2	80.2	110.2	
	SBF	SBF	SBF	

TESTS OF ANB-3066/SD-851-2 PROPELLANT/LINER
BOND UNDER ATMOSPHERIC PRESSURE AT 77°F

Spec. No.:	5-25	5-5	5-7	5-8	5-3
2a', in.	0.4	0.8	0.8	0.8	1.2
R, in./min.	0.50	0.02	0.10	0.50	0.02
U, in.	f, lb/in.	f, lb/in.	f, lb/in.	f, lb/in.	f, lb/in.
.005	8.5	5.4	7.4	9.6	5.5
.010	15.0	9.1	12.3	15.5	9.5
.015	21.4	12.3	16.8	21.4	13.0
.020	27.6	15.8	21.0	27.1	17.0
.025	33.8	19.5	25.4	33.0	19.7
.030	38.8	23.0	30.4	38.4	24.5
.035	45.9	26.7	35.1	44.8	27.5
.040	52.1	30.4	39.6	50.2	32.0
.045	58.0	34.1	44.5	56.3	35.7
.050	63.3	37.1	49.0	61.7	39.5
.055	69.7	40.3	53.9	67.6	43.2
.060	75.9	44.0	58.6	73.1	47.0
.065	81.1	47.7	62.6	78.7	50.2
.070	86.6	50.7	67.3	83.9	54.0
.075	92.6	54.2	71.7	89.1	57.5
.080	97.3	57.1	76.2	93.3	60.5
.085	103.0	60.3	80.1	98.8	63.2
.090	108.0	64.1	84.6	103.3	66.7
.095	112.6	67.0	87.8	107.3	68.5
.100	117.8	70.0	92.0	110.8	71.2
.105	122.3	73.2	96.0	114.6	73.2
.110	125.4	75.7	99.0	117.4	74.7
.115	129.7	78.9	102.2	120.5	76.2
.120	132.8	81.4	104.9	122.8	77.0

SBF

TESTS OF ANB-3066/SD-851-2 PROPELLANT/LINER
BOND UNDER ATMOSPHERIC PRESSURE AT 77°F

Spec. No.:	5-4	5-6	5-42	5-2
2a', in.	1.2	1.2	1.6	1.6
R, in./min.	0.10	0.50	0.02	0.10
U, in.	f, lb/in.	f, lb/in.	f, lb/in.	f, lb/in.
.005	8.0	9.5	4.5	6.3
.010	12.7	15.0	8.0	9.8
.015	17.0	19.7	11.0	13.9
.020	20.5	24.7	14.2	17.6
.025	24.2	29.2	17.5	21.3
.030	27.7	34.2	21.0	25.2
.035	32.0	38.5	24.5	29.4
.040	35.2	43.2	27.5	33.3
.045	38.7	47.7	30.7	37.5
.050	42.5	52.2	34.2	41.4
.055	45.7	57.2	37.5	46.0
.060	49.5	61.7	40.7	50.2
.065	52.5	65.5	43.7	53.9
.070	55.5	69.7	46.7	57.8
.075	59.2	74.7	49.7	61.7
.080	61.7	78.0	52.5	64.9
.085	65.0	82.5	55.2	68.6
.090	67.5	86.2	58.0	71.5
.095	69.8	89.2	60.0	73.7
.100	72.2	93.2	62.0	76.4
.105	74.5	96.5	63.5	
.110	76.5	99.5	64.5	
.115		102.5		

TESTS OF ANB-3066/SD-851-2 PROPELLANT/LINER BOND
UNDER A SUPERIMPOSED PRESSURE OF 500 PSIG AT 77°F

Spec. No.:	5-35	5-21	5-13	5-24	5.20
2a', in.	0.4	0.4	0.4	0.8	0.8
R, in./min.	0.02	0.10	0.50	0.02	0.10
U, in.	f,lb/in.	f,lb/in.	f,lb/in.	f,lb/in.	f,lb/in.
.005	5.8	7.5	9.3	5.8	6.4
.010	10.0	12.7	14.9	10.1	11.1
.015	14.2	18.0	20.3	13.6	15.2
.020	17.8	23.7	26.4	17.4	19.5
.025	22.0	29.5	32.1	20.9	23.8
.030	26.4	35.5	37.9	25.0	28.0
.035	30.1	41.7	43.8	28.2	32.3
.040	34.3	47.0	49.5	32.3	36.1
.045	38.7	53.0	55.8	35.6	40.4
.050	42.1	58.5	61.7	39.3	44.2
.055	46.5	63.5	67.6	42.9	49.0
.060	50.4	68.0	73.5	47.2	52.6
.065	54.1	76.0	78.6	50.5	55.9
.070	58.5	82.2	85.0	53.7	59.7
.075	62.0	87.5	90.9	57.8	63.8
.080	66.1	92.0	96.0	61.8	67.1
.085	70.3	98.7	101.7	64.3	71.1
.090	74.0	104.7	107.8	68.1	75.2
.095	77.9	109.5	112.5	71.2	78.5
.100	81.3	114.7	118.3	75.2	82.6
.105	85.5	120.5	124.2	78.2	85.9
.110	88.7	125.2	129.4	81.0	89.5
.115	92.8	130.2	134.8	84.3	92.8
.120	96.0	135.7	140.1	87.8	95.9
.125	100.2	140.0	144.8	90.6	99.5
.130	103.6	142.7	150.7	93.6	102.6
.135	107.8	150.2	155.6	95.9	106.1
.140	110.5	155.0	159.8	98.4	109.2
	SBF	SBF	SBF	SBF	

TESTS OF ANB-3066/SD-851-2 PROPELLANT/LINER BOND
UNDER A SUPERIMPOSED PRESSURE OF 500 PSIG AT 77°F

Spec. No.:	5-34	5-23	5-18	5-36	5-19
2a', in.	1.2	1.2	1.2	1.6	1.6
R, in./min.	0.02	0.10	0.50	0.10	0.50
U, in.	f, lb/in.	f, lb/in.	f, lb/in.	f, lb/in.	f, lb/in.
.005	5.3	6.3	8.4	5.1	8.4
.010	9.0	10.7	13.8	8.9	13.6
.015	12.2	14.9	18.8	12.1	17.3
.020	15.6	19.1	24.2	15.3	22.7
.025	18.8	22.6	29.2	18.8	26.9
.030	22.0	26.9	34.6	22.0	31.6
.035	25.2	30.6	39.6	25.2	35.6
.040	28.9	34.3	45.0	28.4	40.0
.045	32.1	38.9	50.0	32.1	42.3
.050	35.5	42.4	54.4	35.1	49.2
.055	39.2	46.8	59.9	38.8	53.7
.060	42.6	51.4	65.8	42.0	58.1
.065	46.0	55.1	69.3	45.0	62.1
.070	49.2	59.0	74.7	48.5	66.8
.075	52.9	63.7	79.2	51.9	70.2
.080	56.3	67.1	84.1	54.7	74.2
.085	59.5	71.3	89.1	57.6	78.7
.090	62.9	75.4	93.5	61.3	82.6
.095	66.1	78.4	98.0	64.1	86.8
.100	69.6	82.3	101.4	66.8	90.3
.105	73.0	85.7	106.4	69.5	94.0
.110	75.4	88.7	110.3	72.0	97.2
.115	78.4	92.4	114.8	74.5	101.2
.120	80.8	95.5	118.8	76.9	104.4
.125		98.0			110.3
.130		100.9			111.1
.135		103.4			114.1
.140		105.3			116.8

TESTS OF ANB-3066/SD-851-2 PROPELLANT/LINER BOND
UNDER A SUPERIMPOSED PRESSURE OF 1000 PSIG AT 77°F

Spec. No.:	5-15	5-14	5-17	5-109	5-22
2a', in.	0.4	0.4	0.4	1.2	1.2
R, in./min.	0.02	0.10	0.50	0.02	0.02
U, in.	f, lb/in.	f, lb/in.	f, lb/in.	f/lb/in.	f/lb/in.
.005	6.1	6.6	10.0	6.1	5.7
.010	10.3	12.1	16.1	9.4	10.0
.015	14.8	17.3	22.0	13.5	14.0
.020	21.0	22.8	27.6	17.0	18.0
.025	23.8	28.0	33.3	21.0	22.0
.030	28.7	33.3	39.2	24.8	25.7
.035	33.2	39.0	44.4	28.0	30.2
.040	37.9	44.5	49.7	32.3	34.2
.045	42.6	49.7	55.2	36 2	38.2
.050	47.0	55.2	59.8	40.3	42.5
.055	51.7	60.9	65.4	44.3	46.7
.060	56.4	66.4	70.7	47.9	50.7
.065	61.1	70.9	75.2	51.0	54.2
.070	65.3	76.1	80.7	55.1	58.2
.075	69.8	82.1	85.7	58.4	62.0
.080	74.2	86.4	90.0	61.4	65.2
.085	78.5	91.9	95.2	65.0	69.0
.090	83.1	97.3	100.4	58.1	72.2
.095	86.6	101.6	104.2	71.1	75.0
.100	91.2	106.6	109.0	74.2	77.7
.105	95.2	111.4	114.5	76.5	80.0
.110	98.7	115.9	118.8	76.8	82.2
.115	102.7	120.7	123.8	80.8	83.7
.120	106.4	125.4	128.5	82.1	85.0
.125	110.3	129.5	133.0		
.130	114.2	134.2	138.0		
.135	117.8	138.5	142.8		
.140	120.7	142.6	146.9		
	SBF	SBF	SBF		

TESTS OF ANB-3066 /SD-851-2 PROPELLANT/LINER BOND
UNDER A SUPERIMPOSED PRESSURE OF 1000 PSIG AT 77°F

Spec. No.:	5-37	5-16	5-111	5-114	5-107	5-112
2a', in.	1.2	1.2	1.2	1.2	1.6	1.6
R, in./min.	0.10	0.50	0.50	0.50	0.10	0.10
U,in.	f,lb/in.	f,lb/in.	f,lb/in.	f,lb/in.	f,lb/in.	f,lb/in.
.005	5.4	9.2	6.1	7.7	6.0	6.9
.010	9.6	15.7	10.5	13.4	10.5	11.5
.015	13.1	21.0	14.6	18.0	14.7	15.4
.020	17.0	26.7	18.4	22.6	18.4	19.0
.025	20.5	31.7	22.5	27.5	22.3	22.6
.030	24.2	37.2	26.2	32.7	25.7	25.7
.035	27.8	42.5	30.1	37.1	29.4	29.3
.040	31.4	47.7	34.1	41.8	33.6	32.4
.045	35.3	53.5	38.2	46.3	37.3	36.0
.050	38.8	59.0	42.3	50.9	40.7	39.6
.055	42.8	64.7	46.6	55.9	44.7	43.2
.060	46.5	70.3	50.7	60.8	48.1	46.9
.065	49.7	75.0	53.8	65.2	51.3	50.0
.070	53.7	80.5	58.4	70.1	55.2	53.0
.075	57.6	86.0	61.7	75.0	56.5	57.2
.080	61.1	91.2	65.5	79.6	61.5	60.5
.085	64.8	96.0	69.0	84.2	65.0	64.4
.090	68.3	101.2	73.2	89.4	68.6	67.0
.095	71.5	106.6	76.5	93.8	71.3	70.6
.100	75.2	110.2	80.3	98.4	74.4	73.4
.105	78.7	115.0	83.6	103.0	77.6	76.8
.110	81.6	119.0	86.2	107.2	80.0	79.3
.115	84.9	123.7	89.0	111.3	82.6	84.2
.120	88.1	127.7	81.8	115.9	85.2	84.5
.125	90.9	132.0	93.6	119.5		
.130	94.3	135.7	85.1	122.9		
.135	97.0	139.7	95.9	127.0		
.140	99.7	142.5		130.1		
.145	102.4	146.2				
.150	104.7	149.2				

TESTS OF ANB-3066/SD-851-2 PROPELLANT/LINER
BOND UNDER ATMOSPHERIC PRESSURE AT 0°F

Spec. No.:	5-10	5-52	5-12	5-50	5-30	5-11	5-29
2a', in.	0.2	0.4	0.4	0.4	0.8	0.8	0.8
R, in./min.	0.10	0.02	0.10	0.50	0.02	0.10	0.50
U, in.	f, lb/in.	f, lb/in.	f, lb/in.	f, lb/in.	f, lb/in.	f, lb/in.	f, lb/in.
.005	22.9	18.5	21.8	25.2	13.0	20.2	26.7
.010	40.5	30.5	36.8	45.0	22.5	33.3	43.0
.015	57.3	41.0	50.4	61.8	31.2	45.4	59.0
.020	71.1	51.5	64.0	78.2	40.0	55.5	74.2
.025	86.0	61.5	76.2	94.0	47.5	66.6	87.5
.030	99.7	71.2	88.8	108.9	55.5	76.5	102.2
.035	113.5	80.0	101.9	124.7	63.0	85.8	115.5
.040	126.8	88.5	114.5	137.1	70.5	96.4	127.5
.045	139.6	97.0	126.2	150.4	78.0	106.0	140.0
.050	151.3	105.0	137.3	163.8	85.5	115.6	151.0
.055	163.9	113.0	149.5	177.4	93.5	126.2	161.2
.060	175.9	121.2	160.6	189.3	101.0	135.1	171.0
.065	185.7	128.5	169.9	198.0	107.0	141.6	178.0
.070	195.6	135.7	179.6	211.3	115.0	149.7	185.5
.075	204.5	143.5	188.3	222.7	121.5	155.3	191.7
.080	209.6	150.0	194.6	232.1	128.0	160.3	195.5
.085	213.3	156.5	201.9	242.0	134.5	165.4	
.090	215.5	163.2	207.7	251.2	140.0	169.1	
.095	211.6	168.5	211.6	257.4	144.0	172.2	
.100	215.5	174.5	215.5	265.8	149.0	175.0	
.105	SBF	179.0	SBF	271.7	152.0		
.110				273.7	154.5		
		SBF					
				SBF			

TABLE B-5-4 (Continued)

TESTS OF ANB-3066/SD-851-2 PROPELLANT/LINER
BOND UNDER ATMOSPHERIC PRESSURE AT 0°F

Spec. No.:	5-31	5-26	5-28	5-49	5-27	5-56
2a', in.	1.2	1.2	1.2	1.6	1.6	1.6
R, in./min.	0.02	0.10	0.50	0.02	0.10	0.50
U, in.	f, lb/in.	f, lb/in.	f, lb/in.	f, lb/in.	f, lb/in.	f, lb/in.
.005	15.0	18.0	24.0	11.7	15.8	21.7
.010	24.2	29.5	39.2	19.2	26.2	37.1
.015	32.5	39.6	53.9	26.2	36.1	50.4
.020	40.2	49.5	65.7	31.7	44.5	63.8
.025	48.0	58.7	78.5	36.5	51.9	74.7
.030	55.2	68.1	91.2	42.5	60.6	85.6
.035	62.0	77.2	104.0	48.2	68.8	97.0
.040	69.2	85.5	115.0	53.5	76.4	106.4
.045	76.5	94.2	127.5	58.0	84.4	116.3
.050	83.2	102.2	138.2	63.2	91.5	125.7
.055	89.6	110.7	149.5	68.2	98.7	132.6
.060	96.0	118.7	160.7	73.0	104.7	139.1
.065	101.7	124.7	169.0	76.2	109.9	143.5
.070	107.5	131.5	186.2	80.0	114.3	148.5
.075	113.0	137.5	184.0	83.0	118.8	
.080	117.5	141.7	188.2	85.0	121.2	
.085	122.0	146.0		86.5		
.090	125.7	150.0		99.7		
.095	128.0					
.100	130.2					

TESTS OF ANB-3066 /SD-851-2 PROPELLANT/LINER
BOND UNDER A SUPERIMPOSED PRESSURE OF
500 PSIG AT 0°F

Spec. No.:	5-43	5-41	5-40
2a', in.	0.4	0.4	0.4
k, in./min.	0.02	0.10	0.50
U, in.	f, lb/in.	f, lb/in.	f, lb/in.
.005	20.7	25.7	29.0
.010	33.5	45.2	48.0
.015	44.0	62.0	68.0
.020	55.0	77.7	84.0
.025	65.0	94.4	100.0
.030	76.0	110.1	116.0
.035	86.5	125.2	131.0
.040	95.7	138.8	147.0
.045	105.5	151.5	162.0
.050	115.0	168.1	165.0
.055	125.0	182.3	190.0
.060	135.5	196.4	203.0
.065	144.5	208.0	216.0
.070	154.5	221.9	230.4
.075	164.0	235.8	224.0
.080	172.5	247.4	255.0
.085	182.5	261.1	267.0
.090	193.5	273.2	281.0
.095	201.0	283.8	292.0
.100	211.0	297.4	305.0
.105	220.5	310.1	318.0
.110	229.0	320.2	327.0
.115	239.0	333.3	339.0
.120	249.5	343.9	352.0
.125	257.5	355.0	362.0
.130	267.5	367.6	374.0
.135	276.5	378.7	387.0
.140	285.5	388.8	397.4
	SBF	SBF	SBF

TESTS OF ANB-3066/SD-851-2 PROPELLANT/LINER
BOND UNDER A SUPERIMPOSED PRESSURE OF
500 PSIG AT 0°F

Spec. No.:	5.44	5.39	5.38	5.47	5.46
2a', in.	1.2	1.2	1.2	1.6	1.6
R, in./min.	0.02	0.10	0.50	0.02	0.10
U, in.	f, lb/in.	f, lb/in.	f, lb/in.	f, lb/in.	f, lb/in.
.005	18.5	17.8	28.6	16.2	18.4
.10	31.5	30.6	47.9	26.5	28.6
.015	44.2	42.5	64.5	36.0	40.2
.020	55.2	53.9	80.2	45.5	50.9
.025	65.7	63.8	95.3	54.0	62.1
.030	76.0	74.2	110.4	62.5	72.3
.035	86.5	85.1	123.4	70.7	82.0
.040	96.0	94.0	139.5	78.5	91.7
.045	105.0	103.9	153.6	86.5	101.4
.050	113.5	113.8	167.1	94.5	110.6
.055	123.7	123.7	181.2	102.5	120.3
.060	133.5	133.6	194.7	110.5	130.0
.065	141.5	141.0	205.7	117.0	137.3
.070	151.0	151.4	218.7	125.5	146.6
.075	166.0	160.3	231.2	132.5	156.3
.080	169.7	168.8	241.6	139.5	164.0
.085	178.7	178.2	254.1	146.5	173.3
.090	188.5	188.1	265.6	154.0	181.0
.095	195.5	195.0	272.9	160.0	187.8
.100	204.0	205.9	283.8	166.5	195.6
.105	212.0	213.3	292.7	173.0	203.3
.110	219.5	220.7	301.0	179.0	209.2
.115	226.5	229.7	310.9	185.5	216.0
.120	234.0	236.6	319.2	190.5	221.8
.125	240.0	244.0		195.5	
.130	248.0	252.9		200.0	
.135	254.2	259.9		203.7	
.140	260.0	266.3		207.0	
.145	265.0				
.150	269.0				

TESTS OF ANB-3066/SD-851-2 PROPELLANT/LINER BOND UNDER A SUPERIMPOSED PRESSURE OF 1000 PSIG AT 0°F

Spec. No.:	5-51	5-57	5-58	5-116	5-117
2a', in.	0.4	0.4	0.4	1.6	1.6
R, in./min.	0.02	0.10	0.50	0.10	0.10
U, in.	f, lb/in.	f, lb/in.	f, lb/in.	f, lb/in.	f, lb/in.
.005	24.7	33.3	32.6	20.6	15.3
.010	45.0	56.8	57.4	32.9	28.5
.015	61.3	76.4	78.2	44.3	38.7
.020	77.2	95.0	99.5	54.6	47.9
.025	94.0	113.7	116.8	64.9	57.6
.030	107.4	129.4	132.6	75.2	65.3
.035	122.0	149.0	155.4	84.5	73.9
.040	135.6	166.7	172.2	94.8	84.1
.045	150.0	182.3	193.0	104.1	92.8
.050	162.8	198.0	208.4	113.4	101.0
.055	177.2	215.7	226.7	123.7	109.6
.060	191.5	231.4	245.5	132.9	119.3
.065	202.9	245.0	259.5	141.2	126.5
.070	216.3	262.7	277.2	149.4	135.7
.075	229.2	275.5	293.0	157.7	143.8
.080	240.5	290.2	302.9	165.9	152.0
.085	253.4	303.9	SBF	175.2	160.2
.090	266.8	317.6		181.4	167.3
.095	277.2	332.4		188.6	175.0
.100	289.6	345.1		195.8	183.6
.105	301.9	358.8		204.1	191.3
.110	312.8	366.7		210.3	196.9
.115	325.2	378.4		216.4	204.0
.120	336.6	388.2		221.6	211.2
	SBF	SBF			

TESTS OF ANB-3066/SD-851-2 PROPELLANT/LINER
BOND UNDER A SUPERIMPOSED PRESSURE OF
1000 PSIG AT 0°F

Spec. No.:	5-45	5-113	5-48	5-53	5-119
2a', in.	1.2	1.2	1.2	1.2	1.2
R, in./min.	0.02	0.02	0.10	0.50	0.50
U, in.	f, lb/in.	f, lb/in.	f, lb/in.	f, lb/in.	f, lb/in.
.005	18.3	15.8	21.2	29.7	29.8
.010	30.1	26.8	37.1	49.5	46.3
.015	41.5	36.8	50.9	66.3	63.9
.020	51.9	44.2	63.8	83.1	79.3
.025	60.8	52.6	75.2	98.0	95.3
.030	71.2	61.1	87.6	115.8	111.3
.035	80.6	68.9	100.0	128.7	125.7
.040	90.5	77.4	110.3	143.5	141.2
.045	99.5	85.8	122.7	157.4	154.6
.050	108.9	93.2	133.6	171.2	167.0
.055	118.3	101.6	144.0	183.1	184.0
.060	127.7	110.0	155.4	196.0	195.8
.065	137.1	115.8	164.8	201.9	207.2
.070	146.5	124.7	175.7	217.3	224.7
.075	154.9	131.6	187.1	232.6	235.5
.080	163.8	140.5	196.4	244.5	247.4
.085	173.2	147.4	207.9	257.9	260.8
.090	182.6	155.3	217.8	268.3	271.1
.095	189.6	161.6	227.2	280.1	281.4
.100	199.0	168.4	236.6	292.0	293.8
.105	207.9	176.3	247.0	304.9	306.1
.110	216.3	182.1	255.9	316.8	315.4
.115	224.2	189.5	265.8	328.7	325.7
.120	232.6	195.3	269.3	338.6	337.1
.125	240.0	200.0	282.6	348.5	345.3
.130	249.0	205.8	292.0	359.4	352.5
.135	256.9	211.6	300.4	369.3	361.8
.140	263.8	215.8	308.4	378.2	369.0
.145	270.7			388.1	
.150	277.2			396.0	
˙ ⁊	283.1				
)	287.6				

TESTS OF ANB-3066/SD-851-2 PROPELLANT/ LINER BOND IN COMBINED TENSION AND SHEAR AT A SCARF ANGLE OF 45° AT 77°F

Spec. No.:	6-88	6-74	6-66	6-75
$2a'$, in.	0.44	0.40	0.40	0.40
R, in./min	0.02	0.10	0.20	0.50
$U_n = U_\tau$, in.	$f_n = f_\tau$, lb/in.	$f_n = f_\tau$, lb/in.	$f_n = f_\tau$, lb/in.	$f_n = f_\tau$, lb/in.
.007	2.6	3.3	3.0	1.9
.014	4.6	5.2	5.7	3.1
.021	6.5	7.3	8.1	5.9
.028	8.4	9.8	10.5	8.4
.035	10.6	12.3	12.6	10.8
.042	12.7	14.6	15.0	12.9
.049	14.6	17.1	17.3	15.0
.057	17.3	19.1	19.4	16.9
.064	19.4	21.5	21.4	19.0
.071	21.7	23.6	23.5	21.0
.078	24.0	25.9	25.4	22.7
.085	26.3	27.9	26.8	24.7
.092	28.6	29.9	28.3	26.5
.099	30.7	32.1	29.9	28.1
.106	32.8	34.1	31.7	29.7
.113	35.2	36.0	33.4	31.1
.120	37.2	38.0	35.1	33.6
.127	39.4	39.9	37.2	35.5
.134	41.4	41.7	39.3	38.3
.141	43.6	43.4	41.2	40.7
	SBF		SBF	SBF

TESTS OF ANB-3066/SD-851-2 PROPELLANT-LINER BOND IN COMBINED TENSION AND SHEAR AT A SCARF ANGLE OF 45° AT 77°F

Spec. No.:	6-71	6-70	6-67	6-73
2a', in.	1.20	1.20	1.20	1.20
R, in./min	0.02	0.10	0.20	0.50
$U_n = U_\tau$, in.	$f_n = f_\tau$, lb/in.	$f_n = f_\tau$, lb/in.	$f_n = f_\tau$, lb/in.	$f_n = f_\tau$, lb/in.
.007	1.7	2.4	3.0	2.2
.014	3.4	4.5	5.4	3.4
.021	5.1	6.5	7.6	4.9
.028	6.7	8.5	9.8	7.1
.035	8.5	10.6	12.0	9.2
.042	10.2	12.5	14.3	10.8
.049	12.0	14.6	16.4	13.9
.057	13.8	16.5	18.3	16.6
.064	15.6	18.4	20.6	19.1
.071	17.3	20.3	22.5	21.0
.078	18.9	22.3	24.4	23.2
.085	20.5	24.2	26.3	25.3
.092	22.3	26.1	28.1	27.4
.099	23.8	28.0	29.9	29.4
.106	25.4	29.9	31.8	31.4
.113	27.0	31.8	33.4	33.3
.120	28.4	33.7	35.1	34.9
.127	29.7	35.4	36.7	37.1
.134	31.2	37.2	38.2	39.2
.141	32.4	38.8	39.5	41.0

TESTS OF ANB-3066/SD-85102 PROPELLANT-LINER BOND IN COMBINED TENSION AND SHEAR AT A SCARF ANGLE OF 45° AT 77°F

Spec. No.:	6-90	6-78	6-72
$2a'$, in.	1.60	1.60	1.60
R, in./min	0.02	0.20	0.50

$U_n = U_\tau$, in.	$f_n = f_\tau$, lb/in.	$f_n = f_\tau$, lb/in.	$f_n = f_\tau$, lb/in.
.007	2.1	2.6	2.8
.014	3.8	4.7	4.9
.021	5.6	6.5	7.0
.028	7.1	8.4	9.0
.035	8.9	10.2	11.0
.042	10.8	12.1	12.8
.049	12.6	13.9	14.7
.057	14.3	15.8	16.4
.064	16.2	17.6	18.2
.071	18.0	19.5	20.1
.078	19.8	21.3	21.8
.085	21.6	23.0	23.6
.092	23.2	24.5	25.3
.099	24.9	26.0	26.9
.106	26.6	27.6	28.5
.113	28.1	29.1	30.2
.120		30.6	
.127		32.1	
.134		33.6	
.141		35.1	

TESTS OF ANB-3066/SD-851-2 PROPELLANT-
LINER BOND IN COMBINED TENSION AND
SHEAR AT A SCARF ANGLE OF 45° AT 0°F

Spec. No.:	6-79	6-76	6-77	6-89
$2a'$, in.	0.40	1.20	1.20	1.20
R, in./min	0.50	0.02	0.10	0.50
$U_n = U_\tau$, in.	$f_n = f_\tau$, lb/in.	$f_n = f_\tau$, lb/in.	$f_n = f_\tau$, lb/in.	$f_n = f_\tau$, lb/in.
.007	11.7	3.6	6.4	5.7
.014	19.9	6.1	11.3	10.5
.021	27.3	8.4	15.9	14.9
.028	33.7	10.4	20.2	19.2
.035	40.2	12.3	23.4	23.3
.042	46.1	14.2	26.3	27.3
.049	51.6	16.1	28.5	32.6
.057	56.4	17.6	32.6	38.3
.064	62.0	19.5	36.5	43.5
.071	66.8	21.4	39.9	48.5
.078	71.4	23.1	43.1	53.5
.085	69.3	25.0	46.7	58.3
.092	78.6	26.4	49.9	63.0
.099	83.5	28.3	53.3	68.0
.106	88.7	29.8	56.7	72.6
.113	93.9	31.3	59.8	77.2
.120			63.2	81.9
.127			66.2	86.4
.134			69.6	90.8
.141			73.0	95.0

TESTS OF ANB-3066/SD-851-2 PROPELLANT-
LINER BOND IN COMBINED TENSION AND
SHEAR AT A SCARF ANGLE OF 45° AT 0°F

Spec.No.:	6-80	6-83	6-69
$2a'$, in.	1.6	1.6	1.6
R, in./min	0.02	0.02	0.10

$U_n = U_\tau$, in.	$f_n = f_\tau$, lb/in.	$f_n = f_\tau$, lb/in.	$f_n = f_\tau$, lb/in.
.007	3.3	4.9	7.8
.014	6.3	8.9	13.2
.021	8.8	12.7	17.8
.028	11.4	16.2	21.7
.035	13.5	19.6	24.9
.042	15.9	22.9	28.0
.049	18.3	25.9	31.2
.057	21.0	29.1	32.9
.064	23.3	31.9	33.3
.071	25.6	34.1	35.6
.078	28.5	36.2	39.7
.085	31.1	38.5	43.3
.092	33.6	40.6	46.9
.099	36.2	42.5	49.9
.106	38.6	44.9	53.0
.113	41.1	47.4	55.5
.120	43.5		58.8
.127	46.0		61.5
.134	48.3		64.0
.141	50.5		66.9
.148			68.6
.156			70.7

TABLE B-6-3

TESTS OF ANB-3066/SD-851-2 PROPELLANT-LINER BOND IN COMBINED TENSION AND SHEAR AT A SCARF ANGLE OF 30° AT 77°F

Spec. No.:		6-61		6-59		6-85	
$?a'$, in.		0.4		0.4		0.4	
R, in./min		0.02		0.10		0.10	

U_n,in.	U_τ,in.	f_n lb/in.	f_τ,lb/in.	f_n,lb/in.	f_τ,lb/in.	f_n lb/in.	f_τ,lb/in.
.009	.005	6.3	3.6	5.5	3.2	5.5	3.2
.017	.010	10.9	6.3	10.0	5.8	9.5	5.5
.026	.015	14.5	8.3	13.6	7.8	13.7	7.9
.035	.020	18.4	10.6	18.7	10.8	17.8	10.3
.043	.025	22.4	12.9	23.1	13.3	22.3	12.8
.052	.030	26.9	15.5	27.8	16.0	26.5	15.3
.061	.035	30.6	17.7	32.1	18.5	31.0	17.9
.069	.040	34.6	20.0	36.6	21.1	35.4	20.4
.978	.045	38.6	22.3	41.3	23.8	39.7	22.9
.087	.050	42.2	24.3	45.6	26.3	44.1	25.5
.095	.055	45.8	26.4	50.8	29.3	48.4	27.9
.104	.060	49.8	28.7	55.1	31.8	52.2	30.1
.113	.065	54.0	31.1	59.3	34.2	56.4	32.6
.121	.070	57.5	33.2	63.8	36.8	59.3	34.2
.130	.075	61.5	35.5	68.1	39.3	63.1	36.4
.139	.080	64.3	37.1	72.3	41.7	66.7	38.5
.147	.085	67.2	38.8	76.3	44.0	70.5	40.7
.156	.090			79.8	46.1	73.6	42.5
.165	.095	SBF	SBF	83.8	48.3	77.0	44.4
.173	.100			87.0	50.2	79.9	46.1
				SBF	SBF	SBF	SBF

TESTS OF ANB-3066/SD-851-2 PROPELLANT-
LINER BOND IN COMBINED TENSION AND
SHEAR AT A SCARF ANGLE OF 30° AT 77°F

Spec. No.:		6-62		6-91		6-68	
2a', in.		0.4		0.4		1.2	
R, in./min		0.50		0.50		0.02	

U_n, in.	U_τ, in.	f_n, lb/in.	f_τ, lb/in.	f_n, lb/in.	f_τ, lb/in.	f_n, lb/in.	f_τ, lb/in.
.009	.005	8.0	4.6	6.5	3.7	4.5	2.6
.017	.010	12.9	7.5	11.5	6.6	8.4	4.8
.026	.015	18.4	10.6	16.1	9.3	11.9	6.8
.035	.020	23.4	13.5	20.5	11.8	15.3	8.8
.043	.025	28.7	16.6	24.7	14.2	19.2	11.1
.052	.030	34.0	19.6	28.9	16.7	22.7	13.1
.061	.035	38.5	22.2	33.2	19.1	26.4	15.2
.069	.040	43.3	25.0	37.8	21.8	30.0	17.3
.078	.045	48.1	27.8	42.6	24.6	33.3	19.2
.087	.050	52.6	30.3	47.4	27.3	36.8	21.2
.095	.055	56.9	32.8	52.0	30.0	39.8	23
.104	.060	61.1	35.3	57.0	32.9	42.7	24.6
.113	.065	65.3	37.7	62.1	35.8	45.4	26.2
.121	.070	68.6	39.6	66.9	38.6	47.9	27.6
.130	.075	70.5	40.7	71.5	41.2	50.0	28.8
.139	.080	72.0	41.6	76.1	43.9	51.0	29.5
.147	.085	74.1	42.8	80.4	46.4		
.156	.090	76.3	44.0	85.2	49.2		
.165	.095	77.4	44.6	89.6	51.7		
.173	.100	79.2	45.7	94.0	54.2		
		SBF	SBF	SBF	SBF		

TESTS OF ANB-3066/SD-851-2 PROPELLANT-
LINER BOND IN COMBINED TENSION AND
SHEAR AT A SCARF ANGLE OF 30° AT 77°F

Spec. No.:		6-64		6-55		6-54	
2a', in.		1.6		1.6		1.6	
R, in./min		0.02		0.10		0.50	
U_n, in.	U_τ, in.	f_n, lb/in.	f_τ, lb/in.	f_n, lb/in.	f_τ, lb/in.	f_n, lb/in.	f_τ, lb/in.
.009	.005	4.2	2.4	5.6	3.2	6.8	3.9
.017	.010	7.5	4.3	9.7	5.6	11.5	6.6
.026	.015	10.5	6.0	13.6	7.8	16.2	9.4
.035	.020	13.7	7.9	17.3	10.0	20.7	12.0
.043	.025	17.1	9.9	21.0	12.1	25.1	14.5
.052	.030	20.1	11.6	24.6	14.2	30.4	17.5
.061	.035	23.5	13.6	28.3	16.3	34.5	19.9
.069	.040	27	15.5	31.9	18.4	38.0	21.9
.078	.045	30	17.3	35.7	20.6	41.5	24.0
.087	.050	32.9	18.9	38.9	22.5	45.4	26.2
.095	.055	35.9	20.7	42.6	24.6	49.3	28.4
.104	.060	38.7	22.4	45.8	26.5	53.1	30.6
.113	.065	41.1	23.7	49.3	28.5	57.2	33.0
.121	.070	43.4	25	52.6	30.3	60.6	35.0
.130	.075	44.8	25.8	55.6	32.1	63.8	36.8
.139	.080	45.8	26.4	58.8	34.0	66.8	39.6

TESTS OF ANB-3066/SD-851-2 PROPELLANT-
LINER BOND IN COMBINED TENSION AND
SHEAR AT A SCARF ANGLE OF 30° AT 77°F

Spec. No.:		6-63		6-60		6-65	
2a', in.		1.2		1.2		1.2	
R, in./min		0.10		0.50		0.50	

U_n,in.	U_τ,in.	f_n,lb/in.	f_τ,lb/in.	f_n,lb/in.	f_τ,lb/in.	f_n,lb/in.	f_τ,lb/in.
.009	.005	5.6	3.2	7.0	4.0	6.9	4.0
.017	.010	9.9	5.7	11.6	6.7	12.1	7.0
.026	.015	14.2	8.2	16.4	9.5	17.1	9.8
.035	.020	17.8	10.2	21.2	12.2	21.7	12.5
.043	.025	21.8	12.6	25.9	15.0	26.8	15.4
.052	.030	26.1	15.0	31.0	17.9	31.9	18.4
.061	.035	30.1	17.4	35.5	20.5	36.3	20.9
.069	.040	34.3	19.8	40.4	23.3	40.4	23.3
.078	.045	38.4	22.1	45.4	26.2	44.7	25.8
.087	.050	42.2	24.3	50.0	28.8	49.1	28.3
.095	.055	46.4	26.8	54.7	31.6	53.6	30.9
.104	.060	50.4	29.1	59.3	34.2	57.5	33.2
.113	.065	54.3	31.3	63.8	36.8	62	35.8
.121	.070	57.8	33.3	67.7	39.1	65.7	37.9
.130	.075	62.1	35.9	71.6	41.3	69.9	40.4
.139	.080	65.1	37.6	75.3	43.5	73.7	42.5
.147	.085	67.9	39.2			77.2	44.5
.156	.090	70.7	40.8			80.4	46.4

TABLE B-6-4

TESTS OF ANB-3066/SD-851-2 PROPELLANT-
LINER BOND IN COMBINED TENSION AND
SHEAR AT A SCARF ANGLE OF 30° AT 0°F

Spec. No.:		6-86		6-115		6-82	
2a', in.		0.4		0.4		0.4	
R, in./min		0.02		0.10		0.50	

U_n, in.	U_τ, in.	f_n, lb/in.	f_τ, lb/in.	f_n, lb/in.	f_τ, lb/in.	f_n, lb/in.	f_τ, lb/in.
.009	.005	10.1	5.8	13.9	8.0	13.5	7.8
.017	.010	17.9	10.3	24.7	14.2	23.7	13.7
.026	.015	25.7	14.8	34.9	20.1	35.8	20.6
.035	.020	33.3	19.2	44.6	25.7	45.4	26.2
.043	.025	41.1	23.7	53.0	30.6	55.6	32.1
.052	.030	48.2	27.8	60.7	35.0	65.9	38.1
.061	.035	55.8	32.2	67.1	38.7	75.7	43.7
.069	.040	63.4	36.6	75.5	43.6	84.7	48.9
.078	.045	69.2	40.0	84.3	48.7	94	54.3
.087	.050	77.7	44.8	92.5	53.4	103.2	59.6
.095	.055	84.2	48.6	100.0	58.2	112.2	64.7
.104	.060	90.4	52.2	108.9	62.8	120.5	69.5
.113	.065	97.2	56.1	116.4	67.2	128.2	74.0
.121	.070	103.9	60.0	124.1	71.6	136.1	78.6
.130	.075	110.2	63.6	131.2	75.7	143.2	82.6
.139	.080	116.2	67.1	137.8	79.5	149	86.0
.147	.085	122.1	70.5	144.2	83.2	153	88.3
.156	.090	127.7	73.7	149.5	86.3	154.6	89.3
.165.	.095	132.7	76.6	153.7	88.7		
.173	.100	136.9	79.0	156.8	90.5	SBF	SBF
.182	.105	140.5	81.1	SBF	SBF		
.191	.110	143.3	82.7				
.199	.115	144.1	83.2				
		SBF	SBF				

TESTS OF ANB-3066/SD-851-2 PROPELLANT-LINER BOND IN COMBINED TENSION AND SHEAR AT A SCARF ANGLE OF 30° AT 0°F

Spec. No.:		6-92		6-93		6-87	
2a', in.		1.2		1.2		1.2	
R, in./min		0.02		0.10		0.50	

U_n,in.	U_τ,in.	f_n,lb/in.	f_τ,lb/in.	f_n,lb/in.	f_τ,lb/in.	f_n,lb/in.	f_τ,lb/in.
.009	.005	6.8	3.9	14.5	8.3	12.0	6.9
.017	.010	12.0	6.9	24.4	14.1	24.0	13.8
.026	.015	16.0	9.2	33.3	19.2	34.7	20.0
.035	.020	20.5	11.8	41.4	23.9	42.6	24.6
.043	.025	27.4	15.8	48.2	27.8	51.8	29.9
.052	.030	34.0	19.6	53.5	30.9	61.0	35.2
.06`	.035	40.5	23.3	59.5	34.3	69.9	40.4
.069	.040	46.6	26.9	65	37.5	78.1	45.1
.078	.045	52.0	30.0	70.1	40.5	85.9	49.6
.087	.050	57.4	33.1	74.4	43.0	93.8	54.1
.095	.055	62.8	36.2	78.7	45.4	101.4	58.5
.104	.060	67.3	38.8	82.2	47.5	109.3	63.1
.113	.065	72.0	41.5	84.9	49.0	116.4	67.2
.121	.070			87.6	50.6	123.7	71.4
.130	.075			90.2	52.1	130.7	75.5
.139	.080			92.4	53.3	137.5	79.4
.147	.085					143.9	83.0

TESTS OF ANB-3066/SD-851-2 PROPELLANT-
LINER BOND IN COMBINED TENSION AND
SHEAR AT A SCARF ANGLE OF 30° AT 0°F

Spec. No.:		6-110		6-84		6-81	
2a', in.		1.6		1.6		1.6	
R, in./min		0.02		0.10		0.50	
U_n, in.	U_τ, in.	f_n, lb/in.	f_τ, lb/in.	f_n, lb/in.	f_τ, lb/in.	f_n, lb/in.	f_τ, lb/in.
.009	.005	8.2	4.7	10.5	6.0	14.9	8.6
.017	.010	14.8	8.5	18.9	10.9	24.8	14.3
.026	.015	20.7	11.9	26.4	15.2	33.7	19.5
.035	.020	26.3	15.2	34	19.6	41.1	23.7
.043	.025	31.9	18.4	40.7	23.5	48.2	27.8
.052	.030	37.3	21.5	47.5	27.4	54.9	31.7
.061	.035	42.8	24.7	53.8	31.0	61.4	35.5
.069	.040	47.7	27.5	59.6	34.4	68.4	39.5
.078	.045	52.8	30.5	65.7	37.9	75.2	43.4
.087	.050	58.0	33.5	71.2	41.1	82.2	47.5
.095	.055	62.9	36.3	76.5	44.1	88.5	51.1
.104	.060	67.6	39.0	81.7	47.2	94.8	54.7
.113	.065	72.0	41.6	86.6	50.0	101.1	58.3
.121	.070	76.3	44.0	90.9	52.4	106.9	61.7
.130	.075	80.5	46.5	95	54.8	112.7	65.1
.139	.080	84.3	48.7	98.7	57.0	117.5	67.8

SIMULTANEOUS COOL/STRAIN
TESTING FROM 125 TO 70°F OF
ANB-3066/SD-851-2 PROPELLANT-LINER BOND

Spec. No.:	7-121		7-124		7-133		7-120	
2a', in.	0.8		1.2		1.2		1.6	
R, in./min	0.0003		0.0003		0.0003		0.0003	
ΔT/, °F/hr	6.60		6.60		6.94		6.60	
U, in.	f, lb/in.	T, °F	f, lb/in.	T, °F	f, lb/in.	T, °F	f, lb/in.	T, °F
0.005	1.33	123.2	2.06	123.2	1.44	123.1	3.85	124.2
0.010	3.88	121.3	3.99	121.3	2.52	121.1	5.05	122.3
0.015	5.95	119.5	6.12	119.5	4.21	119.2	6.25	120.5
0.020	7.77	117.7	7.60	117.7	6.49	117.3	7.81	118.7
0.025	10.56	115.8	9.92	115.8	8.17	115.4	9.62	116.8
0.030	12.14	114.0	11.98	114.0	10.2	113.4	11.3	115.0
0.035	14.44	112.2	14.18	112.2	12.7	111.5	13.5	113.2
0.040	16.02	110.3	16.49	110.3	13.7	109.6	15.4	111.3
0.045	17.23	108.5	19.20	108.5	16.6	107.7	17.4	109.5
0.050	19.4	106.7	21.78	106.7	18.6	105.7	19.7	107.7
0.055	21.2	104.8	24.5	104.8	20.7	103.8	21.8	105.8
0.060	23.1	103.0	27.2	103.0	23.0	101.9	23.8	104.0
0.065	24.5	101.2	30.0	101.2	25.2	99.9	25.6	102.2
0.070	27.5	99.3	32.7	99.3	27.3	98.0	26.7	100.3
0.075	30.2	97.5	35.7	97.5	29.3	96.1	27.3	98.5
0.080	32.3	95.7	36.9	95.7	31.0	94.2	26.4	96.7
0.085	35.2	93.8	38.7	93.8	31.9	92.2		
0.090	37.9	92.0	39.9	92.0	32.0	90.3		
0.095	40.9	90.2	40.9	90.2	31.0	88.4		
0.100	42.8	88.3	41.0	88.3				
0.105	43.9	86.5						
0.110	44.2	84.7						

SIMULTANEOUS COOL/STRAIN
TESTING FROM 125 TO 70°F OF
ANB-3066/SD-851-2 PROPELLANT-LINER BOND

Spec. No.:	7-122		7-123		7-125		7-128	
2a', in.	0.8		0.8		0.8		0.8	
R, in./min	$9.38/10^{-4}$		9.38×10^{-4}		9.09×10^{-5}		9.09×10^{-5}	
$\dot{T}$, °F/hr	20.0		20.68		2.0		2.0	
U, in.	f, lb/in.	T, °F	f, lb/in.	T, °F	f, lb/in.	T, °F	f, lb/in.	T, °F
0.005	2.45	123.2	2.52	123.2	-0.3	123.2	1.96	123.2
0.010	4.90	121.3	4.57	121.3	0.93	121.3	4.04	121.3
0.015	6.99	119.5	6.97	119.5	2.80	119.5	6.50	119.5
0.020	9.19	117.7	9.38	117.7	4.81	117.7	8.82	117.7
0.025	11.5	115.8	11.7	115.8	6.73	115.8	11.3	115.8
0.030	13.8	114.0	14.2	114.0	9.02	114.0	13.7	114.0
0.035	16.3	112.1	16.6	112.1	11.3	112.2	16.1	112.2
0.040	18.6	110.3	18.9	110.3	13.6	110.3	18.5	110.3
0.045	21.3	108.5	21.5	108.5	16.0	108.5	22.7	108.5
0.050	23.9	106.6	24.3	106.6	18.8	106.7	23.9	106.7
0.055	26.8	104.8	26.7	104.8	21.5	104.8	26.7	104.8
0.060	29.0	103.0	29.8	103.0	24.3	103.0	29.4	103.0
0.065	31.4	101.1	33.2	101.1	26.8	101.2	31.9	101.2
0.070	33.9	99.3	36.3	99.3	29.4	99.3	34.1	99.3
0.075	36.6	97.5	39.8	97.4	31.5	97.5	35.5	97.5
0.080	39.2	95.6	42.9	95.6	34.3	95.7	36.0	95.7
0.085	41.7	93.8	45.8	93.8	36.5	93.8	34.7	93.8
0.090	44.1	91.9	48.8	91.9	37.0	92.0		
0.095	46.7	90.1	52.3	90.1	38.2	90.2		
0.100	49.0	88.3	54.6	88.3	37.2	88.3		
0.105	50.9	86.4	57.7	86.4				
0.110	52.7	84.6	60.6	84.6				
0.115	53.7	82.7	62.4	82.7				
0.120	53.4	80.9	63.6	80.9				

TABLE B-7-2

SIMULTANEOUS COOL/STRAIN
TESTING FROM 125 TO 40°F OF
ANB-3066/SD-851-2 PROPELLANT-LINER BOND

Spec. No.:	7-105		7-106		7-98		7-108	
2a', in.	0.4		0.8		0.8		1.2	
R, in./min.	0.0003		0.0003		0.0003		0.0003	
$\dot{T}$, °F/hr	10.20		10.20		10.20		10.20	
U, in.	f, lb/in.	T, °F	f, lb/in.	T, °F	f, lb/in.	T, °F	f, lb/in.	T, °F
0.005	-1.79	121.2	0.52	122.2	-1.0	121.2	1.82	120.2
0.010	-1.79	118.3	1.82	119.3	0.75	118.3	4.17	117.3
0.015	0.0	115.5	3.13	116.5	3.0	115.5	6.77	114.5
0.020	3.06	112.7	4.95	113.7	5.0	112.7	9.38	111.7
0.025	7.14	109.8	7.03	110.8	7.25	109.8	11.72	108.8
0.030	10.71	107.0	9.11	108.0	9.5	107.0	14.32	106.0
0.035	14.8	104.2	10.94	105.2	11.75	104.2	16.93	103.2
0.040	19.9	101.3	13.02	102.3	14.25	101.3	19.53	100.3
0.045	24.7	98.5	14.84	99.5	16.75	98.5	22.4	97.5
0.050	29.8	95.7	17.19	96.7	20.5	95.7	27.1	94.7
0.055	34.2	92.8	18.75	93.8	24.3	92.8	31.8	91.8
0.060	38.3	90.0	21.9	91.0	28.0	90.0	35.9	89.0
0.065	41.1	87.2	25.0	88.2	32.0	87.2	39.8	86.2
0.070	44.9	84.3	28.9	85.3	35.5	84.3	43.8	83.3
0.075	47.7	81.5	32.0	82.5	39.5	81.5	46.9	80.5
0.080	50.8	78.7	34.9	79.7	43.0	78.7	49.7	77.7
0.085	53.8	75.8	37.5	76.8	46.5	75.8	51.8	74.8
0.090	57.9	73.0	39.1	74.0	50.0	73.0	53.4	72.0
0.095	62.5	70.2	38.3	71.2	52.5	70.2	54.2	69.2
0.100	66.3	67.3			54.5	67.3	54.9	66.3
0.105	70.9	64.5			55.5	64.5		
0.110	74.0	61.7			56.3	61.7		
0.115	77.6	58.8						
0.120	79.6	56.0						
0.125	80.9	53.2						
0.130	76.5	50.3						

SIMULTANEOUS COOL/STRAIN
TESTING FROM 125 TO 40°F OF
ANB-3066/SD-851-2 PROPELLANT-LINER BOND

Spec. No.:	7-118		7-99		7-100		7-101	
2a', in.	1.6		0.8		0.8		0.8	
R, in./min.	0.0003		1.25×10^{-3}		1.25×10^{-3}		1.25×10^{-3}	
$\dot{T}$, °F/hr.	10.20		31.95		31.95		31.95	
U, in.	f, lb/in.	T, °F	f, lb/in.	T, °F	f, lb/in.	T, °F	f, lb/in.	T, °F
0.005	1.52	122.2	2.81	121.9	3.32	122.8	3.28	123.9
0.010	4.04	119.3	5.10	119.7	5.87	120.7	5.81	121.7
0.015	6.82	116.5	7.40	117.6	8.16	118.6	8.21	119.6
0.020	9.34	113.7	9.18	115.5	10.20	116.5	10.35	117.5
0.025	11.87	110.8	11.48	113.4	12.50	114.4	12.88	115.4
0.030	14.90	108.0	13.78	111.2	14.54	112.2	15.15	113.2
0.035	17.93	105.2	16.07	108.1	16.58	110.1	17.93	111.1
0.040	21.2	102.3	18.11	107.0	18.49	108.0	20.5	109.0
0.045	24.0	99.5	20.4	104.8	20.9	105.8	23.2	106.8
0.050	27.0	96.7	22.8	102.7	23.0	103.7	25.8	104.7
0.055	29.5	93.8	25.3	100.6	25.5	101.6	28.5	102.6
0.060	32.1	91.0	28.1	98.4	27.8	99.4	31.3	100.4
0.065	34.6	88.2	30.6	96.3	30.1	97.3	33.8	98.3
0.070	36.4	85.3	33.4	94.2	32.7	95.2	36.6	96.2
0.075	37.6	82.5	36.5	92.1	35.2	93.1	39.6	94.1
0.080	38.1	79.7	39.3	89.9	37.8	90.9	42.4	91.9
0.085	37.9	76.8	41.8	87.8	40.6	88.8	45.2	89.8
0.090	36.9	74.0	44.6	85.7	43.1	86.7	48.0	87.7
0.095			47.2	83.5	45.4	84.5	50.5	85.5
0.100			49.5	81.4	48.0	82.4	53.0	83.4
0.105			51.8	79.3	50.0	80.3	55.3	81.3
0.110			53.3	77.1	51.8	78.1	56.8	79.1
0.115			54.8	75.0	52.8	76.0		
0.120			55.6	72.9	52.8	73.9		
0.125			54.4	70.8	51.5	71.8		
0.130			55.1	68.6	48.5	69.6		

SIMULTANEOUS COOL/STRAIN
TESTING FROM 125 TO 40°F OF
ANB-3066/SD-851-2 PROPELLANT-LINER BOND

Spec. No.	7-130		7-131	
2a', in.	0.8		0.8	
R, in./min.	9.09×10^{-5}		9.09×10^{-5}	
$\dot{T}$, °F/hr.	3		3.09	

U, in.	f, lb/in.	T, °F	f, lb/in.	T, °F
0.005	0.25	122.3	-2.34	122.2
0.010	1.36	119.5	-0.35	119.3
0.015	3.09	116.7	1.75	116.5
0.020	5.07	114.0	2.34	113.7
0.025	7.18	111.2	3.97	110.9
0.030	9.41	108.5	5.02	108.0
0.035	11.76	105.7	7.01	105.2
0.040	14.11	103.0	8.29	102.4
0.045	16.83	100.2	10.16	99.5
0.050	19.43	97.5	12.03	96.7
0.055	22.2	94.7	13.90	93.9
0.060	24.6	92.0	16.12	91.0
0.065	26.9	89.2	18.93	88.2
0.070	29.1	86.5	22.2	85.4
0.075	31.2	83.7	25.0	82.6
0.080	33.0	81.0	28.3	79.7
0.085	34.7	78.2	31.5	76.9
0.090			35.0	74.1
0.095			37.0	71.2
0.100			39.4	68.4
0.105			42.1	65.6
0.110			44.6	62.7
0.115			47.0	59.9
0.120			51.4	57.1
0.125			54.9	54.3
0.130			56.1	51.4
0.135			60.2	48.6
0.140			61.9	45.8

Runaway CO_2 Injection

Test Anomaly

TABLE B-7-3

SIMULTANEOUS COOL/STRAIN
TESTING FROM 125 TO 0°F OF
ANB-3066/SD-851-2 PROPELLANT-LINER BOND

Spec. No.:	7-104		7-97		7-96		7-98	
2a', in.	0.4		1.6		0.8		0.8	
R, in./min.	4.29×10^{-4}		0.0003		9.38×10^{-4}		9.38×10^{-4}	
$\dot{T}$, °F/hr.	15		15		41		47	

U, in.	f, lb/in.	T, °F	f, lb/in.	T, °F	f, lb/in.	T, °F	f, lb/in.	T, °F
0.0005	2.55	122.1	2.30	120.8	1.77	119.4	2.50	117.8
0.010	5.61	119.2	4.34	116.7	3.28	115.7	4.75	113.6
0.015	8.42	116.3	6.63	112.5	5.56	112.1	7.25	109.5
0.020	11.48	113.3	9.18	108.3	7.58	108.4	9.5	105.3
0.025	15.05	110.4	12.12	104.2	9.60	104.8	12.0	101.1
0.030	18.11	107.5	15.56	100.0	11.87	101.1	14.0	96.9
0.035	21.4	104.6	18.88	95.8	13.89	97.5		
0.040	25.5	101.7	22.2	91.7	16.67	93.8	SBF	SBF
0.045	28.8	98.8	25.5	87.5	19.44	90.2		
0.050	32.9	95.9	28.1	83.3	22.2	86.5		
0.055	37.0	92.9	30.9	79.2	25.0	82.9		
0.060	40.8	9C.0	33.2	75.0	28.0	79.2		
0.065	44.9	87.1	34.4	70.8	31.3	75.6		
0.070	49.2	84.2	35.2	66.7	34.6	71.9		
0.075	53.1	81.3	35.2	62.5	37.9	68.3		
0.080	57.7	78.4	34.9	58.3	40.9	64.6		
0.085	62.2	75.5	33.4	54.2	44.4	61.0		
0.090	67.3	72.6			47.5	57.3		
0.095	72.2	69.6	Test Anomaly		50.0	53.7		
0.100	77.6	66.7			52.8	50.0		
0.105	82.1	63.8			55.0	46.4		
0.110	86.00	60.9			56.3	42.7		
0.115	90.3	58.0			57.3	39.1		
0.120	92.6	55.1			55.06	35.4		
0.125	94.6	52.2			SBF	SBF		
0.130	95.9	49.2						
0.135	95.7	46.3						

SIMULTANEOUS COOL/STRAIN
TESTING FROM 125 TO 0°F OF
ANB-3066/SD-851-2 PROPELLANT-LINER BOND

Spec. No.:	7-102		7-103	
2a', in.	0.8		0.8	
R, in./min.	6.25×10^{-4}		6.25×10^{-4}	
$\dot{T}$, °F/hr.	46.88		47	

U, in.	f, lb/in.	T, °F	f, lb/in.	T, °F
0.005	3.5	118.8	3.09	117.7
0.010	6.0	112.5	6.19	111.5
0.015	9.5	106.3	9.02	105.2
0.020	12.5	100.0	12.37	98.9
0.025	15.5	93.8	15.72	92.7
0.030	19.0	87.5	19.07	86.4
0.035	22.5	81.3	23.2	80.1
0.040	26.5	75.0	27.3	73.9
0.045	30.0	68.8	31.7	67.6
0.050	34.0	62.5	36.1	61.3
0.055	38.5	56.3	41.0	55.1
0.060	42.5	50.0	46.1	48.8
0.065	47.3	43.8	51.0	42.5
0.070	52.0	37.5	55.9	36.3
0.075	57.5	31.3	62.4	30.0
0.080	62.5	25.0	68.6	23.7
0.085	68.5	18.8	74.5	17.5
0.090	74.5	12.5	81.4	11.2
0.095	80.0	6.3	88.7	4.9
0.100	86.5	0.0	97.4	- 1.3
0.105	92.0	- 6.3		

TESTS AT 77°F OF SPECIMENS DISSECTED FROM
MINUTEMAN III MOTOR

Spec. No.:	8-1	8.2	8-3	8-4	8-5
2a', in.	0.4	0.8	0.8	0.8	0.8
R, in./min	0.10	0.02	0.02	0.10	0.10
U, in.	f, lb/in.	f, lb/in.	f, lb/in.	f, lb/in.	f, lb/in.
.005	8.2	6.8	6.5	8.5	7.5
.010	14.2	12.2	11.7	14.4	13.6
.015	19.0	17.3	16.2	20.4	18.6
.020	26.5	22.1	20.7	26.1	23.9
.025	33.2	27.2	25.2	31.3	29.0
.030	39.3	32.3	30.2	37.0	34.5
.035	46.2	37.3	35.0	42.4	39.8
.040	52.7	41.4	40.0	48.0	45.4
.045	59.0	47.7	45.1	53.9	51.0
.050	65.7	52.5	50.1	59.8	56.4
.055	72.0	57.6	55.2	65.1	62.1
.060	78.7	62.5	60.5	70.7	67.6
.065	85.5	67.3	65.5	76.2	73.2
.070	91.5	72.3	70.2	81.6	78.4
.075	97.5	76.7	75.0	87.0	83.8
.080	100.0	81.3	79.5	91.6	88.6
.085		85.8	84.1	96.5	93.0
.090		89.2	88.2	100.7	97.4
.095		92.6	92.1	100.4	101.2
.100			95.5	108.0	
.105			98.5		

TESTS AT 77°F OF SPECIMENS DISSECTED FROM
MINUTEMAN III MOTOR

Spec. No.:	8-6	8-7	8-8	8-9	8-10
2a', in.	0.8	0.8	1.2	1.2	1.6
R, in./min	0.50	0.50	0.10	0.10	0.10
U, in.	f, lb/in.	f, lb/in.	f, lb/in.	f, lb/in.	f, lb/in.
.005	9.8	9.2	7.0	7.1	6.8
.010	17.0	16.1	12.3	12.6	11.9
.015	23.3	22.6		17.6	16.3
.020	29.6	28.6		23.0	20.6
.025	36.6	35.0	26.8	27.9	24.8
.030	42.6	40.9	32.0	32.9	28.6
.035	49.7	47.4	37.1	37.9	32.6
.040	56.0	53.6	42.2	42.8	36.7
.045	62.3	59.7	47.3	48.0	40.8
.050	69.1	66.4	52.2	53.0	44.8
.055	75.5	72.6	57.5	57.9	48.7
.060	81.8	79.1	62.7	62.8	52.8
.065	88.3	85.0	67.6	67.3	56.8
.070	93.6	90.7	72.4	71.4	60.7
.075	97.4	97.1	76.7	75.4	64.4
.080		102.4	81.3	78.5	67.8
.085		106.7	85.1	81.0	70.6
.090		111.3	88.2	83.3	73.5
.095		114.9	90.9		76.0
.100		117.7	93.1		78.3
.105		120.3			

TABLE B-10-1

TESTS AT 77°F OF SPECIMENS DISSECTED
FROM POLARIS A-3 MOTOR

Spec. No.:	10-1	10-2	10-3	10-4	10-5
$2a'$, in.	0.4	0.8	0.8	0.8	0.8
R, in./min.	0.10	0.02	0.02	0.10	0.50
U, in.	f, lb/in.	f, lb/in.	f, lb/in.	f, lb/in.	f, lb/in.
.005	2.5	2.2	2.2	2.7	2.6
.010	4.5	4.3	4.5	4 4	5.3
.015	7.0	6.1	6.6	6.3	7.8
.020	9.2	7.6	8.4	7.9	10.4
.025	11.5	9.1	10.4	9.7	12.7
.030	13.7	11.2	12.2	11.0	15.2
.035	16.0	12.7	14.0	12.3	17.2
.040	18.5	14.7	16.0	13.7	19.4
.045	20.2	16.3	17.5	14.9	21.7
.050	22.5	17.8	19.4	16.3	23.8
.055	24.7	19.6	21.1	17.5	26.0
.060	26.7	21.4	22.7	18.6	28.0
.065	29.0	22.9	24.4	20.1	30.0
.070	31.5	24.7	26.3	21.3	32.5
.075	33.2	26.5	28.0	22.7	34.6
.080	35.2	28.0	29.7	23.7	36.8
.085	37.2	30.1	31.4	24.9	38.8
.090	39.2	31.8	33.1	26.0	40.9
.095	41.2	33.1	34.6	27.2	43.1
.100	43.5	34.9	36.2	28.5	45.0
.105	44.7	36.7	36.6	29.5	47.0
.110	46.7	38.0	39.3	30.6	49.0
.115	48.5	39.5	40.7	31.8	50.9
.120	50.2	41.0	42.2	32.7	52.8
.125	52.2	42.6	43.7	34.0	54.7
.130	53.7	44.1	45.2	35.2	56.4
.135	55.2	45.4	46.5	36.2	58.1
.140	57.2	46.9	47.7	37.2	60.0
.145	58.7	47.9	49.0	38.2	61.8
.150	60.5	48.7	48.3	39.2	63.5
.155	62.0	62.0	51.3		30.5
.160	63.5	63.5	52.4		63.5
.165	65.0	65.0	53.3		65.0
.170			54.2		
.175			54.8		
.180			55.1		

TESTS AT 77°F OF SPECIMENS DISSECTED
FROM POLARIS A-3 MOTOR

Spec. No.:	10-6	10-7	10-8	10-9
2a', in	0.8	1.2	1.2	1.6
R, in./min.	0.50	0.10	0.10	0.10
U, in.	f, lb/in.	f, lb/in.	f, lb/in.	f, lb/in.
.005	2.8	3.0	2.0	2.5
.010	5.5	5.2	4.0	4.6
.015	7.7	7.5	6.0	6.2
.020	10.1	9.6	7.8	8.0
.025	12.5	11.5	9.7	9.5
.030	14.9	13.4	11.5	11.0
.035	17.1	15.4	13.2	12.3
.040	19.6	17.2	15.0	14.0
.045	21.9	19.1	16.6	15.4
.050	24.2	20.9	18.5	17.0
.055	26.2	22.8	20.1	18.4
.060	28.8	24.5	21.7	19.8
.065	31.0	26.5	23.4	21.4
.070	33.3	28.5	25.0	22.7
.075	35.5	30.0	26.6	24.4
.080	37.7	32.0	28.5	25.7
.085	39.8	33.8	30.1	27.3
.090	42.0	35.7	31.9	28.7
.095	44.3	37.6	33.3	30.2
.100	46.3	39.0	34.8	31.4
.105	48.4	40.8	36.5	32.8
.110	50.4	42.3	38.0	34.1
.115	52.4	43.9	39.3	35.2
.120	54.5	45.5	41.0	36.5
.125	56.5	47.1	42.2	37.7
.130	58.3	48.5	43.5	38.8
.135	60.2	49.7	44.9	39.6
.140	62.1	51.1	46.1	40.6
.145	63.7	52.5	47.4	41.2
.150	65.6	53.6	48.3	41.7
.155	67.3	54.6	49.4	42.1
.160	63.5	55.5	50.4	50.4

TABLE B-10-2

TESTS AT 0°F OF SPECIMENS DISSECTED FROM POLARIS A-3 MOTOR

Spec. No.:	10-10	10-11	10-12	10-13	10-14
2a', in.	0.4	0.8	0.8	0.8	0.8
R, in./min	0.10	0.02	0.02	0.10	0.50
U, in.	f, lb/in.	f, lb/in.	f, lb/in.	f, lb/in.	f, lb/in.
.005	10.9	5.8	6.6	8.3	14.1
.010	17.6	11.9	11.4	15.1	23.8
.015	24.0	16.3	15.4	18.1	30.8
.020	29.2	20.1	19.0	25.2	37.2
.025	34.7	23.8	22.3	29.4	43.8
.030	39.0	27.1	25.7	34.0	49.4
.035	44.2	30.5	28.8	37.5	55.0
.040	48.1	33.5	31.6	41.6	60.2
.045	52.1	36.7	34.7	44.3	64.1
.050	56.4	39.6	37.8	47.5	69.4
.055	60.0	42.8	40.7	50.2	74.1
.060	64.0	45.8	43.3	53.1	78.3
.065	58.2	49.0	46.4	55.8	82.5
.070	72.2	52.0	49.5	58.8	86.6
.075	76.2	55.2	52.1	62.2	90.8
.080	79.5	58.0	55.0	65.1	94.4
.085	83.5	60.9	57.6	67.8	97.7
.090	86.8	63.7	60.7	70.5	101.6
.095	90.5	66.4	63.3	73.5	105.2
.100	94.5	69.4	66.1	76.9	108.6
.105	97.5	71.8	68.8	79.6	111.6
.110	100.6	74.6	71.4	82.1	115.8
.115	103.9	77.5	74.0	84.8	118.6
.120	108.8	80.2	76.4	87.9	121.9
.125	110.0	82.8	78.8	91.1	125.0
.130	113.4	85.4	81.4	94.3	128.0
.135	116.1	88.0	83.8	96.8	131.1
.140	119.2	90.6	86.1	99.0	133.6
.145	121.9	93.1	88.3	102.2	136.3
.150	124.6	95.3	90.7	105.1	139.1
.155	127.7	97.8	93.0	107.5	141.6
.160	130.1	100.0	95.2	110.2	144.4
.165			97.6		
.170			100.0		
.175			102.1		
.180			104.2		
.185			105.9		

TESTS AT 0°F OF SPECIMENS DISSECTED
FROM POLARIS A-3 MOTOR

Spec. No.:	10-15	10-16	10-17	10-18
2a', in.	0.8	1.2	1.2	1.6
R, in./min.	0.50	0.10	0.10	0.10
U, in.	f, lb/in.	f, lb/in.	f, lb/in.	f, lb/in.
.005	13.6	8.9	9.4	8.8
.010	21.7	15.3	15.4	14.6
.015	29.2	20.6	21.1	19.6
.020	35.8	25.5	26.0	23.9
.025	41.3	30.6	30.3	27.7
.030	47.0	34.6	34.1	31.3
.035	52.2	38.7	37.9	34.5
.040	57.1	42.3	41.7	37.6
.045	62.1	46.1	45.3	40.6
.060	67.0	49.7	48.8	43.6
.055	71.5	53.3	51.5	46.7
.060	76.2	56.3	55.0	49.7
.065	80.1	59.4	58.3	52.5
.070	84.6	62.7	61.5	55.0
.075	88.8	66.0	64.8	58.0
.080	92.5	68.8	67.8	60.3
.085	96.5	71.6	70.2	63.1
.090	100.2	74.4	73.2	65.6
.095	103.9	77.0	75.9	68.4
.100	108.1	80.1	78.9	71.2
.105	110.8	82.6	81.3	73.2
.110	114.3	85.7	84.0	75.7
.115	117.5	88.7	86.8	78.2
.120	121.2	91.3	89.5	80.8
.125	123.7	93.6	91.9	83.3
.130	126.7	95.9	94.6	85.6
.135	130.6	98.9	97.1	87.1
.140	132.9	101.0	99.8	89.6
.145	136.3	103.8	101.7	91.9
.150	138.8	105.8	104.4	94.1
.155	141.5	108.1	106.3	95.9
.160	144.5	110.2	108.7	97.7
.165				99.7

REPEATABILITY TESTS OF ANB-3600/SD-923
PROPELLANT-LINER BOND AT 77°F AND ATMOSPHERIC
PRESSURE (OPERATOR 1, BATCH 1)

Spec No.:	11-1	11-2	11-3	11-4	11-5
2a', in.	0.4	0.8	0.8	0.8	0.8
R, in./min	0.10	0.02	0.02	0.10	0.50

U, in.	f, lb/in.	f, lb/in.	f, lb/in.	f, lb/in.	f, lb/in.
.005	4.6	2.5	2.0	3.5	2.8
.010	7.7	4.3	3.7	5.8	6.4
.015	10.3	6.2	5.0	8.6	9.0
.020	12.8	8.1	7.3	11.4	12.3
.025	15.4	10.1	8.8	14.0	14.9
.030	18.0	12.2	10.6	16.5	18.0
.035	21.3	14.5	12.3	19.6	20.6
.040	24.7	16.7	14.1	22.4	23.1
.045	28.0	19.1	16.1	25.2	27.0
.050	30.9	21.6	17.9	28.0	30.1
.055	34.0	24.2	20.2	31.3	32.7
.060	38.1	26.9	22.7	34.4	36.0
.065	41.4	29.6	25.2	37.7	39.6
.070	45.1	32.4	27.7	40.8	43.2
.075	48.7	35.4	30.3	44.6	46.9
.080	51.5	38.6	32.8	47.9	50.5
.085	56.1	41.6	35.3	51.2	54.1
.090	59.5	44.8	37.8	54.8	57.9
.095	63.4	48.0	40.4	58.4	61.8
.100	67.2	51.2	43.4	61.7	65.7
.105	71.3	54.4	46.4	65.5	69.5
.110	74.7	57.7	49.2	68.8	73.7
.115	78.8	61.0	53.0	72.4	77.3
.120	82.7	64.2	55.5	76.0	81.4
.125	86.5	67.7	58.8	79.3	85.0
.130	90.2	71.2	61.8	82.9	89.1
.135	94.0	74.5	65.1	86.7	93.5
.140	95.3	77.9	68.1	89.7	97.4
.145	102.0	81.1	70.9	93.1	101.2
.150	105.6	84.4	74.4	96.4	105.4
.155	109.5	88.0	78.2	99.4	109.5
.160	115.7	91.2	81.3	102.8	112.8
.165	117.7		87.1		116.7
.170	120.6		90.4		121.1
.175	123.7		93.4		124.4
.180	127.5		95.9		127.8
.185	130.6		98.4		
.190	133.5		101.0		
.195	136.5		103.5		
.200	139.1				

REPEATABILITY TESTS OF ANB-3600/SD-923
PROPELLANT-LINER BOND AT 77°F AND ATMOSPHERIC
PRESSURE (OPERATOR 1, BATCH 1)

Spec No.:	11-6	11-8	11-7	11-9
2a', in.	0.8	1.2	1.2	1.6
R, in./min	0.50	0.10	0.10	0.10
U, in.	f,lb/in.	f,lb/in.	f,lb/in.	f,lb/in.
.005	2.2	2.2	2.0	2.8
.010	5.0	4.0	4.5	5.1
.015	8.8	6.0	7.3	6.9
.020	11.3	7.5	9.8	9.0
.025	14.3	9.8	12.3	10.3
.030	17.4	11.1	14.8	12.6
.035	20.2	13.1	17.6	14.1
.040	23.2	15.1	20.2	16.4
.045	26.5	17.4	23.2	18.0
.050	29.5	19.4	26.5	20.6
.055	32.3	21.4	29.5	23.1
.060	35.3	24.2	32.5	25.5
.065	38.8	27.0	35.3	27.8
.070	41.6	29.5	38.8	29.8
.075	45.2	32.0	42.4	32.2
.080	47.9	34.8	45.4	35.3
.085	52.0	37.6	48.7	38.6
.090	55.5	40.4	52.5	40.7
.095	59.3	43.4	55.8	43.5
.100	63.8	46.7	59.3	46.3
.105	67.4	50.2	62.6	48.9
.110	71.7	53.0	65.6	52.3
.115	75.7	56.5	69.4	55.4
.120	79.2	60.3	73.2	57.9
.125	83.3	63.1	76.7	60.8
.130	87.1	66.9	80.0	64.1
.135	90.9	69.4	83.3	67.0
.140	95.2	72.9	86.6	70.o
.145	98.9	75.7	90.1	72.9
.150	102.7	78.5	93.4	76.2
.155	106.8	81.5	96.2	79.3
.160	110.8	84.0	99.4	82.4
.164	114.3			85.3
.170	117.6			88.4
.175	121.2			91.2
.180	124.4			94.0
.185				96.3
.190				98.7
.195				101.0
.200				

TABLE B-12

REPEATABILITY TESTS OF ANB-3600/SD-923 PROPELLANT-LINER BOND AT 77°F AND ATMOSPHERIC PRESSURE (OPERATOR 1, BATCH 2)

Spec. No.:	12-1	12-2	12-3	12-4	12-5
2a', in.	0.4	0.8	0.8	0.8	0.8
R, in./min	0.10	0.02	0.02	0.10	0.10
U, in.	f,lb/in.	f,lb/in.	f,lb/in.	f,lb/in.	f,lb/in.
.005	2.8	1.7	1.9	1.9	2.5
.010	5.1	3.5	3.3	4.2	4.3
.015	7.1	4.8	4.8	5.9	6.1
.020	8.9	6.1	6.0	7.4	7.7
.025	11.2	7.3	7.4	9.4	10.0
.030	12.7	8.9	8.7	11.1	11.5
.035	14.5	10.2	10.2	12.6	13.6
.040	16.5	11.7	11.5	14.3	15.4
.045	18.6	13.5	13.1	16.3	17.7
.050	20.4	14.7	14.5	18.3	19.5
.055	22.9	16.5	16.0	20.0	21.9
.060	25.5	18.1	17.6	22.2	24.2
.065	28.0	19.8	19.3	24.5	26.8
.070	30.6	21.9	21.2	26.7	29.1
.075	33.1	23.9	23.1	28.7	31.1
.080	35.7	25.7	24.8	30.9	34.0
.085	38.2	27.8	26.9	33.1	36.8
.090	41.3	30.1	29.0	35.6	39.6
.095	44.3	32.3	31.2	37.8	42.5
.100	47.7	34.6	33.4	40.5	45.1
.105	51.0	36.7	35.7	43.0	47.9
.110	54.3	39.2	38.1	45.7	50.7
.115	57.9	41.5	40.6	48.0	53.6
.120	61.2	44.1	43.2	50.7	56.4
.125	64.7	46.6	45.6	53.2	59.2
.130	68.3	48.7	48.3	56.4	62.1
.135	72.1	51.2	50.8	59.1	65.2
.140	76.0	53.5	53.5	61.8	68.5
.145	79.3	56.1	56.5	64.3	71.3
.150	82.9	58.4	59.3	67.0	74.2
.155	86.7	60.7	62.1	70.2	77.3
.160	90.3	62.7	64.9	73.0	80.1
.165	94.3	64.7	67.6	75.9	82.9
.170	36.4	67.0	70.6	78.9	85.8
.175	58F	68.8	73.2	81.6	58.6
.180			75.7	84.9	91.4
.185			78.4	87.3	93.8
.190			81.2	90.3	
.195			83.6	93.3	
.200			85.8	95.7	
.205			88.0	98.0	
.210			90.3	100.4	
.215				102.4	
.220				104.4	

REPEATABILITY TESTS OF ANB-3600/SD-923
PROPELLANT-LINER BOND AT 77°F AND ATMOSPHERIC
PRESSURE (OPERATOR 1, BATCH 2)

Spec. No.:	12-6	12-7	12-8	12-9	12-10
2a', in.	0.8	0.8	1.2	1.2	1.6
R, in./min	0.50	0.50	0.10	0.10	0.10
u, in.	f, lb/in.	f, lb/in.	f, lb/in.	f, lb/in.	f, lb/in.
.005	4.3	4.3	2.0	2.2	2.0
.010	7.1	6.9	3.7	4.2	3.7
.015	9.4	9.5	5.0	6.0	5.3
.020	11.7	12.1	7.0	7.5	6.9
.025	14.5	14.6	8.5	8.8	8.2
.030	16.3	16.4	10.1	10.3	9.7
.035	18.6	19.0	11.8	12.3	11.2
.040	20.9	21.3	13.6	13.8	12.7
.045	23.7	23.4	15.1	15.4	14.3
.050	26.5	26.0	16.9	17.4	15.9
.055	29.3	28.3	18.6	18.9	17.8
.060	32.3	31.1	20.2	20.9	19.5
.065	35.2	33.7	22.7	22.7	21.4
.070	37.7	36.5	25.2	25.2	23.4
.075	40.8	39.4	27.2	27.5	25.5
.080	43.8	42.5	29.2	29.5	27.7
.085	47.1	45.8	31.5	31.8	29.8
.090	50.5	48.9	34.0	33.8	32.3
.095	53.8	52.0	36.6	36.3	34.6
.100	57.1	55.1	39.1	38.8	37.1
.105	60.7	58.2	41.6	41.1	39.5
.110	64.2	61.8	44.6	43.6	41.9
.115	67.8	64.6	47.4	46.2	44.3
.120	71.9	68.2	50.0	48.4	46.8
.125	75.5	71.6	52.7	51.2	48.9
.130	79.0	74.7	55.0	53.7	51.5
.135	83.1	78.0	57.5	56.3	54.0
.140	86.7	81.1	60.6	58.8	56.2
.145	90.0	84.7	62.8	61.3	58.1
.150	93.8	87.6	65.1	63.8	60.4
.155	94.6	90.2	67.1	66.4	62.1
.160	101.5	93.8	68.9	68.9	64.1
.165	104.5	96.3	71.2	71.4	
.170	107.1	99.2	73.2	73.9	
.175	110.9	102.0		76.0	
.180	113.5	104.1		78.5	
.185				80.8	
.190				83.3	

TABLE B-21

REPEATABILITY TESTS OF ANB-3600/SD-923 PROPELLANT-LINER BOND AT 77°F AND ATMOSPHERIC PRESSURE (OPERATOR 2, BATCH 1)

Spec. No.:	21-11	21-12	21-13	21-14	21-15
2a', in.	0.4	0.8	0.8	0.8	0.8
R, in./min	0.10	0.02	0.02	0.10	0.10
U, in.	f, lb/in.	f, lb/in.	f, lb/in.	f, lb/in.	f, lb/in.
.005	2.5	1.0	1.4	2.5	2.5
.010	5.0	3.0	3.4	5.0	5.1
.015	7.2	5.1	4.9	7.5	7.6
.020	9.2	6.3	6.6	10.0	10.2
.025	11.5	8.1	8.1	12.5	12.7
.030	13.7	10.2	9.9	15.0	15.3
.035	16.0	11.9	11.3	17.2	17.8
.040	18.2	13.5	13.1	20.0	20.6
.045	20.5	15.8	14.6	22.5	23.4
.050	22.7	17.3	16.5	25.0	26.5
.055	25.0	19.1	18.3	28.5	29.3
.060	27.5	20.9	19.8	31.2	32.3
.065	30.0	22.9	22.2	34.5	35.2
.070	32.5	25.0	24.5	37.2	38.0
.075	35.2	27.2	26.7	40.2	40.8
.080	38.0	28.8	28.9	43.7	43.6
.085	40.7	31.1	30.9	47.0	46.4
.090	43.5	33.1	33.4	50.0	49.7
.095	47.2	35.7	35.8	53.5	52.8
.100	50.5	38.0	38.3	56.7	55.6
.105	54.5	40.5	40.8	60.0	58.6
.110	57.5	43.1	44.0	63.5	61.9
.115	61.0	45.6	46.5	67.2	65.0
.120	64.5	47.4	49.5	70.0	67.8
.125	68.2	50.0	51.7	73.7	70.6
.130	72.0	52.8	54.4	76.7	73.4
.135	75.0	55.6	56.9	80.0	76.2
.140	79.0	58.4	59.4	83.5	78.8
.145	82.5	60.9	61.8	86.7	81.6
.150	86.2	63.5	64.3	90.0	83.9
.155	90.0	66.3	67.0	92.5	86.4
.160	94.0	68.8	69.8	95.7	88.0
.165	97.5	71.4	72.5	98.7	
.170	101.2	73.7	75.2	101.7	
.175	105.0	76.2	77.9	104.5	
.180	109.0	79.0	79.9		
.185	112.7	81.6	81.6		
.190	116.7	84.1	84.1		
.195	120.0	86.4	86.6		
.200	122.5		89.1		

REPEATABILITY TESTS OF ANB-3600/SD-923 PROPELLANT-LINER BOND AT 77°F AND ATMOSPHERIC PRESSURE (OPERATOR 2, BATCH 1)

Spec. No.:	21-16	21-17	21-18	21-19	21-20
2a', in.	0.8	0.8	1.2	1.2	1.6
R, in./min	0.20	0.20	0.10	0.10	0.10
U, in.	f, lb/in.	f, lb/in.	f, lb/in.	f, lb/in.	f, lb/in.
.005	3.2	4.6	2.5	2.5	2.2
.010	5.7	8.0	3.8	5.0	5.0
.015	8.0	10.9	5.9	7.0	6.7
.020	10.0	13.5	7.4	8.8	8.5
.025	13.0	16.1	9.0	10.8	10.0
.030	14.5	18.7	10.3	12.6	11.7
.035	16.2	20.8	11.8	15.1	13.5
.040	17.7	23.4	13.6	16.9	14.7
.045	19.8	26.0	14.9	18.9	16.2
.050	22.2	28.6	16.7	21.2	17.7
.055	24.0	31.2	18.8	22.9	19.7
.060	26.0	33.8	20.3	26.2	21.5
.065	28.2	36.4	21.9	27.7	23.0
.070	30.5	38.8	23.9	30.3	25.0
.075	33.1	41.4	26.2	32.8	27.0
.080	35.0	44.4	28.8	34.8	28.7
.085	37.7	47.1	31.9	37.6	30.5
.090	40.0	50.1	36.0	40.4	32.5
.095	42.2	52.8	40.2	42.9	35.0
.100	45.0	55.9	45.1	45.4	37.0
.105	47.2	58.9	48.4	47.9	39.0
.110	49.7	61.8	51.5	50.7	40.7
.115	52.2	64.8	54.3	53.5	42.5
.120	55.0	67.9	57.7	56.5	45.0
.125	57.2	70.5	60.5	59.3	47.5
.130	60.0	73.6	63.9	62.1	49.5
.135	63.1	77.0	67.0	65.4	51.7
.140	65.5	80.0	69.5	68.1	53.5
.145	68.1	83.3	72.9	70.7	55.7
.150	71.2	86.5	76.0	74.2	57.5
.155	74.3	89.5	79.1	76.7	59.7
.160	77.0	92.9	82.4	79.2	61.2
.165	79.6	96.3	85.3	81.8	63.2
.170	82.5	99.4	88.4	84.3	65.0
.175			91.4	86.8	66.7
.180			94.0	88.6	67.7
.185			96.6	90.9	
.190			99.2	93.1	
.195			101.8	94.6	

TABLE B-22

REPEATABILITY TESTS OF ANB-3600/SD-923 PROPELLANT-LINER BOND AT 77°F AND ATMOSPHERIC PRESSURE (OPERATOR 2, BATCH 2)

Spec. No.:	22-11	22-12	22-13	22-14	22-15
2a', in.	0.4	0.8	0.8	0.8	0.8
R, in./min	0.10	0.02	0.02	0.10	0.50
U, in.	f,lb/in.	f,lb/in.	f,lb/in.	f,lb/in.	f,lb/in.
.005	2.5	1.0	1.4	2.5	2.5
.010	4.8	2.5	2.6	5.0	4.5
.015	7.0	3.7	4.3	6.3	6.3
.020	9.1	5.0	5.3	8.0	7.9
.025	10.9	7.3	7.0	10.1	10.2
.030	13.0	8.3	8.0	11.3	11.7
.035	14.6	10.1	9.4	13.1	13.5
.040	16.3	12.1	10.6	15.1	15.3
.045	18.4	13.3	12.1	16.4	17.0
.050	20.4	15.1	13.3	18.1	18.6
.055	22.1	17.1	14.5	20.2	20.4
.060	24.2	18.9	16.5	21.9	22.9
.065	26.1	20.7	18.2	23.7	24.2
.070	28.3	22.7	19.4	25.5	26.2
.075	30.6	25.0	23.3	27.7	28.0
.080	32.6	26.7	25.<	30.3	30.3
.085	34.6	29.0	26.9	32.3	32.3
.090	36.7	31.5	29.1	34.0	34.4
.095	39.0	34.0	31.0	36.6	36.7
.100	41.3	36.3	33.4	39.1	38.2
.105	43.8	38.1	35.1	41.6	40.8
.110	46.6	40.4	37.1	44.1	43.3
.115	48.7	42.9	38.5	46.4	45.9
.120	51.2	45.4	41.2	48.7	47.9
.125	53.8	47.9	43.4	51.2	50.7
.130	56.3	50.2	44.9	53.7	52.8
.135	58.9	52.7	47.3	56.3	55.1
.140	61.8	55.0 .	49.2	59.3	57.3
.145	64.5	56.8	51.4	61.8	59.9
.150	67.3	59.0	53.3	64.3	62.5
.155	70.1	61.3	55.8	66.9	65.0
.160	72.9	63.1	57.5	69.9	67.6
.165	75.7	65.1	59.2	72.4	70.1
.170	78.8	66.9	60.6	75.0	73.4
.175	81.6	69.4	62.8	77.5	76.2
.180	84.8		64.3	79.5	79.0
.185	87.7			80.8	81.6
.190	90.8			83.3	84.1
.195	93.6			85.8	86.7
.200	96.9			87.1	89.2
.205	99.8				91.8
.210	102.8				94.3
.215	105.4				96.6
.220	108.4				98.9

TABLE B-22 (CONTINUED)

REPEATABILITY TESTS OF ANB-3600/SD-923 PROPELLANT-LINER BOND AT 77°F AND ATMOSPHERIC PRESSURE (OPERATOR 2, BATCH 2)

Spec. No.:	22-16	22-17	22-18	22-19	22-20
2a', in.	0.8	0.8	1.2	1.2	1.2
R, in./min	0.50	0.50	0.10	0.10	0.10
U,in.	f,lb/in.	f,lb/in.	f,lb/in.	f,lb/in.	f,lb/in.
.005	3.3	2.5	2.0	1.9	2.4
.010	6.3	5.5	3.8	3.8	4.2
.015	11.4	8.3	5.1	5.3	5.9
.020	11.2	10.8	6.7	7.0	7.3
.025	13.7	13.2	7.9	8.4	8.8
.030	15.8	15.4	9.5	10.2	10.4
.035	17.8	17.4	10.8	11.9	11.9
.040	19.6	19.6	12.2	13.5	13.5
.045	22.1	22.0	13.6	15.0	14.9
.050	24.7	24.7	15.4	16.8	16.5
.055	26.5	27.0	17.7	18.4	18.2
.060	29.0	29.5	19.5	19.8	19.8
.065	31.3	32.0	21.9	21.9	21.6
.070	33.9	34.7	23.9	23.7	23.3
.075	36.7	37.6	26.0	25.5	25.3
.080	39.2	40.4	28.0	27.4	27.3
.085	41.8	43.1	30.1	29.5	29.3
.090	44.6	46.2	31.9	31.3	31.3
.095	47.1	48.9	34.2	33.4	33.3
.100	49.7	52.0	36.3	35.7	35.3
.105	52.5	54.7	38.6	37.6	37.4
.110	55.6	57.5	40.5	39.5	39.6
.115	58.6	61.1	42.7	41.8	41.8
.120	61.8	64.1	45.1	44.1	43.9
.125	65.0	67.1	47.4	46.4	46.0
.130	67.8	70.4	49.7	48.4	47.9
.135	70.7	73.4	51.8	50.7	49.9
.140	73.9	76.7	54.1	53.3	51.8
.145	77.1	79.7	56.1	55.6	53.7
.150	80.3	82.8	58.2	57.9	55.4
.155	83.4	85.8	60.3	60.2	56.8
.160	86.9	88.3	62.6	61.9	58.3
.165	90.0	91.7	64.4	56.5	
.170	93.3	94.4	66.2	67.0	
.175	96.6	97.4	67.9	69.5	
.180	99.7	100.3	69.8	71.6	
.185	103.0			73.7	
.190	106.1			75.3	
.195	108.9			77.2	
.200	112.5			78.9	
.205	115.3			80.7	
.210	118.1			82.1	

B-54

APPENDIX C

THERMAL ANALYSIS OF
THE SCARF-JOINT SPECIMEN
IN SIMULTANEOUS COOLING
AND STRAINING

1. **Analysis of the Heat Transfer in the Scarf-Joint Specimen with Decaying Temperature Boundary Conditions**

The thermal properties of ANB-3066 propellant were taken from the linterature. Corroborative tests of the thermal diffusivity were performed between 70°F and 7°F. As a result the following thermal properties values were used:

    a. Density: 110.59 $1bm/ft^3$

    b. Specific Heat: 0.279 BTU/1bm/°F

    c. Thermal diffusivity: 0.00778 ft^2/hr

Computer simulations to determine the thermal gradients of scarf-joint specimens nominally 1 x 2 x 4-in. in size, subjected to various rates of cooling, used the properties listed above. Separate tests of the unstead state thermal behavior of the scarf-joint specimen were made in a convective conditioning chamber, to ascertain an appropriate test system was like that to be used in the simultaneous straining - cooling tests. A value of 7.0 $BTU/ft^2/°F$ was obtained for this parameter. It turns out that this parameter can vary widely without affecting the thermal gradients in the specimens.

2. **Computer Simulation**

A finite-difference heat transfer solution was utilized, and impletmented to determine the thermal gradients through the thinnest section of the scarf-joint, with a linear temperature-decay boundary condition.

These simulations show that after an initial unsteady state period, during which the temperature profiles are changing, an unchanging gradient is established that decays at the rate of the boundary changes. Further study has shown that this is in agreement with analytic solutions for this type of heat transfer.[1]

---

1. Carslaw H.S., Jarger, J.C., "Conduction of Heat in Solids" 1959 Clarendon Press.

The temperature profile is the computed temperature variation between points in the specimen immediately beneath the surface, on a line perpendicular to the smallest dimension, separated by the grid spacing employed in the finite-difference program. (1/51 inches for all results discussed)

Somewhat surprisingly, the maximum variation in the temperature profile (from the point nearest the specimen surface to the center point) was found to be linearly related to the rate of boundary temperature decay. Figure C-1 shows this relationship. Figure C-2 is a portion of the simulation printout showing parameter values utilized and the change of profile with time.

These data were utilized to provide the test matrix of straining and cooling rates to be used in the simultaneous cooling straining tests in the program. This is shown in Table C-1. It should be noted that 47°F/hr was arbitrarily chosen as the fastest cooling rate to limit profile difference values to a maximum of 5°F.
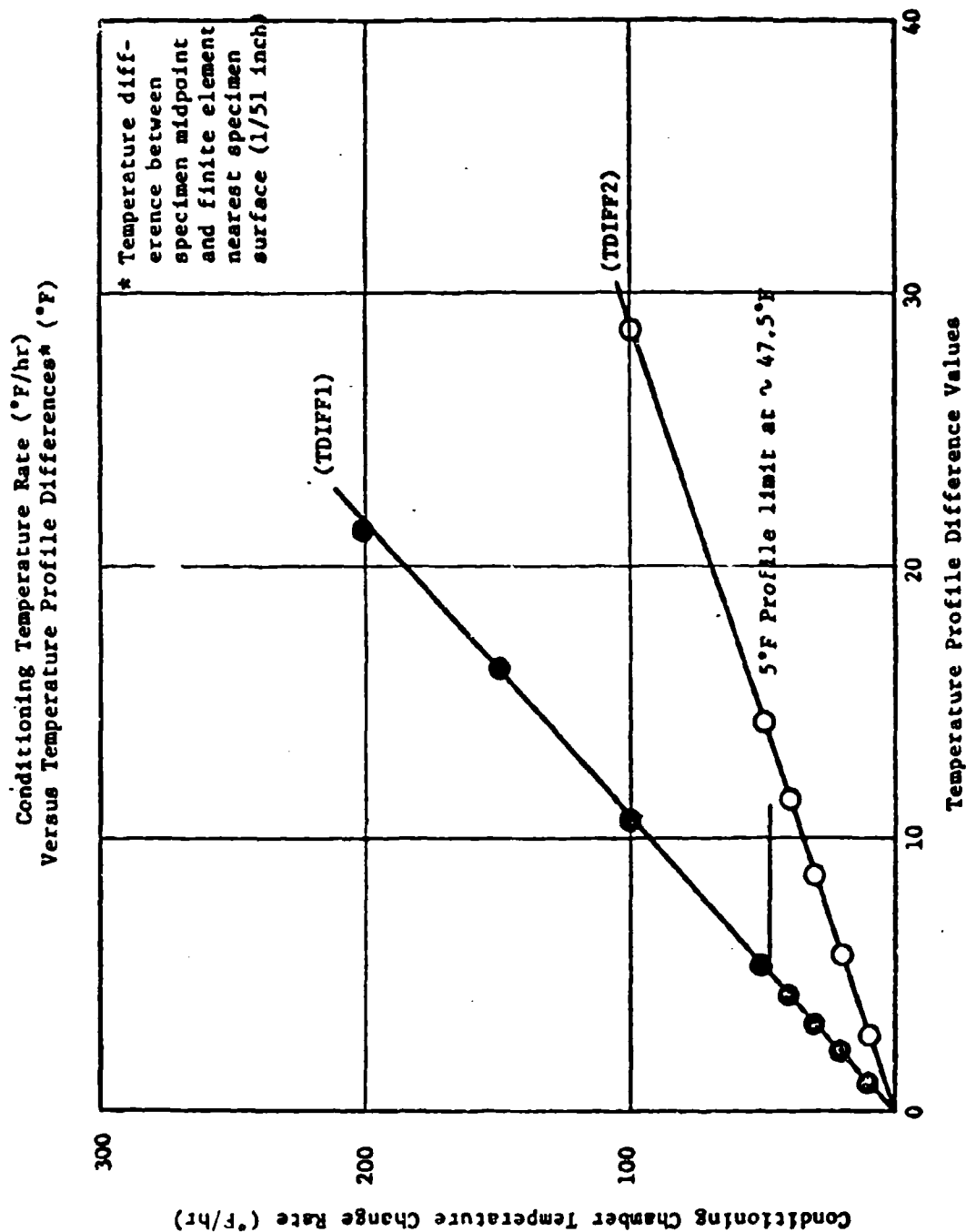
Conditioning Temperature Rate (°F/hr)
Versus Temperature Profile Differences* (°F)

Figure C-1

1008..47.3

HT TRANS CCCF=   1000.00 RATE TEMP DECAY=   47.50 DEC F/ HR ①

TEST SPECF SCINT COOL'NG   SIMULATION DECAY RATE 47.0 DEG F/HR

FK	ALPHA	HTC	TEMP RATE		
.240000	30.050000	1000.00	47.50		
ARINCH	BCINCH				
1000.00	1001.06				
MDIV	NPRNT	DTSEC	TLIMS	TPRNTS	
51	5	180.00	2400.00	900.00	
T INIT	T INS	T OUTS			
125.00	79.00	79.90			

RADII ==== ②
1000.0000 1000.1070 1000.2059 1000.3039 1000.4019 1000.5000
TIME(HR) TIME(MIN) TIME(SEC)

TINS = 125.0000   0.0 ③
0.000000   0.0
125.00   125.00   125.00   125.00   125.00   125.00 ④
   0.0000   0.0000   0.0000   0.0000   0.0000
   TDIFF1   TDIFF2 TIME SEC   T CENTER
   0.00   0.00   0.00   125.00
   1.0000   1.0000

TINS = 113.1250   900.0 ⑤
.250000   15.0
113.18   114.94   116.11   117.41   117.54   117.72
   11.0203   10.1591   9.0881   7.9925   7.4603
   TDIFF1   TDIFF2 TIME SEC   T CENTER
   4.59   4.54   900.00   117.72
   0.0000   0.0000

TINS = 101.2500   1800.0 ⑥ ⑦
.500000   30.0
101.51   103.12   104.53   105.54   106.14   106.34
   11.0784   11.7165   11.5780   11.4602   11.3970   11.3734
   TDIFF1   TDIFF2 TIME SEC   T CENTER
   5.09   5.03   1800.00   106.34
   .9915   .9013

TINS = 89.3750   2700.0
.750000   45.0
89.43   91.27   92.49   93.71   94.32   94.52
   11.0745   11.6582   11.0424   11.0320   11.0245   11.0220
   TDIFF1   TDIFF2 TIME SEC   T CENTER
   5.09   5.09   2700.00   94.52
   .9897   .9997

TINS = 77.5000   3600.0
1.000000   60.0
77.56   79.39   80.82   81.04   82.45   82.65
   11.0750   11.0732   11.0716   11.0703   11.8695   11.8692
   TDIFF1   TDIFF2 TIME SEC   T CENTER
   5.15   5.09   3600.00   82.65
   .9989   .9989

LEGEND

① Thermal properties
   Thermal conductivity
   Specific-heat-density product
   Heat transfer coef
   Conditioning temperature decay rate

② Center of finite element nearest surface AA

③ Center of element - specimen mid thickness
   (BB inch - AA inch = 0.1 inch)

④ Initial temp distribution in spec

⑤ Profile after 0.25 hr conditioning -
   exterior temp tins = 113.25°F

⑥ Maximum temp diff within the spec ③ - ②

⑦ Ratio to previous value printed

Figure C-2